Victor Aulin - Oleg Lyashuk - Olexiy Pavlenko - Denis Velykodnyi - Andrii Hrynkiv
Sergii Lysenko - Dmytro Holub - Yuriy Vovk - Volodymyr Dzyura - Mariana Sokol*

REALIZATION OF THE LOGISTIC APPROACH IN THE INTERNATIONAL CARGO DELIVERY SYSTEM

Fierce rivalry in the transport market raises serious reassessment and implementation of new approaches to logistics companies and trade enterprises in marketing of goods. To maintain the volume of domestic sales and output to the external one, producers and trading firms are forced to expand their trade and economic relations that occur in other regions. The integration of the world economy and policy orientation of foreign trade to free trade greatly simplify the task of setting up the free trade and economic connections, but the question is how quickly and efficiently, with the least costs, it is necessary to put the goods in the right region to the customer.

In modern market conditions, international container transportation of goods between Ukraine and the European Union countries has a prospect of development, as each year the number of orders in transport and logistics enterprises increases. After analyzing the status of orders, the problem has been detected and widely connected with the method of organization of container cargo delivery in international communication and the formation of rational technology of serviced. To solve this problem a method of logistic approach to the system of containers transportation has been proposed based on the cybernetic model „white box". The initial stage of its implementation involves formation of the limitation system of input parameters and factors that are consistent with the needs of the customer firm and the company performing transportation. Ten alternative order services schemes, each of which takes into account the possible combinations of operations, has been proposed.

Based on the company „Inter Trans Logistic", which serviced the order of the company „Agricultural Holding August" for the transportation of rape seeds, 10 tons of corn on demand and a portion of sunflower oil 20,000 liters, according to their applications for transportation, a logistic approach using a cybernetic model „white box" has been implemented. Based on the mathematical models of changes in the total costs of the international container cargo shipping company of the customer, it has been shown that the maximum expenses are occurring in the implementation of the scheme 1 service order. In that case, the costs have been in the range of 848.72 to 7455.41 US $, according to a certain series of experiments. Based on the condition of the minimum cost function for container transportation, scheme 1 has been chosen as limiting scheme of service order against which the assessment carried out changes of the total costs in the implementation of other schemes. In percentage display according to Scheme 1, the following percentage intervals have been deducted for the reduction of sales costs: Scheme 2 - 12.70 to 34.98%; Scheme 3 - 2.93 to 12.00%; Scheme 4 - 2.06 to 10.88%; Scheme 5 - 1.69 to 4.25%; Scheme 6 - 0.87 to 3.28%; scheme 7 - 0.97 to 2.58%; Scheme 8 - 1.64 to 4.45%; Scheme 9 - 2.66 to 11.77%; scheme 10 - 2.33 to 9.94%.

The results of experimental studies indicate that when the proposed methodology of the logistic approach, using the „white box" based on the company „Inter Trans Logistic" to international container transportation of goods in relation to the application of the company „Agricultural Holding August" for transportation, the scheme 2 sequence of transport operations has been effective. In its realization the costs for 12.70 to 34.98% has been decreased in comparison with the marginal service scheme.

Keywords: *logistic approach, transportation technology, container international traffic*

1. Introduction

Transport is a branch of production that provides society vital needs in goods transportation, and is a part of the infrastructure production. By providing the transportation goods, transport makes a significant contribution to development of foreign economic, scientific, technical and cultural, sports and other connections of Ukraine, mainly with the European Union countries. According to this, there is an increasing tendency of demands for international transport services, both in terms of volume and nomenclature [1].

The over-saturation of the market, consumer dictation in the market and rigid competition cause serious difficulties for producers, trading and sales enterprises in the sale of goods. To save sales volumes, manufacturers and trading firms are forced to go on expansion sales at the expense of entering markets that are located in other regions. And while the world economy integration and countries foreign trade policy orientation to free trade greatly simplify this task, so the following question has been raised: how quickly and efficiently, with the least costs, it is necessary to put the goods on the market [2].

* **[1]Victor Aulin, [2]Oleg Lyashuk, [3]Olexiy Pavlenko, [1]Denis Velykodnyi, [1]Andrii Hrynkiv, [1]Sergii Lysenko, [1]Dmytro Holub, [2]Yuriy Vovk, [2]Volodymyr Dzyura, [4]Mariana Sokol**
[1]Department of Maintenance and Repair of Machines, Central Ukrainian National Technical University, Kirovograd, Ukraine
[2]Department of Automobiles, Ternopil Ivan Puluj National Technical University, Ukraine
[3]Department of Transport Technologies, Kharkiv National Automobile and Road University, Ukraine
[4]Foreign Languages Department, Ternopil State Medical University, Ukraine
E-mail: vovkyuriy@ukr.net

Nowadays, in the global market, the process of goods delivery is associated with the process of performing a series of works, operations and services, the complex of which will ensure the efficient goods distribution. In such a situation, transport companies are faced with the task of using efficient tools, developing methods and procedures for handling orders for any cargo owner with the most need for quality services. There is a need to develop a rational technology for servicing orders, while the delivery of goods in containers in international traffic has been organized.

The relevance of international container transportation has been increased [3]. This is evidenced by the existence and creation of new large, modern companies that are specialized precisely in this type of cargo delivery organization. They compete with each other by offering customers the best, more economical, faster, better ways to handle orders and deliver in international containers, and the ability to deliver goods to anywhere in the world. That is why such process necessitates development of the efficient container transportation technologies.

Container transportation between Ukraine and the European Union countries has been recognized as the most modern and high-quality way of international transportation. That allowed reducing the share of transport component in the final price of the goods from 2% to 11%. The selection of rational order service technology and, as a result, the reduction of shipping costs is a priority task for many companies whose main goal is, logistically, to provide the right product in the right amount, quality and at the right time [4]. The use of containers increases transportation efficiency, because the costs associated with the movement, storage and handlings of goods are significantly reduced.

New representative offices of world large companies continue to open in Ukraine. Thus, in January 2017 it became known that the international operator FM Logistic began to work in the segment of the sea container traffic in Ukraine. The third largest company had been opened in Odessa. The company provides multimodal services, interacts with port operators, ship-owners and container lines, customs, railways, carriers to create a single chain of the cargo delivery.

In the first half of 2018, container terminals in Ukraine processed 340155 TEU. It is 4.7% more than the volume processed in the same period of 2017. Growth, compared to previous year's indexes, shows that transshipment increased by 24.4%, of course, it is not so impressive, but encouraging the pace of development and stability.

The developed system solutions in container handling at container terminals allowed improving the efficiency of production management using modern technologies implementation in the ports of China [5-9]. One of the important issues in this system is the return of empty containers, which is solved by using solutions derived from developed gravity models [10]. In addition, the study [10] proposes an effective solution for the container capacity and the container terminal area.

In the international cargo delivery system, rational construction of the port infrastructure, container terminal and adjacent areas is very important, therefore, to determine the optimal configuration of the location, a two-level programming system was used. This system took into account the container movement in time and allowed to determine the shipping costs with the maximum positive effect for the operator [11].

Article [12] presents a new advanced solution for handling the container terminals system. The process of container terminal manufacturing operations has been described according to workflow and Data Flow Diagram (DFD). The integrity and reliability of the new system using the analysis of the Petri Net has been proven. At the same time, the new solution of the problem is to rebuild the logistic processes that have low costs, high quality, greater flexibility, quick and reasonable response to the entire production system of the terminal.

The authors of the article [13] focus on modeling of the products chain supply. However, the subspace identification methods can be used to characterize relations between some parameters of the supply system. This can be useful if the internal structure of the system was complicated. The supply chains can be identified and modeled by deterministic models of linear states space. The accuracy of the identified model reflects the relationship between certain system parameters and their sensitivity estimates [14-17].

After the oil crisis, Japanese "Just-in-Time" logistics systems have been created at long distances of mutual cooperation between the manufacturer of cars, spare parts suppliers, their logistic subsidiaries and third-party logistics suppliers [18].

Processes and operations in goods delivery can be tested, depending on acceptable methods and approaches for cybernetic models "black, white and gray boxes" [19].

In order to protect the critical data and cryptographic keys, drones' delivery has been provided based on developed methodology using the cybernetic model of the "white box" [20]. Experimental results showed that the proposed methodology had been economically efficient and suitable for supply systems with limited resources. Economic grounds for logistics operations are grounded in the works of Petraska et al. [21], Gajewska and Zimon [22], Agbelie [23], Alghaffari, Nguyen, and Chen [24].

In modern market conditions, international container transportation of goods between Ukraine and EU countries has a development perspective, as each year the number of orders has been increased to the address of transport and transport-logistics enterprises. The revealed found the problem associated with the method of organization of the container cargo delivery in international traffic and the formation of rational technology service orders based on cybernetic model of the «white box».

The aim of the study is to develop a methodology for service orders rational technology formation into the organization of goods delivery in containers in international traffic with minimal costs based on the logistic approach of the transportation system using the cybernetic model "white box". The object of research - the process of service orders in the organization of goods delivery in containers in international traffic.

2. Materials and methods

The general scheme of service orders in the organization of container goods delivery in international traffic between Ukraine and the European Union countries may include a lot of main operations using different types of transport (road, rail, sea).

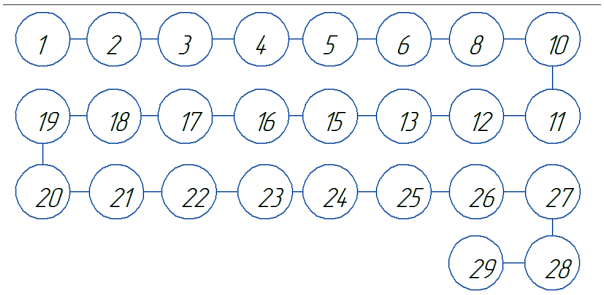

Figure 1 *Set and structure of operations according to cargo delivery technology as per scheme 1*

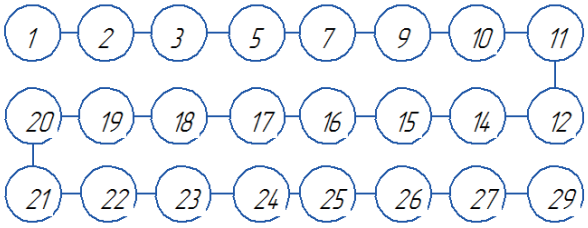

Figure 2 *The sequence of operations as per scheme 2*

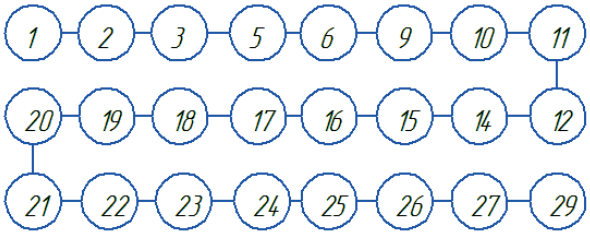

Figure 3 *The sequence of operations as per scheme 3*

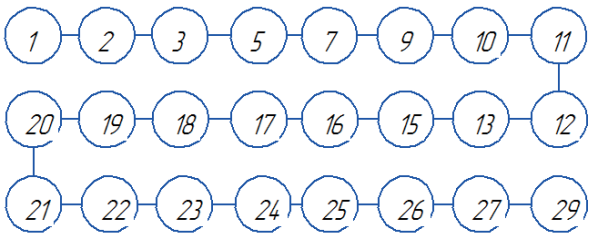

Figure 4 *The sequence of operations as per scheme 4*

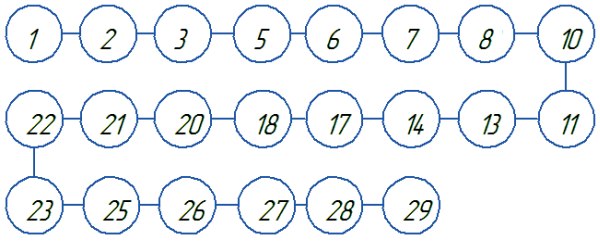

Figure 5 *The sequence of operations as per scheme 5*

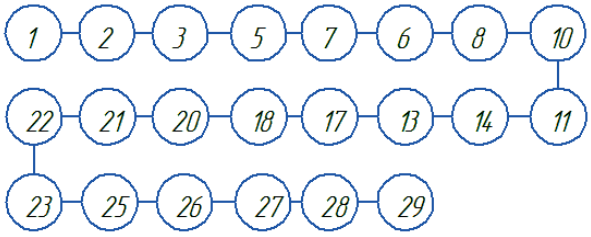

Figure 6 *The sequence of operations as per scheme 6*

As practice shows, in terms of economic considerations, the combination of different modes of transport is usually used.

To minimize the total shipping costs, the task is to select a set of certain operations, taking into account the requirements of the customer serviced.

The schemes of service orders in the organization of goods delivery in containers in international traffic are formed from the list of operations:

1 - Receipt of an application for transportation from a potential client;
2 - Specification of departure and destination ports;
3 - Selection of appropriate container and determination of its availability;
4 - Search for container among partner companies;
5 - Selection of the type of a vehicle for transportation of goods;
6 - Determination of appropriateness of the auto transport usage;
7 - Determination expediency of the rail transport usage;
8 - Search for transport vehicles among their own;
9 - Vehicle rental in partner's firms;
10 - Identification and search of loading and unloading mechanisms;
11 - Choosing customs brokerage office;
12 - Choosing port delivery scheme;
13 - Determination of reasonability of the auto transport in the destination country;
14 - Determination of reasonability of the rail transport in the destination country;
15 - Agreement with the client goods delivery costs;
16 - Contract execution with the contractors and financial-payment, shipping documents;
17 - Supply container and vehicle under load;
18 - Container movement to the terminal;
19 - Transfer and storage of the cargo at the port terminal;
20 - Transfer and overload of the container on the vessel;
21 - Vessel movement to the territory of a foreign state;
22 - Goods transferring into the terminal of the port and unloading the container from the vessel;
23 - Customs clearance in the port;
24 - Storage at the terminal territory;
25 - Vehicle delivery and container loading;
26 - Inside vehicle container movement to its destination;
27 - Unloading the container from the consignee's vehicle;
28 - Cargo unloading outside the container;
29 - Transfer to the recipient.

Ten alternative order schemes have been offered (Figures 1-10), each of which takes into account possible combinations of operations. Thus, for example, the first scheme (Figure 1) has the following features: the transport enterprise does not have its own containers, transport for containers transportation to the port is automobile, there is an own transport vehicle, transportation

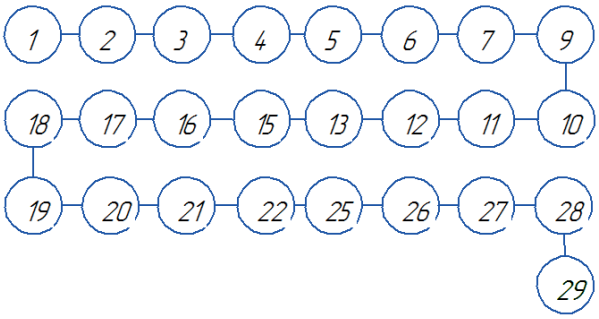

Figure 7 *The sequence of operations as per scheme 7*

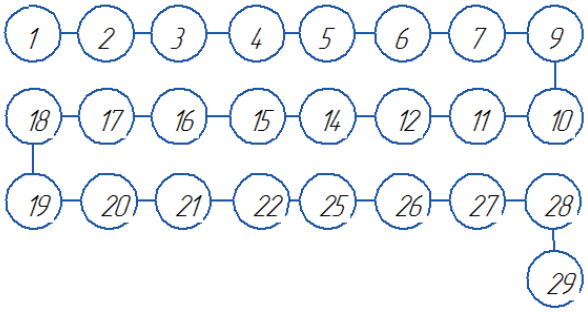

Figure 8 *The sequence of operations as per scheme 8*

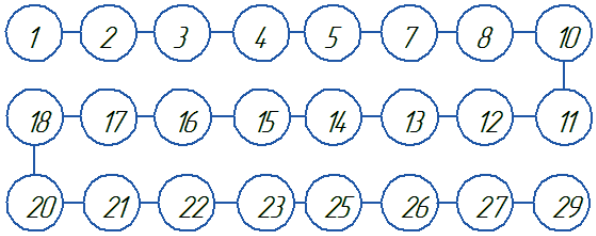

Figure 9 *The sequence of operations as per scheme 9*

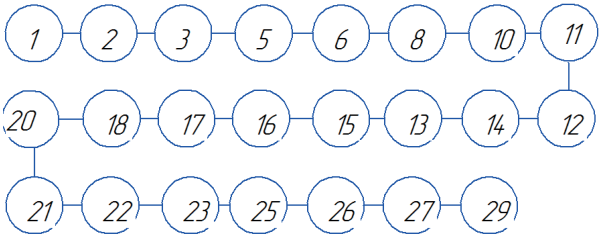

Figure 10 *The sequence of operations as per scheme 10*

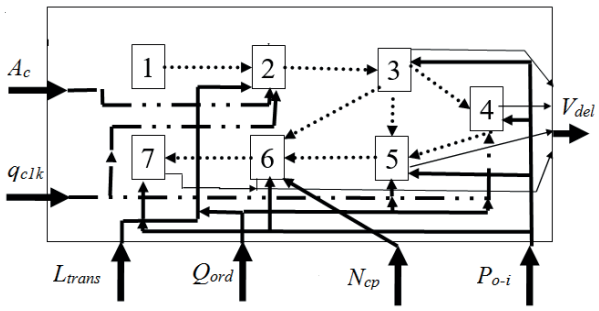

Figure 11 *Schematic of displaying the proposed methodology of the logistic approach to the transportation system based on the cybernetic model "white box"*

from the port is done by the motor transport, an unloading of containers from the vehicle and unloading the cargo is organized.

The difference between the second scheme (Figure 2) from the first (Figure 1) is that the enterprise has its own containers, the transportation to the port comes over the rail transport, vehicles are rented from partner firms, the transportation from the port - by the rail transport, cargo from the containers is not unloaded, and immediately transferred to the recipient (Figure 2).

Alternatively, to the second in the third scheme (Figure 3), the transportation of the cargo to the port is carried out by auto transport, and the transportation from the port - by the rail one.

In the following scheme (Figure 4), the transportation of the cargo to the port is carried out by the rail transport and the transportation from the port - by the automotive one.

The main feature of the scheme (Figure 5) is the combination of the auto and rail transports during the transportation of containers to the port and from the port and cargo unloading outside containers at the transfer to the recipient.

The combination of the rail and auto transport in the process of bringing containers to the port and bringing them off the port is shown in scheme six (Figure 6).

The following combinations of operations are displayed in the scheme (Figures 7-10): combining types of transport, availability of own or rental vehicles, loading and unloading mechanisms, storing containers at the terminal or immediate reloading them into vehicles, transferring to the recipient of the cargo, unloaded from containers or transfer of downloaded containers.

The costs are the most important parameter when choosing the best option for the scheme of service orders when organizing the container cargo delivery in international connections [16]. For this reason, the following research develops a logistic approach to choosing a sequence of operations of the order service scheme, which would provide an opportunity to evaluate and optimize the associated costs of time, resources and funds. The limited resources in the delivery system have been considered, as well.

The use of models in this case requires not only their theoretical development, but the experimental verification on actual materials, as well. The process of processing orders in the organization of the container cargo delivery in international liaison is considered as a complex system, which has a complex of interconnected and interacting subsystems. For a more complete and accurate characteristics of the research object, a schematic representation of the logistic approach, based on the "white box", has been proposed (Figure 11).

This scheme clearly indicates which parameters significantly affect the object of the study and how they are interrelated. [25-26]. The adaptation of the cybernetic model "white box" is based on the four established types of connections between the groups of major processes and the main factors that have been formed in the proposed method, namely: between groups of main processes (1-7); between input parameters (A_c, q_{clk}) and groups of main processes (1-7); between groups of main processes (1-7) and output parameters (V_{del}); between groups of main processes (1-7) and environmental factors (L_{trans}, Q_{org}, N_{cp}, P_{o-i}). The scheme of Figure 2 shows the main processes that occur in organization of containers goods delivery in the international traffic of the company "Inter Trans Logistic": 1 - acceptance of the application for transportation; 2 - evaluation of the company's capabilities for application and choice of service order scheme; 3 - registration

of documents; 4 - loading and unloading work with a cargo; 5 - loading and unloading operations with the container; 6 - customs operations; 7 - moving the container.

3. Results

The input parameters that influence the process of container cargo transportation in international traffic are: number of containers A_c; nominal capacity of one container q_{c1k}. External factors are: distance transportation L_{trans}; volume of one order Q_{ord}; number of customs points N_{cp}; costs of a particular transaction P_{o-i}. As a starting point, from the logistic point of view, the total shipping costs have been chosen V_{del}, as well.

The system constraints, derived from the analysis of order "Agricultural Holding August", which establishes trade and economic ties with partners from Turkey, Italy, Spain, France and the UK for transportation of established packaged rape seeds, 10 tons of corn on demand and part of 20,000 liters of sunflower seeds oil and the possibilities regarding this order of the transport and logistics company "Inter Trans Logistic" have the following form:

$$\begin{cases} 1 \le A_c \le 2 \\ 10 \le q_{c1k} \le 30; \\ 1000 \le A_c \le 9000; \\ 10 \le Q_{ord} \le 30; \\ 2 \le N_{cp} \le 6; \\ 5 \le P_{o-i} \le 100. \end{cases} \quad (1)$$

As a target function for the logistic approach to the transportation system based on the cybernetic model «white box», the function of the total costs of the cargo delivery from a set of parameters and factors has been chosen. Under such conditions, the target costs function should go to its minimum:

$$V_{del} = f(A_c, q_{c1k}, L_{trans}, Q_{ord}, N_{cp}, P_{o-i}) \to \min. \quad (2)$$

For further numerical calculation it is necessary to evaluate the input parameters and factors of the environment in the economic equivalent, namely, in the form of freight costs, consisting of a number of components:

$$V_{del} = V_{l.u.w} + V_{trans} + V_{c.d} + V_c + V_{c.s} + V_{doc}, \quad (3)$$

where $V_{l.u.w}$ - loading and unloading costs, US$; V_{trans} - transportation costs, US$; $V_{c.d}$ - costs of cargo customs declaration, US$; V_c - rental costs of vehicles, containers, US$; $V_{c.s}$ - costs of contractor services, US$; V_{doc} - registration costs of financial-payment, commodity-accompanying documents, US$.

Economic indicators, in the form of costs for specific operations, according to the proposed methodology of the logistic approach to the system of transportation based on the cybernetic model «white box» (Figure 12), have been estimated in stages according to the rates of transport operations of the company «Inter Trans Logistic».

As costs of loading and unloading operations are related to the cargo and containers, they can be calculated by the formula:

$$V_{l.u.w} = V_{l.cargo} + V_{l.cont} + V_{u.cont} + V_{u.cargo}, \quad (4)$$

where $V_{l.cargo}$ - costs of loading the container cargo, US$; $V_{l.cont}$ - costs of loading the cargo container in a vehicle, US$; $V_{u.cont}$ - costs of unloading the container from the vehicle, US$; $V_{u.cargo}$ - costs of unloading the cargo from the container, US$.

The costs of loading and unloading the container by cargo are the following:

$$V_{l.(u.)cargo} = Q_{ord} \cdot C_{l.u}^{cargo}. \quad (5)$$

In formula (5) there are costs of loading or unloading the cargo to / from one container, US$/t.

The costs of loading and unloading the container in / out of the vehicle are:

$$V_{l.(u.)cont} = A_c \cdot C_{l.u}^{cont}. \quad (6)$$

In formula (6), the loading or unloading costs per container are given in US$/unit.

The costs of transportation of containers by different modes of transport are the following:

$$V_{trans} = V_{w.cargo} + V_{AT} + V_{RW} + V_{ST}, \quad (7)$$

where $V_{w.cargo}$ - costs of mileage vehicle unladed, US$; V_{AT} - costs of transportation by road, US$; V_{RW} - transportation costs by rail, US$; V_{ST} - costs of transportation by sea, US$.

It is worth saying that the costs of mileage vehicle unladed have been determined by taking into account the costs of moving a car per one kilometer and the corresponding distance.

The costs of transportation by the road, rail or sea are:

$$V_{AT(RW,ST)} = Q_{ord} \cdot L_{trans}^{AT(RW,ST)} \cdot C_{trans}^{AT(RW,ST)}, \quad (8)$$

where $L_{trans}^{AT(RW,ST)}$ - the distance of transportation by the appropriate type of transport; $C_{trans}^{AT(RW,ST)}$ - transportation costs per one ton-kilometer by the road, rail or sea.

The costs of the cargo customs declaration have been determined by taking into account the time of delay at the customs office $t_{t.i}$ and the cargo delaying costs per one hour at the border office $C_{t.i}$:

$$V_{c.d} = t_{t.i} \cdot C_{t.i} \cdot N_{cp}. \quad (9)$$

Rental costs of vehicles, containers are:

$$V_c = A_c \cdot C_c, \quad (10)$$

where C_c - rental costs of one vehicle (container) per day is defined as the average market in the territory of Ukraine.

The costs of contractor services $V_{c.s}$ take into account costs of brokerage agency services C_{br}, the cargo insurance costs C_{ins} and the security services costs C_{sec}:

$$V_{c.s} = Q_{ord} \cdot (C_{br} + C_{ins} + C_{\text{sec}}). \quad (11)$$

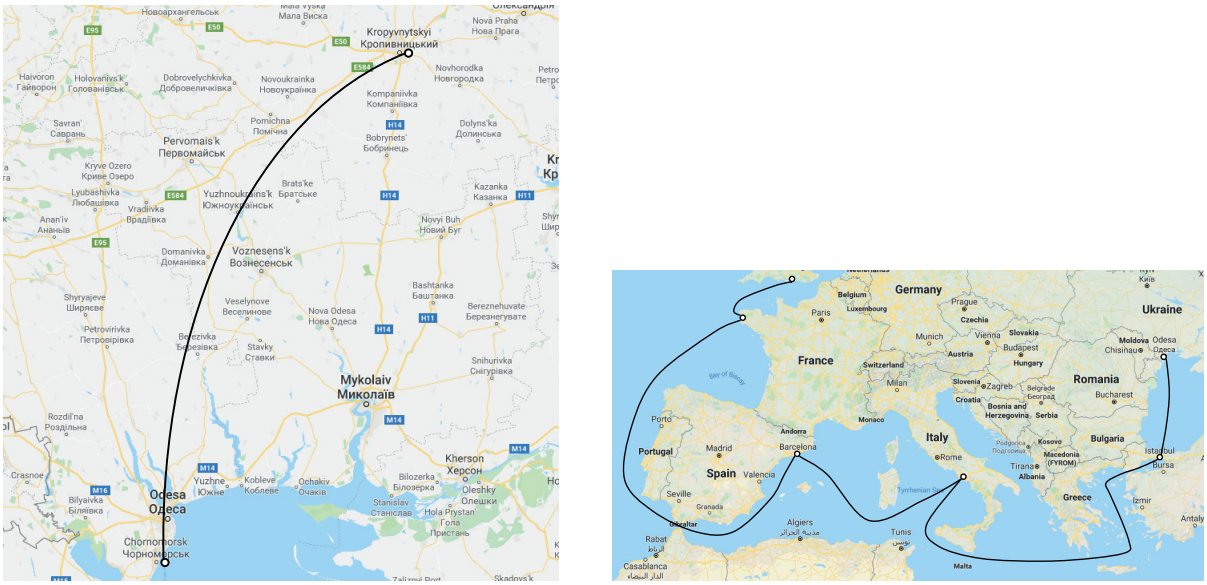

(a) *(b)*

Figure ***12*** *Schemes of container transportations by the company "Inter Trans Logistic" in accordance with the orders of the company "Agricultural Holding August" on the territory of Ukraine (a) and on the international traffic (b)*

Table 1 *Levels of factors variation*

Parameter	Minimum value	Maximum value
Number of customs offices, pcs	2	6
Distance transportation, km	2000	10000
Volume of one order, t	10	30
The costs of a particular operation (service), US$	5	100

Table 2 *Results of the experiment plan with allowance for the limit values*

A series of experiments	Levels of variation			
	Number of customs offices, pcs	Distance transportation, km	Volume of one order, t	The costs of a particular operation (service), US$
1	6	10000	30	5
2	6	10000	10	5
3	6	2000	10	5
4	2	10000	30	100
5	2	2000	30	100
6	2	2000	10	100
7	2	10000	10	100
8	6	2000	30	5
9	2	2000	10	5
10	6	10000	30	100
11	6	2000	10	100
12	6	2000	30	100
13	2	10000	30	5
14	6	10000	10	100
15	2	2000	30	5
16	2	10000	10	5

Table 3 *The calculation results of total costs for the international cargo container delivery for ten alternative service orders*

Series of experiment	Total costs of cargo delivery, US$									
	Scheme 1	Scheme 2	Scheme 3	Scheme 4	Scheme 5	Scheme 6	Scheme 7	Scheme 8	Scheme 9	Scheme 10
1	7455.41	6338.74	6588.74	6644.29	7144.29	7210.96	7262.81	7151.70	6649.85	6714.67
2	2377.63	2075.78	2159.11	2177.63	2251.70	2273.92	2292.44	2255.41	2179.48	2199.85
3	851.70	586.89	623.92	698.00	723.92	786.89	779.48	720.22	629.48	677.63
4	7452.42	6335.75	6585.75	6641.31	7141.31	7207.97	7259.83	7148.72	6646.86	6711.68
5	2874.64	1869.09	1980.20	2202.42	2557.97	2746.86	2720.94	2543.16	1996.86	2145.01
6	848.72	583.90	620.94	695.01	720.94	783.90	776.49	717.23	626.49	674.64
7	2374.64	2072.79	2156.12	2174.64	2248.72	2270.94	2289.46	2252.42	2176.49	2196.86
8	2877.63	1872.07	1983.18	2205.41	2560.96	2749.85	2723.92	2546.15	1999.85	2148.00
9	848.72	583.90	620.94	695.01	720.94	783.90	776.49	717.23	626.49	674.64
10	7455.41	6338.74	6588.74	6644.29	7144.29	7210.96	7262.81	7151.70	6649.85	6714.67
11	851.70	586.89	623.92	698.00	723.92	786.89	779.48	720.22	629.48	677.63
12	2877.63	1872.07	1983.18	2205.41	2560.96	2749.85	2723.92	2546.15	1999.85	2148.00
13	7452.42	6335.75	6585.75	6641.31	7141.31	7207.97	7259.83	7148.72	6646.86	6711.68
14	2377.63	2075.78	2159.11	2177.63	2251.70	2273.92	2292.44	2255.41	2179.48	2199.85
15	2874.64	1869.09	1980.20	2202.42	2557.97	2746.86	2720.94	2543.16	1996.86	2145.01
16	2374.64	2072.79	2156.12	2174.64	2248.72	2270.94	2289.46	2252.42	2176.49	2196.86

The registration costs of financial-payment, commodity-accompanying documents are:

$$V_{doc} = \sum_{j=1}^{k} C_{regj} \cdot n_{rj} . \quad (12)$$

Equation (12) takes into account the costs of processing documents k of type C_{regj} and the number of documents of the appropriate destination n_{rj}.

The method of mathematical planning experiment has been used to implement the developed methodology of the logistic approach to the efficient organization of the container cargo transportation. To this end, a plan of a full-factor experiment has been prepared due to four external factors: the distance of transportation, the volume of one order, the number of customs offices, the costs of a particular operation, the minimum and maximum value of which is determined by the system of restrictions Equation (2) between Ukraine and the European Union countries (Table 1). In forming levels of varying factors that affect goods transportation cost in international connections, it is necessary to set the maximum values that will correspond to the order of the company "Agricultural Holding August" by transporting the cargo by "Inter Trans Logistic" company. The number of customs offices has been taken into account, which can maximally affect the transport costs. The minimum number will be 2 (initial and final), and the maximum number - 6 points for international traffic in relation to the application of the company "Agricultural Holding August" and the established route of rice 3. The volume levels of orders have been formed from firm applications. Costs of operations (services) are reflected in the unit derived from the analysis of costing services company "Inter Trans Logistic".

For given factors, the number of experiments series is 16. As 2 levels of variation has been chosen, so designate them as follows: "-" - 1st level of variation (min), "+" - level 2 (max). After that, all possible combinations of connections and values have been tabulated in Table 2.

Calculations of total costs in the studied ten schemes have been made in Microsoft Excel, and the results are shown in Table 3.

4. Discussion

To substantiate the developed methodology of the logistic approach for choosing a rational technology for servicing orders for international container transportation of goods and e influence of parameters on the criterion of their efficiency (expenses), a regression analysis has been chosen. Among the investigated factors, the following connections have been considered: linear function with nonzero coefficient; linear function with zero coefficient; power function with nonzero coefficient; power function with zero coefficient. To construct the model, the Microsoft Excel program was used, which employs a program for calculating regression mathematical models. Using the above-mentioned cases of analytic regression functions, a regression analysis has been performed for each alternative order service (Figures 1-10). It has been determined that for each operation scheme (Figures 1-10) the linear function with a non-zero coefficient is the best, because in that case the value of determination coefficient R is maximum and equals to 0.9. The regression coefficients have been estimated by: the standard error; the meaning of "t-statistics"; "P-value"; significant indicators. According to results of this assessment, factors such as the number of customs offices and the price of a particular operation have not been taken into account in the mathematical model of costs. Thus, the general formula of the regression model of costs is the following

$$V_{del}^{m} = a_0 + a_1 \cdot L_{trans} + a_2 \cdot Q_{ord} , \quad (13)$$

Table 4 *Determination results of regression models unknown coefficients*

Indicator	The value of unknown coefficients of regression models for the corresponding schemes									
	Scheme 1	Scheme 2	Scheme 3	Scheme 4	Scheme 5	Scheme 6	Scheme 7	Scheme 8	Scheme 9	Scheme 10
a_1	-2254	-2293	-2262	-2279	-2490	-2429	-2466	-2500	-2385	-2345
a_2	0.52	0.48	0.48	0.47	0.48	0.46	0.48	0.48	0.49	0.48
a_3	197.6	158.7	164.7	169.4	178.2	182.5	182.9	178.1	166.1	159.6

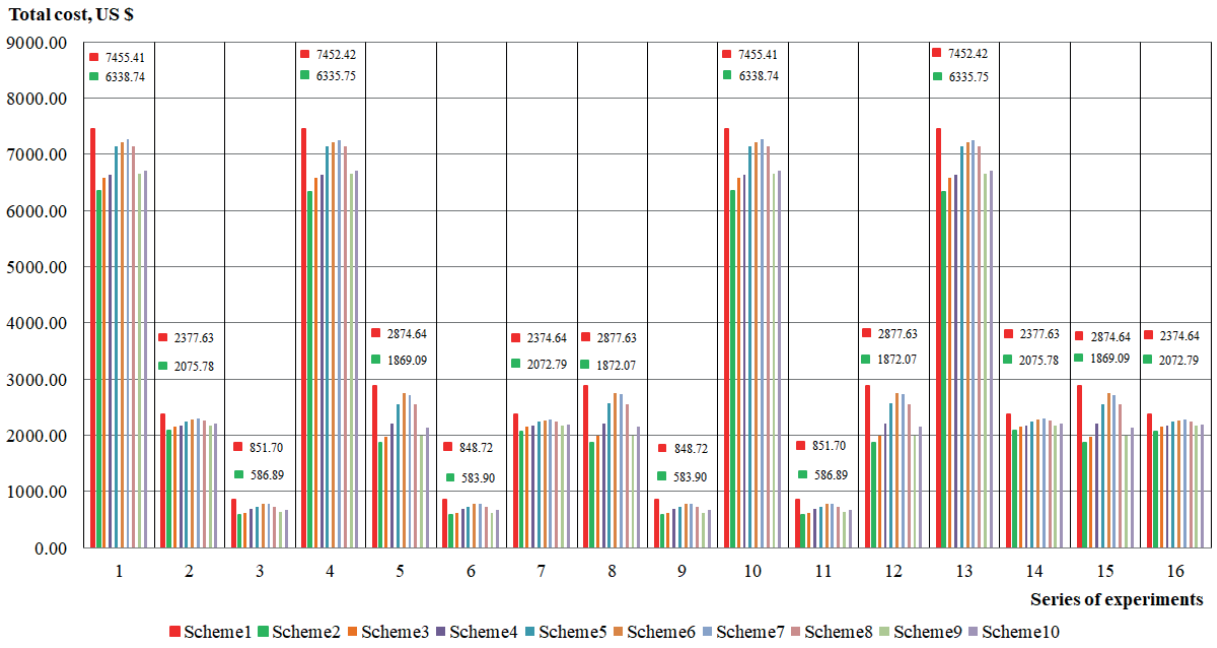

Figure 13 *Total costs for international container delivery according to a series of experiment planning experiments indicating the maximum and minimum costs of the developed transport order schemes*

where m - the number of the corresponding order service scheme, a_0, a_1, a_2 - unknown coefficients of the regression equation L_{trans}, Q_{ord}. Results of determining the coefficients of regression (13) have been presented in Table 4. According to the mathematical model for the ten service schemes, the calculated values of expenditure have been calculated and are presented in the form of a graph in Figure 13.

With implementation of the container delivery company "Inter Trans Logistic", order service company "Agricultural Holding August" for the transportation of rape seeds, 10 tons of corn on demand and a portion of sunflower oil is 20,000 liters, according to the applications have been systematized in Table 1. From the analysis of the graphic representation of the total cost of international container delivery of the goods of the customer firm (Figure 13), it follows that the maximum costs will be according to the scheme of order maintenance. In this case, the costs have been in the range of 848.72 to 7455.41 US $, according to a certain series of experiments. Proceeding from condition (2) and analysis of the data presented in Figure 13, scheme 1 has been selected for the marginal order maintenance service, concerning which the estimation of change of general expenses at realization of other schemes has been carried out. In percentage display according to Scheme 1, the following intervals have been received: reduction of expenses for the implementation of the order: scheme 2 - 12.70 to 34.98%; Scheme 3 - 2.93 to 12.00%; Scheme 4 - 2.06 to 10.88%; Scheme 5 - 1.69 to 4.25%; Scheme 6 - 0.87 to 3.28%; scheme 7 - 0.97 to 2.58%; Scheme 8 - 1.64 to 4.45%; Scheme 9 - 2.66 to 11.77%; scheme 10 - 2.33 to 9.94%

Results of experimental studies indicate that when the proposed methodology of the logistic approach, using the "white box", to international container transportation of goods in relation to the application for transportation, the scheme 2 sequence of transport operations has been effective. In its realization, the costs have been decreased for 12.70 to 34.98% in comparison to the marginal service scheme 1.

In the future it is planned to build based on the obtained results an imitation model based on the developed methodology and models in the environment of Petri Networks taking into account the risk factors at each stage of the process of the container delivery of goods in international traffic.

5. Conclusions

- It has been revealed that the proposed method of logistic approach to the container transportation system, based on the cybernetic model of the "white box" allows to take into account in more detail, form the possibilities of the transport and logistics enterprise in relation to the order and effectively choose the order of the service maintenance with the minimum expenses for carrying out transportation.

- Using the logistic approach to the container transport system, based on the cybernetic model of the "white box", based on the company "Inter Trans Logistic", serving the order of the company "Agricultural Holding August" for the transportation of packaged rape seeds, 10 tons of corn on demand and part of 20,000 liters of sunflower seeds oil, according to applications, maximum expenses 848.72 to 7455.41 US $ have been received according to scheme 1 of service of this order.
- Results analysis of experimental studies of changes in costs during the transportation, at the request of the firm "Agricultural Holding August", indicates that an efficient scheme of transport operations has been Scheme 2, because at the same time costs of 12.70 to 34.98% have been reduced in comparison with the limit scheme 1 of the transport order service by the company "Inter Trans Logistic".

References

[1] SKOROBOGATOVA, O., KUZMINA-MERLINO, I. Transport infrastructure development performance. *Procedia Engineering* [online]. 2017, **178**, p. 319-329. ISSN 1877-7058. Available from: https://doi.org/10.1016/j.proeng.2017.01.056

[2] LORD, J. D. Retail saturation: Inevitable or irrelevant? *Urban Geography* [online]. 2000, **21**(4), p. 342-360. ISSN 0272-3638/eISSN 1938-2847. Available from: https://doi.org/10.2747/0272-3638.21.4.342

[3] WANG, T., CULLINANE, K. The efficiency of European container terminals and implications for supply chain management. In: *Haralambides H.E. (eds) Port Management* [online]. London: Palgrave Readers in Economics, Palgrave Macmillan, 2015, p. 253-272. ISBN 978-1-137-47576-3/e ISBN 978-1-137-47577-0. Available from: https://doi.org/10.1057/9781137475770_12

[4] RYZHENKOVA, N.: Containers market overview in Ukrainian ports in the first half of 2017. Ports of Ukraine [online]. [Viewed 2017-09-25]. Available from: https://ports.com.ua/articles/obzor-rynka-konteynerov-v-portakh-ukrainy-v-i-polugodii-2017

[5] LIU, H. B., et al. A study on operational model of container multi-modal transport virtual enterprise based on multi-agent technology. *Advanced Materials Research* [online]. 2015, **1065-1069**, p. 3310-3313. ISSN 1662-8985/eISSN 1662-8985. Available from: https://doi.org/10.4028/www.scientific.net/AMR.1065-1069.3310

[6] LI, B., WU, C. W., CAO, J. X. The integrated optimization of container port logistics system resources. *Applied Mechanics and Materials* [online]. 2014, **505-506**, p. 878-883. ISSN 1662-7482/eISSN 1662-7482. Available from: https://doi.org/10.4028/www.scientific.net/AMM.505-506.878

[7] QIAN, X. W. The application of SLP with Hungarian method in the spatial layout planning of logistics park-with Chengdu international railway container logistics park as an example. *Advanced Materials Research* [online]. 2014, **838-841**, 1273-1280. ISSN 1662-8985/eISSN 1662-8985. Available from: https://doi.org/10.4028/www.scientific.net/AMR.838-841.1273

[8] CHOU, C. C., et al. Operation management of port logistics in the global supply chain. *Advanced Materials Research* [online]. 2013, **706-708**, p. 2087-2090. ISSN 1662-8985/eISSN 1662-8985. Available from: https://doi.org/10.4028/www.scientific.net/AMR.706-708.2087

[9] XU, C. X., JIANG, M. M., WANG, Z. Y. Contrast research on containers collecting and distributing system of Guangzhou port and Dalian port. *Applied Mechanics and Materials* [online]. 2012, **209-2011**, p. 667-670. ISSN 1662-7482/eISSN 1662-7482. Available from: https://doi.org/10.4028/www.scientific.net/AMM.209-211.667

[10] ZHANG, X., SONG LIN, J., ZHAO, Z. Study of container transport planning model and algorithm. *Advanced Materials Research* [online]. 2013, **605-607**, p. 570-573. ISSN 1662-8985/eISSN 1662-8985. Available from: https://doi.org/10.4028/www.scientific.net/AMR.605-607.570

[11] RUSGIYARTO, F., et al. Discrete event simulation model for external yard choice of import container terminal in a port buffer area. In 3rd International Conference on Engineering, Technology and Industrial Application : proceedings [online]. Vol. 1855(1), AIP Publishing, 2017. ISBN 978-0-7354-1529-4, p. 040014-1-040014-8. Available from: https://doi.org/10.1063/1.4985510

[12] ZHONG, W. Z., FU, X. Q., WANG, Y. P. Petri Net modeling: Container terminal production operation processing system analysis. *Applied Mechanics and Materials* [online]. 2013, **409-410**, p. 1320-1324. ISSN 1662-7482/eISSN 1662-7482. Available from: https://doi.org/10.4028/www.scientific.net/AMM.409-410.1320

[13] VADVARI, T., VARLAKI, P. Identification of supply chains based on input-output data. *Periodica Polytechnica Transportation Engineering* [online]. 2015, **43**(3), p. 162-167. ISSN 0303-7800/eISSN 1587-3811. Available from: https://doi.org/10.3311/PPtr.7931

[14] PAVLENKO, O., VELYKODNYI, D. The choice of rational technology of delivery of grain cargoes in the containers in the international traffic. *International Journal for Traffic and Transport Engineering* [online]. 2017, **7**(2), p. 164-176. ISSN 2217-544X/eISSN 2217-5652. Available from: https://doi.org/10.7708/ijtte.2017.7(2).02

[15] CARLO, H., VIS, I., JANROODBERGEN, K.: Storage yard operations in container terminals: Literature overview, trends, and research directions. *European Journal of Operational Research* [online]. 2014, **235**(2), p. 412-430. ISSN 0377-2217. Available from: https://doi.org/10.1016/j.ejor.2013.10.054

[16] AULIN, V., HOLUB, D. Regulatory and legal support transport systems functioning reliability in Ukraine. Journal of Zhytomyr State Technological University. Technical Sciences Series. 2016, **2**(77), p. 28-35. ISSN 1728-4260/eISSN 2522-1779.

[17] AULIN, V., et al. Substantiation of diagnostic parameters for determining the technical condition of transmission assemblies in trucks. *Eastern European Journal of Enterprise Technologies* [online]. 2018, **2**(1), p. 4-13. ISSN 1729-3774/eISSN 1729-4061. Available from: https://doi.org/10.15587/1729-4061.2018.125349

[18] NOJIRI, W., KANEKO, J., FUJIWARA, T. Long-distance Transportation of automotive parts by third-party logistics providers from the viewpoint of spatial organization of just-in-time systems. *Geographical Review of Japan* [online]. 2012, **85**(1), p. 1-21. ISSN 1883-4388/eISSN 2185-1751. Available from: https://doi.org/10.4157/grj.85.1

[19] ISO/IEC/IEEE 24765:2017 Systems and software engineering - Vocabulary [online]. Available from: https://www.iso.org/standard/50518.html

[20] SEO, S. - H., et al. A security framework for a drone delivery service. In 2nd Workshop on Micro Aerial Vehicle Networks, Systems and Applications for Civilian Use Dro Net 16 : proceedings [online]. New York, NY, USA, ACM, 2016. ISBN 978-1-4503-4405-0, p. 29-34. Available from: https://doi.org/10.1145/2935620.2935629

[21] PETRASKA, A., et al. The algorithm for the assessment of heavyweight and oversize cargo transport routes. *Journal of Business Economics and Management* [online]. 2017, **18**(6), p. 1098-1114. ISSN 1611-1699/eISSN 2029-4433. Available from: https://doi.org/10.3846/16111699.2017.1334229

[22] GAJEWSKA, T., ZIMON, D. Study of the logistics factors that Influence the development of e-commerce services in the customer's opinion. *Archives of Transport* [online]. 2018, **45**(1), p. 25-34. ISSN 0866-9546/e-ISSN 2300-8830. Available from: https://doi.org/10.5604/01.3001.0012.0939

[23] AGBELIE, B. R. D. K. An empirical analysis of three econometric frameworks for evaluating economic impacts of transportation infrastructure expenditures across countries. *Transport Policy* [online]. 2014, **35**, p. 304-310. ISSN 0967-070X. Available from: https://doi.org/10.1016/j.tranpol.2014.06.009

[24] ALGHAFFARI, S., NGUYEN, H., CHEN, P. Critical factors for organisational effectiveness: The case of Saudi Arabian seaports. *Journal of Sustainable Development of Transport and Logistics* [online]. 2018, **3**(2), p. 49-65. eISSN 2520-2979. Available from: https://doi.org/10.14254/jsdtl.2018.3-2.3

[25] AULIN, V., et al. Studying truck transmission oils using the method of thermal-oxidative stability during vehicle operation. *Eastern-European Journal of Enterprise Technologies* [online]. 2019, **1**(6)(97), p. 6-12. ISSN 1729-3774/eISSN 1729-4061. Available from: https://doi.org/10.15587/1729-4061.2019.156150

[26] KRYVORUCHKO, O., SHYNKARENKO, V., POPOVA, N. Quality management of transport services: Concept, system approach, models of implementation. *International Journal of Engineering and Technology (UAE)* [online]. 2018, **7**(4.3), p. 472-476. eISSN 2227-524X. Available from: https://www.scopus.com/inward/record.uri?eid=2-s2.0-85056727889&partnerID=40&md5=bd246aa071591c2 e9699888b3 d9bbd03

Jiri Cejka - Martin Telecky*

INFLUENCE OF ECONOMIC AND POLITICAL FACTORS ON THE PUBLIC RAIL TRANSPORT

The goal of the paper is to assess the territorial development in terms of the public rail transport in conditions of the Czech Republic or, more precisely, in the south of Bohemia. The capacity utilisation of the railway line No. 190 in the direction from Ceske Budejovice to the target station of Strakonice is analysed and the suitable deployment of the set of wagons, intended to be used in providing the basic transport services in the low-populated areas, is evaluated. The paper is concerned with the current situation in utilising the capacities on the railway line No. 190 with respect to the future utilisation of the railway links that will be affected by economic factors in the form of the reduced fare for students and pensioners. To this end, the mathematical and statistical methods, which will pre-define the suitability of the choice of capacities of the set of wagons in providing the basic transport services, will be applied.

Keywords: *public tramsport, the railway links, territory development, expected mean value*

1. Introduction

Principles of the territorial development define the spatial planning documentation for the whole regional territory, while refining and developing the objectives and tasks of the spatial planning in accordance with the territorial development policy. The strategies for achieving these goals are being determined and the planning activities of individual municipalities or towns are being coordinated, [1].

The essential part of the territorial development is to submit the future plans for the construction of a new railway corridor and restoration of other railway lines which will intersect the chosen regions and have a significant influence on building other partial structures. The economic and political factors directly affect future decision-making and have an influence on the investment matters in the process of creating and establishing the living standard of individual citizens, [2-4].

The issue of the low-populated areas is currently being analysed from the viewpoint of providing the transport services by means of the public line transport and the public rail transport. The goal is to interconnect individual modes of transport in order to provide a sufficient transport capacity by means of individual linksinr the current economic, political and living conditions. The preferences of citizens (consumers, passengers) mostly provide, in the form of questionnaires, complaints or other forms of information, the suggestions, which become the subject of the decision making on investments and the future changes in the territorial development. The public transport, as a competitor to a private motor vehicles transport, is being addressed most frequently. The goal is to reduce the volume of the private motor vehicle transport and to support the public line and rail transports due to their environmental friendliness and the related financial savings of citizens, [5].

The economic situation in the Czech Republic has been positive in recent two years. The investment opportunities in the form of building the transport infrastructure (roads, railways, etc.) are on the rise. The economic development and the general life satisfaction increase, [6-8].

Citizens prefer innovation in the quality of the rendered public transport services. They require more frequent providing of the basic transport services in the low-populated areas in more frequent time intervals. The reason is also the problem of an insufficient number of parking places for passenger cars, especially in bigger towns. In Spain, for instance, the high-speed railway corridors are being built and developed to save the passengers´s time and to reduce the mental costs. [9-11].

The paper also deals with the issue of the public rail transport as the offering of the transport services with the expected number of the railway links and the transport capacity being provided.

The mathematical and statistical methods, which evaluate the suitability of the choice of variants being considered in the decision-making under risk in the public rail transport have been applied within the data analysis. The data are taken from the carrier´s internal database. The chosen methods serve for identifying the key factors that are adapted to the issue in question. The analyses have been made for the railway line No. 190, which has provided the current results and expectations for the future volume of passengers travelling in the Ceske Budejovice - Strakonice section[1]. The data contain the number of passengers transported within providing the basic transport services on working days in the low-populated areas per a specific period of time (July 2018).

The following two basic approaches have been chosen in the decision-making under risk:

- Rule of the expected mean value,
- Rule of the expected mean value and variance.

In determining the subjective probabilities allocated to individual random phenomena, the relative size method was chosen. This method works on the principle of the limited number

1 by RegioPanter 650, Locomotive 240+Bdt+BDs

* **Jiri Cejka, Martin Telecky**
Institute of Technology and Business in Ceske Budejovice, Czech Republic
E-mail: cejka@mail.vstecb.cz

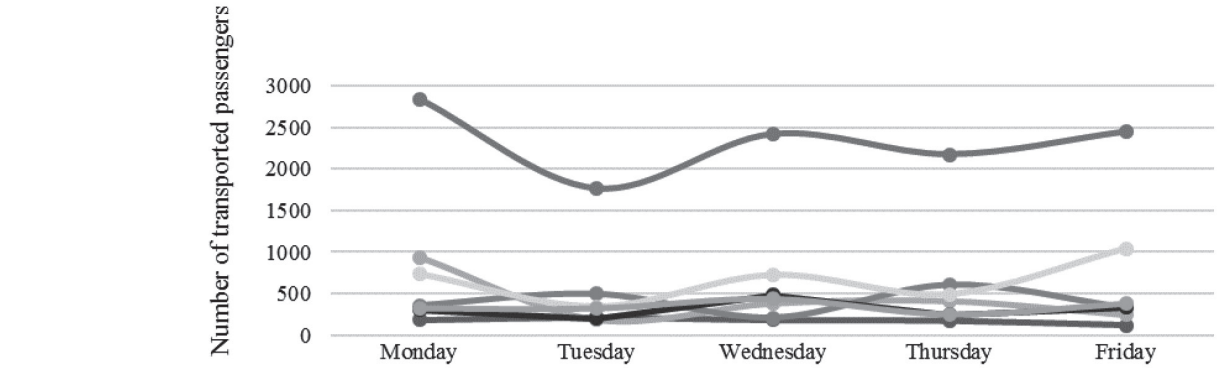

	Monday	Tuesday	Wednesday	Thursday	Friday
04:55 - 06:00	182	215	182	173	116
06:16 - 07:22	937	187	382	410	245
07:30 - 08:35	357	499	207	611	330
10:18 - 11:20	306	197	482	240	332
12:18 - 13:20	732	340	718	489	1037
14:30 - 15:32	322	323	442	248	383
Total number of passengers transported	2836	1761	2413	2171	2443

Figure 1 *Evaluation of individual railway links on the railway line No. 190 (Ceske Budejovice - Strakonice)*

Table 1 *Capacity utilisation and number of passengers transported on the railway line No. 190*

Time of railway link	Monday	Tuesday	Wednesday	Thursday	Friday	Number of passengers transported as per railway links
04:55 AM - 06:00 PM	182	215	182	173	116	868
06:16 AM - 07:22 AM	937	187	382	410	245	2161
07:30 AM - 08:35 AM	357	499	207	611	330	2004
10:18 AM - 11:20 AM	306	197	482	240	332	1557
12:18 PM - 13:20 PM	732	340	718	489	1037	3316
14:30 PM - 15:32 PM	322	323	442	248	383	1718
Total number of passengers transported	2836	1761	2413	2171	2443	
	The highest volume of passengers transported on a working day					

of random phenomena on condition that individual probabilities of random phenomena equal to one, as follows

$$probability = p_1 + p_2 + p_3 + \cdots + p_n = 1 \quad (1)$$

The rule of the expected mean value E(x) is determined according to the following formula:

$$expected\ mean\ value = \sum_{i=1}^{n} xi * pi \quad (2)$$

If the maximizing criterion applies to the entering table, the variant containing the greatest value will be optimal. In case of the minimizing criterion, on the other hand, the variant with the lowest value is taken into account.

The rule of the expected mean value and variance D(x) is determined according to the following formula:

$$variance = \sum_{i=1}^{n} [xi - E(x)]^2 * pi \quad (3)$$

The variant is chosen based on the lowest variance value [12-13].

The input data and the calculation are shown in the results.

2. Results

The data provided by Ceske drahy, a.s. for the South Bohemian Region have been analysed.

Table 2 *Expected number of transported passengers after the application of the decision-making theory method of risk*

Choice of a suitable capacity/ expected number of passengers transported within 1 working day by means of 6 railway links	Maximizing criterion				
	1000	1500	2000	2500	3000
150 (900)	-21150	-21150	-21150	-21150	-21150
200 (1200)	-18540	-9720	-9720	-9720	-9720
250 (1500)	-20340	1710	1710	1710	1710
300 (1800)	-22140	-90	13140	13140	13140
350 (2100)	-23940	-1890	20160	24570	24570
400 (2400)	-25740	-3690	18360	36000	36000
450 (2700)	-27540	-5490	16560	38610	47430
Probability of a random phenomenon	0.6	0.2	0.1	0.05	0.05

Table 3 *Results of the method of expected mean value and variance*

Rule of the expected mean value	EX		
150 (900)	-21150		
200 (1200)	-15012		
250 (1500)	-11520		
300 (1800)	-10674		
350 (2100)	-10269	Appropriate to deploy the InterPanter with five wagons	
400 (2400)	-10746		
450 (2700)	-11664		
Rule of the expected mean value and variance	Variance	Standard deviation	
150 (900)	0	0	Appropriate to deploy RegioPanter
200 (1200)	18670176	4320.89991	
250 (1500)	116688600	10802.2498	
300 (1800)	214707024	14652.8845	
350 (2100)	340147269	18443.0819	
400 (2400)	448084224	21168	
450 (2700)	539490294	23226.9304	

Figure 1 shows the average numbers of passengers transported in July 2018 on working days by means of six railway links. Railway links on the railway line No. 190 represent the complete offering of passenger trains. Fast trains and express trains, which do not serve the low-populated areas, were not included. The above Table shows individual railway links and the number of passengers transported by them in selected time intervals, as well as the total evaluation.

Overall, Monday is the busiest working day with a total number of 2836 passengers. The busiest railway link on working days is the train departing from Ceske Budejovice at 12:18 and arriving at Strakonice at 13:20, see Table 1.

In July 2018, the average number of transported passengers was 11624. Monday was the busiest working day. Taken in an ascending order, the order is as follows: Monday, Friday, Wednesday, Thursday and Tuesday.

The government and the Ministry of Transport of the Czech Republic have decided on the grant of discounts for students and the persons above 65 years of age. The above groups of passengers will pay 25 % of the fare only. The remaining 75 % will be compensated to the carriers from public budgets (of the state, municipalities or towns/cities). The prerequisite for the grant of discounts for students is that the students must hold a valid ISIC card (full-time study) and the passengers below 15 must be holders of the pupil´s ID card. The decision on the grant of discounts became effective in September 2018. Table 2 assumes the random phenomena (number of passengers in certain values), options of the set of wagons deployment as per the provided capacities and stating of subjective probabilities for individual random phenomena based on of the relative size method. The random phenomenon (1000 passengers) becomes the most probable consideration with a probability of 60 %.

The following data upon which the entering table will be set are under consideration. Considering the following structure of passengers:

a) 60 % students (pupils) and passengers above 65, who pays 25 % of the fare,
b) 10 % passengers - reduced fare - 25 %,
b) 10 % passengers - reduced fare - 50%,
d) 20 % passengers paying the full fare.

Structure of sales from passengers transported on the railway line No. 190 (Ceske Budejovice - Strakonice):

a) Students (full-time study) and pupils, pensioners: CZK 23[2],
b) Passengers entitled to a reduced fare (25 %): CZK 70,
b) Passengers entitled to a reduced fare (50 %): CZK 47,
d) Passengers paying the full fare: CZK 93.

Based on the economically substantiated costs, the costs per one travelled kilometre, in the case of passenger trains, are as follows as per the type of the set of wagons deployed and the allowable capacity:

1) Capacity of 150 places: CZK 169 per train-kilometre
2) Capacity of 200 places: CZK 174 per train-kilometre
3) Capacity of 250 places: CZK 179 per train-kilometre
4) Capacity of 300 places: CZK 184 per train-kilometre
5) Capacity of 350 places: CZK 189 per train-kilometre
6) Capacity of 400 places: CZK 194 per train-kilometre
7) Capacity of 450 places: CZK 199 per train-kilometre.

The total number of travelled train-kilometres according to the timetable amounts to 60 train-kilometres. The total capacity of 6 railway links is set. The train (wagon) turnover is not considered. All values have been taken from the primary reports on costs and sales from transport operations in the public rail transport.

The Table 3 inputs contain the negative values. This is why the revenues from passenger transport fail to sufficiently cover the operating costs of selected railway links. If the rule of the expected mean value is applied, the variants will have negative values. It means that the economic result is expected to be always negative and not positive. From the loss minimization viewpoint, it is appropriate to choose the variant of the set of wagons with a capacity of 350 passengers within one railway link. With 6 railway links deployed, the total capacity is 2100 passengers.

The rule of the expected mean value and variance reviews the appropriate variant based on the assumption of remote distances from the expected mean value. The lowest value will represent the most advantageous variant. In this case, it is appropriate to choose the first variant, i.e. the deployment of the set of wagons with a capacity of 150 passengers within one railway link.

2 Exchange rate 1 EUR = 25.778 CZK (Czech National Bank)

3. Conclusion

Economically substantiated costs are always higher than the price of (revenue from) the fare in the South Bohemian Region. The reason is the lower number of transported passengers and the preference of the private motor vehicles transport. The public rail transport is, as a rule, in the red. The economic result is negative (loss). For the future providing of the basic transport services by the public rail transport, it is necessary to compensate the loss with the financial means from public budgets. This implies that the economically substantiated costs are compensated (to zero) and the carrier will continue to obtain the compensation or an adequate profit, which is stipulated in the public service contract. The data have been analysed for the period of July 2018 when the students and the persons above 65 were not granted a discount of 75 % off the regular fare. The results show that a total number of passengers transported by means of the six railway links on the line No. 190 (Ceske Budejovice - Strakonice) amounted to 11624. The number of passengers is expected to considerably increase when the carrier offers a reduced fare (75 %). The goal is to prefer the public transport over the private motor vehicles transport. The carriers strive to serve the low-populated areas, while innovating the provided services and coordinating the railway network. The results point to the possibilities of selection of chosen variants, which may be expected after applying the mathematical and statistical rules (approaches).

Another problematic area is the reduction of the value added tax rate (VAT) on fares, effective since February 2019. The VAT is the main source of income for funding the public transport. In the last months, the passengers were still paying the first reduced rate of VAT, i.e. 15 %. The Senate of the Czech Republic strives for the VAT rate reduction to 10 % of the fare within the amendment of the VAT Act. This will result in the further monetary outflow, i.e. the lack of income going into public budgets. The paper contains the assumptions of the considered changes, which will become the basis for drawing-up the next publication.

Acknowledgement

This specialised paper is drawn-up within the RUMOBIL project.

References

[1] MAIER, K., et al. *Sustainable development of territory* (in Czech). 1. ed. Prague: Grada Publishing, 2012. ISBN 978-80-247-4198-7.
[2] PROVAZNIKOVA, R. *Financing of towns, municipalities and regions* (in Czech). 3.ed. Prague: Grada Publishing, 2015. ISBN 978-80-247-5608-0.
[3] PEKOVA, J., KADERABKOVA, J. *Local government - sustainable development and finance* (in Czech). Prague: Wolterskluwer, 2012. ISBN 978-80-735-7910-4.
[4] MAJEROVA, V., KOSTELECKY, T., SYKORA, L. *Social capital and development of the region* (in Czech). 1. ed. Prague: Grada Publishing, 2011. ISBN 978-80-4093-5.
[5] BAGIORVA, A. P., NOTMAN, O. V., VERESS, J. Methods of integrated assessment of megalopolis's micro-districts on the basis of residents' opinions. *Economy of region* [online]. 2017, **4**(4), p. 1138-1150. ISSN 2072-6414. Available from: https://doi.org/10.17059/2017-4-13
[6] TELECKY, M., CEJKA, J. *Implementation of value-creating processes and financial management in transport practice* (in Czech). 1. ed. Brno: CERM Academic Publishing house, 2018. ISBN 978-80-7204-975-2.

[7] TELECKY, M. *Factors affecting financial health of public transport companies from the viewpoint of accounting, financing and other disciplines* (in Czech). 1.ed. Ceske Budejovice: Faculty of Economics of the University of South Bohemia, 2016. ISBN 978-80-7394-630-2.

[8] KAMPF, R., et al. The application of ABC analysis to inventories in the automatic industry utilizing the cost saving effect. *Nase More* [online]. 2016, **63**(3), p. 120-125. ISSN 0469-6255/eISSN 1848-6320. Available from: https://doi.org/ 10.17818/NM/2016/SI8

[9] MOTA, C., LOPEZ, M. A., MARTINEZ-RODRIGO, A. A mathematical study of accessibility and cohesion degree in high-speed rail station connected to an urban bus transport network. *Open Physics* [online]. 2017, **15**(1), p. 160-174. ISSN 2391-5471. Available from: https://doi.org/10.1515/phys-2017-0017

[10] DELAPLACE, M., DOBRUSZKES, F. Editorial: Thinking beyond the cost-benefit analysis: The wider impact of high-speed rail on local development. *Belgeo* [online]. 2016, **3**. ISSN 13772368. Available from: http://journals.openedition.org/belgeo/18166

[11] KAMPF, R., ZEMAN, K., BENES, P. The determination of the optimal variant of public bus line transport vehicles in the daily circulation. *Nase More* [online]. 2015, **62**(3), p. 119-125. ISSN 0469-6255/eISSN 1848-6320. Available from: https://doi.org/10.17818/NM/2015/SI6

[12] DOSTAL, P., RAIS, K., SOJKA, Z. *Advanced methods of managerial decision-making* (in Czech). 1. ed. Prague: Grada Publishing, 2005. ISBN 978-80-247-1338-1.

[13] FOTR, J., SOUCEK, I. *Investment decision-making and project management* (in Czech). 1. ed. Prague: GradaPublishing, 2011. ISBN 978-80-247-3293-0.

Jindrich Cyrus - David Krcmarik - Reza Moezzi - Jan Koci - Michal Petru*

HOLOLENS USED FOR PRECISE POSITION TRACKING OF THE THIRD PARTY DEVICES - AUTONOMOUS VEHICLES

A completely new area of HoloLens usage is proposed. The Hololens is an augmented reality device, which provides the high precision location information. Such an information is normally used to accurately position holograms within the real space with respect to the viewer (user of HoloLens). The information is precise enough to use it for reporting the position for the purpose of autonomous driving. Several experiments have been executed in vast areas (20 m x 40 m) in order to find out the potential error coming from vibrations or other effects when moving the HoloLens. The results show that the technology can be used for spaces, which are previously known by the system - pre-scan of the space is needed. The big advantage of the system is its readiness for indoor positioning applications with no additional infrastructure needed, simultaneous localization and mapping, complex space mapping and reached precision. The disadvantage is mainly the costs.

Keywords: *position tracking, Microsoft HoloLens, infrastructure-less*

1. Introduction

The precise position tracking is an important thing on the way to the so-called Industry 4.0. The device, which is being operated autonomously, needs to know its current position and according to required trajectory adjust its movement. Positioning is a hot topic outdoors and indoors. Outdoors positioning relies mainly on the built infrastructure of satellite belts around Earth - Glonass, Beido, GPS or Galileo. The precision of the GPS, with cooperation of other global positioning systems, can achieve the order of tens of millimeters [1]. The trend of combining the multiple systems in order to enhance accuracy of positioning information is an interesting concept, especially in urban areas [2]. The demand for precise positioning is mainly due to the expansion of autonomous vehicle control into real life. The precise outdoor and indoor positioning requires very often some kind of infrastructure (external referencing systems). In the outdoor case, that is mainly global positioning system, mobile network [3] or other built speciality proprietary infrastructure [4]. Such systems are susceptible to failures due to unavailability of the required infrastructure [5].

As a result, there is a demand to solve the precise positioning for various purposes without any additional infrastructure [6]. This demand is accented especially for indoor position tracking. There is a huge potential of autonomous vehicle control in well-known spaces for tedious manipulation. One can name a few examples: transportation of medical material within hospitals [7] or paper manipulation in data centers [8]. In [7] a powerlink interface for a fast data transmission was used. The Pathfinder used front and rear lidar and special software available from GitHub for the precision position tracking.

The LIDARs (light detection and ranging) are often used as a part for autonomous SLAM (simultaneous localization and mapping) [9]. The LIDARs costs can be as small as 100$ and hence readily employable for even low cost small autonomous vehicles - Figure 1.

Disadvantage of the LIDARs can be the fact that the devices scan the environment usually only in one plane and they can have problems with glass obstacles (imagine e.g. glass doors) [10]. The LIDARs, when correctly used with appropriate software for the SLAM task, provide reliable information on the current position with the high level of accuracy typically in the range of millimeters (defined as a mean error distance between the estimated location and the real location) [11].

An interesting device, for very precise position tracking using the depth camera, is Intel RealSence D435 - Figure 2. The measuring depth reaches as far as 10 m. In [12] it was used even for the health treatment outcome (gait analysis and facial tracking).

There are other proposed ways how to accurately, to a certain level, track the position using some kind of small infrastructure - RFID [13], RSSI [14].

A promising technology for position tracking is utilization of the ultra-wide band (UWB) localization. One of the best working devices is SEWIO [15]. As reported, since it is a relatively new system, the accuracy and tag's battery life has to be further improved. The UWB technology needs a grid of anchors, whose proper placement is crucial for obtaining good positioning results [16]. The worst scenario for the UWB localization systems is a narrow corridor. The estimated position of the robot from the UWB system is fluctuating in the order of tens of centimeters [16]. Remedy to this can be a denser anchor grid. Nevertheless, the needed infrastructure is relatively easy to implement.

2. Autonomous AR-based position tracking

For this project of autonomous transport vehicle, an easy-to-deploy and ready-to-use system was sought, which would not need

* **Jindrich Cyrus, David Krcmarik, Reza Moezzi, Jan Koci, Michal Petru**
Technical University of Liberec, Czech Republic
E-mail: jindrich.cyrus@tul.cz

Figure 1 *LIDAR DF-DFR0315*

Figure 2 *Intel RealSence D435*

Figure 3 *Microsoft HoloLens head-mounted kit - user tracking corridor*

any additional infrastructure. Based on the above search for up-to-date used technologies was decided to examine another SLAM device, which was to the best of authors' knowledge, not yet used.

In the past, some SLAM methodologies were proposed and implemented on autonomous robot, such as LSD-SLAM, REMODE, ORB-SLAM. Their differences can be distinguished based on the type of method, which ORB and REMODE use the feature-based, but LSD-SLAM implements direct method. The ORB and LSD visualization are built-in, while the REMODE utilizes ROS/R Vis feature. The REMODE has no camera trajectory module, but ORB and LSD SLAM do have [17].

The Microsoft HoloLens, Figure 3, which is direct based, has built-in visualization and no camera trajectory module; is a head-mounted device used to project augmented reality (AR) into the users' field of view. The HoloLens is an optical see-through device with many sensors - gyroscope, magnetometer and accelerometer. It also includes the positional tracking subsystems - depth camera with 120° x 120° FOV (field of view) and four grayscale cameras. Nowadays, the big limitation of the HoloLens is its cost (thousands of USD) and from the user point of view very disturbing small field of view 30°H and 17.5°V. It is used for many purposes ranging from educational deployments to easy robot manipulation programming [18].

The HoloLens has a database of environments in which the device was operated. If a new environment is presented it is added to the database list. The HoloLens possesses a unique algorithm, which is based on the depth camera and four grayscale cameras with cooperation from other sensors (gyroscope, accelerometer). The device is constantly monitoring its neighborhood as far as 5 meters away from its cameras. It uses a proprietary correlation algorithm to find the actual position based on the data coming from various sensors.

In this project, the focus was on an autonomous vehicle control in known environment. As already previously stated such a scenario is widely implementable for many real world usages. Hence, one can scan the environment in which the vehicle is moving using the HoloLens. A special program in Unity and Microsoft Visual Studio was created and loaded into the HoloLens. The program was taking system generated location information from the HoloLens and sending it to a Ubuntu based server where a Node-RED server was installed.

A simple code, generating actual position string, is added to the Main Camera object within the Unity scene. This GameObject is moving with the move of the glasses.

A string was created, which is composed of position (x, y, z) and rotation (a, b, c) information. This string is sent both to glasses (in order the user to see his actual position) and also to server via the UDP.

For sending information, a UDP packet was preferred since it is a simple connectionless protocol without any handshaking. There was no need for any guarantee of delivery, ordering or protection, since the packets are sent with high frequency and hence few packets loss is not crucial.

In the code, the SendUDPMessage method was used from the UDPCommunication class, which is defined to be available for no Unity environments - hence the statement "#if !UNITY_EDITOR". When the code is loaded to HoloLens all the code within pragmas "#if !UNITY_EDITOR" is processed.

The UDPCommunication class is all in the "#if !UNITY_EDITOR" statement, since this functionality is not supported in the Unity (but it is supported in HoloLens). For sending an async and threading principles are used. A helper function for memory stream was used, as well.

The messages are sent to a convenient server where the Node-RED is installed. In a simple flow, it was possible to parse the received data and send it immediately to a MSSQL database. The Node-RED interface (Figure 4) was chosen for easy implementation ability and availability of immediate responses to certain not valid data obtained from the UDP messages. Moreover, it enables easily debugging of the whole application.

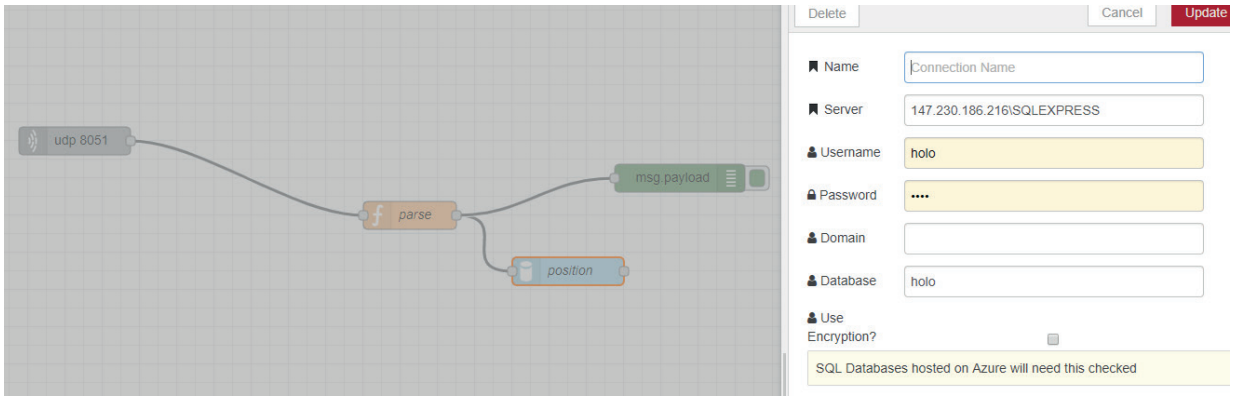

Figure 4 *The Node-RED interface for sending data to database*

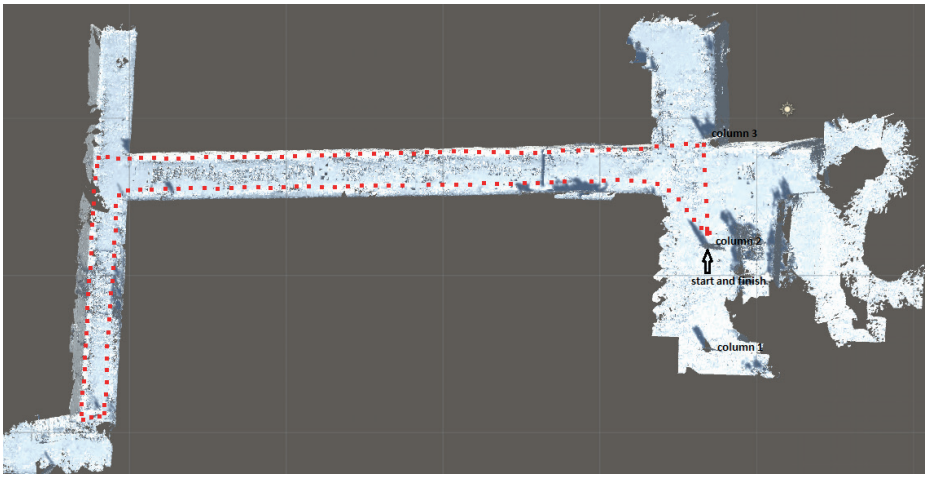

Figure 5 *Autonomous vehicle movement along the designated path - red dots real measurements, distance in x direction is 38 m and distance in y direction is 13.5 m from the origin at the column*

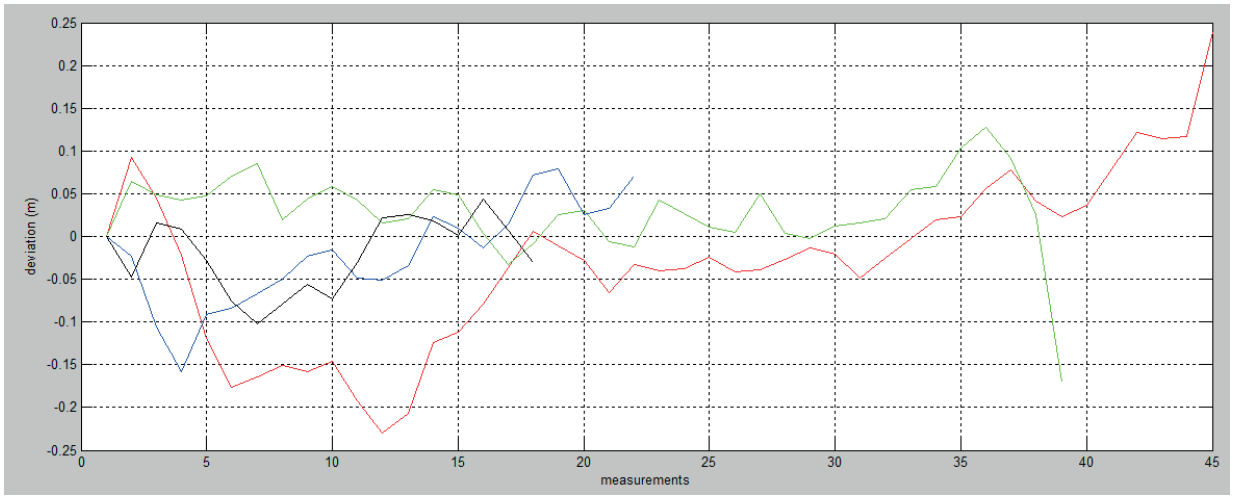

Figure 6 *Deviation of reported position by the HoloLens with respect to the real position; red and green - horizontal movement, blue and black - vertical movement*

3. Tests

The preciseness of position determination was tested. On the testing polygon in vestibule of Institute for Nanomaterials, Advanced Technologies and Innovation, Liberec a sufficiently big space (roughly 50 x 30 m) was at disposition for testing autonomous vehicles. The polygon is shown in Figure 5. The application was started when leaning on the middle column (start of red dots - column 2) and looking directly to the uppermost column (column 3). In such a way it was certain that the coordinate system is positioned well. The vestibule and the connecting corridors were prior scanned also with the help of the HoloLens. It was tried to move the vehicle close to the walls of the corridors in order to evaluate the measured position. As visible from Figure 6 the positions are quite precise following the walls of the corridor.

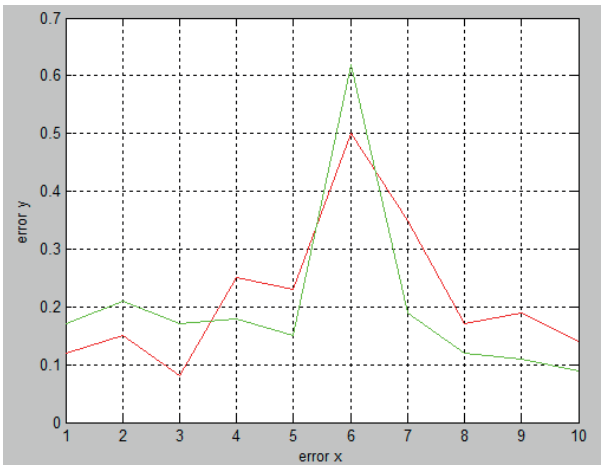

Figure 7 *Errors in position location at the start/finish column (green x direction, red y direction)*

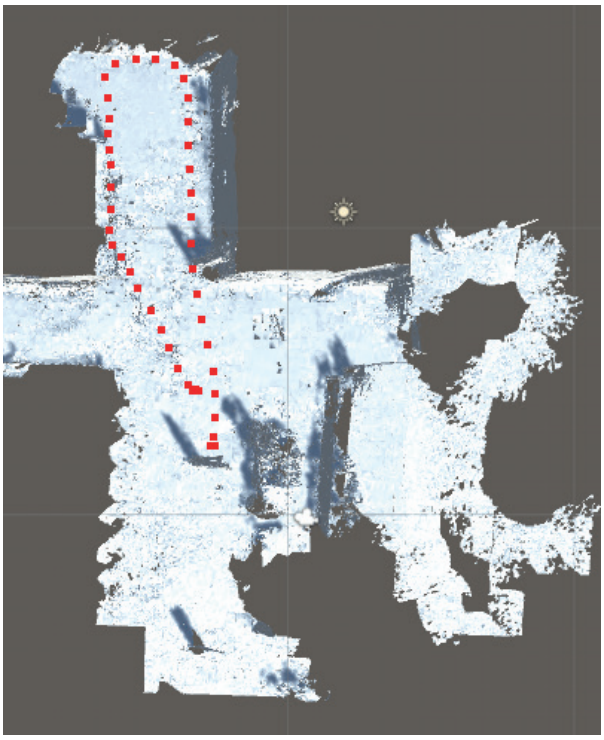

Figure 8 *Autonomous vehicle movement trajectory in "free space"*

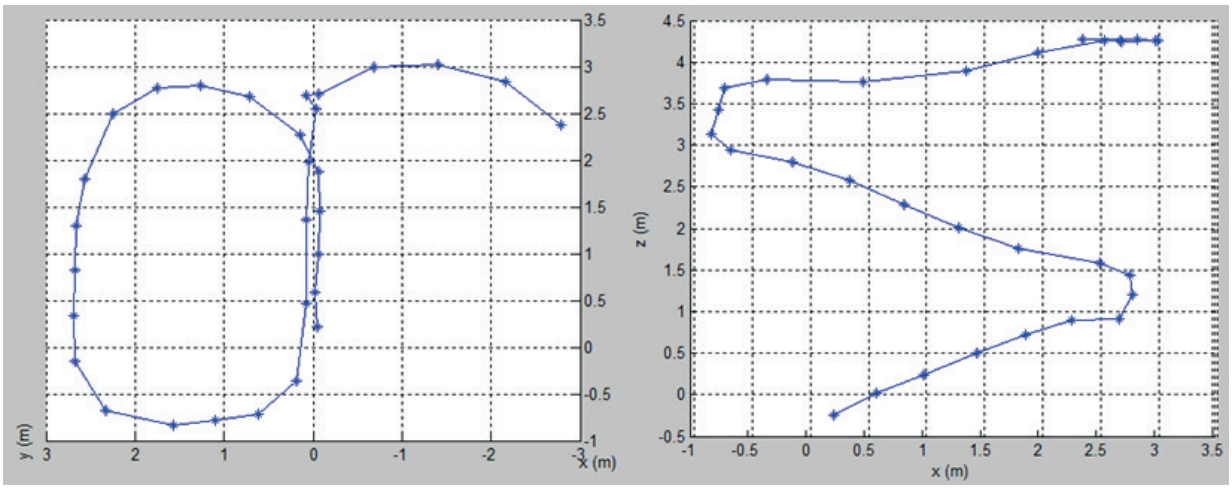

Figure 9 *Left - ground plan projection of moving on the staircase, right - vertical projection*

In these tests the focus was on movement within corridors. As stated in [16] such a setup is challenging for precise position monitoring for the UWB based positioning devices. The corridor was 2.5 m wide. Compared to the results from [16] the better deviations from the real movement were achieved. The movement was a simple inline movement along the walls. Figure 6 shows similar results of maximum deviation not exceeding approximatelly ± 20 cm from the projected trajectory. Red and green lines are measurements when the vehicle was moving along the „horizontal" long corridor and blue and black lines are measurements when moving along the „vertical" short corridor - see Figure 5.

The measurements were repeated many times. The trajectory was starting always at one of the columns (column 2 from Figure 5) and finishing at the same place. The error was measured as an absolute value of the difference of x and y position coordinates between the start and finish. Ideally it should be 0. The results are shown in Figure 7.

In Figure 7 an abnormal peak in error measurement between start/finish for measurement number 6 is visible. It was no clear what has caused it. It could be some excessive vibration during the movent of the vehicle.

The measurement in the free space - vestibule, was continued. The vehicle was moving again along the walls in order to be able to compare measured positions with the real ones. The trajectory is visible in Figure 8. The position error was up to ± 28 cm in x and y axes.

The potential of monitoring the elevation of autonomous vehicle was further tested. One can imagine the use in the case as when the vehicle is driving to elevated areas for freight loading. In this case, the HoloLens only mounted on the head when moving on the staircase was used. The results are shown in Figure 9 as

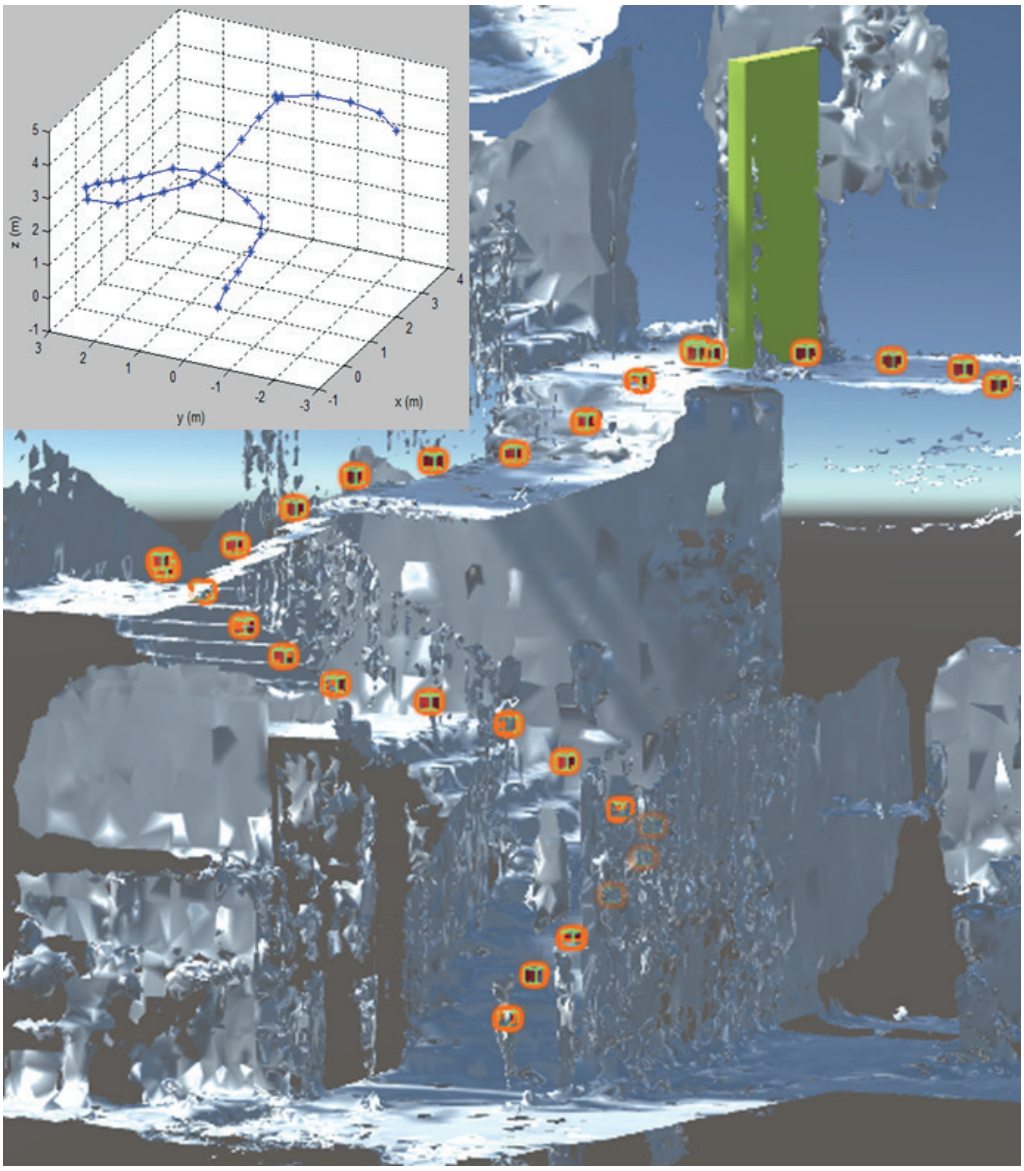

Figure 10 *Measured points when moving along the staircase; detail the points depicted in the graph*

x-y and x-z rectangular projections. The 3D trajectory is clearly visible. The measured and real elevations were compared and the fluctuations were no more than 32 cm - Figure 10.

Several tests were performed in order to find out the feasibility of using the HoloLens for position tracking. This approach was used in order to construct an autonomous vehicle with the new concepts of controlling. The next task will be a design of a system for controlling more vehicles in one area. The idea is to develop an industrial autonomous vehicle and for such cases cooperation of several units is a necessity [19]. It is perceived that proposed solution can be in these days costly but a strong decline in the price is anticioated as the AR platform spread accross.

4. Conclusion

The achieved experiment showed feasibility of the HoloLens for easy and readily available position tracking. A program for the HoloLens was presented. The program is reporting the current position of HoloLens. The position data is stored into MSSQL database. A third party device (e.g. web browser) is depicting the data onto the real map of the space. It was even tried to monitor the posible precise location in the 3D space - the staircase use case. The precision of position tracking was evaluated and the results show precision up to 30 cm. Important thing about the proposed system is its infrastructure-less functioning.

Acknowledgement

This result was obtained through the financial support of the Ministry of Education, Youth and Sports of the Czech Republic and the European Union (European Structural and Investment Funds - Operational Programme Research, Development and Education) in the frames of the project “Modular platform for autonomous chassis of specialized electric vehicles for freight and equipment transportation”, Reg. No. CZ.02.1.01/0.0/0.0/16 _025/0007293.

References

[1] GUO, J., LI, X., LI, Z., HU, L., YANG, G., ZHAO, CH., FAIRBAIRN, D., WATSON, D., GE. M. Multi-GNSS precise point positioning for precise agriculture. *Precision Agriculture* [online]. 2018, **19**(5), p. 895-911. ISSN 1385-2256, eISSN 1573-1618. Available from: https://doi.org/10.1007/s11119-018-9563-8

[2] LI, T., ZHANG, H., GAO, Z., CHEN, Q., NIU, X. High-accuracy positioning in urban environments using single-frequency multi-GNSS RTK/MEMS-IMU integration. *Remote sensing* [online]. 2018, **10**(2), p. 205-225. ISSN 2072-4292. Available from: https://doi.org/10.3390/rs10020205

[3] PEREZ-DIAZ-DE-CERIO, D., HERNANDEZ-SOLANA, A., VALDOVINOS, A., VALENZUELA, J. L. A low-cost tracking system for running race applications based on Bluetooth low energy technology. *Sensors* [online]. 2018, **18**(3), p. 922-937. ISSN 1424-8220. Available from: https://doi.org/10.3390/s18030922

[4] NIAZI, A. U., CHIN, K. J., JIN, R., CHAN, V. W. Real-time ultrasound-guided spinal anesthesia using the SonixGPS ultrasound guidance system: a feasibility study. *Acta Anaesthesiologica Scandinavica* [online]. 2014, **58**(7), p. 875-881. ISSN 0001-5172, eISSN 1399-6576. Available from: https://doi.org/10.1111/aas.12353

[5] NERI, A., FILIP, A., RISPOLI, F., VEGNI, A. M. An analytical evaluation for hazardous failure rate in a satellite-based train positioning system with reference to the ERTMS train control systems. 25th International Technical Meeting of the Satellite-Division of the Institute-of-Navigation : proceedings. 2012, p. 204-235.

[6] CHEN, L.-W., CHOU, P.-C. BIG-CCA: Beacon-less, infrastructure-less, and GPS-less cooperative collision avoidance based on vehicular sensor networks. *IEEE Transactions on Systems, Man, Cybernetics: Systems* [online]. 2016, **46**(11), p. 1518-1528. ISSN 2168-2216, eISSN 2168-2232. Available from: https://doi.org/10.1109/TSMC.2015.2504040

[7] BACIK, J., DUROVSKY, F., BIROS, M., KYSLAN, K., PERDUKOVA, D., PADMANABAN, S. Pathfinder-development of automated guided vehicle for hospital logistics. *IEEE Access* [online]. 2017, **5**, p. 26892-26900. ISSN 2169-3536. Available from: https://doi.org/10.1109/ACCESS.2017.2767899

[8] BLOKDYK, G.: *Autonomous logistics*. 3. ed., CreateSpace Independent Publishing Platform: South Carolina, US, 2018, p. 86-110. ISBN 978-1985683686.

[9] GRISETTI, G., KUMMERLE, R., STACHNISS, C., BURGARD, W. A tutorial on graph-based SLAM. *IEEE Intelligent Transportation Systems Magazine* [online]. 2010, **2**(4), p. 31-43. ISSN 1939-1390. Available from: https://doi.org/10.1109/MITS.2010.939925

[10] KIM, J., CHUNG, W. Robust localization of mobile robots considering reliability of LiDAR Measurements. IEEE International Conference on Robotics and Automation (ICRA) : proceedings [online]. 2018. eISSN 2577-087X, p. 1-19. Available from: https://doi.org/10.1109/ICRA.2018.8460648

[11] ASVADI, A., GARROTE, L., PREMEBIDA, C., PEIXOTO, P., NUNES, U. J. Multimodal vehicle detection: fusing 3D-LIDAR and color camera data. *Pattern Recognition Letters* [online]. 2018, **115**, p. 20-29. ISSN 0167-8655. Available from: https://doi.org/10.1016/j.patrec.2017.09.038

[12] SIENA, F. L., BYROM, B., WATTS, P., BREEDON, P. Utilising the Intel RealSense camera for measuring health outcomes in clinical research. *Journal of Medical Systems* [online]. 2018, **42**(3), p. 53-62. ISSN 0148-5598, eISSN 1573-689X. Available from: https://doi.org/10.1007/s10916-018-0905-x

[13] YANG, Q., TAYLOR, D. G., DURGIN, G. D. Kalman filter based localization and tracking estimation for HIMR RFID systems. IEEE International Conference on RFID : proceedings [online]. 2018. eISSN 2573-7635, p. 1-14. Available from: https://doi.org/10.1109/RFID.2018.8376199

[14] PENG, Y., NIU, X., TANG, J., MAO, D., QIAN, CH. Fast signals of opportunity fingerprint database maintenance with autonomous unmanned ground vehicle for indoor positioning. *Sensors*. 2018, **18**(10), p. 3419-3447. ISSN 1424-8220. Available from: https://doi.org/10.3390/s18103419

[15] CONTIGIANI, M., PIETRINI, R., MANCINI, A., ZINGARETTI, P. Implementation of a tracking system based on UWB technology in a retail environment. 12th IEEE/ASME International Conference on Mechatronic and Embedded Systems and Applications (MESA) : proceedings [online]. 2016, p. 15-61. Available from: https://doi.org/10.1109/MESA.2016.7587123

[16] CERNOHORSKY, J., JANDURA, P., RYDLO, P. Real time ultra-wideband localisation. 19th International Carpathian Control Conference (ICCC) : proceedings [online]. 2018. ISBN 978-1-5386-4762-2, p. 445-450. Available from: https://doi.org/10.1109/CarpathianCC.2018.8399671

[17] BUYVAL, A., AFANASYEF, I., MAGID, E. Comparative analysis of ROS-based monocular SLAM methods for indoor navigation. 9th International Conference on Machine Vision (ICMV) : proceedings [online]. 2016, 103411K. Available from: https://doi.org/10.1117/12.2268809

[18] NEVES, J., SERRARIO, D., PIRES, J. N. Application of mixed reality in robot manipulator programming. *Industrial Robot - The International Journal of Robotics Research and Application* [online]. 2018, **45**(6), p. 784-793. ISSN 0143-991X. Available from: https://doi.org/10.1108/IR-06-2018-0120

[19] XIDIAS, E., ZACHARIA, P., NEARCHOU, A. Path planning and scheduling for a fleet of autonomous vehicles. *Robotica* [online]. 2016, **34**(10), p. 2257-2273. ISSN 0263-5747, eISSN 1469-8668. Available from: https://doi.org/10.1017/S0263574714002872

Sergey Goolak - Juraj Gerlici - Viktor Tkachenko - Svitlana Sapronova - Tomas Lack - Kateryna Kravchenko*

DETERMINATION OF PARAMETERS OF ASYNCHRONOUS ELECTRIC MACHINES WITH ASYMMETRICAL WINDINGS OF ELECTRIC LOCOMOTIVES

This article is devoted to development of a method for calculating the parameters of an asynchronous motor of an electric locomotive with asymmetrical windings of stator and rotor. A method for determining self and mutual inductances of the stator and rotor phases of an asynchronous motor with asymmetric windings and their relations to mechanical variables is proposed. It is based on comparing two equations of stored magnetic energy, one equation calculated through induction, magnetic field strength and geometrical dimensions and another equation calculated through the parameters of the motor circuits. It is shown that the obtained solutions correspond to the previously existing methods, but they give the additional possibilities in mathematical modeling. The proposed technical solution allows higher accuracy developing of a mathematical model of a drive with an asynchronous motor having asymmetrical stator and rotor windings for studying dynamic processes during the operation of the specified drive, in particular, the drive of auxiliary machines for electric locomotive, where an asynchronous motor with asymmetrical stator windings is used as a phase release.

Keywords: *magnetic field induction, mutual inductance, self-inductance, magnetic field strength*

1. Introduction

The search for effective methods for obtaining a picture of dynamic processes in an electric drive with an asynchronous electric motor and the study of the operating modes of electric machines for specific technical applications require a reasonable choice of the most appropriate method for the given case of mathematical modeling of the indicated electric drives. Considering the possibility of building a mathematical model of an asynchronous electric machine, it is necessary to take into account that such a selection should assume the possibility of accounting a number of assumptions [1-7]. First, it shall be deemed that the system of voltage of the asynchronous motor is symmetrical and sinusoidal and the stator and rotor windings are symmetrical. It is also necessary to assume that the stator and the rotor of the asynchronous machine are smooth.

In this regard, one interesting circumstance should be noted. Although the actual supply voltage system is asymmetric and non-sinusoidal and stator and rotor windings of the asynchronous motor are not always symmetrical, the methods for asynchronous machines modeling, when the stator and the rotor windings are symmetrical and the power supply system is sinusoidal, are widely used. The works on the asynchronous machines modeling can be a proof of the same [8-13]. The mathematical models, obtained with the help of these methods, allow to investigate dynamic processes in electric drives with asynchronous motors and to study the operating modes of electric machines under the condition of symmetry of the stator and the rotor windings and with a high-quality power supply system of the electric machine. This is an evidence that the topic of researches devoted to the development of mathematical models of asynchronous motors with asymmetrical windings and with asymmetry and non-sinusoidal of the supply voltage system, as well as the development of methods for determining the parameters of an asynchronous motor applied in these models, is relevant.

2. Analysis of methods for determining the parameters of asynchronous motors

When building each of the models of an asynchronous motor analyzed in [1-13], its own system of motor parameters is required, and, respectively, its own method of determining these parameters.

Calculations of parameters using catalog and reference data of an asynchronous motor have a large inaccuracy and can only be used for the qualitative assessment of the energy, operating and mechanical characteristics of the motor [14]. The calculation of the parameters according to the results of the experiments is highly accurate and can be used to assess the energy efficiency of asynchronous motors, but with the time invariant parameters of asynchronous motors. With an asymmetrical non-sinusoidal power supply system, stator winding induction harmoniously depends on the angle between the phase currents of the stator and the rotor. This angle is variable in the conditions of a poor voltage supply system. This imposes certain restrictions on the use of the solutions proposed in [14]. The method of determining parameters with reference to a specific time interval is based on

* [1]Sergey Goolak, [2]Juraj Gerlici, [1]Viktor Tkachenko, [3]Svitlana Sapronova, [2]Tomas Lack, [2]Kateryna Kravchenko
[1]Department of Traction Rolling Stock, State University of Infrastructure and Technologies, Kyiv, Ukraine
[2]Department of Transport and Handling Machines, Faculty of Mechanical Engineering, University of Zilina, Slovak Republic
[3]Department of Carriages and Carriage Economy, State University of Infrastructure and Technologies, Kyiv, Ukraine
E-mail: goolak@duit.edu.ua

the processing and recording of available information about a motor such as phase currents and voltages [15]. It provides the ability to select the desired method of determining parameters with reference to time for a specific type of motor model. However, the following question remains, i.e. what parameters of an asynchronous motor can be determined having an information about phase currents and voltages, which is relevant for creating a mathematical model of an asynchronous motor under conditions of power supply from the system with a source of poor-quality electrical energy.

In [16], mathematical relations between the parameters of an asynchronous motor and its phase currents and voltages are given for a model of a generalized two-phase asynchronous machine for coordinates α - β, d - q. But the mathematical tool and the algorithm of its use for determining motor parameters are provided only conceptually. It has been mentioned above that the models in coordinates d - q and x - y are strictly connected to the field speed of the stator or rotor and can be used only in the case of powering the stator with only sinusoidal voltage.

In [17], the authors adapted the model of an asynchronous motor in coordinates d - q to a non-sinusoidal voltage supply by switching from the model in coordinates a, b, c to model in d - q by applying the Park's transformation. The transition to the model in a, b, c from model in coordinates d - q is carried out using the inverse Park's transformation. Model parameters are calculated using equivalent - T. The calculation of the parameters of an asynchronous motor for equivalent - T is given in [18], it does not take into account such phenomena as displacement of the rotor current, steel loss and magnetic circuit saturation. In the study [19], a method was developed for determining the parameters from the catalog data using an equivalent scheme for an asynchronous motor taking into account current displacement and capacity losses of steel, but the authors did not consider the phenomenon of saturation of the motor magnetic circuit. This problem is considered in [20], where reactivity is scrutinized as a function of the saturation level of the magnetic circuit.

The solutions obtained in [18-20] allow one to determine parameters of an asynchronous motor, but under the condition that its stator and rotor windings are symmetrical. The operation of an asynchronous motor with electric or magnetic asymmetry of the stator windings leads to an uneven distribution of losses in copper through the stator phases and the occurrence of variable components of the electromagnetic moment and power consumption [21].

The asymmetry of active resistances and inductances can be considered as their deviation from similar parameters when motor windings are symmetrical [22]. This algorithm will allow us to calculate and build a model of an asynchronous motor with asymmetry of windings. But the question regarding the calculation of parameters of asynchronous motors, which are powered from a single-phase power supply network, which is important for the class of asynchronous motors, used to break down a single-phase power supply system into a three-phase one, still remains open.

In [23] it was assumed that a single-phase motor for transforming parameters could be represented as an ideal transformer and the coefficient of voltage deviation from the symmetrical mode was replaced by the ratio of voltages. However, the mathematical tool and the algorithm of its application are given only conceptually in [23-24].

Determining the parameters of asynchronous motors in the specified modes powered by a single-phase network allows one to build a mathematical model to find the energy, mechanical and performance characteristics of this motor in the given mode with a great accuracy [25]. Due to asymmetry, not only transient processes, but also the established modes are dynamic, therefore, in any coordinate system, they are described by differential equations. To obtain static parameters as a function of a variable, this system is differentiated analytically, after which it is integrated numerically with respect to this variable. When performing differentiation, there may be a question of method convergence. In addition, this technique does not show the dependence of inductance on the geometrical dimensions of the corresponding windings, which is important when the windings of an asynchronous motor are asymmetrical.

When modeling the drive for auxiliary machines of electric locomotives of the series VL-80$^{T.K}$, the phase release, which is an asynchronous motor with a square-cage rotor powered by a single-phase network, can be replaced by a system of asymmetric voltage sources [26]. To set the asymmetry of voltage sources, vector diagrams of currents and voltages shall be built and the asymmetry parameters shall be determined using a vector diagram of voltages. For building of diagrams, it is necessary to know such parameters of a real asynchronous machine as the active resistances of the stator and rotor windings and the self and mutual inductances of these windings.

The proposed method for determining the phase and mutual inductances of an asynchronous motor can be applied during the modeling of dynamic processes of drives with asynchronous motors, which have asymmetrical stator and rotor windings and can be powered by poor quality power systems, in particular, to simulate dynamic processes for drive of auxiliary machines of electric locomotives of the VL-80$^{T.K}$ series.

3. Development of requirements for the magnetic structure and phase zones arrangement in a generalized model of an asynchronous motor

Consideration of electric machines in the article is based on the fundamental assumption that machines can be represented by linear circuit systems with lumped parameters that move relative to each other. Since the two elements of the electric machine (the stator is a fixed element, the rotor is a rotating element) are in relative motion, the question arises about the choice of a suitable coordinate system for recording the equations of motion. There is some freedom in choosing a coordinate system for studying any specific devices and a specific task and the desired form of equations of motion usually dictate this choice. The true coordinates shall be used when choosing the Lagrange function to record the equations of motion [27].

In practice, various methods of electric machines building are used, one of which is shown in Fig. 1 [28]. The considered machine consists of six groups of concentrated coils (one coil per group is shown), which are called phase zones. Three of these phase zones are located in the slots of the static magnetic system

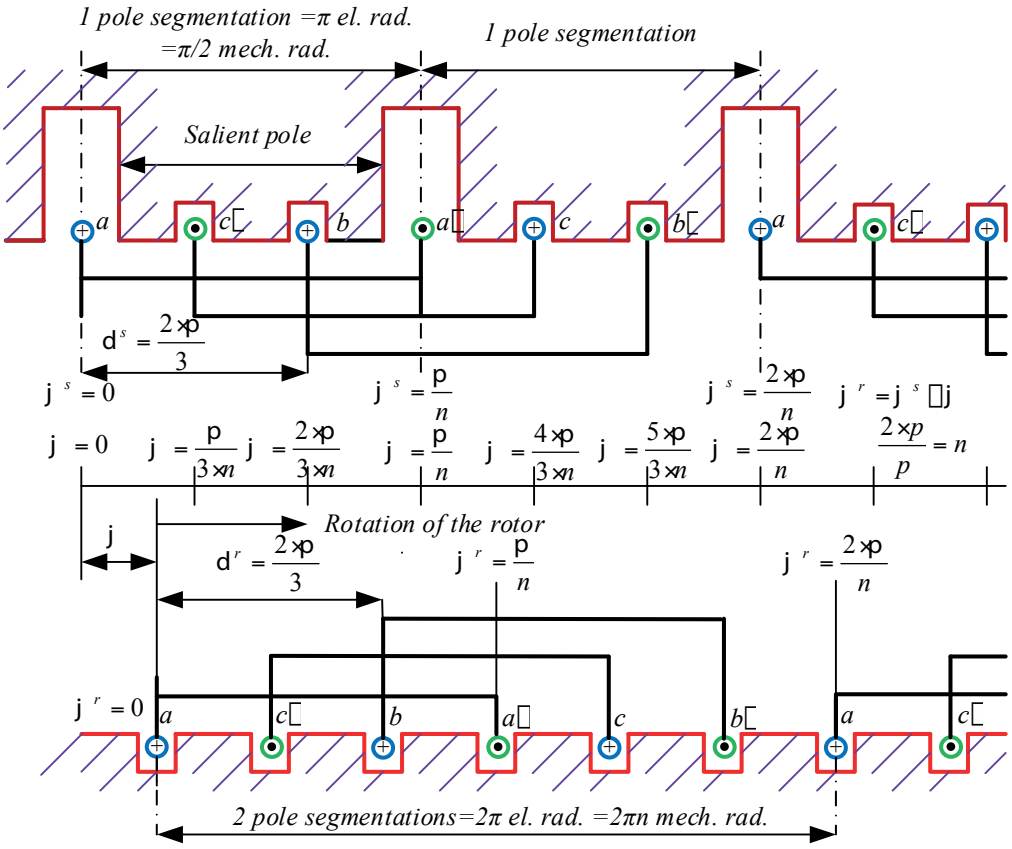

Figure 1 *The salient-pole machine having 3 axels and 2 p poles*

called the stator, the other three - in the slots of the magnetic system, which rotates are called the rotor. For the analyzing tasks, the boundaries of the magnetic system and the phase winding shown in Figure 1 as concentrated will be represented in the form of the continuous structure represented in Figure 2 [28]. Here, the phase zones are sinusoidally distributed main layers and the stator poles projections are shown by radial conductivity, which varies as a function of the angle. It is assumed that the magnetic structure and phase zones arrangement in the generalized physical model (Figure 2) should satisfy the conditions, the main of which are as follows [28]:

1. Electric spatial angle ϕ_{el} and mechanical spatial angle ϕ are related by the following expression:

$$\varphi_{el} = p \cdot \varphi = n \cdot \varphi \qquad (1)$$

where φ_{el} - angle in electrical spatial radians; φ - angle in mechanical spatial radians; p - the number of machine pole pairs; n - the number of periods of the spatial distribution of the current layer.

2. It is assumed that in the generalized model, the coils are sinusoidally distributed in space, so that the current i, connected to the clamps of the phase zone, creates a surface current density $K(\varphi) = i \cdot Z \cdot \cos n \cdot \varphi$, where $Z = w/l$ - the linear density of the conductor current layer, w - the number of turns of the winding, l - the length of the winding.
3. The phase zones of both the stator and the rotor are shifted in space by *120* electrical degrees, i.e. magnetic axes of the phase zones are shifted by $2\pi/3$ of electrical radians or by $2\pi/3n$ mechanical radians.
4. Stator-to-rotor gap is space between the magnetic systems of the stator and the rotor. It is assumed that one side of the stator-to-rotor gap is magnetically “smooth” and the other has magnetic irregularity (pole projections) periodically repeated through π of electrical spatial radians or through $\pi/2$ of mechanical radians.
5. When determining the strength in salient-pole machines, the stator-to-rotor gap will be uniform, which value is g and is equal to the average size of the stator-to-rotor gap for a salient-pole structure. The unevenness of the stator-to-rotor gap will be taken into account in the idealized model, using the radial magnetic inductivity, which is changing in space:

$$\mu_{rad} = \mu - \mu_2 \cdot \cos(2 \cdot \pi \cdot \varphi^8). \qquad (2)$$

6. Each of the three phase zones, located on the stator, has different number of turns. The rotor phase zones also have different numbers of turns.
7. The stored electrical energy, which is used to describe the machine, is considered only as a zero-order field energy or a static magnetic field energy. The energy of the electrostatic field is neglected, which allows ignoring the effect of capacitors inside the windings and between them. All the electric fields, created by a change in time of magnetic fields or relative motion in a magnetic field, are not included in the energy function describing the system. These electric fields

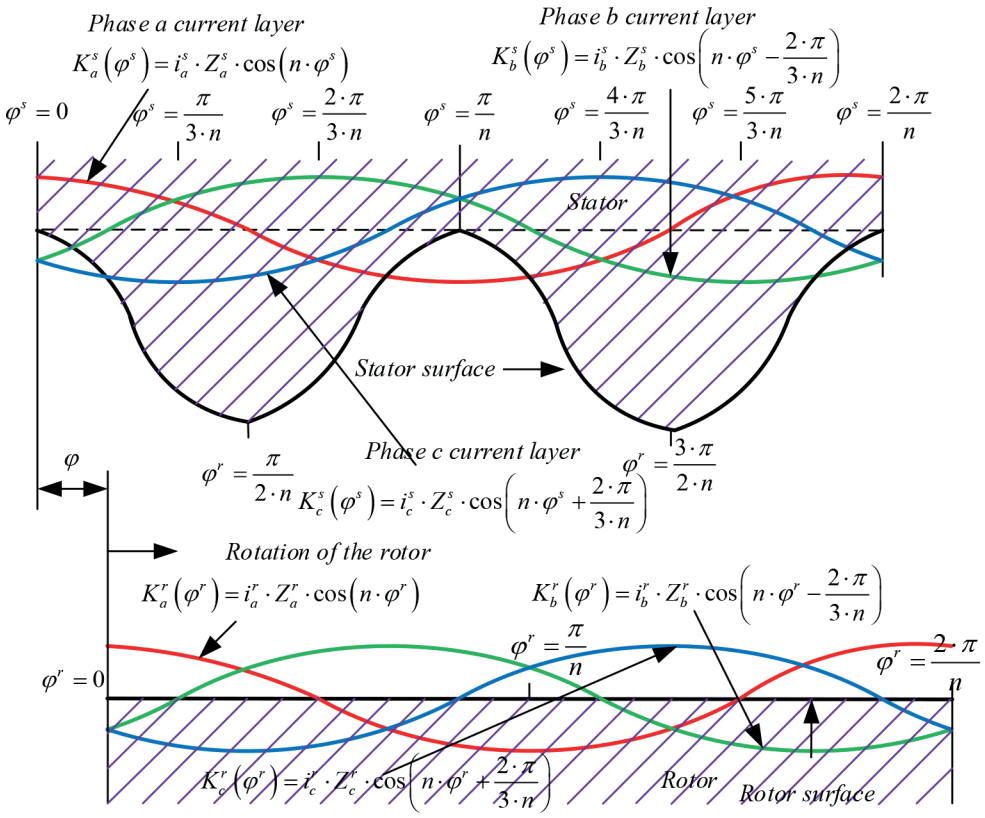

Figure 2 *Current layers created by sinusoidally distributed coils in a generalized machine*

occur when deriving the equations of motion from the energy function of the system written for the magnetic field energy.

4. Development of an algorithm for determining self and mutual inductances of stator and rotor

To determine the inductions of a generalized machine and their connections with mechanical variables, two equations of stored magnetic energy are used, namely, one through the magnetic induction B, the magnetic field strength H and dimensions: $W_m = \frac{1}{2} \cdot \int H \cdot B \cdot dv$ [29] and another one through chain parameters: $W_m = \frac{1}{2} \cdot \sum_i \sum_j L_{ij} \cdot i_i \cdot i_j$ with subsequent equating of these two equations.

The first step to calculate the machine inductance is calculation of the magnetic induction at all the points of the machine. Significant reserve of magnetic energy is only in the stator-to-rotor gap and the inductances can be calculated using the values B and H in the gap, which are obtained from the calculation of the machine static field pattern in accordance with clause 7. Only the influence of the magnetic field existing in the stator-to-rotor gap should be taken into account when considering a generalized machine. In this case, the generalized machine will be a model of a real machine, which reflects its properties related to the transformation of energy.

The presence of the salient-poles is taken into account by the fact that the magnetic inductivity is different at various points in space; therefore, the salient-poles will only affect the magnitude of the magnetic induction B [28]. The magnetic field strength H is found from the assumption of the salient-poles absence. The magnetic field strength H is determined for a system with a uniform stator-to-rotor gap, which is considered in cylindrical coordinates ρ, φ^s, z. At the same time, rotor surface radius is $\rho = r_s$, radial dimension of stator-to-rotor gap $g = r_s - r_r$ and axial length of stator-to-rotor gap l_β. Six current layers determine the six laws of distribution of the surface current density, i.e. three for the rotor and three for the stator. These surface currents flow in the axial direction *(z)*. In accordance with Figure 2 and taking into account the fact that when finding H, the surface of the stator bore is assumed to be smooth and six current layers create the following surface current densities.

Internal stator surface is *($\rho = r_s$)*:

$$k_a^s(\varphi^s) = a_z \cdot i_a^s \cdot Z_a^s \cdot \cos(n \cdot \varphi^s), \tag{3}$$

$$k_b^s(\varphi^s) = a_z \cdot i_b^s \cdot Z_b^s \cdot \cos n \cdot \left(\varphi^s \frac{2 \cdot \pi}{3 \cdot n}\right), \tag{4}$$

$$k_c^s(\varphi^s) = a_z \cdot i_c^s \cdot Z_c^s \cdot \cos n \cdot \left(\varphi^s \frac{2 \cdot \pi}{3 \cdot n}\right), \tag{5}$$

where Z_a^s, Z_b^s i Z_c^s are linear densities of conductors of the three stator current layers.

Similarly, the magnetic field strength on the rotor surface *($\rho = r_r$)* is determined with taking into account that $\varphi^r = \varphi^s - \varphi$.

Using the conclusion given in [16], the equation for finding the magnetic field strength of *a* phase can be written as follows:

$$H_a^s \approx -a_\rho \cdot \frac{r_r}{n \cdot g} \cdot i_a^s \cdot Z_a^s \cdot \sin(n \cdot \varphi^s). \quad (6)$$

The magnetic strengths for the other two phases of the stator and the three phases of the rotor are determined similarly.

The resulting field in the stator-to-rotor gap is found by adding:

$$H_\rho = H_a^s + H_b^s + H_c^s + H_a^r + H_b^r + H_c^r. \quad (7)$$

The equation for magnetic induction B is obtained from equation for H and the magnetic inductivity is taken as a variable. Then

$$B = a_\rho \cdot (\mu - \mu_2 \cdot \cos(2 \cdot n \cdot \varphi^s)) \cdot (H)_\rho, \quad (8)$$

where (H_ρ) is given in Equation (7).

Equations (7) and (8) can be used to determine the accumulated energy by the spatial integral over volume of the stator-to-rotor gap. The stator-to-rotor gap of an idealized model of a salient-pole machine corresponds to a change in the axial coordinate z from O to l_β, angle φ^s from 0 to 2π, coordinate ρ^r from 0 to g, moreover, g is the average value of the stator-to-rotor gap of a salient-pole machine.

Total energy in the stator-to-rotor gap is as follows:

$$W_m = \int_0^{l\beta}\int_0^{g}\int_0^{2\pi} \frac{1}{2} \cdot B \cdot H \cdot (r_r d\rho^r d\varphi^s dz) = \int_0^{l\beta}\int_0^{g}\int_0^{2\pi} \frac{1}{2} \cdot \cdot \left[(\mu - \mu_2 \cdot \cos(2 \cdot n \cdot \varphi^s)) \cdot (H)_\rho^2\right] \cdot (dz \cdot r_r d\rho^r \cdot d\varphi^s). \quad (9)$$

Substituting Equations (7) and (8) into Equation (9), the energy in the stator-to-rotor gap is determined by integration.

The accumulated energy, determined by Equation (9), can be equated to the stored energy expressed through the following circuit parameter:

$$W_m = \frac{1}{2} \cdot \sum_i \sum_j L_{ij} \cdot i_i \cdot i_j. \quad (10)$$

Adjusting Equations (9) and (10) and assuming that the mutual inductance L_{ij} shall be equal to L_{ji} in the assumption of a linear system, the following equations for inductance is obtained:

$$L_{aa}^{ss} = L_{aa\mu}^{ss} + L_{aa\mu_2}^{ss}, \quad (11)$$

$$L_{bb}^{ss} = L_{bb\mu}^{ss} + L_{bb\mu_2}^{ss} \cdot \cos\left(\frac{4 \cdot \pi}{3}\right), \quad (12)$$

$$L_{cc}^{ss} = L_{cc\mu}^{ss} + L_{cc\mu_2}^{ss} \cdot \cos\left(\frac{4 \cdot \pi}{3}\right), \quad (13)$$

$$L_{ab}^{ss} = L_{ba}^{ss} = (L_{ab\mu}^{ss} + L_{ab\mu_2}^{ss}) \cdot \cos\left(\frac{2 \cdot \pi}{3}\right), \quad (14)$$

$$L_{ac}^{ss} = L_{ca}^{ss} = (L_{ac\mu}^{ss} + L_{ac\mu_2}^{ss}) \cdot \cos\left(\frac{2 \cdot \pi}{3}\right), \quad (15)$$

$$L_{bc}^{ss} = L_{cb}^{ss} = L_{bc\mu}^{ss} \cdot \cos\left(\frac{4 \cdot \pi}{3}\right) + L_{bc\mu_2}^{ss}, \quad (16)$$

$$L_{aa}^{rr} = L_{aa\mu}^{rr} + L_{aa\mu_2}^{rr} \cdot \cos 2 \cdot n \cdot \varphi, \quad (17)$$

$$L_{bb}^{rr} = L_{bb\mu}^{rr} + L_{bb\mu_2}^{rr} \cdot \cos 2 \cdot n \cdot \left(\varphi + \frac{2 \cdot \pi}{3 \cdot n}\right), \quad (18)$$

$$L_{cc}^{rr} = L_{cc\mu}^{rr} + L_{cc\mu_2}^{rr} \cdot \cos 2 \cdot n \cdot \left(\varphi + \frac{2 \cdot \pi}{3 \cdot n}\right), \quad (19)$$

$$L_{ab}^{rr} = L_{ba}^{rr} = L_{ab\mu}^{rr} \cdot \cos\frac{2 \cdot \pi}{3} + L_{ab\mu_2}^{rr} \cdot \cdot \cos 2 \cdot n \cdot \left(\varphi + \frac{2 \cdot \pi}{3 \cdot n}\right), \quad (20)$$

$$L_{ac}^{rr} = L_{ca}^{rr} = L_{ac\mu}^{rr} \cdot \cos\frac{2 \cdot \pi}{3} + L_{ac\mu_2}^{rr} \cdot \cdot \cos 2 \cdot n \cdot \left(\varphi + \frac{2 \cdot \pi}{3 \cdot n}\right), \quad (21)$$

$$L_{bc}^{rr} = L_{cb}^{rr} = L_{bc\mu}^{rr} \cdot \cos\frac{4 \cdot \pi}{3} + L_{bc\mu_2}^{rr} \cdot \cos 2 \cdot n \cdot \varphi, \quad (22)$$

$$L_{aa}^{sr} = L_{aa}^{rs} = (L_{aa\mu}^{sr} + L_{aa\mu_2}^{sr}) \cdot \cos n \cdot \varphi, \quad (23)$$

$$L_{ab}^{sr} = L_{ba}^{rs} = (L_{ab\mu}^{sr} + L_{ab\mu_2}^{sr}) \cdot \cos n \cdot \left(\varphi + \frac{2 \cdot \pi}{3 \cdot n}\right), \quad (24)$$

$$L_{ac}^{sr} = L_{ca}^{rs} = L_{ac\mu}^{rs} \cdot \cos n \cdot \left(\varphi - \frac{2 \cdot \pi}{3 \cdot n}\right) + + L_{ac\mu_2}^{rs} \cdot \cos n \cdot \left(\varphi - \frac{2 \cdot \pi}{3 \cdot n}\right), \quad (25)$$

$$L_{ba}^{sr} = L_{ab}^{rs} = L_{ba\mu}^{rs} \cdot \cos n \cdot \left(\varphi - \frac{2 \cdot \pi}{3 \cdot n}\right) + + L_{ba\mu_2}^{rs} \cdot \cos n \cdot \left(\varphi - \frac{2 \cdot \pi}{3 \cdot n}\right), \quad (26)$$

$$L_{bb}^{sr} = L_{bb}^{rs} = L_{bb\mu}^{sr} \cdot \cos n \cdot \varphi + L_{bb\mu_2}^{sr} \cdot \cos n \cdot \left(\varphi - \frac{2 \cdot \pi}{3 \cdot n}\right), \quad (27)$$

$$L_{bc}^{sr} = L_{cb}^{rs} = L_{bc\mu}^{ss} \cdot \cos n \cdot \left(\varphi + \frac{2 \cdot \pi}{3 \cdot n}\right) + L_{bc\mu_2}^{ss} \cdot \cos n \cdot \varphi, \quad (28)$$

$$L_{ca}^{sr} = L_{ac}^{rs} = L_{ca\mu}^{sr} \cdot \cos n \cdot \left(\varphi + \frac{2 \cdot \pi}{3 \cdot n}\right) + + L_{ca\mu_2}^{sr} \cdot \cos n \cdot \left(\varphi - \frac{2 \cdot \pi}{3 \cdot n}\right), \quad (29)$$

$$L_{cb}^{sr} = L_{bc}^{rs} = \left(L_{bc\mu}^{sr} \cdot \cos n \cdot \left(\varphi - \frac{2 \cdot \pi}{3 \cdot n}\right) + L_{bc\mu_2}^{sr} \cdot \cos n \cdot \varphi\right), \quad (30)$$

$$L_{cc}^{sr} = L_{cc}^{rs} = L_{cc\mu}^{sr} \cdot \cos n \cdot \varphi + L_{cc\mu_2}^{sr} \cdot \cos n\left(\varphi + \frac{2 \cdot \pi}{3 \cdot n}\right), \quad (31)$$

Equations (11)-(31) determine all the self and mutual inductances with respect to six pairs of electrical terminals. The nature of these inductances is of the considerable interest. Inductances that have index $\mu(L_\mu^s, L_{\mu 2}^{sr})$ are functions of magnetic inductivity μ, while an index $\mu(L_{\mu_2}^s, L_{\mu_2}^{sr})$ correspond to inductances, which are functions of inductivity μ_2.

The method of expressing magnetic inductivity (8) allows one to conclude that all the terms with index μ will be present in equation for any machine with a uniform stator-to-rotor gap, while terms with index μ_2 will occur in the case of a salient-pole machine, that is, a machine with uneven stator-to-rotor gap. In equations for the non-salient-pole machine, all these terms will be equal to zero. Obviously, for a machine with a uniform stator-to-rotor l_β gap, all the self-inductances are constant and all the mutual inductances are cosine-shaped functions of the spatial angle $n \cdot \phi$ between the respective coils on the stator and the rotor. This kind of spatial change in mutual inductance can be expected when sinusoidally distributed coils rotate relative to each other. Terms appearing due to the presence of the salient poles are similar to terms included in the equations for the non-salient-pole machines, except for the rotor self- inductances. The

Table 1 *Comparison of the results of the calculation of inductance carried out by using the proposed method and data obtained experimentally*

ℓ	Parameter	Calculated	Experimental	Inaccuracy
1	Phase inductance of stator winding for phase A	0.242 mH	0.235 mH	-2.97%
2	Phase inductance of stator winding for phase B	0.694 mH	0.684 mH	-3.31%
3	Phase inductance of stator winding for phase C	0.822 mH	0.836 mH	1.67%
4	Phase inductance of rotor winding for phases A, B, C	0.076 mH	0.079 mH	3.95%
5	Mutual inductance	0.391 mH	0.39 mH	-2.56%

self-inductances of stator are constant and the mutual inductances of the stator and the rotor are changed in proportion to the cosine of the spatial angle $n{\cdot}\phi$. This follows from the fact that the rotor is magnetically smooth and, accordingly, the stator inductances should not depend on its position and the mutual inductances of the stator and rotor should be similar to those for machines with a uniform stator-to-rotor gap. The latter is a consequence of the energy conservation law, which leads to equality of mutual inductances. It is easy to see that the self inductance of the rotor due to the salient polarity is a function of the rotor position and varies according to the cosine law of the double electrical spatial angle $2{\cdot}n{\cdot}\phi$. This is a consequence of the fact that the angular coordinate of the full cycle of changes in the size of the stator-to-rotor gap is equal to half the phase zone. Thus, the change in the mechanical spatial angle ϕ to 2π corresponds to $2{\cdot}n$ cycles of change of the rotor induction due to the presence of salient poles at the stator.

Thus, inductances are shown as functions of an independent coordinate φ.

To verify the adequacy of the method, the phase and mutual inductances of the asynchronous motor NB-455A, which is used as a phase release on electric locomotives of VL-80^{T,K} series were calculated and compared to results obtained experimentally [13]. This motor has symmetrical rotor windings and asymmetrical stator windings. The results are listed in Table 1.

As can be seen from the Table 1, inaccuracy of inductance calculations does not exceed 5% of the data obtained experimentally. This indicates that the proposed method for determining the inductance of an asynchronous motor with a square-cage rotor having asymmetrical windings is adequate.

5. Conclusion

The problem of finding the phase and mutual inductances of an asynchronous motor with asymmetrical stator and rotor windings is considered in the article. The method for determining the phase and mutual inductances of asynchronous motor stator and rotor phases of asynchronous motor with asymmetric windings and their relations with mechanical parameters has been improved. The method is based on a comparison of the two equations of stored magnetic energy:

- the equation written through induction, magnetic field strength and geometrical dimensions;
- the equation written through the parameters of the motor circuits.

Comparison of results of an asynchronous motor parameters calculation to results obtained experimentally indicates a high accuracy of the proposed method.

References

[1] KUZNETSOV, V. V., NIKOLYENKO V. V. Models of operating asynchronous engines at poor-quality electricity (in Russian). *East European Advanced Technology Journal* [online]. 2015, **1**(8(73)), p. 37-42. ISSN 1729-3774/eISSN 1729-4061. Available from: https://doi.org/10.15587/1729-4061.2015.36755

[2] PUSTOVYETOV, M., SOLTUS, K., SENYAVSKIY. I. *Computer simulation of asynchronous motors and transformers. Examples of interaction with power electronic converters* (in Russian). Monograph. Saarbrucken, Deutshland, Lap Lambert Academic Publishing, 2013. ISBN 3659407763, 9783659407765.

[3] GERLICI, J., et al. Investigation of influence of separator magnetic system configuration with permanent magnets on magnetic field distribution in working area. *Electrical Engineering and Electromechanics* [online]. 2017, **2**, p. 13-17. ISSN 2074-272X. Available from: https://doi.org/10.20998/2074-272X.2017.2.02

[4] GERLICI, J., LACK, T., HARUSINEC, J. Realistic simulation of railway operation on the RAILBCOT test stand. *Applied Mechanics and Materials* [online]. 2014, **486**, p, 387-395. ISSN 1662-7482. Available from: https://doi.org/10.4028/www.scientific.net/AMM.486.387

[5] DIZO, J., STEISUNAS, S., BLATNICKY, M. Vibration analysis of a coach with the wheel-flat due to suspension parameters changes. *Procedia Engineering* [online]. 2017, **192**, p. 107-112. ISSN 1877-7058. Available from: https://doi.org/10.1016/j.proeng.2017.06.019

[6] SMETANKA, L., ST'ASTNIAK, P., HARUSINEC, J. Wear research of railway wheelset profile by using computer simulation. *MATEC Web of Conferences* [online]. 2018, **157**(2), 03017. ISSN 2261-236X. Available from: https://doi.org/ 10.1051/matecconf/201815703017

[7] GERLICI, J., et al. Assessment of innovative methods of the rolling stock brake system efficiency increasing. *Manufacturing Technology* [online]. 2018, **18**(1), p. 35-38. ISSN 1213-2489/ISBN 978-80-7414-325-0. Available from: https://arl.ujep.cz/arl-ujep/en/csg/?repo=ujeprepo&key=59578862639

[8] RUAN, J. Y., WANG. S. M. Magnetizing curve estimation of induction motors in single-phase magnetization mode considering differential inductance effect. *IEEE Transactions On Power Electronics* [online]. 2016, **31**(1), p. 497-506. ISSN 0885-8993/eISSN 1941-0107. Available from: https://doi.org/10.1109/TPEL.2015.2401835

[9] CHIONCE, C.P., et al. Vector control structure of an asynchronous motor at maximum torque. IOP Conference Series: Materials Science and Engineering : proceedings. Vol. 106(1). International Conference on Applied Sciences ICAS 2015, 012005.

[10] PAKKIRAIAH, B., SUKUMAR, G. D. A new modified artificial neural network based mppt controller for the improved performance of an asynchronous motor drive. *Indian Journal of Science and Technology* [online]. 2016, **9**(45), p. 1-10. ISSN 0974-6846/eISSN 0974-5645. Available from: https://doi.org/10.17485/ijst/2016/v9i45/105313

[11] GUO, Z., WEI ZHANG Q. The study on mathematical model and simulation of asynchronous motor considering iron loss. *Journal of Physics Conference Series* [online]. 2018, **1060**(1), p. 1-6. ISSN 1742-6588. Available from: https://doi.org/10.1088/1742-6596/1060/1/012085

[12] DEMENTYEV, Y. N., UMURZAKOVA A. D. The engine mechanical coordinates measuring in the asynchronous motor. *MATEC Web of Conferences* [online]. 2014, **19**, 01027. ISSN 2261-236X. Available from: https://doi.org/10.1051/matecconf/20141901027

[13] BALARA, D., et al. Neural networks application for mechanical parameters identification of asynchronous motor. *Neural Network World* [online]. 2017, **3**, p. 259-270. ISSN 1210-0552/eISSN 2336-4335. Available from: https://doi.org/10.14311/NNW.2017.27.013

[14] MUGALIMOV, R. G., HRAMSHIN, W. Y., MUGALIMOVA, A. R. Comparative analysis of the methods for calculating the parameters of electric circuits for the replacement of induction motors (in Russian). *Electrical Engineering: Network Electronic Scientific Journal*. 2016, **3**(1), p. 36-40. eISSN 2313-8742.

[15] TERYOHIN, A. A., DADYENKOV, D. A. An overview of how to identify the parameters of an asynchronous electric drive (in Russian). *Vesnik of the Perm National Research Polytechnic University. Electrical Engineering, Information Technology, Control Systems*. 2017, **2**, p. 55-66. ISSN 2224-9397/eISSN 2305-2767.

[16] GOOLAK, S. O., et al. Determination of dynamic variables of a generalized asynchronous motor (in Ukrainian). *Collection of scientific works of the State economic-technological university of transport. Series: Transport Systems and Technologies*. 2016, **29**, p. 143- 153.

[17] NIKOLAYEV, A. A., MUTALLAPOVA, F. F. Development of an improved block diagram of an asynchronous motor in the d-q coordinate system relative to the rotor without reference to the reference vector (in Russian). *Russian Internet Journal of Electrical Engineering* [online]. 2017, **4**(2), p. 3-12. ISSN 2313-8742. Available from: https://doi.org/10.24892/RIJEE/20170201

[18] EPSHTEIN, I. I. Calculation of parameters of the asynchronous motor. Energy saving (in Russian). *Energetics. Energy audit*. 2014, **8**(126). p. 57-61. ISSN 2218-1849/eISSN 2313-8890.

[19] SIVOKOBYLENKO, V. F., TKACHENKO, S. N., DERKAYOV, S.V. Determination of the parameters of equivalent circuits and characteristics of asynchronous motors (in Russian). *Electricity*. 2014, **10**, p. 38-44. ISSN 0013-5380/eISSN 2411-1333.

[20] LING, Z., et al. Equivalent circuit parameters calculation of induction motor by finite element analysis. *IEEE Transactions on Magnetics* [online]. 2014, **50**(2), p. 1-2. ISSN 0018-9464. Available from: https://doi.org/10.1109/TMAG.2013.2282185

[21] ZAGIRNYAK, M., et al. Correction of the operating modes of an induction motor with asymmetrical stator windings at vector control. International Conference on Electrical Drives and Power Electronics EDPE : proceedings [online]. 2015. p. 74-79. eISSN 1339-3944. Available from: https://doi.org/10.1109/EDPE.2015.7325303

[22] NGUYEN, V., et al. A Method for incipient interturn fault detection and severity estimation of induction motors under inherent asymmetry and voltage imbalance. *IEEE Transactions on Transportation Electrification* [online]. 2017, **3**(3), p. 703-715. eISSN 2332-7782. Available from: https://doi.org/10.1109/TTE.2017.2726351

[23] GHIAL, V. K., SAINI, L. M., SAINI, J. S. Parameter estimation of permanent-split capacitor-run single-phase induction motor using computed complex voltage ratio. *IEEE Transactions on Industrial Electronics* [online]. 2014, **61**(2), p. 682-692. ISSN 0278-0046/eISSN 1557-9948. Available from: https://doi.org/10.1109/TIE.2013.2253067

[24] TKACHENKO, V., at al. Research into resistance to the motion of railroad undercarriages related to directing the wheelsets by a rail track. *Eastern-European Journal of Enterprise Technologies* [online]. 2017, **5/7**(89), p. 65-72. ISSN 1729-3774/eISSN 1729-4061. Available from: https://doi.org/10.15587/1729-4061.2017.109791

[25] MALYAR, V. S., MALYAR, A. V. Steady-state modes and static characteristics of a three-phase asynchronous motor powered by a single-phase network (in Russian). *Energetics. News of Higher Educational Institutions and Energy Associations of the CIS*. 2016, **6**, p. 536-548. ISSN 1029-7448/eISSN 2414-0341.

[26] GOOLAK, S. O., YERMOLENKO, E. K. Development of a mathematical model for the investigation of the operation of supplementary machines of electric locomotives of series of VL-80$^{T.K.}$, working in not-sinusoidal and not-symmetrical modes (in Ukrainian). *Visnyk of the Volodymyr Dahl East-Ukrainian National University.* 2018, **2**(243), p. 80-92. ISSN 1998-7927.

[27] KESSLER, M., ANDRES, M., SCHMITT, T. Control and characteristic map generation of permanent magnet synchronous machines and induction machines with squirrel cage. 10th International Modelica Conference : proceedings [online]. Linkopings Iniversitet : Linkoping University Electronic Press, 2014. ISBN 978-91-7519-380-9, p. 1151-1160. Available from: https://doi.org/10.3384/ecp14096

[28] GOOLAK, S.: Methodological recommendations for the application of the model of physical processes in three-phase asynchronous motor (in Ukrainian). *Collection of scientific works of the State economic-technological university of transport. Series: Transport Systems and Technologies*. 2018, **1**(32), p. 4-13.

[29] MARTINEZ, J., BELAHCEN, A., ARKKIO A. 3D permeance model of induction machines taking into account saturation effects and its connection with stator current and shaft speed spectra. *IET Electric Power Applications* [online]. 2015, **9**(1), p. 20-29. ISSN 1751-8660. Available from: https://doi.org/10.1049/iet-epa.2014.0013

Daniel Kajanek - Branislav Hadzima - Matej Brezina - Martina Jackova*

EFFECT OF APPLIED CURRENT DENSITY OF PLASMA ELECTROLYTIC OXIDATION PROCESS ON CORROSION RESISTANCE OF AZ31 MAGNESIUM ALLOY

Impact of applied current density during the plasma electrolytic oxidation (PEO) process on corrosion resistance of AZ31 magnesium alloy was studied. The PEO coatings were prepared using four different current densities with values of 0.025 A/cm^2, 0.05 A/cm2, 0.1 A/cm^2 and 0.15 A/cm^2 in electrolyte consisting of 10 g/l Na_3PO_4.12H2O and 1 g/l KOH. Morphology and chemical composition of the coatings was examined using the scanning electron microscopy and EDS analysis respectively. Electrochemical characteristics of ground and coated samples were measured by means of electrochemical impedance spectroscopy (EIS) in 0.1 M NaCl solution. Obtained data in form of Nyquist diagrams were analysed by equivalent circuit method. Results of experiments showed that value of applied current density had significant effect on protective performance of the PEO coatings prepared on AZ31 magnesium alloy surface.

Keywords: *magnesium alloy, plasma electrolytic oxidation, corrosion resistance*

1. Introduction

The main reason, which impedes the wider usage of magnesium alloys in technical applications is their high reactivity and the resulting low corrosion resistance in most of the practical environments. The high rate of corrosion degradation is attributed to presence of inclusions in the structure of the Mg alloys which form microgalvanic cells and thus promote corrosion of the Mg matrix or grain boundaries. Particularly harmful elements are nickel, cobalt and iron. Another cause of insufficient corrosion resistance is the presence of a naturally created surface film based on $MgO/Mg(OH)_2$. The chemical composition of this film depends on the environment to which the alloy is exposed. According to the E-pH diagram, this film is stable only in strongly alkaline environments. In acidic and neutral conditions it does not provide adequate protection [1-3]. Nowadays, there are several well-known methods of protecting Mg alloys such as cathodic protection, platting and preparation of various coatings. The last category is one of the most evolving methods. The surface of the magnesium alloys can be modified in various ways depending on the desired final properties, with surface pre-treatment being very important as well. Frequently used surface treatment methods are cathodic electrodeposition techniques or anodic oxidation. A perspective technique called plasma electrolytic oxidation is getting a lot of scientific attention as it is a method for preparation of protective coatings on Mg alloy in a non-expensive way. In this process, unlike conventional anodic oxidation, much higher voltages are reached/applied and the obtained coatings have a ceramic-like character. The disadvantage is the porosity of these layers resulting from nature of the PEO process. The advantage of the PEO is that there is a variety of environmentally acceptable electrolytes and secondly it is also possible to use both DC and AC power sources. The preparation of such layers is relatively complicated in terms of the obtained coating properties as there is a number of variables in the PEO process such as the value of applied current/voltage, time of preparation, optimal composition of the electrolyte and the applied frequency in the case of alternating power sources. Those parameters have significant impact on the overall properties of the PEO layers [4-6]. This paper is focused on the effect of applied current density on the morphology and chemical composition of prepared layers and on corrosion protective function in an aggressive chloride containing environment.

2. Experimental material and methods

The experimental material AZ31 magnesium alloy produced by continuous casting has been homogenizing at 420° C for 16 hours. Its chemical composition, detected by the EDXRF analysis on the ARL QUANT'X EDXRF Spectrometer is shown in Table 1.

Metallographic samples have been prepared according to the standard metallographic procedures recommended for magnesium alloys. The AZ31 Mg alloy microstructure has been observed by optical microscope ZEISS Axio Observer Z1.m. The images have been created using AxioVision Rel 4.5 software. An etchant consisting of 2.5 ml of acetic acid, 2.1 g of picric acid, 5 ml of demineralized water and 35 ml of ethanol has been used to visualize the microstructure. The etching time has been set to 10 seconds. In the end samples have been rinsed by demineralized water, ethanol and dried by stream of air.

Prior to the PEO coating process, each sample has been ground by an emery paper p1000 to provide the same roughness across the treated surface. Subsequently, samples have been rinsed by demineralized water, ethanol and air-dried. The plasma

* [1,2]Daniel Kajanek, [2]Branislav Hadzima, [3]Matej Brezina, [2]Martina Jackova
[1]Department of Materials Engineering, Faculty of Mechanical Engineering, University of Zilina, Slovakia
[2]Research Centre, University of Zilina, Slovakia
[3]Faculty of Chemistry, Brno University of Technology, Czech Republic
E-mail: daniel.kajanek@fstroj.uniza.sk

Table 1 *Chemical composition of AZ31 magnesium alloy*

Component	Al	Zn	Mn	Si	Cu	Fe	Mg
wt. %	3.31	0.65	0.23	0.114	0.004	0.001	balance

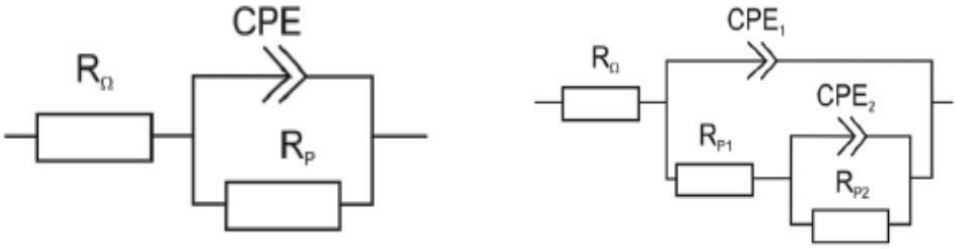

a) *b)*

Figure 1 *Equivalent circuits for diagrams with one capacitance loop (a) and two capacitance loops (b)*

electrolytic oxidation has been carried out using a laboratory DC power source Keysight N8762A with parameters 600 V/ 8.5 A and output of 5100 W. The two-electrode system has been used with the sample AZ31 involved as an anode. The cathode has been provided by stainless steel plate. The PEO has been carried out in an electrolyte composed of 10 g/l $Na_3PO_4.12H_2O$ and 1 g/l KOH and its pH has been stabilized at 12.3. During the PEO procedure, the electrolyte has been cooled with water and constantly stirred with a laboratory stirrer for better distribution of species. The electrolyte temperature was kept below 50° C. Four current densities with values of 0.025 A/cm^2, 0.05 A/cm^2, 0.1 A/cm^2 and 0.15 A/cm^2 have been applied on the surface with the preparation time of 10 minutes. Applied current has been maintained at a constant value. The morphology of the prepared PEO coatings has been observed using the Carl Zeiss Merlin scanning electron microscope and chemical composition has been examined by EDS analysis.

Electrochemical impedance spectroscopy has been used as a tool for evaluation of the corrosion resistance of the ground and PEO coated samples. Measurements have been performed in 0.1 M NaCl at the temperature of 22 ± 1° C on a laboratory potentiostat VSP Biologic. The measured frequencies have been ranged from 100 kHz to 10 mHz. The amplitude of the applied voltage has been set to 15 mV. The mean value of the sine voltage has been equal to the open circuit potential reached after 24 hours of exposure. The outputs of these measurements are the Nyquist diagrams, which can be quantitatively described using the equivalent circuit method (Figure 1). Simple Randels circuit (Figure 1a) has been used for analysis of diagrams with one capacitance loop. Diagrams with two capacitance loops has been analysed by circuit shown in Figure 1b. The most important circuit element for evaluation of corrosion resistance is R_p called the polarization resistance. The higher the R_p value is obtained the higher corrosion resistance is provided. If the Nyquist diagram is formed by the two capacitance loops, the resulting resistance of the surface is given by the sum of the partial resistors R_{p1} and R_{p2}. The element R_Ω expresses the resistance of the electrolyte and the element CPE (constant phase element), which replaces the capacitance C in the circuit, simulates the inhomogeneity of the measured surface [7].

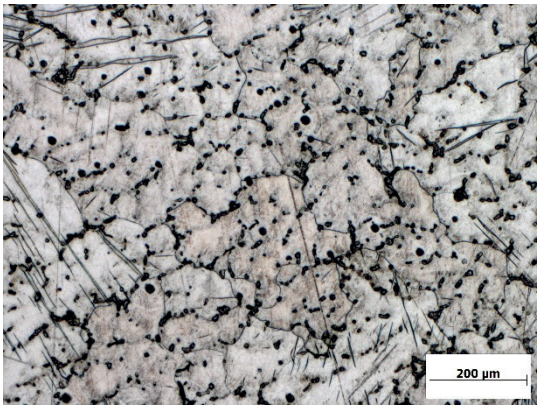

Figure 2 *Microstructure of AZ31 Mg alloy*

3. Results and discussion

The AZ31 magnesium alloy microstructure (Figure 2) is formed by polyhedral grains of solid solution of aluminum, zinc and other alloying elements in magnesium. The intermetallic phase of $Mg_{17}Al_{12}$ is also present in the microstructure. The average grain size is 220 µm. It is also possible to observe twins that were probably formed by deformation during the cutting and samples preparation [8].

The SEM images in Figure 3 show the PEO coatings prepared at a current density of 0.025 A/cm^2 (a) 0.05 A/cm^2 (b), 0.1 A/cm^2 (c) and 0.015 A/cm^2 (d). From the photo documentation, it can be seen that all the layers exhibit a porous structure typical for the PEO process. The formation of micropores is associated with the presence of molten oxides and gas bubbles produced during the discharges occurred on the surface of samples [6]. It is also possible to observe several microcracks resulting from stresses in the PEO layer during rapid solidification of molten substances in a contact with cold electrolyte [9, 10]. Chemical composition of the coatings obtained by EDS analysis is shown in Table 2. It can be seen that from this point of view there is not a significant difference within individual coatings. Therefore it can be assumed that applied current density does not have marginal impact on the chemical composition of PEO coatings. Moreover, it is clear that PEO coatings are consisting of elements present in the electrolyte (P, Na, O) and elements, which came from Mg substrate (Mg, Al). This claim is in good agreement with work [11].

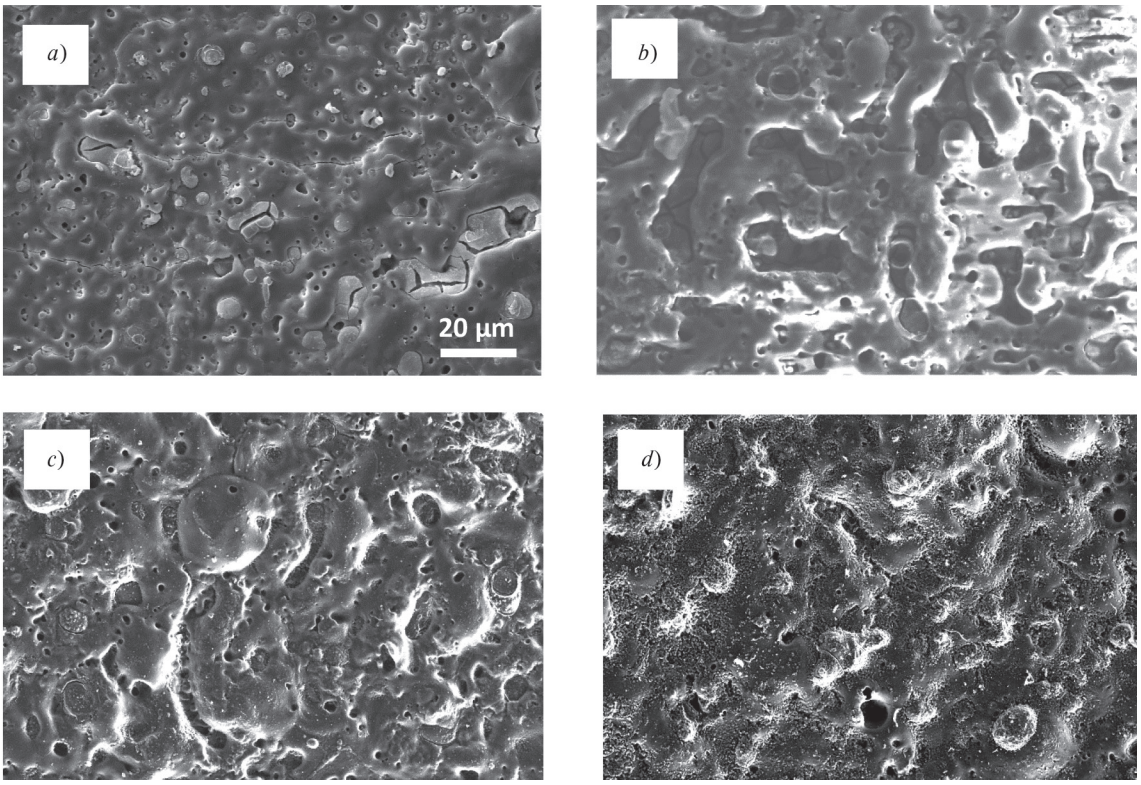

Figure 3 *Morphologies of PEO coatings prepared at 0.025 A/cm² (a), 0.05 A/cm² (b), 0.1 A/cm² (c) and 0.15 A/cm² (d), mag. 2000x*

Table 2 *Chemical composition of AZ31 magnesium alloy*

at. %	0.025 A/cm²	0.05 A/cm²	0.1 A/cm²	0.15 A/cm²
Mg	14.7	12.2	11.5	10.8
O	28.3	26.1	24.5	29.2
P	13.3	14.6	12.4	14.2
Al	0.34	0.14	0.15	0.16
Si	-	0.04	0.04	0.03
Na	1.16	1.74	1.89	2.68

Table 3 *Roughness parameters of the PEO coating prepared with different applied current density*

	0.025 A/cm²	0.05 A/cm²	0.1 A/cm²	0.15 A/cm²
Ra [µm]	0.884	1.016	1.698	2.041
Rz [µm]	8.412	8.763	14.300	17.317

It can be seen that with the increasing current density the layers are more rugged. This is also confirmed by roughness measurements (Table 3) which show increasing trend of Ra and Rz parameters with increasing energy input. Prepared coatings are formed on the surface of the magnesium alloy by intensive discharges which are responsible for formation of the layers. The higher the applied current density the more intensive/larger the discharges are occurring on the surface. However, they are less in numbers [9]. More intensive discharges consequently melt a greater amount of material and form a more rugged layer. Layers prepared at 0.1 A/cm² and 0.15 A/cm² exhibit imperfections in the form of small particles located around the pores and their occurrence is more extensive at the highest applied current density. For a more detailed description of their effect on the quality of the layer, its chemical composition will be performed and deeply studied in the future experiments.

The Nyquist diagrams for different PEO layers and ground samples measured in 0.1 M NaCl after 24 h of exposure are shown in Figure 4. In all the cases, except for 0.1 A/cm², the diagrams are created by two capacitive loops. Occurrence of one capacitance loop in diagram assumes homogeneous conditions on the measured surface during dissolution and two capacitance loops point to the presence of areas with different electrochemical behaviour [7]. Corresponding electrochemical characteristics are shown in Table 4. When comparing polarization resistances, it can be seen that all of the PEO layers exhibit a significantly higher R_p compared to the ground sample with the value of 6765 Ω.cm² and thus have a positive influence on the corrosion resistance. It is resulting from the formation of an effective barrier, which slows down penetration of solution and thus provides sufficient protection for the Mg substrate against harmful activity of the chloride ions present in testing environment. When comparing

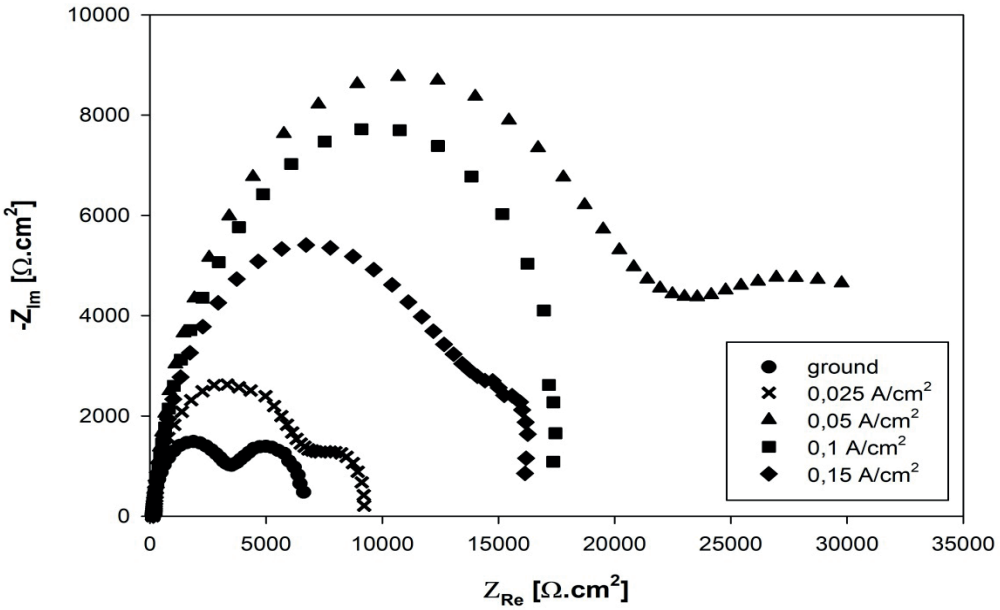

Figure 4 *Nyquist plots of ground PEO treated samples of AZ31 Mg alloy measured in 0.1M NaCl*

Table 4 *Electrochemical characteristics of ground and PEO coated samples of AZ31 Mg alloy in 0.1 M NaCl*

	R_Ω ($\Omega.cm^2$)	R_{p1} ($\Omega.cm^2$)	R_{p2} ($\Omega.cm^2$)	R_p ($\Omega.cm^2$)	CPE_1 [$F.s^{n-1}$]	CPE_1 [$F.s^{n-1}$]	n_1	n_2
ground	115	3699	3066	6765	1.10^{-5}	2.10^{-3}	0.9	0.9
0.025 A/cm²	120	5875	3340	9215	7.10^{-6}	4.10^{-4}	0.9	0.9
0.05 A/cm²	119	18 909	15 592	34 501	6.10^{-6}	2.10^{-4}	0.9	0.7
0.1 A/cm²	128	18 399	-	18 399	6.10^{-6}		0.9	
0.15 A/cm²	133	11 313	5874	17 187	7.10^{-6}	2.10^{-4}	0.9	0.8

the individual layers, differences in the polarization resistance values have been observed. It is obvious that polarization resistance has increased with the increasing applied current density from the 9215 $\Omega.cm^2$ reached by 0.025 A/cm up to the applied current density of 0.05 A/cm², where the maximum of R_p with the value of 34 501 $\Omega.cm^2$ has been reached. With a layer prepared at 0.1 A/cm² decrease of the resistance has been observed from 18 399 $\Omega.cm^2$ to the 17 187 $\Omega.cm^2$ reached by the 0.15 A/cm². This trend can be explained by the synergic effects of several factors. As it was mentioned before, the roughness of the layers has increased with increasing applied current density and the occurrence of heterogeneities and larger pores associated with intensive discharges has been observed. Heterogenities and porosity has increased surface roughness and therefore larger electrochemically active area has been in contact with electrolyte [3, 4, 12]. That is why the PEO layers formed at higher current densities (0.1 A/cm² and 0.15 A/cm²) have been attacked more intensively by aggressive chloride ions compared to a more uniform layer obtained at a current density of 0.05 A/cm². In the case of the layer prepared at 0.025 A/cm² its thickness and compactness are probably not high enough due to the insufficient energy input which has resulted in less intensive sparking effect and thus less promoted formation of the coating. Therefore, the lowest polarization resistance across the prepared layers has been reached. These observations are in good agreement with the results presented in works of [11, 13].

4. Conclusions

According to the performed experiments and analysis several conclusions can be stated:

- Prepared PEO coatings revealed porous structure typical for plasma electrolytic oxidation process.
- Roughness of the PEO coatings increased with the increasing applied current density. In the cases of 0.1 A/cm² and 0.15 A/cm² heterogeneities were observed.
- All of the created PEO layers reached higher values of the polarization resistance compared to the ground samples in 0.1 M NaCl and thus positively influenced the corrosion resistance of AZ31 Mg alloy.
- The highest corrosion resistance was provided by the PEO coating created with current density of 0.05 A/cm², which reached more than 5-times higher polarisation resistance value of 34 501 $\Omega.cm^2$ compared to the ground samples, which reached R_p value of 9215 $\Omega.cm^2$.

Acknowledgement

The research was supported by the Scientific Grant Agency of the Ministry of Education, Science, Research and Sport of the Slovak Republic under the contract VEGA no. 1/0045/17 and by project ITMS 26220220121.

References

[1] DRABIKOVA, J., et al. Improvement of bio-compatible AZ61 magnesium alloy corrosion resistance by fluoride conversion coating. *Koroze a ochrana materialu* [online]. 2016, **60**(50), p. 132-138. ISSN 1804-1213. Avalible from: https://doi.org/10.1515/kom-2016-0021

[2] UHRICIK, M., et al. Change of internal friction on magnesium alloy with 5.48% Al and 0.813% Zn. *Proceedia Engineering* [online]. 2017, **177**, p. 568-575. eISSN 1877-7058. Avalible from: https://doi.org/10.1016/j.proeng.2017.02.262

[3] SONG, G. L. *Corrosion of Magnesium Alloys*. 1. ed., Woodhead Publishing: Philadelphia, 2011. ISBN 9781845697082.

[4] MHAEDE, M., PASTOREK, F., HADZIMA, B. Influence of shot peening on corrosion properties of biocompatible magnesium alloy AZ31 coated by dicalcium phosphate dihydrate (DCPD). *Materials Science and Engineering C* [online]. 2014, **39**, p. 330-335. ISSN 0928-4931/eISSN 1873-0191 . Avalible from: https://doi.org/10.1016/j.msec.2014.03.023

[5] DOROZHKIN, S. Calcium orthophosphate coatings on magnesium and its biodegradable alloys. *Acta Biomaterialia* [online]. 2014, **10**(7), p. 2919-2934. ISSN 1742-7061/eISSN 1878-7568. Avalible from: https://doi.org/10.1016/j.actbio.2014.02.026

[6] YEROKHIN, A. L., et al. Plasma electrolysis for surface engineering. *Surface and Coatings Technology* [online]. 1991, **122**(2-3), p. 73-93. ISSN 0257-8972/eISSN 1879-3347. Avalible from: https://doi.org/10.1016/S0257-8972(99)00441-7

[7] AMIRUDIN, A., THIERRY, D. Application of electrochemical impedance spectroscopy to study the degradation of polymer-coated metals. *Progress in Organic Coatings* [online]. 2016, **26**(1), p. 1-28. ISSN 0300-9440. Avalible from: https://doi.org/10.1016/0300-9440(95)00581-1

[8] KAJANEK, D.,PASTOREK, F., HADZIMA, B. Corrosion resistance of AZ31 magnesium alloy influenced by conventional cutting fluid. *Materials Engineering - Materialove Inzinierstvo* [online]. 2017, **24**(3), p. 67-71. ISSN 1335-0803/eISSN 1338-6174. Avalible from: http://fstroj.uniza.sk/journal-mi/PDF/2017/08-2017.pdf

[9] DARBAND, G. B., et al. Plasma electrolytic oxidation of magnesium and its alloys: Mechanism, properties and applications. *Journal of Magnesium and Alloys* [online]. 2017, **5**(1), p. 74-132. ISSN 2213-9567. Avalible from: https://doi.org/10.1016/j.jma.2017.02.004

[10] WANG, H. M., CHEN, Z. H., LI, L. L. Corrosion resistance and microstructure characteristics of plasma electrolytic oxidation coatings formed on AZ31 magnesium alloy. *Surface Engineering* [online]. 2010, **26**(5), p. 385-3920. ISSN 0267-0844/eISSN 1743-2944. Avalible from: https://doi.org/10.1179/026708410X12506873242822

[11] MORI, Y., et al. Characteristics and corrosion resistance of plasma electrolytic oxidation coatings on AZ31B Mg alloy formed in phosphate - Silicate mixture electrolytes. *Corrosion Science* [online]. 2014, **88**, p. 254-262. ISSN 0010-938X/eISSN 1879-0496. Avalible from: https://doi.org/10.1016/j.corsci.2014.07.038

[12] KAJANEK, D., et al. Corrosion performance of AZ31 magnesium alloy treated by ultrasonic impact peening (UIP). *Materials Today: Proceedings* [online]. 2018, **5**(13), p. 26687-26692. eISSN 2214-7853. Avalible from: https://doi.org/10.1016/j.matpr.2018.08.136

[13] DURDU, S., USTA, M. Characterization and mechanical properties of coatings on magnesium by micro arc oxidation. *Applied Surface Science* [online]. 2012, **261**, p. 774-782. ISSN 0169-4332. Avalible from: https://doi.org/10.1016/j.apsusc.2012.08.099

Marketa Weisheitelova - Karel Klouda - Stanislav Lasek*

EFFECTS OF PASSIVE AND ACTIVE DECONTAMINATION ON METAL MATERIALS CONTAMINATED BY SULPHUR MUSTARD (YPERITE)

This paper reports the results of the experimentally determined effects of decontaminating agents on metal surfaces resulting from passive and active decontamination after sulphur mustard (Yperite) contamination. The paper includes an analysis of the experimentally obtained results for each metal (Zinc, Nickel, Aluminium, Brass, Steel, Copper).

Keywords: *decontamination, yperite, metal, surface, pH potential*

1. Introduction

Decontamination refers to a set of methods, procedures and means used to remove effectively contaminating substances. Since the complete removal of contaminating substances is rarely perfect (due to residual / secondary contamination), the definition can be amended by saying that the goal of decontamination is to reduce the harmful effect of contamination to a safe level or to eliminate it.

This paper deals with the effect of decontaminating agents on the surfaces of decontaminated metals contaminated with sulphur mustard (HD), known as active decontamination, or uncontaminated with HD, the so-called passive decontamination. Knowledge of the effects may indicate the necessity to use a different material or surface treatment for the selected metal.

The most frequently used chemical procedures for decontamination during the liquid phases are strong oxidizing agents in hydrogen peroxide type solutions, ozonization and decomposition with strong acids or alkalis. Decontaminating agent application then depends directly on the form and extent of decontamination and on the type of the decomposed substance.

2. Experiments

For the purpose of the experiments, the decontaminating solutions Hvezda SCH [1-2] a two-component agent with combined decontaminating effects, were selected. The component trade name CC contains in particular hydrogen peroxide, while the component trade name AB includes an ethoxylated fatty alcohol, sodium hydroxide. The key component is quaternary alkyl (C_{12}-C_{16}) benzyl dimethyl ammonium chloride and a hypochlorite mixture - solution containing 2.5 % by weight active chlorine and 2 % by weight sodium hydroxide.

During the experiments, the focus was on the materials used for the construction of critical infrastructure, specifically on those used for the construction of Prague's Metro, an important constituent part of municipal transport in Prague. Thanks to the long-time cooperation with the Prague Public Transport Company, the operator of Prague's Metro, the surface testing samples of materials, which were actually used, were acquired, see Table 1.

3. Passive decontamination

Surfaces of the samples were scanned using digital microscopes. Time of exposure to decontaminating solutions was 1 and 3 hours, and the solutions were applied by manual spraying. The surfaces of metal samples (0.4 m^{-2}) were divided into 4 areas with defined circular zones for testing the content of 7 cm^{-2}. The H1 and H3 regions were reserved for the Hvezda solution with the times of exposure 1 and 3 hours, while the hypochlorite mixture was applied to the N1 and N3 regions with the times of exposure 1 and 3 hours. After exposure to decontaminating solutions, the surfaces of individual samples were dried up, washed with distilled water and scanned. A total of 8 samples were processed in the aforementioned manner. The scanned images were compared. Changes on the surfaces were so significant that it was decided to have these changes examined and assessed at the Department of Material Engineering at VSB - Technical University of Ostrava.

Both of the used decontaminating solutions were alkaline (pH 13-14) with oxidizing nature (having the potential metals $E_{cor} \approx 0.5$-1 V if a standard hydrogen electrode is used). Based on the E-pH diagrams, it was possible to assess the thermodynamic possibility of formation (stability) and the type of corrosion products in the given region. However, E-pH diagrams do not allow the rate of corrosion formation (kinetics) to be determined. Both peroxide and hypochlorite have the strong oxidizing effects. The pH values of individual environments were ascertained directly by measurement or calculated based on composition. The value of potential taken up by the metal was determined as a

* [1,2]Marketa Weisheitelova, [1]Karel Klouda, [1]Stanislav Lasek
[1]VSB - Technical University of Ostrava, Czech Republic
[2]National Institute for NBC Protection, Milin, Czech Republic
E-mail: weisheitelova@sujchbo.cz

Table 1 *Overview and designation of used materials*

No.	Name	No.	Name
K 1	Zinc-plated metal sheet	K 5	Stainless steel (18/8)
K 2	Nickel	K 6	Stainless ferritic steel (Cr12)
K 3	Aluminium (99 %)	K 7	Copper (99 %)
K 4	Brass (CuZn30)	K 8	Zinc - iron

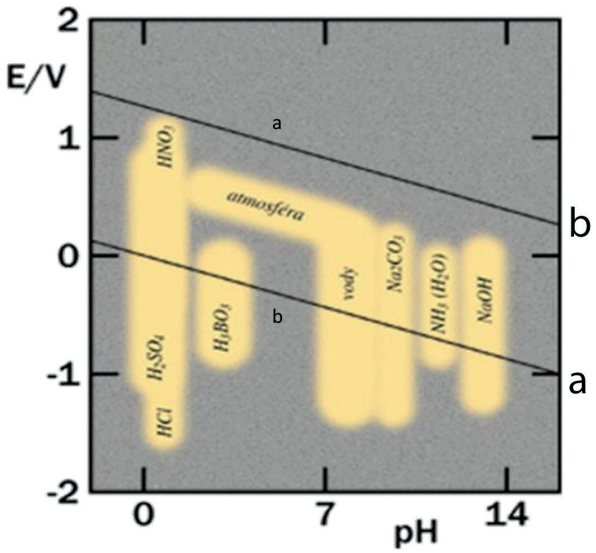

Figure 1 *The potential-pH diagrams for various environments*

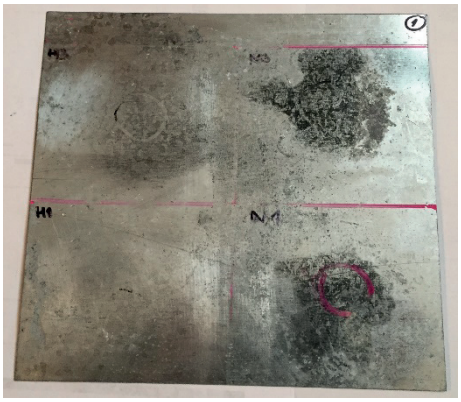

Figure 2 *The K1 sample after passive decontamination*

compromise between the oxidizing properties of the environment and the grade of the metal concerned [3].

The E potential-pH diagram, Figure 1 shows the designated regions with depicted corrosion potentials of metals in selected environments. The higher the value of (corrosion) potential metals, the stronger the oxidizing effect of the environment. Aerated waters and solutions have their potential in the upper part of the respective region, while deaerated ones in the lower part of the respective zone (highlighted in yellow). The area of thermodynamic stability is delimited by the a-b line segments. (The pH-dependent range of potential values in which the water is stable, the thermodynamically stable oxygen gas above the line b and the gaseous hydrogen below the line a).

Detailed assessment of changes in metal surfaces after the passive decontamination was carried out by the stereomicroscope and metallographic examination microscope focusing on the areas designated by the circles (magnification 400 times). Table 2 provides an overview of changes on surfaces of each metal following the passive decontamination.

Assessment of changes in the K1 sample - zinc-plated steel metal sheet, Figure 2.

In the dark areas in samples N1 and N3, clusters of microscopic corrosion pits (dots) with hemispherical profile were detected. The dark areas were formed by aggregates of the dark adhesive corrosion products. The H1 and H3 samples did not include such microscopic dots, but shallow microscopic irregular depressions with rougher inner surface were discovered in them. Under the microscope, it was further detected that the dark areas did not result from different corrosion of zinc cells with different roughness. In addition, light stains, typical of zinc corrosion products (ZnO, $Zn(OH)_2$, etc.), could be seen on the zinc-plated sheet metal.

The more intense change in the colour shade for N1 and N3 (compared to H1 and H3) corresponds to the corrosive effect of chlorides on the exposed zinc-plated surfaces. The Zinc corrosion can proceed in both acidic and alkaline environments (pH 12-14).

Assessment of changes in the K2 sample - nickel. The surface of the K2 metal remained unchanged after having been exposed to the decontaminating agents.

Assessment of changes in the K3 sample - aluminium (99 %), Figure 3.

Numerous darker stains (with the size of 0.01-0.1 mm) and numerous dark dots (with the diameter ranging from 1 to 10 μm) can be seen under the microscope, when the gauge line is observed in the forming process direction on the original surface not exposed to the decontaminating agents. After the exposure to the decontaminating solutions, all regions (H1-N3) were covered with thin, uneven, nearly continuous layers of the light grey deposits of salts, very likely of the $Al(OH)_3$ based corrosion products. According to the E-pH diagram Figure 4, aluminium and its alloys are subject to corrosion in alkaline environments (pH ≥13). On the surface of the regions under review, black dots were observed in the field of view of the stereomicroscope, as well.

The observed surface included microscopic pits and corroded borders of grains, which were greater the longer they were exposed and for the hypochlorite mixture [4]. The more extensive affected areas H1 and H3, compared to N1 and N3, result from application of the tenside that increases the wettability of

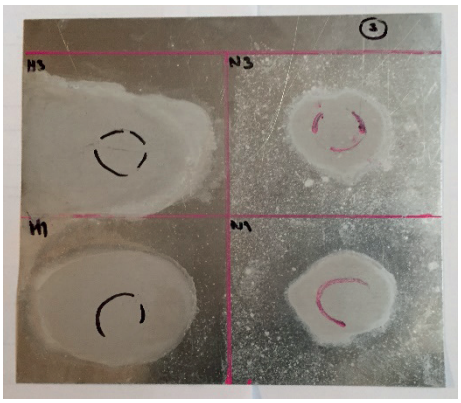

Figure 3 *The K3 sample after passive decontamination*

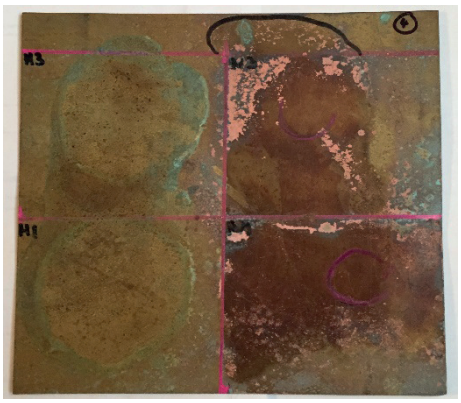

Figure 5 *The K4 sample after passive decontamination*

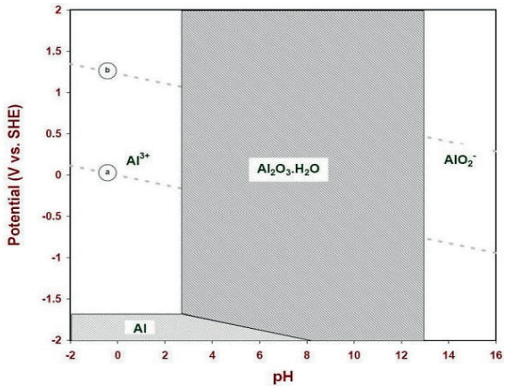

Figure 4 *The E-pH diagram (Pourbaix) for aluminium exposed to water, area "Al" - Immunity region, area "Al^{3+} and AlO_2^-"- Corrosion region, area "$Al_2O_3.H_2O$"- Passive region*

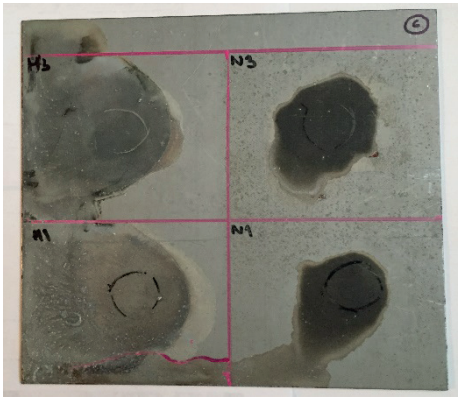

Figure 6 *The K6 sample after passive decontamination*

the surface where the solution was applied (with the application of the same quantity of solution in all cases).

Aluminium Al (Standard potential E_o = -1.66 V) is well resistant to atmospheric exposure and effects of the neutral solutions, since in the given environment (with pH values ranging from 4 to 10), it is protected by a thin layer of oxide and which is thermodynamically stable. In acidic or alkaline environments, Al oxides dissolve and Al metal corrodes faster emitting hydrogen. Solutions containing Cl^- ions ($Cl_xO_y^-$) cause pit corrosion (pitting) where the passive decontamination is applied (Al_2O_3) [5].

Assessment of changes in the K4 sample - brass (CuZn30), Figure 5.

Outside the exposed areas, under the microscope, depressions of mechanical origin (bruises, scratches), lengths of the order of tenths of millimeters and widths of the order of hundredths of a millimeter, were found. This concerns a copper alloy containing zinc with the concentration of 30 % by weight (CuZn30). The alloy contains copper with a high electrochemical grade and zinc with a low electrochemical grade. Brass is generally resistant to atmospheric corrosion. This resistance is slightly worse than in the case of pure copper and decreases with the increasing content of zinc. This alloy is prone to the selective (extraction) corrosion of zinc in certain environments due to the transport of zinc atoms to the solution or due to the development of corrosion products, the so-called surface dezincification.

The E-pH diagram for the specified brass probably exists. However, it is possible to use the E-pH diagram for copper and zinc where corrosion can be expected in alkaline aqueous solutions with oxidizing effect, leading to the anodic stripping of the ZnO_2^{2-} and CuO_2^{2-} anions (see section covering zinc-plated sheet metal and copper). The greenish or green and blue areas may be deposits of chlorides (hypochlorites) of copper.

Assessment of changes in the K6 sample -Stainless ferritic steel sheet, Figure 6.

Depending on the degree of darkening of the exposed areas, increasing the time of exposure increases the degree of surface corrosion; further, the solution that includes sodium hypochlorite has the more intense effects. The K6 sample included numerous microscopic pits (with the diameters ranging from 0 to 50 μm, with the depth ranging from 10 to 20 μm), which were the same inside the exposed regions as well as outside of them. The pits were formed during the final treatment of the sheet metal and not as a result of exposure to the solutions. The surfaces also included light dots in these places. The microscope revealed local deposits of salts under which areas with a metallic lustre had formed with the same pits as in other areas.

According to the E-pH diagram, Figure 7 and other findings, steel materials are passivated in oxidizing environments. If the solution with oxidizing effects contains chlorides, or where applicable hypochlorite, the pit corrosion develops particularly in solutions with oxidizing effects.

Because the Diagram E-pH for the steel sample CR12 shows a diagram for steel AISI 304 (CrNi18-10) and 316 (CrNiMo17-11-2), areas of uniform corrosion, immunity, pit corrosion (dots)

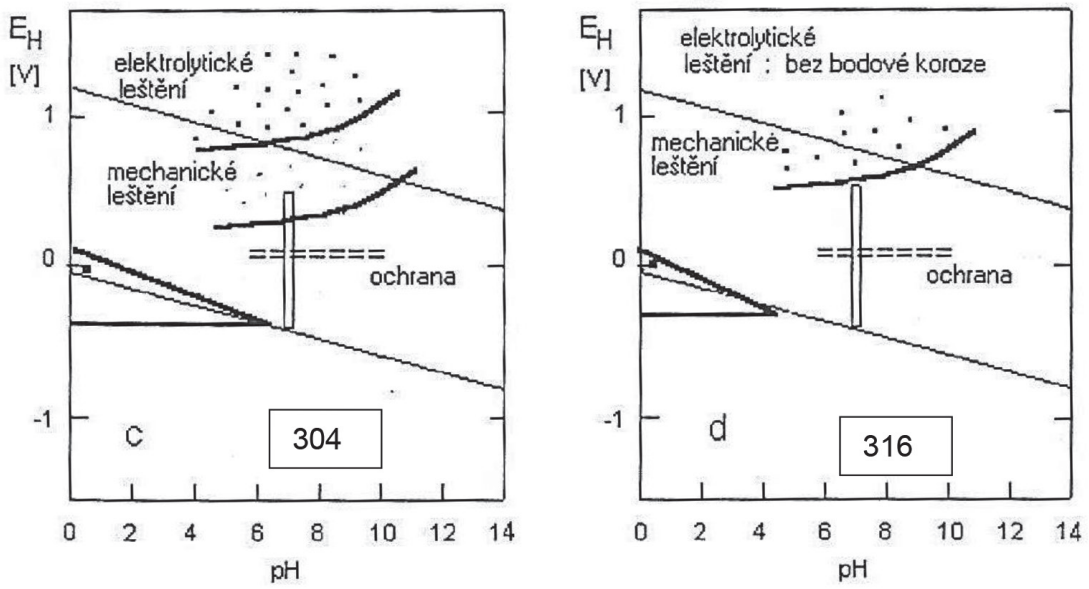

Figure 7 *The E-pH diagram for steel 304 and 316 in the aqueous solution of 0.1 mol/l NaCl (Key: electrolytic polishing/elektrolyticke lesteni, mechanical polishing/mechanicke lesteni, protection/ochrana, electrolytic polishing: without pit corrosion/elektrolyticke lesteni: bez bodove koroze, mechanical polishing/mechanicke lesteni, protection/ochrana)*

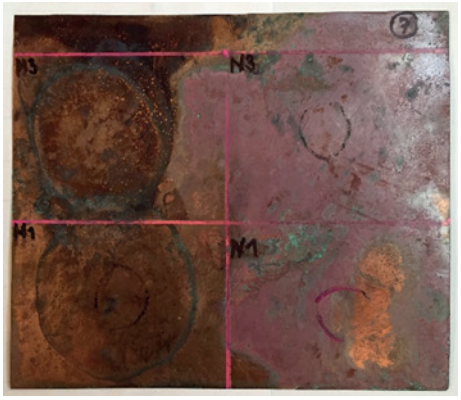

Figure 8 *The K7 sample after the passive decontamination*

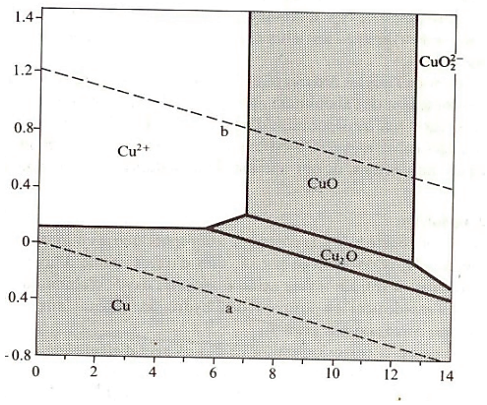

Figure 9 *The E-pH diagram for copper in water, area "Cu" - Immunity region, area "CuO and Cu_2O"- Corrosion region, area "Cu^{2+} and CuO_2^{2+}"- Passive region*

and passivity of steel AISI 304 and 316 in the aqueous solution of 0.1 mol/l NaCl (3.5g/l Cl) at the temperature of 25 °C were experimentally determined. Under the protective potential (protection in the diagram), the perfect passivity occurred; above this potential, passivity was imperfect. The areas of uniform, as well as pit corrosion, are more extensive in the case of AISI 304 steel. The pit corrosion is also affected by the surface treatment (such as polishing) [3]. Steel Cr12 has the point of occurrence of the point corrosion slightly shifted to the lower values of breakdown potential compared to CrNi18-10 even in alkaline region. In alkaline environments, all the aforementioned steel materials are subject to an increased potential of pit corrosion (pitting) breakdown with increasing pH values.

Assessment of changes in the K7 sample - copper (99 %), Figure 8.

Three types of pit corrosion can develop on copper in aqueous solutions. The brown areas are likely to represent copper oxides, green copper chloride dihydrate.

Copper shows good resistance to atmospheric corrosion, cold as well as warm water, unless the flow rate exceeds several meters per second. The standard potential of copper (standard potential Eo = + 0.34 V, SHE) is higher than that of the hydrogen electrode. In the absence of oxidizing substances, copper therefore resists corrosion in acidic environments (non-oxidizing acids).

On the other hand, in the presence of oxidizing substances with a higher reduction potential, Cu dissolves (the Cu^{2+} region) such as in the aqueous solutions of HNO_3, in aerated H_2SO_4 acid, in the solution of $FeCl_3$ or in the solution containing peroxide, or where applicable hypochlorite NaClO (with oxidizing effects) depending on concentration. Corrosion also develops in strong alkaline solutions (pH 13-14) with oxidizing effects (E > 0.4 V, the area of CuO_2^{2-}), or where applicable copper oxides are formed (CuO) with protective effects (pH 10-12), Figure 9.

Assessment of changes in the K8 sample - zinc - iron, Figure 10.

The description is similar to K1. The N3 and N1 solutions acted on a smaller area (compared to the K1 sample); darker

Table 2 *Overview of changes on the surfaces of metals*

No.	Hvezda		Hypochlorite solution	
	H1	H3	N1	N3
K1	no changes	grey stains	dark grey areas and stains	dark grey and black stains
K2	no changes	no changes	no changes	no changes
K3	light grey and dull appearance, smaller area	light grey and dull appearance, larger area	light grey appearance	light grey appearance
K4	the rim of the area is green with brown dots inside	the rim of the area is greenish with more distinctive brown dots inside	large brown areas, light orange and pink stains	large brown areas, light orange and pink stains
K5	no changes	no changes	no changes	no changes
K6	grey area, light dots with residues of salt	grey area, light dots with residues of salt	dark grey area, light dots (with salt)	dark grey area, light dots (with salt)
K7	brown areas and light dots	darker brown areas and light dots	dark brown dots, turning pink	dark brown dots, turning pink
K8	minor changes, weak darkening	minor changes, weak darkening	dark grey areas, light as well as dark cells	sharp-cut grey (black) area, cells corroded to various extent

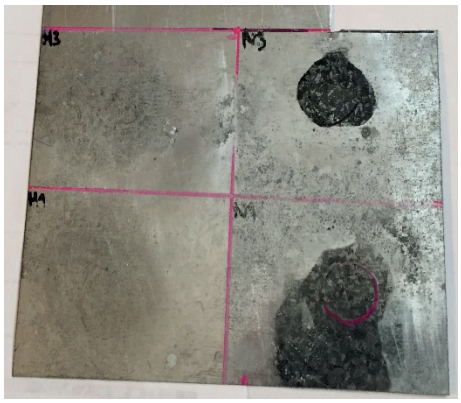

Figure 10 *The K8 sample after passive decontamination*

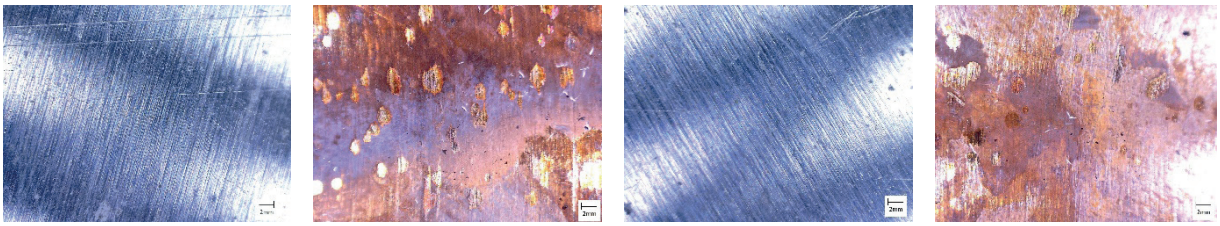

Figure 11 *An example of the scanned K7 sample (magnification 80 times), on the left is a photograph of the delimited area prior to the application of the N - hypochlorite mixture decontaminating solution and after exposure to the hypochlorite mixture after 1 hour (N1) and 3 hours (N3)*

appearance of exposed areas (using the same amount and concentration of solution on both plates K1 and K8).

Figure 11 shows images of the K7 sample surfaces before and after exposure to the decontaminating solution. Significant changes on the surfaces due to exposure to the hypochlorite mixture and changes in colour with light or dark dots can be seen here.

4. Active decontamination

Surfaces of samples were scanned using digital microscopes. The surfaces were contaminated with HD and after 30 minutes the decontaminating solutions were applied with a manual sprayer. The contaminating substance in the place of “HD” application was removed only by using a paper pad. After 60 minutes from the beginning of the test, the liquid (mixture resulting from

Figure 12 *The effect of HD on the K4 sample (on the left, the surface prior to exposure to HD and after the exposure to HD)*

Table 3 *Overview of changes on the surfaces of each metal following the active decontamination*

No.	Type of metal	Effects on surface		
		HD	Hvezda	Hypochlorite mixture
K1	Zinc-plated metal sheet	no changes	no changes	blackening
K2	Titanium zinc (99 % Zn)	no changes	change, dulling stain	blackening
K3	Aluminium (99 %)	no changes	no changes	dulling
K4	Brass (CuZn30)	visible drops of HD	Change	change and visible drops of HD
K5	Stainless steel (18/8)	no changes	no changes	no changes
K6	Stainless ferritic steel	no changes	no changes	no changes
K7	Copper (99 %)	no changes	no changes	visible drops of HD
K8	CU anodised aluminium	no changes	disruption of the surface layer	destruction of the surface layer

decontamination) was removed, the surface washed with distilled water and dried; changes on the surfaces were visually assessed.

Samples with the dimensions 50×50 mm were used for the tests. The K2 - nickel sample was replaced by a titanium - zinc sample (the originally used sample was not affected by the decontaminating solutions) and the K8 sample - zinc - iron (which is almost identical with the K1 sample) was replaced by a sample of Cu anodised aluminium that is widely used in Prague's Metro.

The surface of the metal samples was divided into 4 regions: top left - the original surface, top right - contamination with HD, bottom left - Hvezda solution, bottom right hypochlorite solution.

Exposure to HD without subsequent decontamination resulted in no visual changes on the surfaces of the metal samples, with the exception of the K4 sample with traces remaining in the place of contact with applied HD drops, Figure 12.

The effects of HD and follow-up decontamination left visible changes on the surface of the K1 through K4, K7, and K8 samples. Considering the shorter time of exposure to the decontaminating solutions compared to the passive decontamination, those changes were less intense and affected smaller areas than in the case of the passive decontamination. The surface of the K2 sample, which remained unchanged after application of passive decontamination, visually changed after active decontamination, which can be ascribed to the concurrent effects of HD and decontaminating agents. Table 3 provides an overview of changes on surfaces of each metal following the active decontamination.

After the material has been decontaminated, the secondary contamination of the space may occur temporarily due to the delayed release of the contaminant (or decomposition products formed by the HD reaction with the decontaminant) sorbed on the surface or within the structure of the exposed material. Therefore, it is extremely important to know not only the effects of the contaminating substance and decontaminating agents on the surfaces of the materials, but also the efficiency of decontamination and the related potential of the secondary contamination.

Additional tests ascertained the efficiency of active decontamination and residual concentration of HD. The samples of metals were covered with a special paper reacting to HD released from the material or its surface by changes in colour. The changes were observed within a time interval of 15 minutes. No residual contamination was proven in any of the samples of metals.

5. Conclusion

The samples of metals made of nickel and stainless steel were not affected by the processes of decontamination. In the remaining samples, changes in colour of the surface following both passive and active decontamination appeared. Such changes do not always have a negative effect on the quality of the metal surface. Some components of the decontaminating solutions create a protective layer as well (such as metal oxides). On the other hand, the changes make the surface of metal look inaesthetic. The results of the tests imply that it is advisable to treat the surface of the metals prior to their use.

References

[1] Safety Data Sheets of Hvezda AB and CC [online] [accessed 2015-21-05]. Avaliable from: http://www.mpd.cz

[2] DECOMKOV Prague s.r.o. *Agents and methods for decontamination.* 2003-2005: Research and Development Project supported by MIT CR no. FF-P2/115.

[3] NOVAK, P. *Corrosion engineering*. Institute of Chemical Technology in Prague, Department of Metallic Materials and Corrosion Engineering, Prague, 2002.

[4] YAKOUT, S. M. Monitoring the changes of chemical properties of rice straw-derived modified by different oxidizing agents and their adsorptive performance for organics. *Bioremediation Journal* [online]. 2015, **19**(2), p. 171-182. ISSN 1088-9868/eISSN 1547-6529. Available from: https://doi.org/10.1080/10889868.2015.1029115

[5] POURBAIX, M. *Analysis of current problems caused by localized corrosion*. *Study of their industrial impact and proposals for action*. Final report. CEBELCOR, Brussels, 1986.

Oleksij Fomin - Juraj Gerlici - Mykola Gorbunov - Alyona Lovska
Kateryna Kravchenko - Oleksii Burlutski - Tomas Lack*

STUDY INTO IMPROVEMENT OF THE HATCH COVERS OF GENERAL-PURPOSE OPEN WAGONS TO PROVIDE STRENGTH UNDER OPERATIONAL LOADING DIAGRAMS

The article presents the results of research into the strength of the hatch covers of general-purpose open wagons. It was detected that strength of the standard hatch covers is not provided in operational loading diagrams. Therefore, new designs of the hatch covers for open wagons were proposed. The results of the strength calculation, implemented with the finite element method, make it possible to conclude that at basic and additional operational loading diagrams the strength values for proposed designs of hatch covers do not exceed the admissible values. The research conducted can contribute to a higher strength of the carrying structures of the bodies of general-purpose open wagons in operation, thus, guaranteeing a higher operational efficiency of the rail transport.

Keywords: *hatch cover, locking support, framing, strength calculation*

1. Introduction

The development of foreign economic relations between Eurasian countries mostly depends on the transport industry, the leading component of which is railways. In order to provide the fail-safe transportation it is necessary to supply railways with adequate rolling stock [1-2].

One of the most damaged elements in the carrying structure of open wagon bodies, as the most popular types of wagons in operation, is the hatch cover (Figure 1). It is caused by its considerable operational loading, because this structural element forms the floor of an open wagon.

A frequent cause of damages of the hatch covers in operation is the loading/unloading of open wagon bodies at sea ports and private enterprises.

In order to provide strength of the hatch covers of open wagons, it is necessary to determine and analyze the strength values in operational loading modes.

2. Analysis of recent studies

The study into the stress-strain state of the hatch cover of open wagons, when part of freight falls on it, is presented in [3]. The results of calculation made it possible to conclude that the standard hatch cover design does not satisfy the strength conditions. The strength research into the hatch cover of open wagons under other loading diagrams is not conducted in the study.

Study [4] deals with results of research into the character and influence of different freight bogies on strength of the carrying structures of wagons.

The methods to improve the carrying capacity of open wagon bodies, to provide their fastening strength on the deck of a train ferry, are given in [5].

However, in that study is not covered the problem of the strength research for the hatch covers of open wagons in operational conditions.

Influence of round tubes, introduced in the carrying systems of freight wagons, on the physical-mechanical properties, is studied in [6-7]. The research into dynamic loading and strength of the open wagon body does not consider the hatch covers in the structure. Thus, the model takes into account the elements rigidly interacting.

A longer service life for obsolete open wagons is substantiated in [8]. In order to determine the dynamic loading on the body of an open wagon at shunting impacts the mathematical model was designed, the solution of which was considered for the research into strength of the body of an open wagon with consideration of operational wear of structural elements.

Besides that, the works do not study the strength of the hatch covers in open wagons for operational loading modes.

The observation of structural peculiarities of open wagons is provided in [9]. It considers advantages and disadvantages of the failure-proof designs of open wagons and tendencies of their improvement.

However, methods to improve hatch covers for open wagons are not considered.

Problems of the rolling stock design for heavy-cargo transportation are studied in [10-11]. Dynamics and strength

* [1]Oleksij Fomin, [2]Juraj Gerlici, [3]Mykola Gorbunov, [4]Alyona Lovska, [2]Kateryna Kravchenko, [5]Oleksii Burlutski, [2]Tomas Lack
[1]Department of Cars and Carriage Facilities, State University of Infrastructure and Technology, Ukraine
[2]Department of Transport and Handling Machines, University of Zilina, Slovakia
[3]Department of Rail Transport, Institute of Transport and Logistics, Volodymyr Dahl East Ukrainian National University, Ukraine
[4]Department of Cars, Ukrainian State University of Railway Transport, Ukraine
[5]Department of Mechanics and Machine Design, Ukrainian State University of Railway Transport, Ukraine
E-mail: fominaleksejviktorovic@gmail.com

a *b* *c* *d*

Figure 1 *The basic damages in the hatch covers of open wagons in operation: a - break in the framing, b - tear of the locking support, c - damages in the framing, d - tear of the sheet*

are studied with advanced methods using ProMechanica and CosmosWorks software. While designing the carrying structure of a carrier, the possibility to use various materials for it is investigated, as well.

The influence of friction between the body and the bogie on dynamic values of a wagon motion is presented in [12]. The modelling was conducted with mathematical techniques in DYNRAIL software.

However, the studies mentioned do not pay attention to determination of the strength values for the hatch covers of general-purpose open wagons.

Research into the dynamics of a wagon with multi-body methods is presented in [13]. The computation was made in the MSC Adams software complex. Study [14] determines the influence of structural peculiarities of wheel sets on the motion of transport facilities on curve sections.

All investigations mentioned above do not study the strength of the structural elements of transport facilities under operational loading.

3. Objective of the article

The study presents possibilities to improve hatch covers for general-purpose open wagons to provide adequate strength at operational loading diagrams. To achieve the objective the following tasks are presented:

1. Strength calculation of the hatch covers of a general-purpose open wagon. Substantiation of its required improvement;
2. Improvements of the hatch covers of a general-purpose open wagon to provide adequate strength at operational loading diagrams;
3. Strength calculation of the improved hatch covers for general-purpose open wagons;
4. Durability calculation of the improved hatch covers for general-purpose open wagons.

4. Presentation of the basic material of the article

In order to determine the strength values of the hatch covers for the general-purpose open wagons, the spatial model of a hatch cover was built in the SolidWorks software and strength was calculated with the finite element method in the CosmosWorks software.

The strength calculation was made at basic loading diagrams for hatch covers in compliance with normative documents [15-17]:

- effect of the equally distributed loading P_g = 69.9 kN of the hatch cover area which consists of the gravity force of the hatch cover and dynamic loading;
- effect from a load of P'_g = 50 kN distributed in the center (25x25 cm) of the hatch cover;
- effect from cyclic impact loads on the hatch cover, the numerical values of which equal 500; and
- fall of 150-kg freight on the hatch cover from a height of 3 m.

The calculations conducted demonstrated that when 150-kg freight fell on the hatch cover from a height of 3 m, the maximum

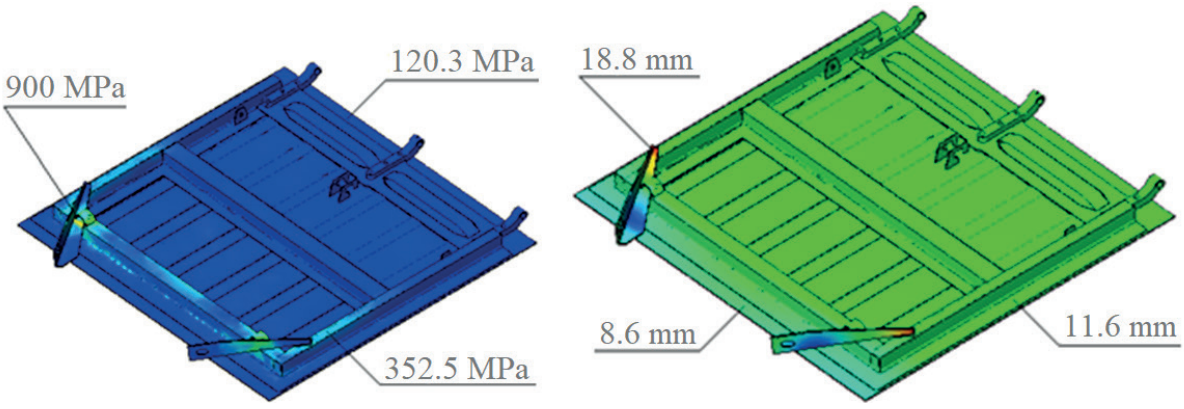

Figure 2 *Results of the strength calculation for the hatch cover of an open wagon when 150-kg freight falls on the hatch cover from a height of 3 m, a - stress state, b - displacements in the units*

equivalent stresses appeared in the locking supports and equaled approximately 900 MPa (Figure 2a), the maximum displacements in the structural units were fixed at the locking supports and equaled 18.8 mm (Figure 2b), the maximum strains were $1.72 \cdot 10^{-2}$. Thus, at a given loading diagram the strength of the hatch cover was not provided [15-17].

At other basic loading diagrams, the strength values of the hatch cover were within the admissible ones.

For improved strength research of the hatch cover of an open wagon the additional diagrams of possible loads in operation were considered:

1) simulation of the hatch cover opening while unloading the freight - non-torsion (without consideration of operation of torsion(s)) and non-simultaneous (at first for one of the supports) impact of the hatch cover against the supports of the intermediate beams of the wagon frame with the maximum opening angle;
2) simulation of the hatch cover opening while unloading freight - non-torsion (without consideration of operation of torsion(s)) and simultaneous impact of the hatch cover against supports of the intermediate beams of the wagon frame with the maximum opening angle;
3) non-simultaneous opening of the hooks - the hatch cover of the loaded wagon rests on one hook and one support (with one hook open and one closed); and
4) tightening (closing) of the hatch cover of an unloaded wagon with force.

The calculations conducted showed that at a non-torsion non-simultaneous impact against the supports of the intermediate beams of the wagon frames the maximum equivalent stresses on the hatch cover appeared at the hinge and equaled approximately 400 MPa; the maximum displacements in the structural units were fixed in the corners of the hatch cover from the locking supports and were approximately 11.7 mm; the maximum strains were $2.6 \cdot 10^{-3}$.

For non-simultaneous opening of the hooks of the hatch cover the maximum equivalent stresses appeared in the hinges, diametrically placed to the locking supports, the mechanism of which was closed; they equaled approximately 400 MPa. The maximum displacements in structural units were detected in the area of the locking supports, whose mechanism was closed; they equaled approximately 11.5 mm, the maximum strains were $7.6 \cdot 10^{-3}$.

At other additional loading diagrams the strength values for the hatch cover were within the admissible ones.

In order to provide strength of the hatch cover the authors proposed essentially new structures (Figure 3).

The design description of a polymaterial framing of variant I for the hatch cover with standard fastenings (Figure 3a):

- plane of the hatch cover consisted of the upper and lower sheets with the gap of elastic (viscous-elastic) substance;
- the upper 2.5-mm corrugated sheet;
- the lower 2.5-mm corrugated sheet. The corrugations reflected the upper sheet on the admissible sections;
- framing was made with an E-shaped profile of a 5-mm curved sheet filled with elastic (viscous-elastic) substance along the perimeter and in the middle of the hatch cover. Its height was adopted for installation of standard fastening elements on the cross beam and lower framing of an open wagon;
- hinges of the hatch covers (elements interacting with the center sill) were welded on the hatch cover (not riveted); and
- fastening supports to the lower framing of the side walls of a standard structure.

A feature of the hatch cover in variant II was the structure of the two horizontal sheets with a substance of elastic-viscous damping characteristics in between. The framing of the hatch cover was of E-shaped profile (Figure 3b) curved of a sheet and filled with an elastic (viscous-elastic) substance along the perimeter and in the middle part of the hatch cover. Its height was adopted for mounting standard fastening elements to the center sill and the lower framing of an open wagon. The hinges of the hatch cover (elements that interact with the center sill) were welded on the hatch cover (not riveted) and the supports were mounted to the lower framing of the side walls of a standard structure.

Variant III of the hatch cover was characterized by the coating made of a plain sheet (Figures 3c, 3d) of a convex configuration (pre-loaded), to provide the adequate strength at impact loading. Besides, the hatch cover framing was filled with a viscous substance of damping characteristics.

The variants of the hatch cover for open wagons proposed were designed for strength at the basic and additional loading

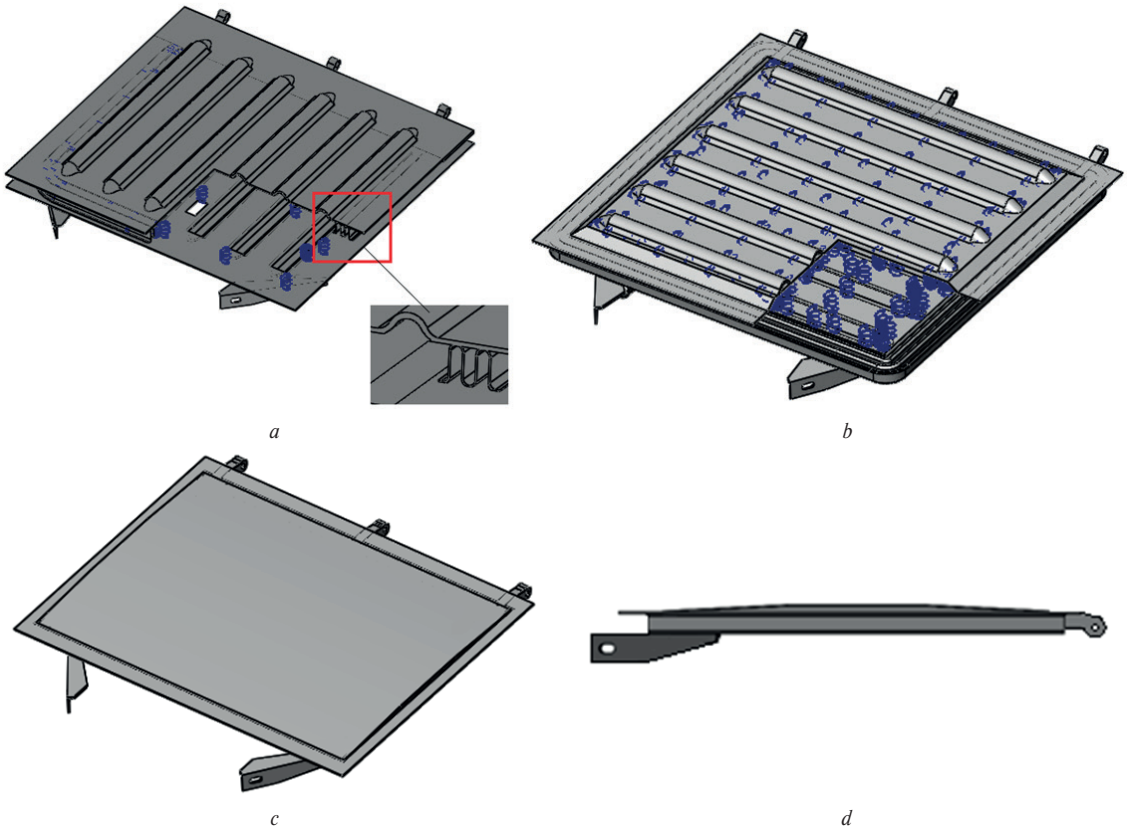

a *b* *c* *d*

Figure 3 *The improved structures of the hatch covers, a - variant I, b - variant II, c and d - variant III*

diagrams mentioned above. The results of the calculation are given in Table 1. The maximum loading of the hatch covers proposed could be observed when 15-kg freight fell on it from a height of 3 m and the strength of the hatch covers was provided [15-17]. Results of the strength calculations of the improved hatch covers at the least favorable diagram are given below.

The improved structures of the hatch covers were also calculated for reliability at the least favorable loading modes.

At a symmetric loading cycle the reliability of the hatch covers (in loading cycles) was determined by the safety factor of fatigue strength [18]:

$$N = N_0 \cdot n^m, \tag{1}$$

where
N_o is the test base;
n is the safety factor of fatigue strength;
m is the parameter of a fatigue curve.

$$n = \frac{\sigma_{-1}}{\sigma_a}, \tag{2}$$

where
σ_{-1} is the endurance limit, MPa;
σ_a is the amplitude stress, MPa.

$$m = \frac{\ln N_0 - \ln N}{\ln \sigma_a - \ln \sigma_{-1}}, \tag{3}$$

where N is the number of cycles before damage.

For steel the endurance limit values can be determined as:

$$\sigma_{-1} \approx (0,1 - 0,5) \cdot \sigma_{BP}, \tag{4}$$

where σ_{BP} is the strength limit, MPa;

Considering a non-symmetric loading cycle the hatch cover reliability was determined as:

$$N = N_0 \cdot \left(\frac{\sigma_{-1}}{\sigma_a + \psi_1 \cdot \sigma_m} \right)^m, \tag{5}$$

where σ_m is the average stress value, MPa;

ψ_1 is the variable, the numeric value of which can be determined as $\psi_1 = \frac{2 \cdot \sigma_{-1} - \sigma_0}{\sigma_0}$;

σ_0 is the endurance limit at the zero additional loading mode, MPa.

The calculations conducted for all the variants of improved hatch covers demonstrated that the adequate strength was provided.

5. Conclusions

From results of the research conducted the following conclusions can be made:

1. In order to provide the adequate operational strength of the hatch covers of a general-purpose open wagon the authors proposed some improvements.
2. Results of the strength calculation of improved hatch covers showed that strength values at basic and additional operational loading diagrams are provided.

Table 1 *Results of the strength calculations of the improved hatch covers*

Loading diagrams	Maximum equivalent stresses, MPa			Displacements in the structural units, mm			Deformations		
Basic	I	II	III	I	II	III	I	II	III
effect from the uniformly distributed load across the hatch cover area	150	170	140	13	7	14	$5.34 \cdot 10^{-1}$	$1.2 \cdot 10^{-1}$	$1.61 \cdot 10^{-3}$
effect from the distributed load on the center (25x25) of the hatch cover	130	140	130	10	4	10	$6.87 \cdot 10^{-3}$	$7.91 \cdot 10^{-3}$	$1.14 \cdot 10^{-3}$
drop of 150-kg freight on the hatch cover from a height of 3 m	220	220	220	13	7	13	$5.91 \cdot 10^{-1}$	$1.18 \cdot 10^{-1}$	$1.91 \cdot 10^{-3}$
Additional									
non-torsion non-simultaneous impact of the hatch cover on the supports of the intermediate beams of the frame	120	150	183.5	4	10	3.41	$8.5 \cdot 10^{-2}$	$3.4 \cdot 10^{-2}$	$1.24 \cdot 10^{-3}$
non-torsion simultaneous impact of the hatch cover against the supports of the intermediate beams of the frame	60	90	85.9	3	9	0.94	$6.7 \cdot 10^{-2}$	$2.68 \cdot 10^{-2}$	$7.06 \cdot 10^{-4}$
non-simultaneous opening of the hooks	200	200	214.2	14.4	9	17.9	$5.2 \cdot 10^{-1}$	$2.65 \cdot 10^{-2}$	$2.1 \cdot 10^{-3}$
tightening (closing) of the hatch cover of an unloaded wagon with force	75	100	6.3	5.1	9	0.36	$2.24 \cdot 10^{-2}$	$2.44 \cdot 10^{-2}$	$3.75 \cdot 10^{-5}$

3. The calculation for reliability of the improved hatch covers at symmetrical and non-symmetrical loading cycles was conducted. The results made it possible to conclude that for all the variants of improved hatch covers the reliability is provided.
4. Implementation of the proposed hatch covers for open wagons in operation can decrease the amount of damaged freight and encourage higher efficiency of open wagons.

References

[1] FOMIN, O., et al. Dynamic loading of the tank container on a flat wagon considering fittings displacement relating to the stops. *MATEC Web of Conferences* [online]. 2018, **234**(2), 05002. ISSN 2261-236X. Available from: https://doi.org/10.1051/matecconf/201823405002

[2] GORBUNOV, M., et al. New principle schemes of freight cars bogies. *Manufacturing Technology* [online]. 2018, **18**(2), p. 233-238. ISSN 1213-2489/ISBN 978-80-7414-325-0. Available from: https://doi.org/10.21062/ujep/83.2018/a/1213-2489/MT/18/2/233

[3] PUTIATO, A. V. Modelling of stress-strain state of the hatch cover of an open wagon when part of freight drops on it. Simulation of the stress-strain state of the gondola cover when falling pieces of cargo. Mechanics. Research and teaching materials. 2011, **5**, p. 113-122.

[4] FOHR, J., et al. Metal and composite intermodal containers in comparative cold tests with wood chips. *Journal of Sustainable Bioenergy Systems* [online]. 2015, **5**(01), p. 32-39. ISSN 2165-400X/eISSN 2165-4018. Available from: https://doi.org/ 10.4236/jsbs.2015.51003

[5] LOVSKA, A. A. Peculiarities of computer modeling of strength of body bearing construction of gondola car during transportation by ferry-bridge. *Metallurgical and Mining Industry* [online]. 2015, **1**, p. 49-54. ISSN 2076-0507/eISSN 2078-8312. Available from: http://www.metaljournal.com.ua/assets/Journal/english-edition/MMI_2015_1/10%20Lovska.pdf

[6] FOMIN, O. V., et al. The influence of implementation of circular pipes in load-bearing structures of bodies of freight cars on their physico-mechanical properties. *Scientific Bulletin of National Mining University*. 2017, **6**(162), p. 89-96. ISSN 2071-2227/eISSN 2223-2362.

[7] FOMIN, O.V. Modern requirements to carrying systems of railway general-purpose gondola cars. *Metallurgical and Mining Industry*. 2014, **5**, p. 31-43. ISSN 2076-0507.

[8] OKOROKOV, A. M., et al. Research into a possibility to prolong the time of operation of universal semi-wagon bodies that have exhausted their standard resource. *Eastern-European journal of enterprise technologies* [online]. 2018, **3**(7)(93), p. 20-26. ISSN 1729-3774/eISSN 1729-4061. Available from: https://doi.org/10.15587/1729-4061.2018.131309

[9] MYAMLIN, S. V., KEBAL, I. U., KOLESNYKOV S. R.: Design review of gondola car. Science and transport progress (in Ukrainian). *Bulletin of the Dnepropetrovsk National University of Railway Transport*. 2014, **6**(54), p. 136-145.

[10] PRIYA DIVYA, G., SWARNAKUMAR, I. A. Modeling and analysis of twenty tonne heavy duty trolley. *International Journal of Innovative Technology and Research* [online]. 2014, **2**(6), p. 1568-1580. ISSN 2320-5547. Available from: http://www.ijitr.com/index.php/ojs/article/view/421/pdf

[11] DIZO, J., et al. Modification and analyses of structural properties of a goods wagon bogie frame. *Diagnostyka* [online]. 2019, **20**(1), p. 41-48. ISSN 1641-6414/eISSN 2449-5220. Available from: https://doi.org/10.29354/diag/99853

[12] MYAMLIN, S., et al. Research of friction indices influence on the freight car dynamics. *TEKA. Commission of Motorization and Energetics in Agriculture* [online]. 2013, **13**(4), p. 159-166. Available from: http://eadnurt.diit.edu.ua/bitstream/123456789/2160/1/159-166.pdf

[13] WOJCIK, K., et al. Multi-body simulations of railway wagon dynamics. *Journal of KONES. Powertrain and Transport* [online]. 2012, **19**(3), p. 499-506. ISSN 1231-4005/eISSN 2354-0133. Available from: https://doi.org/10.5604/12314005.1138164

[14] HAUSER, V., et al. Impact of wheelset steering and wheel profile geometry to the vehicle behavior when passing curved track. *Manufacturing Technology*. 2017, **17**(3), p. 306-312. ISSN 1213-2489/ISBN 978-80-7414-325-0.

[15] GOST UA 7598:2014. Freight wagons. General requirements for the calculation and design of new and upgraded rail wagons 1520 mm (non-self-propelled) (in Ukrainian). 2015.

[16] GOST 33211-2014. Freight wagons. Requirements for strength and dynamic qualities (in Russian). Moscow, 2016.

[17] EN 12663-2. Railway applications - structural requirements of railway vehicle bodies. Part 2: Freight wagons.

[18] USTYCH, P. A., KARPYCH, V. A., OVECHNYKOV, M. N.: *Reliability of rail non-tractive rolling stock* (in Russian). Moskow, Variant, 1999.

Miroslav Pavelek - Pavol Spanik - Michal Frivaldsky*

VOLTAGE STRESS REDUCTION ON COMPENSATION CAPACITORS OF WIRELESS CHARGING SYSTEMS FOR TRANSPORT AND INDUSTRIAL INFRASTRUCTURE

The paper deals with a proposal for circuit configuration of series-series (SS) compensated wireless power transfer (WPT) system with reduced voltage stresses on compensation capacitors. Nowadays, a huge effort is given for the development of reliable, efficient and robust wireless charging systems and therefore the circuit configuration and component selection are crucial to meet suitable operational characteristics. For this purpose, the current trends in WPT systems are outlined in the first section. Next, the analysis of frequently utilized WPT system configuration is provided and the most critical issues related to practical utilization are discussed. Consequently, the proposal of how to eliminate negative aspects is given. All theoretical statements are supported by mathematical apparatus of the proposed system and consequently by the simulation analysis.

Keywords: *wireless power transfer, resonance, capacitor, voltage stress*

1. Introduction

Development of power electronics in last decades enables the massive rise of consumer and industrial electronic devices. Together with this rise, the autonomy of electronics becomes also very important. This means that self-operation without the necessity of component supplement with grid electricity acts as a major feature how to become independent. The way of such realization is the utilization of energy storage systems like accumulators or super capacitors. Nowadays, almost in every application, the usage of long-durability accumulators is necessarily inevitable (cell-phones, laptops, lighting, biomedical, etc.) [1-3]. Current trends in energy recharge are still mostly based on the wired chargers, but the wireless power transfer (WPT) is increasingly getting into the forefront of technology when talking about advanced charging systems [4-5].

IPT (inductive power transfer), as well as CPT (capacitive power transfer), are the most pervasive methods used for wireless charging [6-8]. IPT is most common and is applicable to many power levels and gap distances. CPT is only applicable for power transfer with inherently small distances. There are also various requirements for main circuit configuration e.g. configuration of resonant compensation network etc. This affects the system transfer characteristics and electrical behavior of key circuit components [9-10]. It is now well known that series-series compensation is the most suitable for the wide spectrum of practical applications. However, one disadvantage is typical and must be carefully considered, it is voltage stress of compensation capacitors. This voltage stress is several times higher (it depends on the operational quality factor) against the supply voltage. For that reason, the structural design of optimal compensation capacitor is quite a difficult issue. A possible way is to use either a special high-voltage capacitor which is very expensive or series-parallel connection of several capacitors even with high-voltage sustainability. This can be a limiting factor for many applications especially when the cost comes into account.

This paper proposes a solution for SS compensation system with reduced voltage stress of compensation capacitors. Given recommendations are initially expressed by the mathematical apparatus, while dependencies of critical variables (compensation capacitor voltage) are identified. The principal operation of system proposal is then verified by the simulation model with high level of validity.

2. Series-series resonant compensated WPT system

The equivalent circuit of the WPT system with resonant compensation configured in series-series topology is shown in Figure 1. The compensation capacitors C_1 and C_2 are connected to the primary and the secondary coil in series. Based on this, the resonant tank acts as a band-pass filter with relatively good selectivity.

It is generally known that to maximize the output power, both parasitic resistances (R_1 and R_2) must be minimized as much as possible [11]. To evaluate the behavior of the system, the basic circuit analysis was performed. The simulation parameters are taken from two identical experimental prototypes of coupling coils. Their values are therefore the same on the primary and the secondary side. The principal design procedure has been already described in [12-13], therefore it won´t be discussed here more in detail. The self-inductances are equal to L_1=L_2=127.4 μH, parasitic resistances are R_1=R_2=0.447 Ω and the load is R_L=30 Ω. The operational frequency range is set according to the main resonant frequency (f_{range}=290 kHz÷340 kHz). Both compensation capacitors have also the same capacity C_1=C_2=2 nF.

* **Miroslav Pavelek, Pavol Spanik, Michal Frivaldsky**
Department of Mechatronics and Electronics, Faculty of Electrical Engineering and Information Technology, University of Zilina, Slovakia
E-mail: michal.frivaldsky@fel.uniza.sk

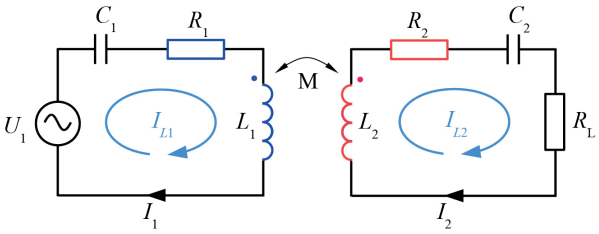

Figure 1 *The equivalent circuit of WPT with series-series resonant compensation*

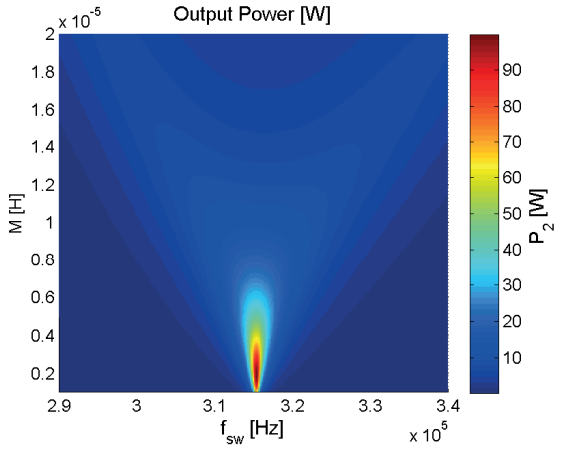

Figure 2 *Power delivered to the load in case of resonant coupling with series-series compensation*

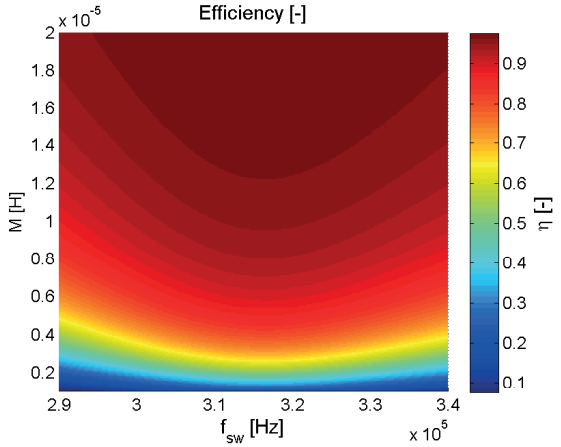

Figure 3 *Transmitting efficiency in case of resonant coupling with series-series compensation*

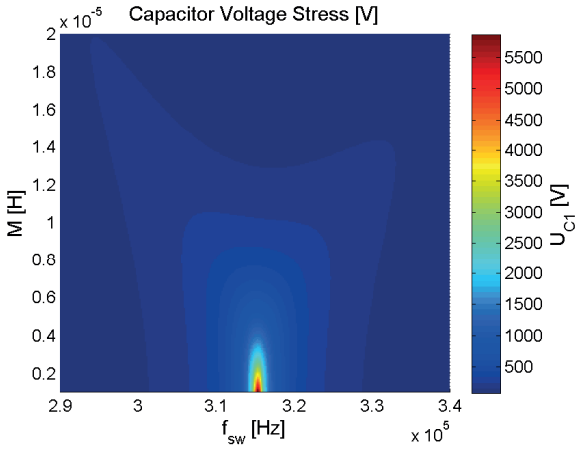

Figure 4 *The voltage on the compensation capacitor C_1 for standard SS WPT system*

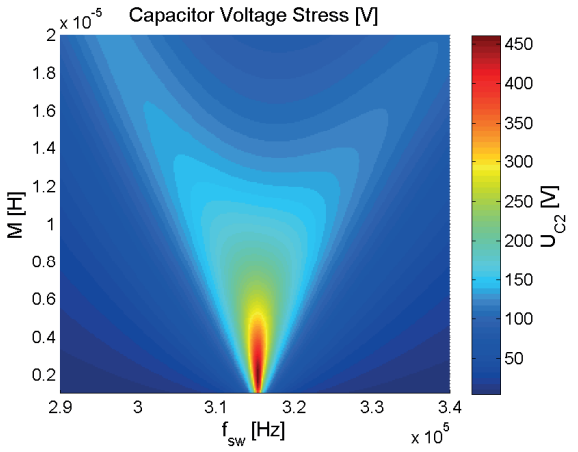

Figure 5 *The voltage on the compensation capacitor C_2 for standard SS WPT system*

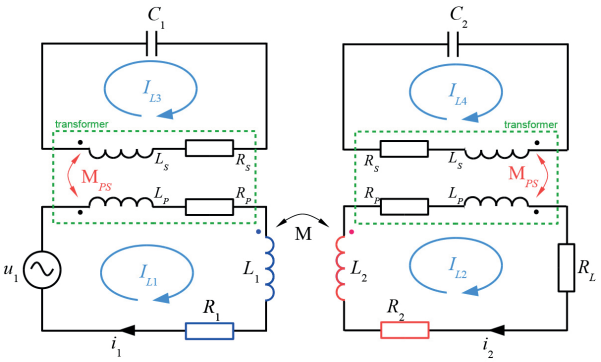

Figure 6 *The equivalent circuit of WPT with series-series resonant compensation and reduced voltage stress on compensation capacitors*

In the simulation, the minimal mutual inductance M_{min}=1 μH corresponds to the transmitting distance 55 cm while its maximal value M_{max}=20 μH represents the distance 10 cm. Simulated distance range was chosen according to requirements for battery charging of electrical vehicles, i.e. for the transportation systems.

Power delivered to the load and the resulting efficiency is seen in Figures 2 and 3. The figures are constructed (using MATLAB) as follows. The operating (switching) frequency is given in x-axis while the y-axis represents the various mutual inductance. It is therefore, a 3D interpretation of particular quantities expressed as a function of two variables.

Based on this, it is clear that the operation of the system can be ensured under various conditions. It depends on the target application and actual system conditions whether high power and mid-range efficiency or very high efficiency and mid-range power are required. Mentioned parameters are strictly dependent on the optimal load (value of R_L) of the WPT system, which is for individual cases different and must be therefore exactly identified [13].

$$\begin{bmatrix} \hat{U}_1 \\ 0 \\ 0 \\ 0 \end{bmatrix} = \begin{bmatrix} \left\{ \begin{matrix} R_1 + R_P + \\ j\omega(L_1 + L_P) \end{matrix} \right\} & -j\omega M & -j\omega M_{PS} & 0 \\ -j\omega M & \left\{ \begin{matrix} R_P + R_2 + R_L \\ j\omega(L_1 + L_P) \end{matrix} \right\} & 0 & -j\omega M_{PS} \\ -j\omega M_{PS} & 0 & \left\{ \begin{matrix} R_S - \\ j\frac{1}{\omega C_1} + j\omega L_S \end{matrix} \right\} & 0 \\ 0 & -j\omega M_{PS} & 0 & \left\{ \begin{matrix} R_S - \\ j\frac{1}{\omega C_2} + j\omega L_S \end{matrix} \right\} \end{bmatrix} x \begin{bmatrix} \hat{I}_{L1} \\ \hat{I}_{L2} \\ \hat{I}_{L3} \\ \hat{I}_{L4} \end{bmatrix} \tag{1}$$

$$f_o = \frac{1}{2\pi\sqrt{L_S C_{1,2}}},\ L_S = \frac{L_P}{n^2} \tag{2}$$

$$\begin{aligned} U_{C1} &= \left| \frac{\left[R_2 + R_L + j\left(\omega L_2 - \frac{1}{\omega C_2} \right) \right] \hat{U}_1}{\left[R_1 + j\left(\omega L_1 - \frac{1}{\omega C_1} \right) \right] \cdot \left[R_2 + R_L + j\left(\omega L_2 - \frac{1}{\omega C_2} \right) \right] + (\omega M)^2} \right| \cdot \frac{1}{n\omega C_1}, \\ U_{C2} &= \left| \frac{j\hat{U}_1 \omega M}{\left[R_1 + j\left(\omega L_1 - \frac{1}{\omega C_1} \right) \right] \cdot \left[R_2 + R_L + j\left(\omega L_2 - \frac{1}{\omega C_2} \right) \right] + (\omega M)^2} \right| \cdot \frac{1}{n\omega C_2}. \end{aligned} \tag{3}$$

Figures 4 and 5 show the voltage stress of particular compensation capacitors (C_1, C_2). It can be seen that even for the very low value of supply voltage (in this case 30 V), the peak voltage at each component is several times higher than the supply voltage. The situation is most critical when the system operates at a resonant frequency, or at its close range and also when the low value of mutual inductance is formed by high operational distance. Carefully designed capacitor structure and its physical configuration is therefore the most difficult issue [14-17].

3. WPT system with reduced voltage stresses on compensation capacitors

As previously mentioned, most limiting factor for practical use of S-S compensated WPT system is high voltage stress on compensation capacitors. A possible way how to solve this problem is to use either an appropriate series-parallel connection of discrete capacitors with the required value of capacitance and voltage sustain level or special high voltage capacitors which are usually very expensive [18-19]. Another possibility is to lower the coils' inductance which reduces the overall stress voltage across the resonant tank. This solution may debase the value of the coil's quality factor and consequently shorten the usable distance range.

Figure 6 shows proposed resourceful circuit modification which significantly reduces voltage stress on compensation capacitors. The solution uses ordinary components and is therefore cheaper. The system may be sufficiently described by the loop current method as seen in Equation (1). It is considered that the variables marked with ^ are considered as peak values.

Both compensation capacitors are replaced with a combination of capacitors and transformers whose secondary circuits are tuned at the resonant frequency given in Equation (2). The system behavior is quite sensitive to the selection of primary inductance *Lp* and transformer voltage ratio *n*. Its leakage inductance must be minimized as much as possible.

With the simplification of (1) in the way the transformers are considered as ideal with voltage ratio *n*, we may derive a general equation for voltages on compensating capacitors (3) in dependency on the frequency.

4. Frequency analysis of proposed system

In order to validate the proposed circuit solution, the system analyses have been done using Equation (1). The output power, transmitting efficiency and voltage stress on C_1 and C_2 corresponds to a voltage ratio of compensation transformer n=2.

The simulation parameters are same as used in the previous model and thus the self-inductance equals to L_1=L_2=127.4 μH, parasitic resistance is R_1=R_2=0.6 Ω and the load is R_L=30 Ω. The analyzed frequency range f_{range}=310 kHz÷320 kHz is not as wide as found in the previous case. Primary inductance of both compensation transformer on the transmitting and receiving side is set to L_P=10 μH. Secondary inductance is calculated from Equation (3), L_S=2.5 μH. The parasitic resistances on the secondary side of the compensation transformer plays an important role and was therefore minimized R_S=0.025 mΩ. Primary resistances are considered within resistances R_1 and R_2. Finally, compensation capacitors C_1 and C_2 were determined from Equation (4) and C_1=C_2=110 nH. Minimal mutual inductance is M_{min}=1 μH while its maximal value M_{max}=20 μH.

Simulation results for the low value of transformer ratio are shown on Figures 7-10. As mentioned before, frequency operational range became narrower which is obvious from all discussed results.

Principal aim for our modified S-S system is to reduce voltage stress on compensation capacitors. Compared to the standard solution the voltage (Figures 4 and 5) on the compensation capacitors is due to compensation transformer reduced up to 3-times (Figures 9 and 10) for individual operating regions.

On the contrary, it can be seen (Figure 8) that even low value of parasitic resistances measured on the secondary side

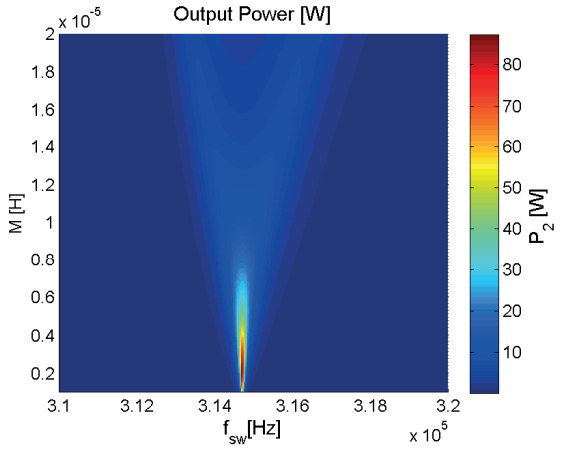

Figure 7 Power delivered to the load (n=2)

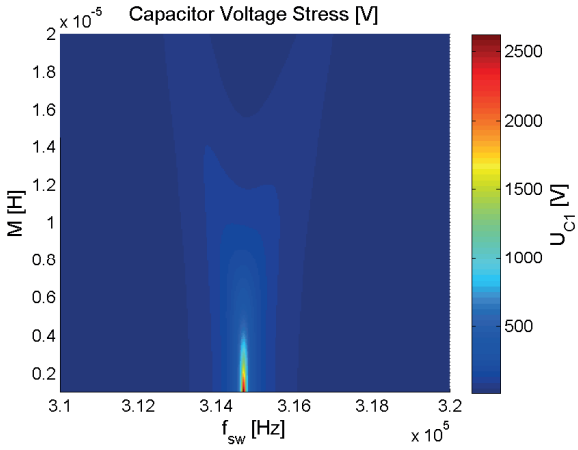

Figure 9 The voltage on the transformed (n=2) compensation capacitor C_1

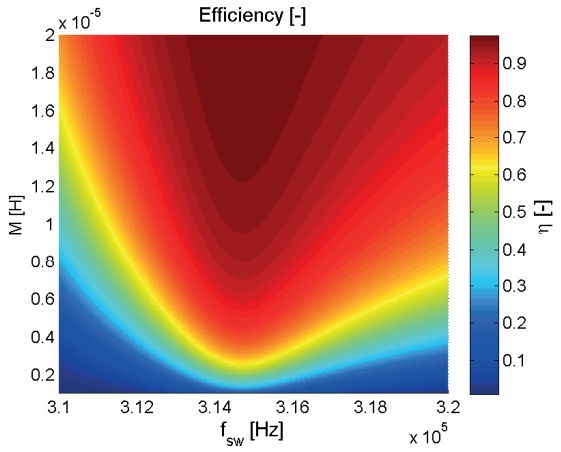

Figure 8 Transmitting efficiency (n=2)

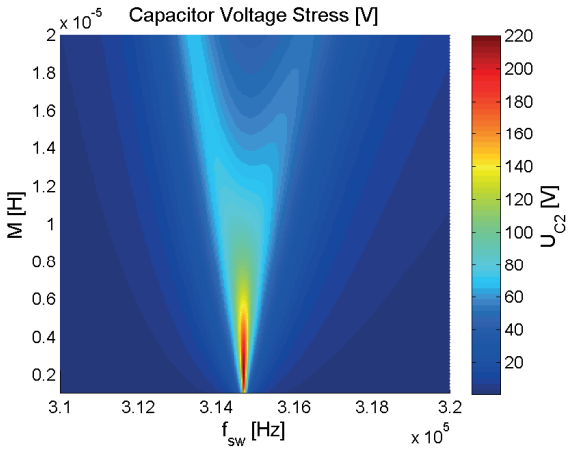

Figure 10 The voltage on the transformed (n=2) compensation capacitor C_2

of compensation transformers greatly influences transmitting efficiency. Similarly, to other variables, the frequency range became narrower whereby area with high efficiency (above 90%) became smaller as compared to Figure 3.

The previously described analysis of the proposed system behavior was further verified by the circuit simulation in time-domain, whose results are shown within the next chapter.

5. Simulation analysis of proposed system

The proposed circuit solution was verified also with the use of transient simulation (Figures 14 and 15) implemented as PSpice model. Figure 11 shows the full circuit configuration which is suitable for charging or supplying various devices in this case for demonstration lap-tops, tablets or LCD displays, but it is not explicitly excluded that the proposed methodology is suited just for this kind of application. All key circuit components are set according to the previous model described in section IV. i.e.:

- U_1=30 V
- L_1=L_2=127.4 µH
- R_1=R_2=0.6 Ω
- R_L=30 Ω.
- f_{range}=310 kHz÷320 kHz
- L_P=10 µH.
- L_S=2.5 µH.
- R_S=0.025 mΩ.
- C_1=C_2=110 nH.
- M_{min}=1 µH
- M_{max}=20 µH.

Only two mutual positions (mid-distance and maximal distance) of transmitting and receiving coils are simulated. The minimal considered distance is 25 centimeters which corresponds to the coupling coefficient between respective coils k=0.09 (M=11 µH). The maximal distance investigated is 55 cm which changes the coupling coefficient in k=0.04 (M=5 µH).

Investigation of the transfer properties of standard SS resonant WPT system and WPT system with compensation transformer were realized within frequency sweep analyses. It is obvious that for selected mutual positions the system reaches the maximal available power and efficiency precisely at the resonant point. This operating state is optimal for the transmitting power and the efficiency but in case of standard circuit configuration (Figure 1) it is highly stressful for the resonant capacitors (Figure 12), where maximum of the voltage stress is achieved for the resonant point of operation [10]. Similar situation but for the system with compensation transformer is shown in Figure 13. The maximal power delivery and efficiency are achieved again close to the resonant point, and capacitor voltage stress is at its peak, but compared to results from Figure 12, it is half of its value. It must be mentioned here, that the resonant points are different when standard and optimized WPT systems are considered. This is caused by the slightly different capacitor value when compensation transformer is considered, while its value is

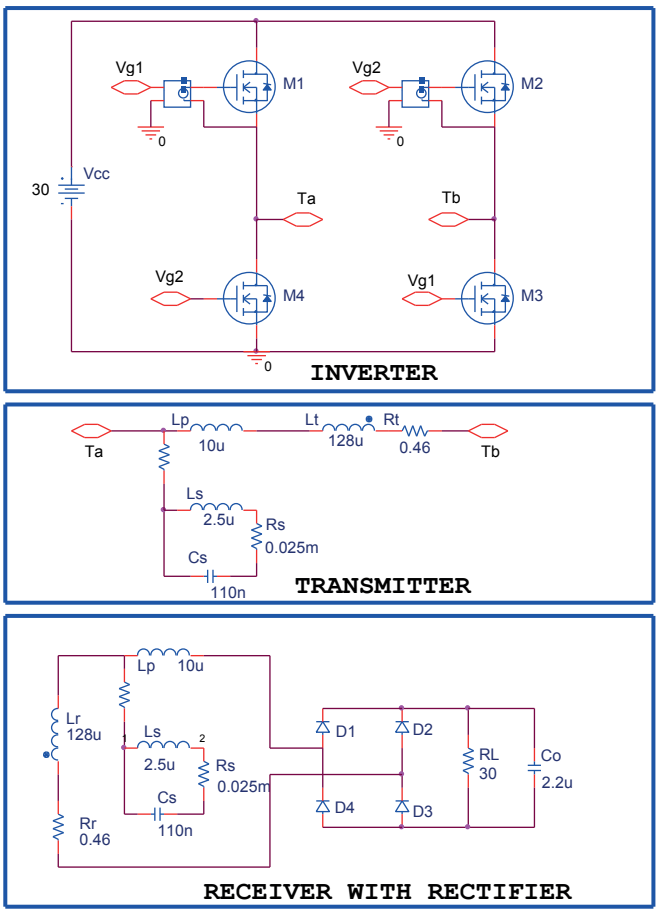

Figure 11 A simulation model of the proposed WPT system voltage on the transformed (n=2) compensation capacitor C1

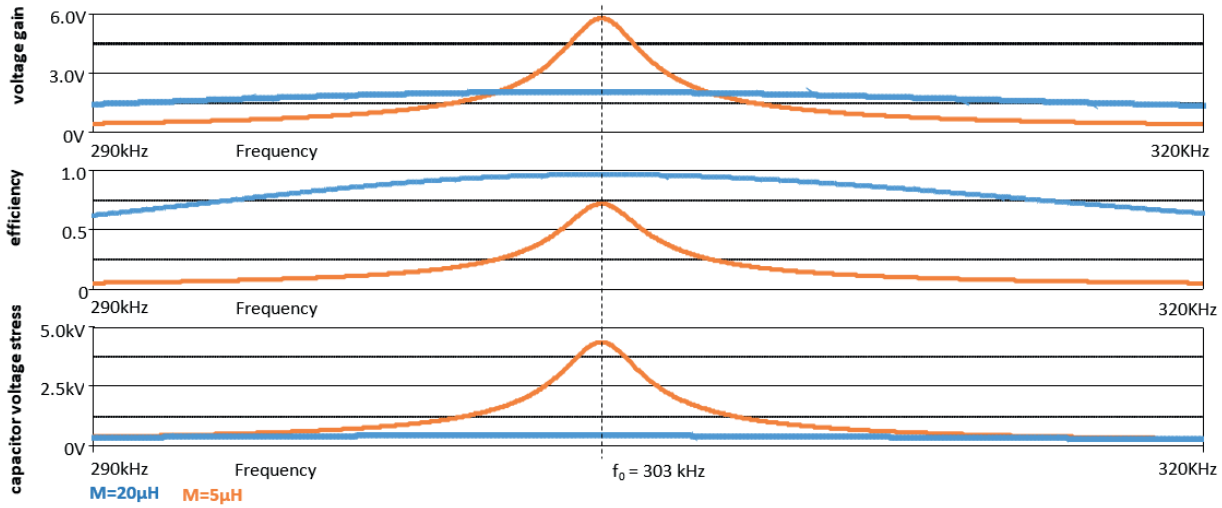

Figure 12 Transfer characteristic for standard SS resonant compensated WPT system (resonant point = 303 kHz)

dependent on the integer value of the number of compensation transformer turns.

On the other hand, the achievable power transfer was decreased from 110 W to 55W and efficiency from 80% to 65%. This was expected because of the existence of parasitic components of compensation transformer (parasitic resistances of windings, leakage inductance). Those must be decreased as much as possible that will be the main topic for the future works, which will be related to optimization works on the compensation transformers as well as on the experimental verifications of the system proposal.

Consequent simulation experiments have been done within time-domain (Figures 14 and 15), while the mutual distance between the transmitting and receiving side was considered for the situation, where M = 5 µH (distance = 55 cm). In comparison to the proposed compensation technique the voltage stress of

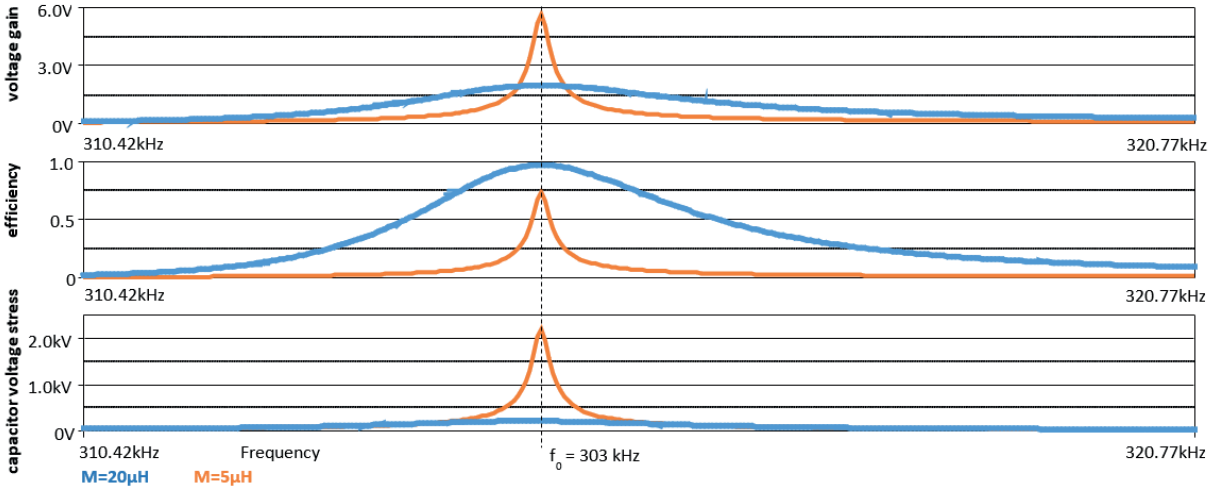

Figure 13 *Transfer characteristic for WPT system with compensation transformer (resonant point = 315 kHz)*

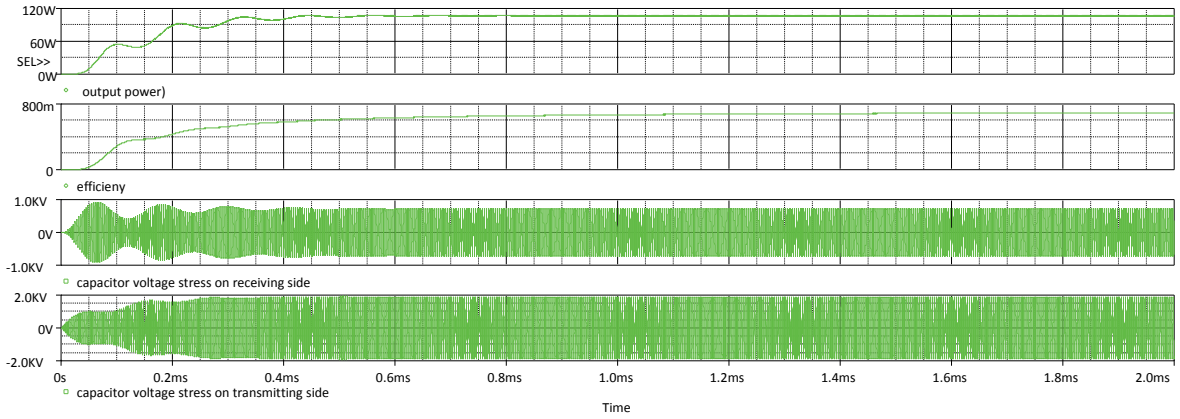

Figure 14 *Simulation results of WPT system without compensation transformer (standard SS compensated system) operated at the the resonant point*

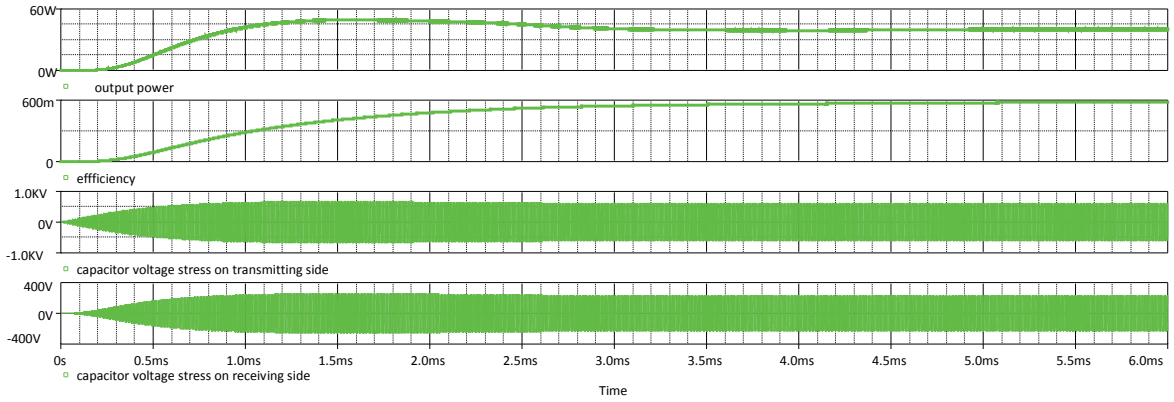

Figure 15 *Simulation results of WPT system with compensation transformer operated at the resonant point*

capacitors in the case of standard SS compensated WPT system is almost 4 times higher. Capacitor voltage stress for standard solution is around 2 kV for transmitting side, while for receiving side it is around 750 V (Figure 14). Proposed solution is acting as follows; transmitting side has voltage stress at the level of 600 V, while receiving side around 200 V (Figure 15).

6. Conclusion

In this paper, a new compensation technique for the resonant WPT system is presented. The simple design procedure is given, whereby the negative effect of individual circuit components is identified. The proposed solution significantly reduces the voltage stress of compensation capacitors. This is basically dependent on the design of the compensation transformer. Within proposed

system, reduction of the voltage stress was achieved up to 3-times lower compared to standard WPT system. Simulation clearly shows all fundamental advantages and disadvantages for further practical use. It was found that the proper design of the compensation transformer will be important issue for future works, thus it has the most significant impact on the whole system behavior while thinking about system efficiency and power delivering capability. Practically all investigated variables are influenced by the values of parasitic resistances on the transformer secondary side where high circulating current occurs. In other words, the higher transformer ratio enables to reduce voltage stress markedly, but on contrary it increases circulating secondary currents. Therefore, it is necessary to find out a suitable compromise that will meet all design requirements.

Future work will be focused on the practical verification of proposed solution and on its system optimization.

Acknowledgment

The authors wish to thank to Slovak National Grant Agency VEGA for the finnacial support within project Nr. 1/0119/18 - Research of the methodology for optimization of EMC of WPT systems, and for project Nr. 1/0547/18 - Research of the possibilities for system optimization of WPT systems.

References

[1] DAI, J., LUDOIS, D. C. A survey of wireless power transfer and a critical comparison of inductive and capacitive coupling for small gap applications. *IEEE Transactions on Power Electronics* [online]. 2015, 30(11), p. 6017-6029. ISSN 0885-8993 eISSN 1941-0107. Available from: https://doi.org/10.1109/TPEL.2015.2415253

[2] ZOSSAK, S., STULRAJTER, M., MAKYS, P. Self-Sensing Control of Pmsm at Zero and Low Speed . *Communications - Scientific Letters of the University of Zilina* [online]. 2018, **20**(1), p. 13-19. ISSN 1335-4205/eISSN 2585-7878. Available from: http://komunikacie.uniza.sk/index.php/communications/article/view/39

[3] HUI, S. Y. R., ZHONG, W., LEE, C. K. A critical review of recent progress in mid-range wireless power transfer. *IEEE Transactions on Power Electronics* [online]. 2014, **29**(9), p.4500-4511. ISSN 0885-8993/eISSN 1941-0107. Available from: https://doi.org/10.1109/TPEL.2013.2249670

[4] KINDL, V., KAVALIR, T., PECHANEK, R. Construction Aspects of System for Wireless Low Power Transfer on Moving Parts of Electric Machinery. *Communications - Scientific Letters of the University of Zilina* [online]. 2015, **17**(1A), p. 77-82. ISSN 1335-4205/eISSN 2585-7878. Available from: http://komunikacie.uniza.sk/index.php/communications/article/view/416

[5] GOVIC, G. A., BOYS, J. T. Modern trends in inductive power transfer for transportation applications. *IEEE Journal of Emerging and Selected Topics in Power Electronics* [online]. 2013, **1**(1), p.28-41. ISSN 2168-6777/eISSN 2168-6785. Available from: https://doi.org/10.1109/JESTPE.2013.2264473

[6] ZHAI, H., PAN., H. K., MINGYU, L. A practical wireless charging system based on ultra-wideband retro-reflective beamforming. In Antennas and Propagation Society International Symposium : proceedings. 2010. ISBN 978-1-4244-4967-5, p. 1-4.

[7] KAVALIR, T., et al. Upgrading of the single point laser vibrometer into a laser scanning vibrometer . *Communications - Scientific Letters of the University of Zilina* [online]. 2018, **20**(1), p. 61-66. ISSN 1335-4205/eISSN 2585-7878. Available from: http://komunikacie.uniza.sk/index.php/communications/article/view/47

[8] SUKJIN, K., et al. High-efficiency PCB- and package-level wireless power transfer interconnection scheme using magnetic field resonance coupling. *IEEE Transactions on Components, Packaging and Manufacturing Technology* [online]. 2015, **5**(7), p. 863-878. ISSN 2156-3950/eISSN 2156-3985. Available from: https://doi.org/10.1109/TCPMT.2015.2446613

[9] NOBILE, G., et al. Multi-criteria experimental comparison of batteries circuital models for automotive applications . *Communications - Scientific Letters of the University of Zilina* [online]. 2018, **20**(1), p. 97-104. ISSN 1335-4205/eISSN 2585-7878. Available from: http://komunikacie.uniza.sk/index.php/communications/article/view/54

[10] TOMMASO, A. O. D., GENDUSO, F., MICELI, R. A small power transmission prototype for electric vehicle wireless battery charge applications. In International Conference on Renewable Energy Research and Applications : proceedings [online]. 2012, p. 1-6. Available from: https://doi.org/10.1109/ICRERA.2012.6477432

[11] MUSAVI, F., EBERLE, W. Overview of wireless power transfer technologies for electric vehicle battery charging. *IEEE Transactions on Power Electronics* [online]. 2014, **7**(1), p. 60-66. ISSN 1755-4535/eISSN 1755-4543. Available from: https://doi.org/10.1049/iet-pel.2013.0047

[12] Kindl, V., et al. Transfer properties of various compensation techniques for wireless power transfer system including parasitic effects. *COMPEL - The International Journal for Computation and Mathematics in Electrical and Electronic Engineering* [online]. 2017, 36(4), p. 1198-1219. ISSN 0332-1649. Available from: https://doi.org/10.1108/COMPEL-04-2016-0143

[13] PIRI, M., et al. Wireless (power transfer) transmission of electrical energy (electricity) intended for consumer purposes up to 50 W. *Advances in Electrical and Electronic Engineering* [online]. 2016, **14**(1), p. 40-48. ISSN 1336-1376/eISSN 1804-3119. Available from: https://doi.org/10.15598/aeee.v14i1.1573

[14] SZABO, L., et al. Torque smoothing of a fault tolerant segmental stator switched reluctance motor. *Communications - Scientific Letters of the University of Zilina* [online]. 2015, **17**(1A), p. 95-101. ISSN 1335-4205/eISSN 2585-7878. Available from: http://komunikacie.uniza.sk/index.php/communications/article/view/419

[15] KIANI, M., GHOVANLOO, M. The circuit theory behind coupled-mode magnetic resonance-based wireless power transmission. *IEEE Transactions on Circuits and Systems I: Regular Papers* [online]. 2012, **59**(9), p. 2065-2074. ISSN 1549-8328. Available from: https://doi.org/10.1109/TCSI.2011.2180446

[16] JOLANI, F., YIQIANG , Y., CHEN, Z. Enhanced planar wireless power transfer using strongly coupled magnetic resonance. *Electronics Letters* [online]. 2015, **51**(2), pp.173-175. ISSN 0013-5194/eISSN 1350-911X. Available from: https://doi.org/10.1049/el.2014.4104

[17] AIELLO, G., et al. A high efficiency interleaved PFC front-end converter for EV battery charger. *Communications - Scientific Letters of the University of Zilina* [online]. 2018, 20(1), p. 86-91. ISSN 1335-4205/eISSN 2585-7878. Available from: http://komunikacie.uniza.sk/index.php/communications/article/view/52

[18] SOHN, Y.H., et al. General unified analyses of two-capacitor inductive power transfer systems: Equivalence of current-source SS and SP compensations. *IEEE Transactions on Power Electronics* [online]. 2015, **30**(11), p. 6030-6045. ISSN 0885-8993/eISSN 1941-0107. Available from: https://doi.org/ 10.1109/TPEL.2015.2409734

[19] CHO, S.Y., et al. Series-series compensated wireless power transfer at two different resonant frequencies. In ECCE Asia Downunder (ECCE Asia) : proceedings. 2013. ISBN 978-1-4799-0482-2, p. 1052-1058.

Vladimir Kindl - Miroslav Byrtus - Bohumil Skala - Vaclav Kus*

KEY ASSEMBLING ISSUES RELATING TO MECHANICAL VIBRATION OF FABRICATED ROTOR OF LARGE INDUCTION MACHINES

In many applications, where rotating machines of high power are used, high demands on reliability and safety are laid. Precise manufacturing procedures has to be kept even in case of machines retrofits when e.g. rotors are newly assembled. Even small inaccuracies or misguiding the precise technological procedure can lead to improper running of the machine and it can result in shut-down of complete drive. In case of primary circuits of nuclear power plants, it further means the shut-down of the whole power plant. Consequently, it results in significant financial losses (foregone profit and cost given by problem fixing). The paper presents a methodology of vibration origin investigation in case of large rotating machines which are part of drives like pump, compressors etc. The methodology is based on the detection of undesirable vibration using a diagnostic system on-site and further it uses mathematical modelling of corresponding mechanical parts to reveal the vibration origin. The modelling along with the measurement showed that the detected dangerous vibration is caused by misguided assembling of the rotor of the machine.

Keywords: *induction, machine, rotor, vibration, unbalance, assembling*

1. Introduction

Not only the industry but the whole today's society is virtually dependent on a continuous supply of electric energy. With the electricity our work is easier which increases the comfort of our lives and gives us a sense of safety. A smooth operation of power plant is therefore very important aspect for a successful and continuous development of our civilization.

Key function elements of conventional thermal, nuclear, and hydroelectric power plants are rotating electrical machines. Besides the power generator the power plant utilizes a large amount of supporting drives (conveyors, pushers, ...) and auxiliary systems (mills, pumps, ...), which together form a huge functional unit. Even a brief function drop-out of any auxiliary system may lead to incidental power plant downtime and thus the power outage.

The power plant operation puts very high operational demands on machines, especially in terms of wide range of dynamic loads. Therefore, it is very important to regularly monitor the vibration of the machines and perform any maintenance earlier than necessary and as planned. This is particularly relevant to large power machines whose rotors have a complicated structure.

One of the major properties of electric machine rotors is their mechanical stiffness [1-6]. Rotors must resist mechanical stress, which primarily comprises centrifugal forces, rotor vibrations, thermal dilatation and the interference press fit [7-12]. In addition to tangential forces producing the machine torque, rotors are also affected by electromagnetic forces in a radial direction [13-18]. These forces gain much higher amplitudes, but they are mutually cancelled [19-21] due to the symmetric mounting of the rotor. If this symmetry is destroyed, for instance, as a result of faulty balancing of the rotor or its eccentric mounting, a unilateral magnetic force occurs [22].

In motors of small dimensions, whose diameter hardly exceeds one meter, the rotor magnetic circuits can be punched from a single sheet. In such a case, the issue of clamping forces can be ignored [23-25]. With a segment layout of rotor laminations, the sufficient clamping force must be achieved by a design with a proper number of clamping bolts, their proper diameter and position taking into account the magnetic flux and saturation of the magnetic circuit.

Rotors of large diameters constitute a different situation. In this case, the number, size and location of the holes for clamping bolts are not critical. The size of the magnetic yoke makes the design trouble-free. The major problem, however, is the size of the mass rotating along the large diameter of the rotor. This leads to substantial centrifugal forces and to the necessity of large friction forces between the individual lamination segments. The necessary friction force is achieved by a large clamping pressure. The maximum value of the clamping force is predominantly limited by the stiffness in the area of ventilation ducts. If the clamping force is insufficient, the segments are loosened, which leads to an imbalance of the rotor. A small clamping force results in loosened ventilation sheets and their shift to the ventilation gap.

The aim of the article is to present a methodology of determining the source of vibration of large machines. The methodology is based on on-site vibration measurement and on analysis of related phenomena like rotor-stator dynamics, analysis of material stress and clamping force of the rotor packet. Other works relating to rotor vibration can be followed in [25-37].

In many applications, only the vibration measurement, which is usually part of a diagnostic system, is presented.

* **Vladimir Kindl, Miroslav Byrtus, Bohumil Skala, Vaclav Kus**
University of West Bohemia, Faculty of Electrical Engineering, RICE, Pilsen, Czech Republic
E-mail: vkindl@rice.zcu.cz

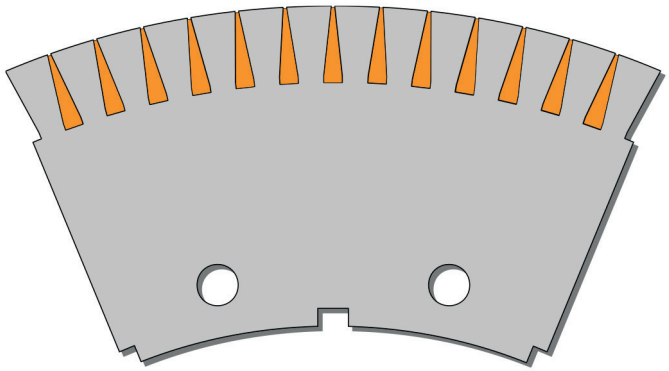

Figure 1 *Annular ring segment of a large asynchronous machine*

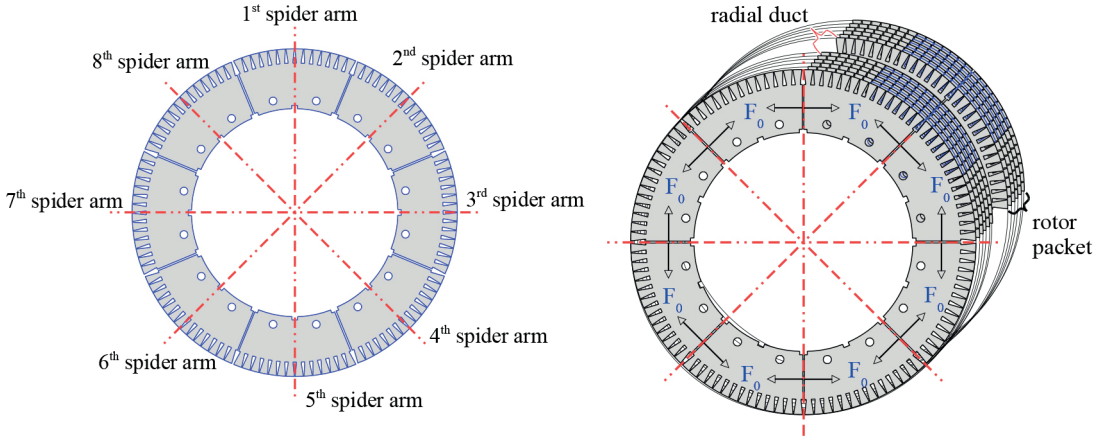

Figure 2 *Rotor packed mounted on the spider arms - odd lamination layer on the left side and even lamination layer on the right side*

The diagnostics can only determine whether the vibration is acceptable or not, since the methodology presented here goes behind and tries to propose a particular procedure for the vibration origin determination.

2. Rotor packet assembling design

A rotor stack is assembled by stacking up steel laminations (see Figure 1). In a steady-state, a magnetic flux with a slip frequency (fractions of Hz up to several Hz) passes through the rotor. However, during the rotor run-up or during a more significant load, the frequency is large and the iron core losses are higher. Therefore, a laminated structure of rotors is necessary.

A rotor stack with a diameter larger than one meter is assembled by stacking up annular segmented steel ring. All odd lamination layers are stacked to even lamination layers with a half overlap (see Figure 2). During assembling, the segments are put on the clamping bolts through the punched-out holes.

Rotor stack is constructed with diameter smaller than the diameter of the rotor spider. Then it is mounted on the rotor spider with an overlap achieved by heating up the lamination, or this method can be combined with super-cooling of the rotor spider with liquid nitrogen. This gives rise to significant radial force acting on the rotor even if it is stopped.

Figure 2 clearly shows that every even layer of lamination is forced to gape in the direction from the radial wedges on the spider arms. This is a serious design error which increases the peripheral stress of the lamination ring by the F_o force. The size of the segments is influenced by many factors [22]. The technological clearance between the sheets in one layer within the contact plane is usually around 0.5 mm. After compression with the relevant pressure, the rotor stack is clamped with clamping rings and bolts. The bolts must exert a sufficient clamping force, thus creating a pre-stressed bolted joint.

Apart from mechanical forces, other forces are also acting in the rotor, namely electromagnetic forces, dynamic forces and forces caused by thermal dilatation [22-24].

3. Requirements for bolts tightening torque

Loosening of a lamination segment is prevented by the friction force between the sheets which is exerted by the clamping pressure. This pressure is created by continuous pressure on the lamination stack as early as during the rotor manufacture. In order to prevent a drop in this pressure as a result of vibrations during the motor operation, the entire rotor pack is clamped with bolts, thus creating a pre-stressed bolted joint. The nuts on the bolts must be tightened with a relevant tightening torque and secured with a weld to prevent loosening.

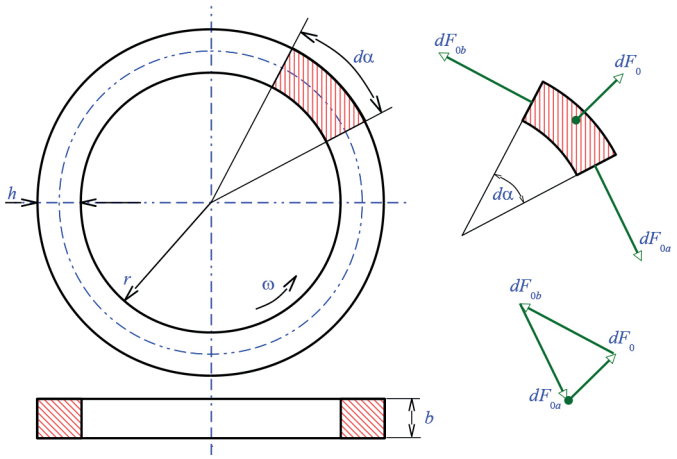

Figure 3 *Forces acting in rotating ring*

If the friction specified above is not sufficient, lamination segments are loosened and the bolts experience both tensile stress and bending stress. This has a negative impact on the rotor dynamics.

The allowable tightening torque of the bolts themselves is from the mechanical point of view many times greater, which means that the mechanical potentialities of bolts are not fully utilized. Their task is completely different - namely to ensure an even clamping pressure along the entire perimeter. According to the required clamping pressure, the number of clamping bolts is determined. However, although the clamping pressure must make the stack compact, it should not be too intense, as it could cause a collapse of ventilation spacers. The stack can be mounted onto the rotor spider in two ways.

First, by attachment with an interference press fit, where the clamping force between the spider arm and the rotor stack will ensure fixing in radial direction. The torque is transferred via tangential wedges because the clamping itself does not exert any additional friction force able to transfer the torque.

Second, by attachment without an interference press fit. Tangential wedges are used for the same reason as above. However, the pack is not secured in the radial direction. This paradoxically increases the need for a greater tightening torque of the bolts.

The large tightening torque is necessary in order to achieve the resistance of the pack to dynamic shocks. During the rotor operation, clearances sometimes occur as a result of various thermal dilatations of the spider arms and the rotor stack. If the structural clamp of the laminations is insufficient and their shift within the stack occurs, the rotor becomes unbalanced and vibrations occur. These vibrations are a further and much stronger source of dynamic forces, which then, in turn, affect the stack lamination (known as additive feedback). Therefore, the calculation of the tightening torque of bolts is the key factor affecting the reliability of operation of large rotors.

4. Analysis of clamping forces

Rotors of large rotating machines are usually operated at a constant speed. With respect to rotor stack dimensions, the effects of field of centrifugal forces cannot be neglected. Moreover, it is a significant source of mechanical loads. The magnitude of clamping force has to take into account the way how the stack segments are fixed to each other.

4.1 First insight calculation

Let us assume, the rotor rotates with an operational speed ω. Further let us suppose a ring with radius r and height h (see Figure 3). Let us consider an infinitesimal small element of mass dm wich corresponds with an angular sector which is given by angle da. The magnitude of the centrifugal force acting on the assumed element can be then expressed in following form

$$dF_o = \omega^2\left(r+\frac{h}{2}\right)dm \approx \omega^2 r^2 \rho b h d\alpha\,. \tag{1}$$

The effect of centrifugal dF_o has to be balanced by inner circumferential tensile forces F_{oa} and F_{ob}, which are of the same size. As for the size of the elementary force dF_o, the following must hold

$$dF_o = Fd\alpha\,. \tag{2}$$

Comparing Equations (1) and (2), one can arrive to the expression of the inner tensile force

$$F = \omega^2 r^2 \rho b h\,, \tag{3}$$

which causes inner tensile stress

$$\sigma = {}^{F}\!/_{bh} = \omega^2 r^2 \rho\,. \tag{4}$$

The centrifugal forces will cause the circumference of the revolving ring to increase. In order to calculate the relative lengthening, the Hook Law can be used, in which the following holds

$$\varepsilon = \frac{2\pi(r+\Delta r)-2\pi r}{2\pi r} = \frac{\Delta r}{r} = \frac{\sigma}{E} = \frac{\omega^2\rho}{E}r^2 \tag{5}$$

The increase in the radius of the rotating ring is expressed after rearrangements as follows

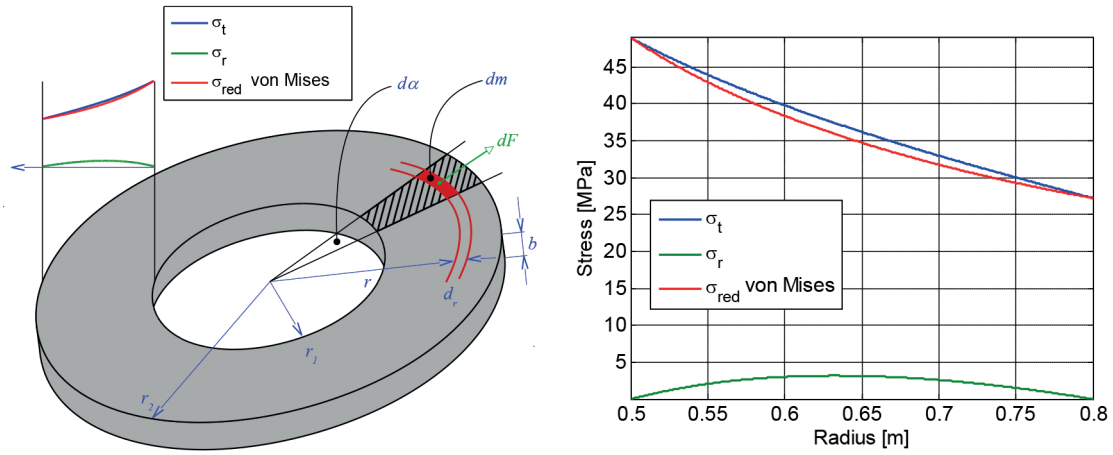

Figure 4 *Stress analysis of the rotating ring corresponding to the rotor packet*

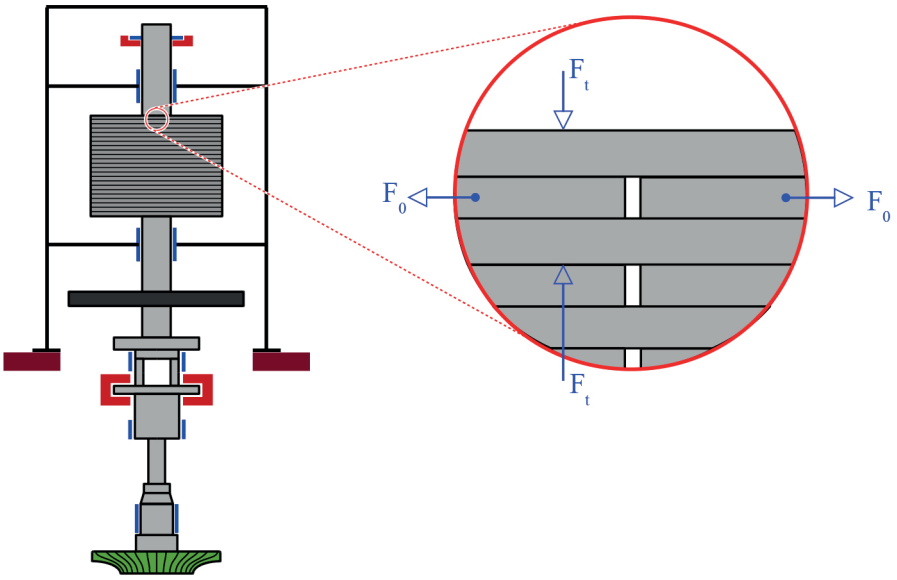

Figure 5 *Friction force and tensile force per partial lamination segments*

Table 1 *Tensile force*

Calculation approach	Tensile force [MN]	Tensile stress [MPa]
First inside approach	16.08	47
Using stress analysis	12.94 (integral value)	depends on the radial position
Data given by manufacturer	17.49	5.33

$$\Delta r = \frac{\omega^2 \rho}{E} r^3 . \tag{6}$$

This increase of the radius results in the decrease of the interference fit and the decrease in the clamping force across the spider arms.

4.2 Calculation using stress analysis

Further, the rotating rotor packet can be considered as a rotating ring loaded by centrifugal force F, which causes following two principal stresses

$$\sigma_r(r) = D_1 - \frac{D_2}{r_2} - (3+\nu)\frac{\rho\omega^2}{8} r^2, \tag{7}$$

$$\sigma_t(r) = D_1 - \frac{D_2}{r_2} - (1+3\nu)\frac{\rho\omega^2}{8} r^2, \tag{8}$$

where $\sigma_r(r)$ stands for radial stress and $\sigma_t(r)$ for tensile stress in the ring. These two quantities are dependent on the radial position r [37]. Considering the nominal speed of the investigated machine, the particular values of the stresses (see Table 1) are presented in Figure 4 along with the ring view. To determine the stresses, an infinitesimal element of the ring is used to formulate a general stress equilibrium. Details can be found in [37].

The manufacturer used an approach for clamping force determination which led to values presented in Table 2. The quantities seem to have inadequate values. They are insufficient to guarantee to compactness of the rotor during its operation.

Table 2 *Clamping force determination*

Calculation approach	Clamping force [kN]	Used bold capacity [%]
First inside approach	166.7	47
Using stress analysis	164.7	46.7
Data given by manufacturer	86.2	24.4

Figure 6 *Plastic distortion of the ventilation sheet (see the upper hole)*

5. Clamping pressure determination

As bolts must not be subjected to shear stress, the tensile force given by Equation (7) can be transferred by friction forces between lamination layers only. The friction coefficient between varnished sheets has usually a value of μ = 0.1. As the number of lamination layers is known, it is possible to determine the tensile force per one overlap of the layer (Figure 5).

The necessary clamping force is expressed as

$$F_T = \frac{2F_O}{\mu}, \tag{9}$$

and the corresponding clamping pressure as

$$p = 2\frac{F_T}{S_S}, \tag{10}$$

where S_s signifies the surface area of one lamination segment.

The tightening torque allowed across the M_{36} bolt is M_{36}=2456 Nm, which would exert the clamping force F_{36}=352.87 kN in the bolt. The bolts capacity that will be used, can be determined as

$$\eta_{36} = \frac{F_T}{F_{36}} \tag{11}$$

6. Stress analysis of a rotor packet segment in centrifugal force field

After rotor disassembling, a distortion of the ventilation sheets has been found (Figure 6). To investigate where the origin of the distortion is, a limit case has been considered, i.e. it has been assumed that the ventilation sheet is not fixed by clamping force and is loaded by the field of centrifugal forces.

This case was modelled by finite element model and the stress analysis was performed. From the results, it can be seen that, if there is almost none clamping force, a radial shift of laminations and a plastic distortion around the bolt occur. Figure 7 clearly shows that in the critical areas, the stress exceeds the value yield strength.

7. Eccentricity due to rotor packet segment sliding

Based on the finding presented above, the mechanism of eccentricity is caused by rotor segment sliding due to insufficient rotor packet clamping. As presented in Figure 8, there are two possibilities of the segment releasing: the first comprises two segment releasing (Figure 8 left), the second lies in releasing of three segment (Figure 8 right). These two mechanisms are coupled and arise mutually.

The resulting value of imbalance of the rotor packet was determined based on the estimate of the shift of the segments. The shift is supposed to be 1mm radially into the ventilation gap of the machine.

8. Vibration source detection in a circulating pump drive

The objective was to design the model of the machine in such a way that it could be used to determine the size of vibrations. Here the source of vibrations is the loosening of several segments and their radial shift leading to an imbalance. This imbalance is further affected by a unilateral magnetic pull which causes a further increase in vibrations. The model must be able to simulate an arbitrary imbalance in any spot of the rotor (see Figure 3). The model takes into account the basic properties of a stator as well.

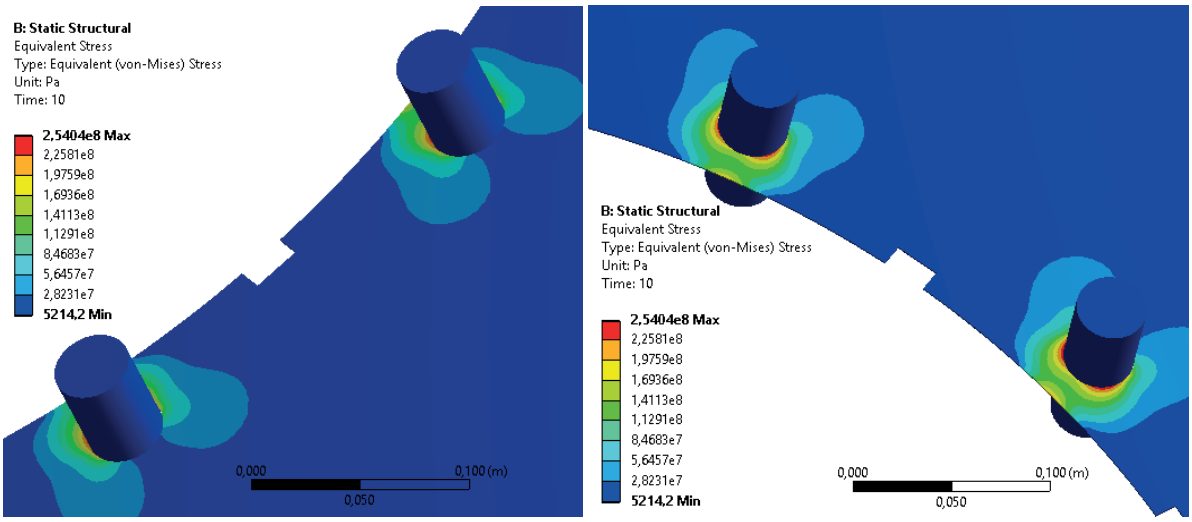

Figure 7 *Simulation of the stress applied to the ventilation sheet due to centrifugal forces*

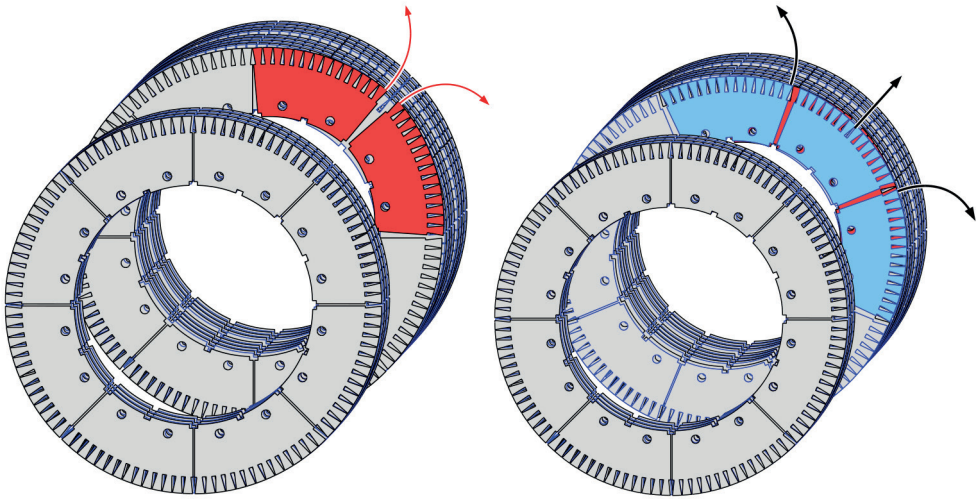

Figure 8 *The mechanism of eccentricity origin - even and odd segments releasing*

8.1 Dynamical model of the drive for vibration analysis

The mathematical model of the rotor can be generally expressed in a matrix form in a non-rotating coordinate system

$$\boldsymbol{M}_R\ddot{\boldsymbol{q}}_R+(\omega\boldsymbol{G}_R+\boldsymbol{B}_R)\dot{\boldsymbol{q}}_R+(\boldsymbol{C}_R+\boldsymbol{K}_R)\boldsymbol{q}_R=\boldsymbol{f}_R(t), \tag{12}$$

where the matrix $\boldsymbol{M}_R$ represents the mass matrix, $\omega\boldsymbol{G}_R$ represents the gyroscopic effect matrix, $\boldsymbol{B}_R$ the damping matrix, $\boldsymbol{C}_R$ the circulation matrix and $\boldsymbol{K}_R$ the rotor stiffness matrix. The vector $\boldsymbol{q}_R$ corresponds to the vector of generalized coordinates defining the configuration space in which the mathematical model is created. The vector $\boldsymbol{f}_R(t)$ defines the external load of the rotor. The matrices listed above are obtained through the finite element method. The shaft is considered to be a one-dimensional continuum if the Euler-Bernoulli theory is adopted assuming that the cross-section area of the shaft is not distorted and remains perpendicular to the distorted axis of the shaft. This assumption can be employed in case of small distortions. Here the influence of the circulation matrix is ignored.

When modelling the rotor of an electric motor, the torsional and bending stiffness of the lamination pack is taken into account. The pack is divided into a suitable number (namely 6) of stiff discs, among which the torsional and bending stiffnesses are considered. The discs are mounted at the corresponding discretization nodes of the rotor.

The mathematical model of the rotor was further supplemented with the model of the stator so that it was possible to simulate the vibration of the stator as a result of the imbalance on the rotor [23-31]. Similarly, with respect to the rotor model, the mathematical model of the stator can generally be expressed in the matrix form

$$\boldsymbol{M}_S\ddot{\boldsymbol{q}}_S+\boldsymbol{B}_S\dot{\boldsymbol{q}}_S+\boldsymbol{K}_S\boldsymbol{q}_S=\boldsymbol{f}_S(t), \tag{13}$$

where the $\boldsymbol{M}_S$ represents the mass matrix, $\boldsymbol{B}_S$ stands for the damping matrix and $\boldsymbol{K}_S$ the stator stiffness matrix. The vector $\boldsymbol{q}_S$ corresponds to the vector of generalized coordinates defining the configuration space in which the mathematical model is created. As the stator is considered to be a rigid body fixed to the frame flexibly, the vector of the generalized coordinates is $\boldsymbol{q}_S=[x,y,z,\varphi_x,\varphi_y,\varphi_z]^T$, where the listed coordinates define the deflections of the stator centre of mass and its angular deflections the relevant coordinate axes. The vector $\boldsymbol{f}_R(t)$ defines the external load of the rotor. The

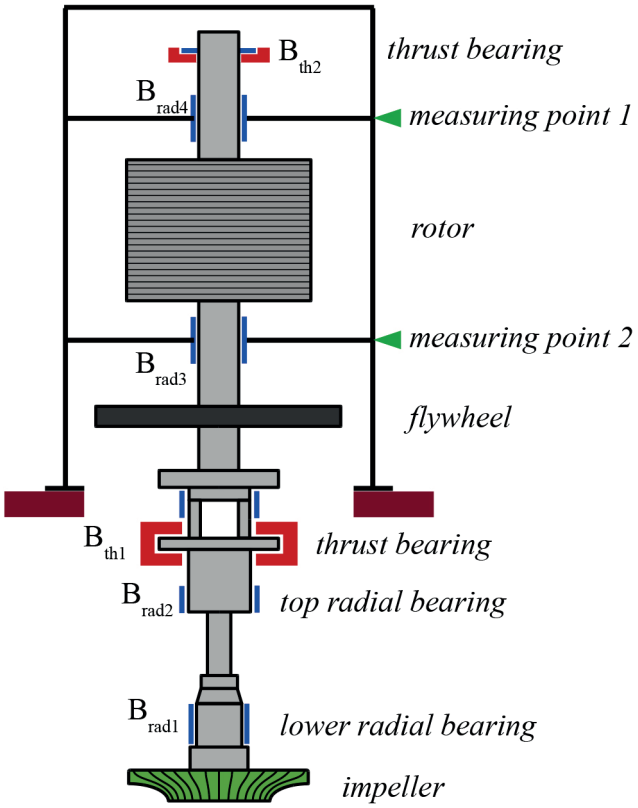

Figure 9 *Diagram of the arrangement of the machine stator and rotor*

matrices of damping and stiffness only take into account the damping and stiffness parameters of the stator fixing.

The stator and rotor are mutually coupled by means of bearings. The rotor rests on four radial and two axial journal bearings. Figure 10 shows the position of the bearings and their designation. In order to mathematically interconnect the subsystem of the rotor with the subsystem of the stator, an overall mathematical model of the system was created in the configuration space, which is defined by the vector of generalized coordinates in the form of $\boldsymbol{q} = [\boldsymbol{q}_R^T, \boldsymbol{q}_S^T]^T$. Then the complex mathematical model has following general matrix form

$$\boldsymbol{M}\dot{\boldsymbol{q}} + (\boldsymbol{B} + \boldsymbol{B}_L)\dot{\boldsymbol{q}} + (\boldsymbol{K} + \boldsymbol{K}_L)\boldsymbol{q} = \boldsymbol{f}(t). \tag{14}$$

Presented matrices can be expressed as

$$\boldsymbol{M} = \begin{bmatrix} \boldsymbol{M}_R & \boldsymbol{0} \\ \boldsymbol{0} & \boldsymbol{M}_S \end{bmatrix}, \boldsymbol{B} = \begin{bmatrix} \omega \boldsymbol{G}_R + \boldsymbol{B}_R & \boldsymbol{0} \\ \boldsymbol{0} & \boldsymbol{B}_S \end{bmatrix},$$
$$\boldsymbol{K} = \begin{bmatrix} \boldsymbol{C}_R + \boldsymbol{K}_R & \boldsymbol{0} \\ \boldsymbol{0} & \boldsymbol{K}_S \end{bmatrix} f(t) = \begin{bmatrix} \boldsymbol{f}_R(t) \\ \boldsymbol{f}_S(t) \end{bmatrix}. \tag{15}$$

Matrices $\boldsymbol{B}_L$ and $\boldsymbol{K}_L$ represent the matrices of damping and stiffness of bearing couplings. As the rotor is placed in a vertical position, the determination of the stiffness of the radial bearings is a very sophisticated problem in general. For the first approach, the stiffness of radial bearings can be estimated based on their type, their geometrical parameters and the oil viscosity according to [9]. However, this approach assumes horizontal position of the rotor and therefore the main load of the bearing is given by gravity load. Here, the main radial load is estimated based on the vertical rotor position and is determined for nominal operating speed of the rotor.

8.2 Critical speeds determination

In order to analyse basic dynamical properties of the system, especially the location of the critical speeds, the Campbell diagram was determined, i.e. the dependency of the natural frequencies on the rotor speed, see Figure 4 [7, 9, 14]. The diagram shows that the intersection point of the revolution start-up line and the curve of the second natural frequency depicted is located near the operating speed. However, this situation is not dangerous from the operational point of view because the corresponding natural shape describes the system vibration in an axial direction and therefore is not dominantly excitable due to the rotor imbalance and the unilateral magnetic pull.

The computational model created was used to determine the upper effective estimations of the radial velocities at measurement points 1 and 2, as shown in Figure 10. These spots correspond to the operational measurement points. The speed of rotor is assumed to be the nominal.

8.3 Steady-state response to imbalance forces due to rotor packet sliding

The vector of excitation forces $\boldsymbol{f}(t)$ in (14) comprises the effect of centrifugal forces. The extent of the stack bulging is simulated in

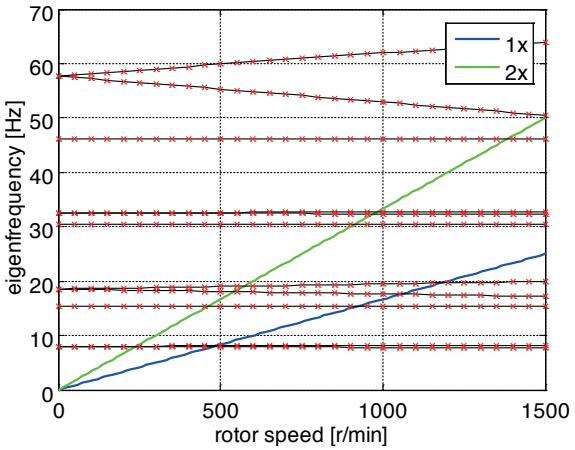

Figure 10 *Campbell diagram of the rotor-stator system*

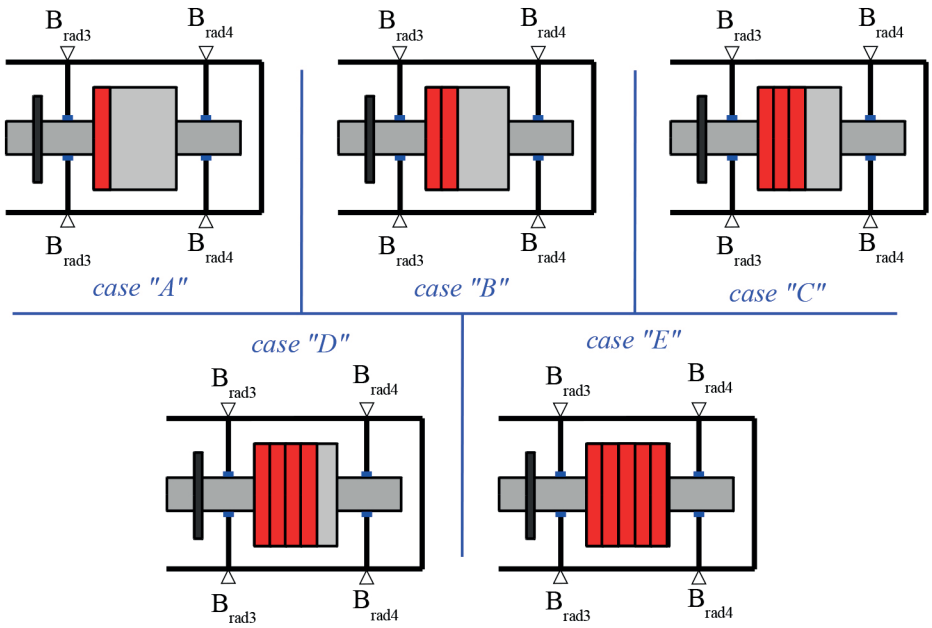

Figure 11 *Computational cases of the position of the imbalance within the rotor*

Table 3 *Determined upper effective estimations of the radial velocities at the reference points of the stator for various configurations of the considered rotor stack imbalance*

Calculation event	Upper Effective Estimation of the Velocity Amplitude in the Radial Direction [mm/s]		Location of the packet sliding
	point 2: V_{Brad3}	point 2: V_{Brad4}	
1	1.4	5.0	case “A”
2	3.1	10.4	case “B”
3	5.2	16.2	case “C”
4	7.7	22.3	case “D”
5	10.5	28.7	case “E”

a way which makes it possible to calculate the induced imbalance. Based on the findings on the rotor after its disassembling, the imbalance is given by the rotor bulging. The rotor was divided into 5 uniform segments and at each segment the imbalance due to bulging was simulated separately. The imbalance of one segment is given by the mass $\Delta m_{1/5} = 0.328\,\text{kg}$, which results in a centrifugal force of $\Delta F_{1/5} = 2.83\,\text{kN}$ under nominal speed. The computational cases of the position of the imbalance within the rotor is displayed in Figure 11. The cases were taken into account to determine what vibration level is caused by different amounts of imbalance and how it corresponds to vibration measurement.

8.4 Evaluation of vibration measurement and calculation

During the rotor operation, a vibration measurement was performed. The positions, where the vibration were recorded are designated in Figure 9 as measuring points 1 and 2. The

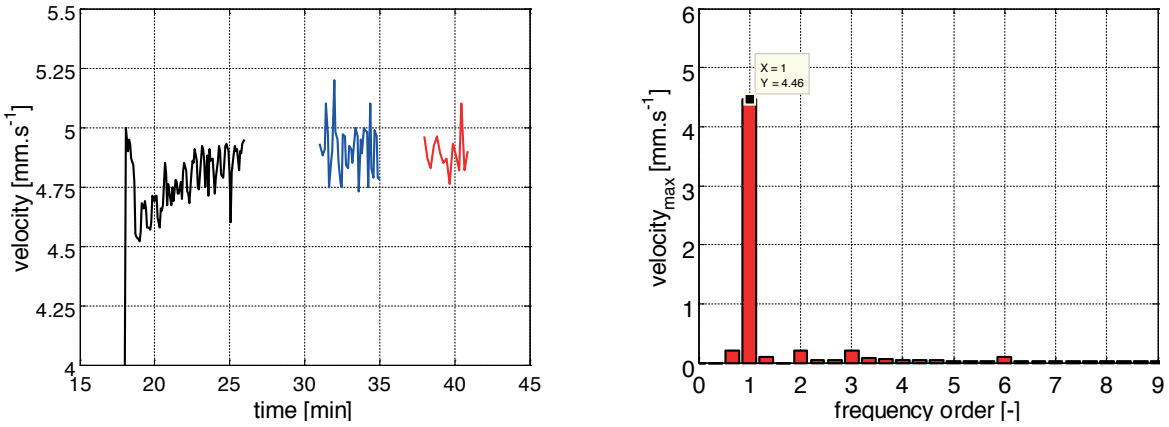

Figure 12 *Mechanical vibration measurement and FFT analysis*

measurement has been used as an indicator of vibration level of the complex equipment. The recordings (Figure 12) show that the vibration level measured by the velocity reached up to 5 mm/s, which has indicated the equipment is not capable to be operated.

The calculations were performed to confirm or disprove the source of undesirable vibration. Comparing results presented in Table 3 and measurement in Figure 12 gives good agreement for the computational case "A". It can be concluded that the amount of imbalance is given by bulging of approximately one fifth of the rotor packet. This conclusion is moreover confirmed by the frequency analysis of the measured vibration velocity. The dominant frequency contained in there corresponds to rotor spin speed frequency which gives the first order frequency (Figure 12 left).

9. Conclusion

The paper proposes a methodology how to investigate the origin of vibrations in a high performance induction motor. The methodology is based on vibration measurement and on the physical findings at the rotor after its disassembling.

In practice, the rotor vibration measurement is continuously performed on-site within a rotor diagnostic system. The vibration measurement can detect if the rotor vibration exceeds safety limits but it is not capable to decide on the vibration origin. Therefore, after analysis of the recorded vibration signal, it was found out that the dominant vibration frequency corresponds to rotor spin speed frequency. Based on that, one can conclude that the vibration source could correspond to one sided magnetic pull forces or/and to imbalance force which have the same fundamental frequency.

Based on finding after rotor disassembling, the main problem consisted in the rotor mounting, especially in its clamping. It has been found, that the improper rotor clamping resulted in rotor imbalance which further gave rise to undesirable vibrations which led to that the rotor had to be put out of operation.

The created mathematical and computational model of the machine made it possible to simulate an arbitrary imbalance of the rotor. The output of the model was the intensity of vibrations of the stator. The model was verified by a practical measurement and proved to be in very good agreement. In addition, the loosened ventilation sheet was simulated and the stress acting on it was calculated. The model predicted possible plastic distortions which were subsequently confirmed by a finding obtained after the dismantling of the machine. One of the rotor stacks exhibited an inadmissible eccentricity and the relevant ventilation sheet even suffered from a plastic deformation.

The analysis proved that an insufficient clamping force can lead to put the rotor out of operation which can finally result in high secondary financial losses, e.g. if the rotor is operated primary circuit within nuclear power plants.

Acknowledgement

This research has been supported by the Ministry of Education, Youth and Sports of the Czech Republic under the RICE - New Technologies and Concepts for Smart Industrial Systems, project No. LO1607 and by funding program of the University of West Bohemia number SGS-2018-009.

References

[1] FINLEY, W., LOUTFI, M. SAUER, B. J. Motor vibration problems - Understanding and identifying. In *2013 IEEE-IAS/PCA Cement Industry Technical Conference : proceedings* [online]. Orlando, FL, USA, 2013, p. 1-20. Available from: https://doi.org/10.1109/CITCON.2013.6525282

[2] MISTRY, R., et al. Influencing factors on motor vibration & rotor critical speed in design, test and field applications. In 2014 IEEE Petroleum and Chemical Industry Technical Conference (PCIC) *Conference : proceedings* [online]. *San Francisco, CA, USA, 2014,* p. 227-236. Available from: https://doi.org/10.1109/PCICon.2014.6961887

[3] YAMAZAKI, K., WATANABE, Y. Interbar current analysis of induction motors using 3-D finite-element method considering lamination of rotor core. *IEEE Transactions on Magnetics* [online]. 2006, **42**(4), p. 1287-1290. ISSN 0018-9464. Available from: https://doi.org/10.1109/TMAG.2006.871423

[4] FERKOVA, Z. Comparison of two-phase induction motor modeling in ANSYS Maxwell 2D and 3D program. In 10th International Conference ELEKTRO 2014 *: proceedings*. Zilina: Faculty of Electrical Engineering, 2014, p. 279-284.

[5] KALAMEN, L., et al. A novel method of magnetizing inductance investigation of self-excited induction generators. *IEEE Transactions on Magnetics* [online]. 2012, 48(4), p. 1657-1660. ISSN 0018-9464. Available from: https://doi.org/10.1109/TMAG.2011.2173312

[6] PYRHONEN, J., et al. Harmonic loss calculation in rotor surface permanent magnets - New analytic approach. *IEEE Transactions on Magnetics* [online]. 2012, 48(8), p. 2358-2366. ISSN 0018-9464. Available from: https://doi.org/10.1109/TMAG.2012.2190518

[7] MARQUES CARDOSO, A. J., et al. Rotor cage fault diagnosis in three-phase induction motors, by Park's vector approach. IAS '95. Conference Record of the 1995 IEEE Industry Applications Conference Thirtieth IAS Annual Meeting : *proceedings* [online]. Vol. 1. Orlando, FL, USA, 1995, p. 642-646. ISBN 0-7803-3008-0/ISSN 0197-2618. Available from: https://doi.org/10.1109/IAS.1995.530360

[8] BINDU, S., THOMAS, V. V. Diagnoses of internal faults of three phase squirrel cage induction motor - A review. In 2014 International Conference on Advances in Energy Conversion Technologies (ICAECT) : *proceedings* [online]. Manipal, India, 2014, p. 48-54. Available from: https://doi.org/10.1109/ICAECT.2014.6757060

[9] NAHA, A., et al. A method for detecting half-broken rotor bar in lightly loaded induction motors using current. *IEEE Transactions on Instrumentation and Measurement* [online]. 2016, **65**(7), p. 1614-1625. ISSN 0018-9456. Available from: https://doi.org/10.1109/TIM.2016.2540941

[10] VALLES-NOVO, R., et al. Empirical mode decomposition analysis for broken-bar detection on squirrel cage induction motors. *IEEE Transactions on Instrumentation and Measurement* [online]. 2015, **64**(5), p. 1118-1128. ISSN 0018-9456. Available from: https://doi.org/10.1109/TIM.2014.2373513

[11] SOUALHI, A., CLERC, G., RAZIK, H. Detection and diagnosis of faults in induction motor using an improved artificial ant clustering technique. *IEEE Transactions on Industrial Electronics* [online]. 2013, **60**(9), p. 4053-4062. ISSN 0278-0046/eISSN 1557-9948. Available from: https://doi.org/10.1109/TIE.2012.2230598

[12] CEBAN, A., PUSCA, R., ROMARY, R. Study of rotor faults in induction motors using external magnetic field analysis. *IEEE Transactions on Industrial Electronics* [online]. 2012, **59**(5), p. 2082-2093. ISSN 0278-0046/eISSN 1557-9948. Available from: https://doi.org/10.1109/TIE.2011.2163285

[13] ROMERO-TRONCOSO, R. J., et al. FPGA-based online detection of multiple combined faults in induction motors through information entropy and fuzzy inference. *IEEE Transactions on Industrial Electronics* [online]. 2011, 58(11), p. 5263-5270. ISSN 0278-0046/eISSN 1557-9948. Available from: https://doi.org/10.1109/TIE.2011.2123858

[14] KIA, S. H., HENAO, H., CAPOLINO, G. A. A high-resolution frequency estimation method for three-phase induction machine fault detection. *IEEE Transactions on Industrial Electronics* [online]. 2007, **54**(4), p. 2305-2314. ISSN 0278-0046/eISSN 1557-9948. Available from: https://doi.org/10.1109/TIE.2007.899826

[15] RANGEL-MAGDALENO, J. d. J., et al. Novel methodology for online half-broken-bar detection on induction motors. *IEEE Transactions on Instrumentation and Measurement* [online]. 2009, 58(5), p. 1690-1698. ISSN 0018-9456. Available from: https://doi.org/10.1109/TIM.2009.2012932

[16] OJAGHI, M., NASIRI, S. Dynamic simulation of eccentric squirrel cage induction motors by including saturable reluctances of individual teeth. *IET Electric Power Applications* [online]. 2014, **8**(6), p. 232-239. ISSN 1751-8660/eISSN 1751-8679. Available from: https://doi.org/10.1049/iet-epa.2013.0381

[17] BERNAT, P., KACOR, P. Operational non-contact diagnostics of induction machine based on stray electromagnetic field. *Communications - Scientific Letters of the University of Zilina* [online]. 2015, **17**(1A), p. 89-94. ISSN 1335-4205/eISSN 2585-7878. Available from: http://komunikacie.uniza.sk/index.php/communications/article/view/418

[18] ORSAG, O., et al. Influence of rotor slot shape on the parameters of induction motor. IEEE International Conference on Environment and Electrical Engineering and IEEE Industrial and Commercial Power Systems Europe (EEEIC/I&CPS Europe 2017) : proceedings [online]. Milan, Italy, 2017. ISBN 978-1-5386-3916-0. p. 1-6. Available from: https://doi.org/10.1109/EEEIC.2017.7977673

[19] BANGURA, J. F., et al. Diagnostics of eccentricities and bar/end-ring connector breakages in polyphase induction motors through a combination of time-series data mining and time-stepping coupled FE-state-space techniques. *IEEE Transactions on Industry Applications* [online]. 2003, **39**(4), p. 1005-1013. ISSN 0093-9994/eISSN 1939-9367. Available from: https://doi.org/10.1109/TIA.2003.814582

[20] JOKSIMOVIC, G. M. Dynamic simulation of cage induction machine with air gap eccentricity. *IEE Proceedings - Electric Power Applications* [online]. 2005, **152**(4), p. 803-811. ISSN 1350-2352/eISSN 1359-7043. Available from: https://doi.org/10.1049/ip-epa:20041229

[21] SILWAL, P., et al. Numerical analysis of the power balance of an electrical machine with rotor eccentricity. *IEEE Transactions on Magnetics* [online]. 2016, **52**(3), p. 1-4. ISSN 0018-9464. Available from: https://doi.org/10.1109/TMAG.2015.2477847

[22] PYRHONEN, J., JOKINEN, T., HRABOVCOVA, V. Design of rotating electrical machines. Wiley, 2014. ISBN 978-1-118-58157-5

[23] OBAID, R. R., HABETLER, T. G., GRITTER, D. J. A simplified technique for detecting mechanical faults using stator current in small induction motors. 2000 IEEE Industry Applications Conference, Thirty-Fifth IAS Annual Meeting and World Conference on Industrial Applications of Electrical Energy : conference record [online]. Vol. 1. Rome, Italy, 2000. ISBN 0-7803-6401-5/ISSN 0197-2618, p. 479-483. Available from: https://doi.org/10.1109/IAS.2000.881153

[24] KOSTIC-PEROVIC, D., ARKAN, M., UNSWORTH, P. Induction motor fault detection by space vector angular fluctuation. 2000 IEEE Industry Applications Conference, Thirty-Fifth IAS Annual Meeting and World Conference on Industrial Applications of Electrical Energy: conference record [online]. Vol. 1. Rome, Italy, 2000. ISBN 0-7803-6401-5/ISSN 0197-2618, p. 388-394. Available from: https://doi.org/10.1109/IAS.2000.881140

[25] ELKASABGY, N. M., EASTHAM, A. R., DAWSON, G. E. Detection of broken bars in the cage rotor on an induction machine. *IEEE Transactions on Industry Applications* [online]. 1992, **28**(1), p. 165-171. ISSN 0093-9994/eISSN 1939-9367. Available from: https://doi.org/10.1109/28.120226

[26] CAMERON, J. R., THOMSON, W. T., DOW, A. B. Vibration and current monitoring for detecting airgap eccentricity in large induction motors. *IEE Proceedings B - Electric Power Applications* [online]. 1986, **133**(3), p. 155-163. ISSN 0143-7038/eISSN 2053-7913. Available from: https://doi.org/10.1049/ip-b:19860022

[27] DORRELL, D. G., THOMSON, W. T., ROACH, S. Analysis of airgap flux, current, and vibration signals as a function of the combination of static and dynamic airgap eccentricity in 3-phase induction motors. *IEEE Transactions on Industry Applications* [online]. 1997, **33**(1), p. 24-34. ISSN 0093-9994/eISSN 1939-9367. Available from: https://doi.org/10.1109/28.567073

[28] NANDI, S. AHMED, S., TOLIYAT, H. A. Detection of rotor slot and other eccentricity related harmonics in a three phase induction motor with different rotor cages. *IEEE Transactions on Energy Conversion* [online]. 2001, **16**(3), p. 253-260. ISSN 0885-8969. Available from: https://doi.org/10.1109/60.937205

[29] TOLIYAT, H. A., AREFEEN, M. S., PARLOS, A. G. A method for dynamic simulation of air-gap eccentricity in induction machines. *IEEE Transactions on Industry Applications* [online]. 1996, **32**(4), p. 910-918. ISSN 0093-9994/eISSN 1939-9367. Available from: https://doi.org/10.1109/28.511649

[30] CARDOSO, J. M., SARAIVA, E. S. Computer-aided detection of airgap eccentricity in operating three-phase induction motors by Park's vector approach. *IEEE Transactions on Industry Applications* [online]. 1993, **29**(5), p. 897-901. ISSN 0093-9994/eISSN 1939-9367. Available from: https://doi.org/10.1109/28.245712

[31] AL-NUAIM, N. A., TOLIYAT, H. A novel method for modeling dynamic air-gap eccentricity in synchronous machines based on modified winding function theory. *IEEE Transactions on Energy Conversion* [online]. 1998, **13**(2), p. 156-162. ISSN 0885-8969. Available from: https://doi.org/10.1109/60.678979

[32] BONNETT, A. H., SOUKUP, G. C. Analysis of rotor failures in squirrel-cage induction motors. *IEEE Transactions on Industry Applications* [online]. 1988, **24**(6), p. 1124-1130. ISSN 0093-9994/eISSN 1939-9367. Available from: https://doi.org/10.1109/28.17488

[33] BOGH, D., CROWELL, J., AMSTUTZ, R. IEEE 841 motor vibration. *IEEE Industry Applications Magazine* [online]. 2005, **11**(6), p. 32-37. ISSN 1077-2618. Available from: https://doi.org/10.1109/MIA.2005.1524734

[34] STACK, J. R., HABETLER, T. G., HARLEY, R. G. Effects of machine speed on the development and detection of rolling element bearing faults. *IEEE Power Electronics Letters* [online]. 2003, **1**(1), p. 19-21. ISSN 1540-7985/eISSN 1558-3767. Available from: https://doi.org/10.1109/LPEL.2003.814607

[35] BANGURA, J. F., et al. Diagnostics of eccentricities and bar/end-ring connector breakages in polyphase induction motors through a combination of time-series data mining and time-stepping coupled FE-state-space techniques. *IEEE Transactions on Industry Applications* [online]. 2003, **39**(4), p. 1005-1013. ISSN 1077-2618. Available from: https://doi.org/10.1109/TIA.2003.814582

[36] OBAID, R. R., HABETLER, T. G., GRITTER, D. J. A simplified technique for detecting mechanical faults using stator current in small induction motors. 2000 IEEE Industry Applications Conference. Thirty-Fifth IAS Annual Meeting and World Conference on Industrial Applications of Electrical Energy : conference record [online]. Vol. 1. Rome, Italy, 2000. ISBN 0-7803-6401-5/ISSN 0197-2618, p. 479-483. Available from: https://doi.org/10.1109/IAS.2000.881153

[37] DEN HARTOG, J. P. Advanced Strength of Materials. Dover Civil Mechanical Engineering, Dover Publications, 1987. ISBN 978-0486654072.

Matej Kubis - Miroslav Gutten - Daniel Korenciak - Matus Danko*

COMMUNICATION OF CLUSTER USING CAN BUS

The paper deals with the communication between the infotainment elements and the drive component of the car using the CAN bus. In the introduction, there is briefly described the communication bus used in cars. It describes its basic features, benefits and utilization. The main task is graphically programmed and builds a dashboard that will resemble to a real dashboard from a Volkswagen Golf 5. Using the dashboard built in LabVIEW, it controls the real dashboard.

Keywords: *communication, CAN bus, LabVIEW, automotive*

1. Introduction

Fieldbuses are now part of every automobile power supply, which are used for receiving, processing and sending of data between sensors, actuators and controllers. Sending the information between devices, for example about the position of the accelerator, it is preferable to encode the information and send it through cheap wires (two twisted wires), as in case that a separate cable will be used for each informative state. The disadvantage is the need for encoders and decoders, and with that the associated need for complex, diagnostic tools. However, if the bus is used in the vehicle, wiring will be simplified, the number of wires reduced as well as terminal blocks and the speed of communication increased [1].

Transmission simulating systems are the important annulus in car factory total assembly workshop automation equipment. By applying the fieldbus technology, it made more reliable transmission system operation, maintenance convenience, which also greatly reduced the overall cost [2].

2. Description of automotive CAN bus

In 1980, Bosch brings to the stage the technical world of networking controllers called CAN - bus. CAN bus is not used only in the automotive industry. CAN bus is a system for the current communication (real time) of control units. It is not used for the direct connection of sensors or actuators, but only to link controllers. The other elements of the system, such as sensors and actuators, are linked by indirect method. In the case of exchange of information via the CAN data bus, all data is transmitted only through two wires. Both bidirectional conductors will carry the same data, regardless of the number of control units and the amount of transmitted data. Transmission of information through the CAN bus has meaning only in case when we need to send a lot of information between multiple controllers [3].

While one unit is connected to the bus transmits data, other units receive them and evaluate them as well. If the unit recognizes the important information, further processes them and sends a signal to actuator. If information is unnecessary, remains passive. For example, the transmission of the information of the vehicle speed display: management control unit measures the value of the speed sensors and the coded sequence to a series of ones and zeros will send it to the CAN bus control unit of the instrument panel. The control unit must decode the message and ensure that it is comprehensible displayed, for example with a digital position indicator or speedometer [4].

The bus may be in two states - the dominant state (dominant) or a recessive (recessive), shown in Figure 1. The dominant state occurs when at least one unit transmits, i.e. “switch is open”, the voltage on the bus is about 2 V. On the other hand, recessive condition occurs when the “switch is turned off” and the voltage on the bus is 0 V, it means the “silent bus”, there is no sending unit, or any unit can begin transmitting. In case of recessive (silent) mode, the voltage of both wires (CAN-High and CAN-Low) is 2.5 V to the chassis, against each other to 0 V. The CAN-H has a voltage of 3.5 V and CAN-L has 1.5 V in the dominant mode. It is referred differential voltage of 2V. The differential voltage between conductors is very important; therefore, bus is from this perspective differential [5].

The most basic data chip versions are: Basic and Full CAN. In Basic CAN, there is a message identified and controlled by the processor of connected device. Full CAN has a filter in the communication chip that decides whether to accept the message or send it to the processor. Full CAN version burdens less own processor of connected device [6].

These two different versions are still used today although not in the exactly same form. Due to the wide range of chips, it is currently available for more than 60 chips of about sixteen producers. Full CAN has two variants: variant A, the 11-bit identifier and variant B (i.e. magnification) with 29 bits. The versions are not compatible. The rate depends not only on the variant of the protocol, but also on the length of the bus.

* **[1]Matej Kubis, [1]Miroslav Gutten, [1]Daniel Korenciak, [2]Matus Danko**
[1]Department of Measurements and Applied Electrical Engineering, Faculty of Electrical Engineering and Information Technology, University of Zilina, Slovakia
[2]Department of Mechatronics and Electronics, Faculty of Electrical Engineering and Information Technology, University of Zilina, Slovakia
E-mail: matej.kubis@fel.uniza.sk

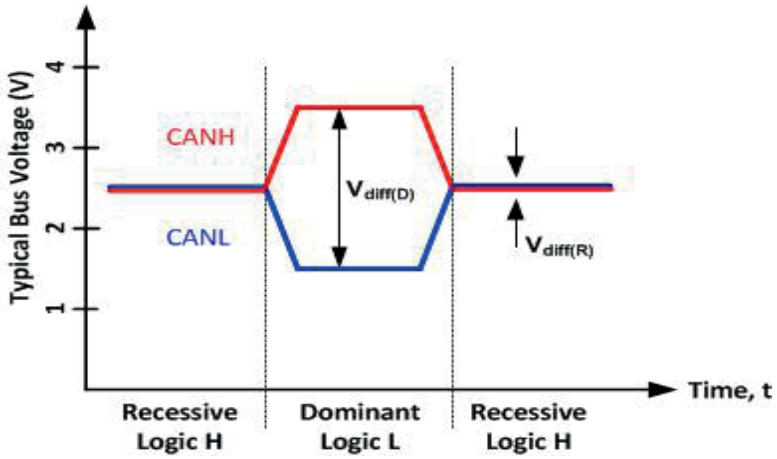

Figure 1 *Voltage level on the CAN*

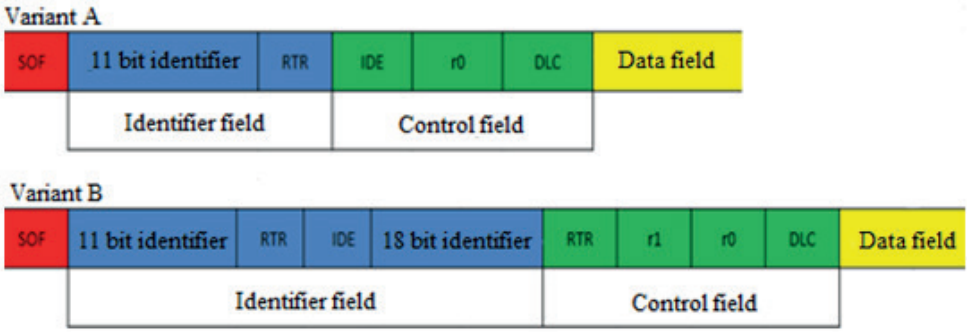

SOF - Start of frame - initialization and synchronization field
RTR - Remote Request - bit, which is dominant in the data frame
SRR - Substitute Remote Request - RTR replaced by the variant B
IDE - Identifer Extension - bit, which allows to distinguish variants of what it is
DLC - Data Length Code - Code for the length of the data field
r1, r0 - reserved bits (complement DLC)

Figure 2 *Format data frame*

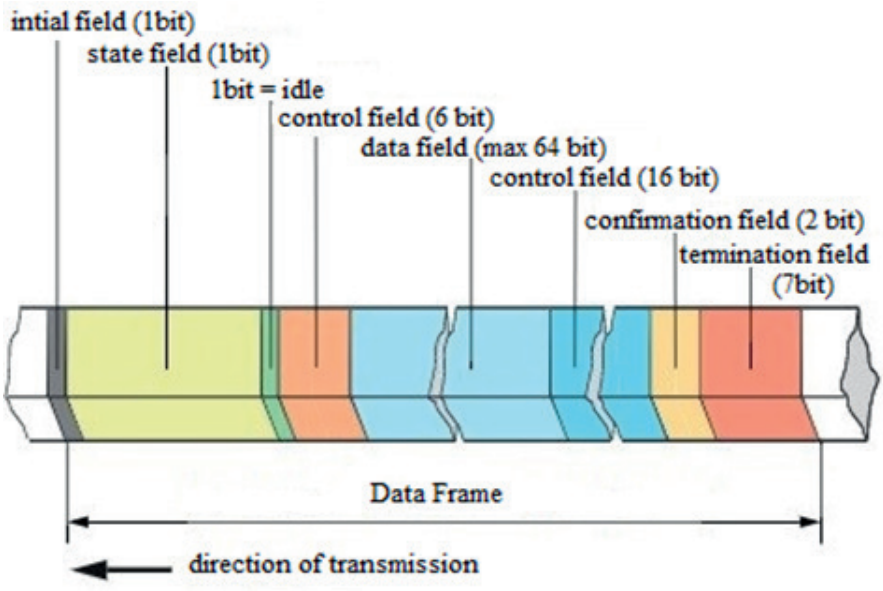

Figure 3 *Field data frame*

A comparison of variant A and variant B is plotted in Figure 2.

Data frame consists of several fields: Start framework, decision-making field, control field, data field, a checksum field, the confirmation field and end frame. Composition data frame is shown in Figure 3.

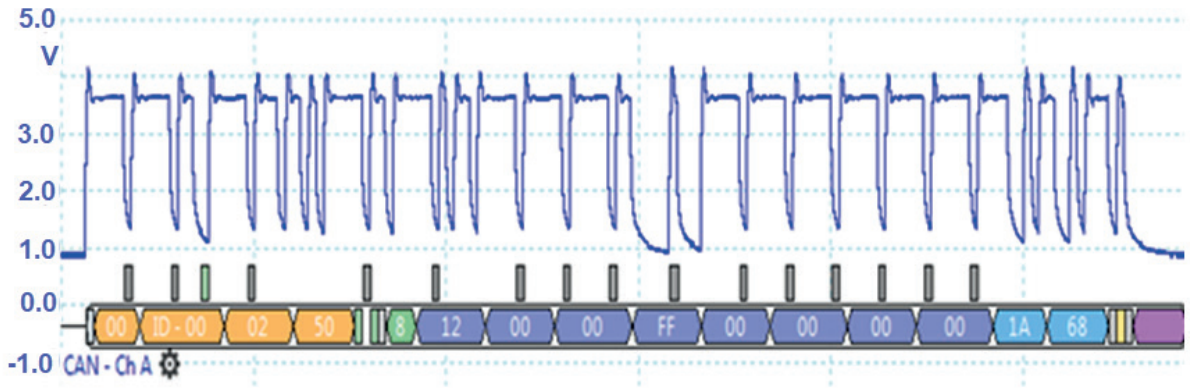

Figure 4 *Extended data frame*

There are three types of CAN buses that are different data rates, use and construction (mainly type exciter):

- HSCAN - high speed CAN bus (High Speed),
- LSCAN - low-speed CAN bus (Low Speed).

Their direct connection is not possible; interconnect through a gateway (gateway). HSCAN is two-wire, control voltage is between drivers about 2V at the end of the interconnected resistors 120 Ohm, unlike LSCAN, consisting of one active conductor and ground and recessive voltage of about 4V (use LSCAN is mostly less intensive systems such as. for comfort electronics.

3. Design and simulation test system dashboard

Implementation of communication was carried out on the data bus CAN. We have chosen CAN bus, because it is the most used bus in automotive applications. Loaded progress on the CAN bus is implemented by using a Pico PC Oscilloscope, sending broadcast messages is provided by the software of bussmaster, where are sent only randomly generated messages [7].

The difference between standard CAN 2.0 A and CAN 2.0 B is the number of bits of the identifier. The standard data frame in the arbitration field contains of 11 - bit identifier and the RTR bit. In Figure 4 there is an enlarged data frame which contains the extended 29 -bit ID, and the RTR bit SRR bit in the arbitration field [8].

The identifier is randomly selected to 0 x 250, other bits are gradually complemented by value, as can be seen in the data frame. This is for showing of data and their generation without using real elements of the car. Behind 0x250 HEX is 8 bits sequentially.

Data analysis was carried out using the CAN hardware Kvaser Leaf SemiPro and software bussmaster. In between each 10 m with a different message is sent over the bus, which sends the real instrument panel, and is, for example: error codes of missing sensor, missing immobilizer, the absence of the control unit of the airbag etc.

In Figure 5 there are shown values of individual bits on the bus along with identifiers that are purposefully deleted due to copyright manufacturer. Inspiring information offers a single interface, where you can record real-time log data without further attachment.

The main task was to program and graphically construct the instrument panel, which will resemble a real dashboard of the car Volkswagen Golf 5.

The first report processes data for speedometer, a given message can be up to 8 bytes and 1 byte can have a value from 0 to 255. If there is needed a larger value, we must use more bytes. There are needed 2 bytes for simulation of the rpmmeter: the second byte as eight low-order bits, the third byte as eight upper bits. Subsequently, the resulting value is divided by four and we get a real running speed. By dividing with the rest, we determine whether the bit is zero or unity. If the final bit is zero, the number is even; therefore, it must be divided by two because of the zero residues. To find out the remaining bits, we must use the logical rotation, so the bit, whose value we want to determine, stands at the end point. In the second report, there are data processed for the temperature and a fuel gauge.

The fuel gauge is one of the few that is not used for its function, CAN bus, but it operates analog, thus it was used only for simulation. The signal for the temperature of the motor is transmitted by the first byte. The signal must firstly be necessary arranged; therefore, he is divided by ¾. The temperature can also be negative; however, we have only positive numbers, so we should subtract the value of 48.

The pointer of the temperature of engine is non-linearized because of the constantly moving pointer on the temperature which is graphically illustrated in Figure 6.

The real temperature of the motor measured by the sensor is displayed to 90 °C. The temperature between 90 °C and 110 °C is working temperature of the engine, and so we have not seen constant movement of a hand for a little change of temperature this tolerance is continuously displayed as 90 °C on the indicator. From 110° C to 130 °C, the pointer indicates the real value to avoid overheating of the motor. The curve is easily adjusted by using the equation of the line:

$$y = k + q \quad (1)$$

$$90 = 110k\text{-}q$$

$$130\ 130k + q =$$

Message Window - CAN

Time ...	Tx/Rx	Channel	Msg	ID	Message	DLC	Data Byte(s)
15:22:5...	Rx	1	s	0x	0x	8	3A 01 FF 01 00 00 00 B9
15:22:5...	Rx	1	s	0x	0x	8	00 00 00 00 00 00 00 00
15:22:5...	Rx	1	s	0x	0x	8	00 99 00 00 00 00 00 00
15:22:5...	Rx	1	s	0x	0x	8	00 00 E1 14 00 00 00 00
15:22:5...	Rx	1	s	0x	0x	5	00 00 80 FF 10
15:22:5...	Rx	1	s	0x	0x	8	55 C4 00 00 80 EF 1B 04
15:22:5...	Rx	1	s	0x	0x	4	01 FF 15 90
15:22:5...	Rx	1	s	0x	0x	8	00 00 00 00 00 57 56 57
15:22:5...	Rx	1	s	0x	0x	7	EF 1B 04 00 00 8C 02
15:22:5...	Rx	1	s	0x	0x	2	85 01
15:22:5...	Rx	1	s	0x	0x	8	FF FF FF FF FF FF FF 03
15:22:5...	Rx	1	s	0x	0x	8	81 FF FF 00 00 FF FF 00

Figure 5 *Bus data analyzed using the software Bussmaster*

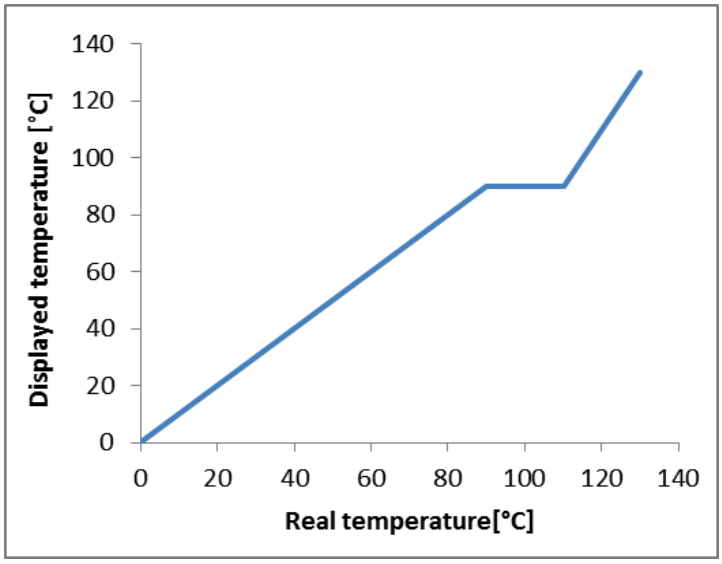

Figure 6 *Characteristics of the pointer to engine temperature*

90 - 130 = 110k - 130k

20k = 40

k = 2

90 * 2 = 110 + Q

q = -220 + 90

q = -130

Final, the third report is essential for processing of engine speed. Motor speed data is transmitted by the second and the third bytes. The second byte is lower eight bits and the third byte is upper eight bits of the resulting number. The resulting number must be divided by 100, so we get speed. Simulated speedometer is shown in Figure 7. The real instrument alarms from the VW Golf V were graphically implemented in LabVIEW and associated with the code.

The real instrument alarms from the VW Golf V were then graphically implemented in LabVIEW and associated with the code. Using CAN analyzer can be analyzed and read messages saved on the SD card. The necessary data to display speed and temperatures have been mentioned above. The basis of these alarms forms a variable speed with the speed of which is completed by the water temperature and the fuel indicator. Because the simulated data processing speed according to predetermined ID instrument manufacturer. In this case, it is a car manufacturer VW Group. Specific identifiers along with the necessary bits administration were associated with a virtual environment and the real-time output. As well as for the engine speed is used in various identifiers for engine temperature and speed. In addition to the fuel level indicator going over the bus all the information, which are needed for the driver. Graphic visualization of the instrument panel is in Figure 8.

We watered the real dashboard by a regulated power supply. The value of the resources we have set at about 12 V. The creation of a network CAN we used industrial computer cRIO containing the CAN card. Test communication of the virtual instrument panel with a real instrument panel shown in Figure 9.

For connecting wires CAN-H and CAN-L, we used a modified connector DSUB9. After starting the communication, we can see that communication takes place in real time, which means

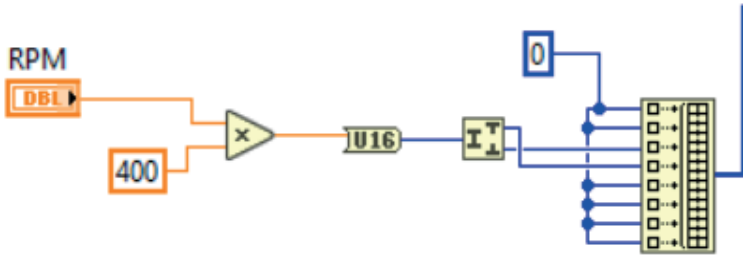

Figure 7 *Rpmmeter in LabView*

Figure 8 *Graphic instrument panel in LabView*

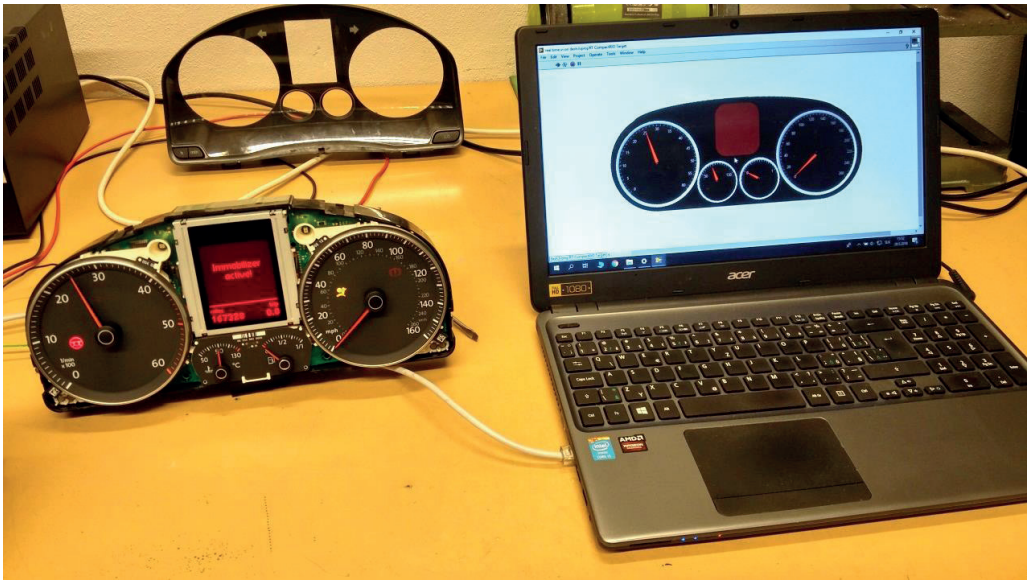

Figure 9 *Dashboard communication test*

that if you deviate rpmmeter needle or needle pointer engine temperature, so we deflect the needle on a real instrument panel. The function of the speedometer is due to the complexity of the simulation omitted because real dashboard compares multiple messages, that structure is complex. The fuel gauge is analogue and is the only part of the instrument panel which does not use the CAN bus.

4. Conclusion

The aim of the paper was to handle the issue of using of control and communication systems for automotive applications. In the theoretical part of the article we dealt with general CAN bus. From the outset the random data were generated by using of the software bussmaster and later were sent to the bus. In the second part of the implementation, the main task was simulation of the real dashboard of the car Volkswagen Golf 5 by using the software LabVIEW and controlling of it in real time.

The rpmmeter and engine temperature indicator were dominated by us. The fuel gauge was controlled analogue, so it was used only for simulation. Speedometer was not operated by us due to the difficulty of simulation and the need of the other control units.

Acknowledgements

This article is the result of a project implementation: Modern methods of teaching of control and diagnostic systems of engine vehicles, ITMS code 26110230107, supported by the Operational Programme Educational.

References

[1] BOSCH R. Bosch automotive electrics and electronics [online]. Plochingen: Robert Bosch GmbH., 2007. ISBN 978-3-658-01783-5/ eISBN 978-3-658-01784-2. Available from: https://doi.org/10.1007/978-3-658-01784-2

[2] LEI Y., HAIHONG W. The design of car transport line control system based on fieldbus technology. World Automation Congress (WAC) : proceedings. Piscataway, NJ: IEEE, 2012. ISBN 9781467344975.

[3] STERBA P.: Electronic equipment car (in Czech). Brno: Computer Press, 2004. ISBN 978-8-025-10211-4.

[4] SEBOK M., et al: Diagnostics of ignition systems. *JEE - Journal of Electrical Engineering* [online]. 2013, **13**(4), p. 181-186. ISSN 1582-4594. Available from: http://jee.ro/articles/WH1360660218W511a06fad8ebe.pdf

[5] SHINDE, A. CAN - Controller area network. LAP Lambert Academid Publishing, 2012. ISBN 978-3659284946

[6] FRIVALDSKY M., DRGONA P., SPANIK P.: Experimental analysis and optimization of key parameters of ZVS mode and its application in the proposed LLC converter designed for distributed power system application. *International Journal of Electrical Power & Energy Systems* [online]. 2013, **47**(1), p. 448-456. ISSN 0142-0615/eISSN 1879-3517. Available from: https://doi.org/ 10.1016/j.ijepes.2012.11.016

[7] Automotive oscilloscopes. Pico Technology 2018 [online]. Available from: https://www.picoauto.com/products/automotive-oscilloscope-kit/overview

[8] CAN in modules. Bosch invented for life 2017 [online]. Available from: http://www.bosch-semiconductors.com/ip-modules/

Taisiya V. Shepitko - Elena S. Shepitko - Vladimir S. Afanasev*

COMPUTER SIMULATION MODELS FOR CONSIDERATION OF SEASONAL TRENDS INFLUENCE ON THE STRUCTURAL DYNAMICS OF BRIDGES

Elimination of seasonality temperature trends in a structural health monitoring of bridges is considered in the article. On example of a beam bridge, eigenfrequencies are plotted against seasonal fluctuations of environmental temperature. Next, analysis of a time series, formed from a data of frequency changes in the bridge, was made. To describe the time series, two different methods were implemented: ARIMA model based on a statistical relationship between the data and LSTM model of a recurrent neural network.

Keywords: *computer simulation, seasonality elimination, structural health monitoring, time series, forecast, SHM, ARIMA, recurrent neural network*

1. Introduction

In general, long-term structural health monitoring of bridges can be described as a process of detecting damage and strategies for describing structures using mathematical models. Appearance of damages inevitably leads to a change in the dynamic response of an object, but this change can also be related to environmental factors (impacts of temperature, seasonal changes in soil characteristics and etc.) or even with dynamic loads (wind pressure, different types of transport), which also significantly affect the dynamics. For example, a daily or seasonal temperature change that deforms the contour of a bridge deck due to heating, or severe, stable wind that deflects the bridge deck. These changes may persist for a certain period of time before returning to normal condition. Standard instruments, such as accelerometers, can give only instant local vibration, but cannot detect stable deformation of the bridge deck, so an absolute displacement was left undetected. Such limitations in detecting an initial condition of the structure would lead to errors in modal parameter estimation. Studies of bridges show that environmental influence leads to deviation of the eigenfrequencies of the structures to 1.52% [1], which can mask the change in frequencies due to damage.

Therefore, before determining the presence of damage in a structure, it is necessary to evaluate an influence of environment on the dynamic response of a structure. The process of the damage identification, based on the operational modal analysis with the filtering of influence, is shown in Figure 1.

Parameter u_k represents "white noise", stationary Gaussian process across the entire frequency band, x_k is a response of a structure in time, $u^{env}{}_k$ is an environmental impact, w_k is modal contribution from random loads, v_k is a noise from external sources, y_k is measured response of the structure, all arrows denote signal vectors, and k denotes discrete time index. The impact of environment and loads on the measured response is estimated based on the correlation dependence between them, for example, using the regression models [2]. In addition, influence of different types of excitation were studied (measured and controlled harmonic oscillations, hammer impact, recording of "white noise") for identification of damages [3].

There are monitoring systems in which an impact of wind speed and temperature are measured (Wind and Structural Health Monitoring Systems). As an example, a system is installed on the Stonecutters Bridge, Hong Kong, China [4]. Such long span bridges are often a subject to various aggressive environmental influences, such as ultra-high wind speed or uneven heating. To prevent detrimental effect on the results of the modal analysis, the characteristics of the wind flow and temperature of the heating of elements are fixed on the bridge. Further, using these data, the modal parameters are adjusted, as well as maximum displacements of the girder and pylons and forces in pylon basement. This approach is called "the model update method" - a process of iterative change in individual parameters of finite element model to minimize the difference between experimentally measured and calculated structural response [5]. However, some studies are aimed to eliminate the influence of environmental factors without their direct measurement. This will simplify the monitoring of objects by reducing the number of measured parameters.

2. Statement of the problem

Influence of environment, in particular the temperature changes that affect the eigenfrequencies of bridges, was considered in this paper. As an object for research was chosen an overpass - large road demountable bridge. The span of the structure has a length of 53.5 m and a width of 8.6 m, it consists of two main beams, assembled from six middle and two end sections,

* **Taisiya V. Shepitko, Elena S. Shepitko, Vladimir S. Afanasev**
Institute of the Railway Track, Construction and Structure, Russian University of Transport (MIIT), Moscow, Russia
E-mail: vla.afanasev@gmail.com

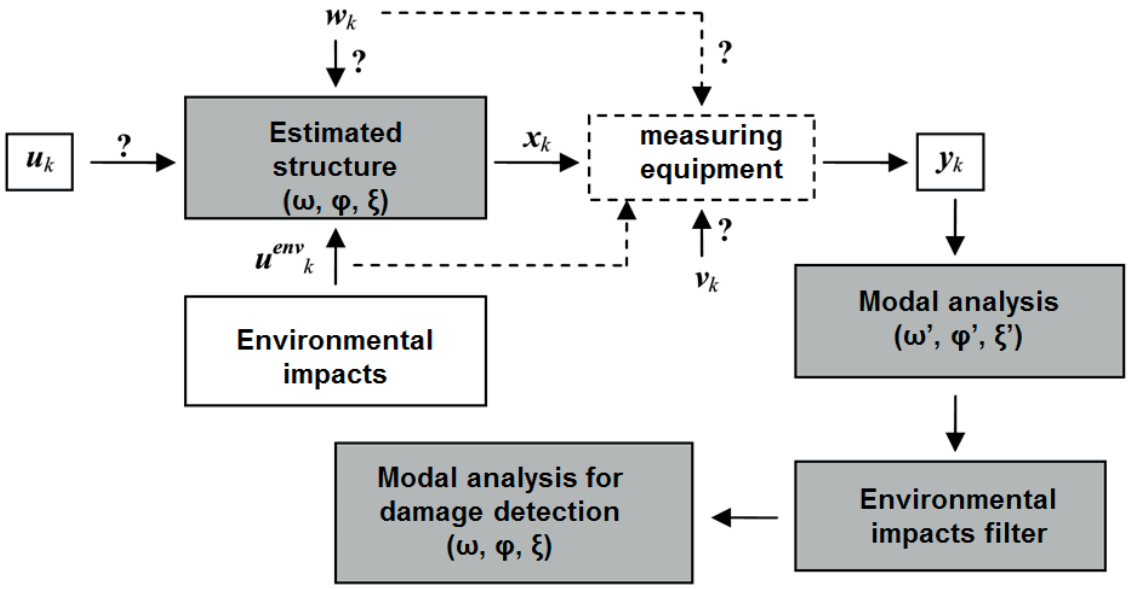

Figure 1 *Sequence of the operational modal analysis process for fault identification*

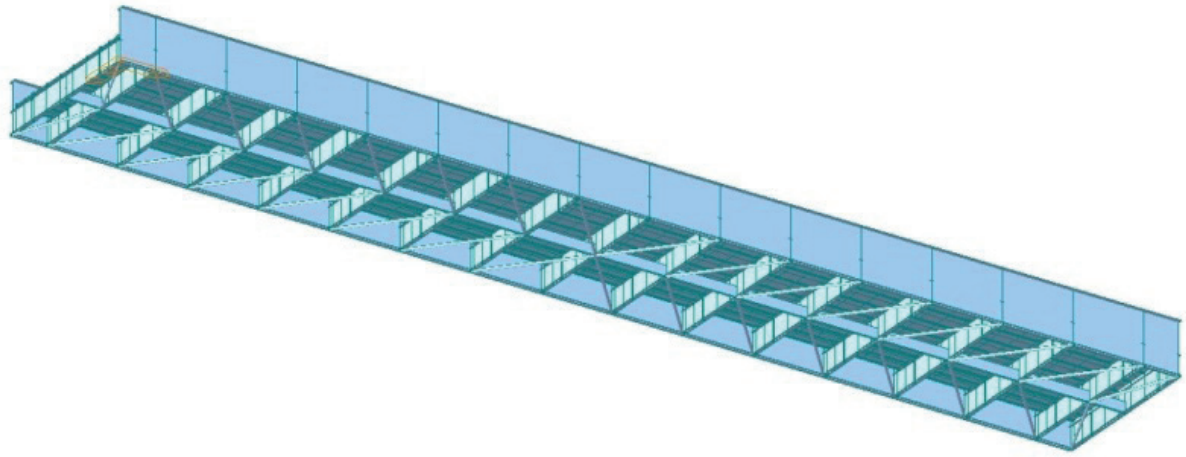

Figure 2 *Spatial model of the BARM road bridge, bottom view*

interconnected by transverse beams of the I-section. The deck lays on this system, made in a form of an orthotropic plate.

A spatial model of the structure was created using the Midas Civil software (Figure 2). The model is made up of beam elements in the form of I-beams for the main and transverse beams and I-beams ℓ14 for the flooring. The deck is represented by plate elements of a given thickness and is rigidly connected to the transverse beams. Eigenfrequencies and eigenvalues for the model were calculated.

To study the effect of temperature on dynamic characteristics of the bridge, a table of average monthly air temperatures is compiled taking into account the number of sunny days (Table 1). For the temperature influence an assumption was made that during the sunny weather an additional solar heating of the span structure takes place, which was calculated according to the "Recommendations for calculating the temperature effects" [6].

Heat of hydration analysis was made for each month with and without additional heating. Further, additional stresses in the main beams of the model due to heating were determined. At the next step, those stresses were applied as initial conditions for calculating the eigenfrequencies of the bridge. As a result, obtained data on the example of fluctuations of first eigenfrequency of bridge can be represented in form of the graph in Figure 3. In the case of annual fluctuations in temperature of the beam, change of the first eigenfrequency will correspond to the graph of Figure 3.a. In order to trace the possible patterns Figure 3.b was constructed, corresponding to change of the first eigenfrequency for 3 years and the weighted moving average (marked red) was calculated.

3. Creation of the predictive models for the data set

Generated data is represented in form of time series - sequentially measured data describing a time-consuming process. The first thing that needs to be done when analyzing this type of data is to estimate the stationarity of the time series - the absence of a trend, seasonality, data releases, etc. According to the moving average (red in graph in Figure 3.b) there is a pronounced

Table 1 *Average temperature of air and bridge per year and additional influence of solar radiation*

month	sunny days in mounth	t air, C		additional solar heating	t of heated bridge, C
		min, night	max, day		
1	2	-10	-7.5	5.12	-2.38
2	2	-7.4	-4	2.73	-1.27
3	3	-5	-0.4	0.27	-0.13
4	8	2.7	9.6	6.56	16.16
5	15	10.7	20	13.66	33.66
6	14	13.3	22.7	15.50	38.20
7	17	15.3	25.1	17.14	42.24
8	19	14.1	23.8	16.26	40.06
9	9	8.9	15.7	10.72	26.42
10	6	3	6.9	4.71	11.61
11	6	-1.5	1.4	0.96	2.36
12	2	-5.9	-3.4	2.32	-1.08

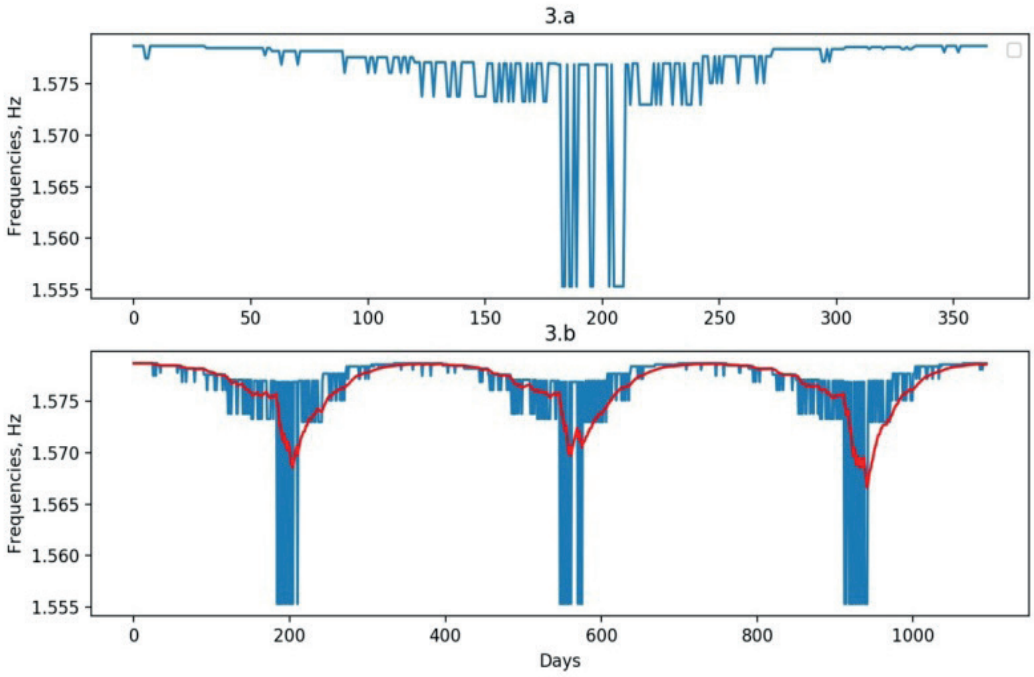

Figure 3 *Change in the first eigenfrequency of the bridge in a year (3.a) and in three years (3.b)*

seasonality of the data - a regular frequency change that repeats over a period of time, in this case annually. Emissions and stable trends are absent - moving average does not change from year to year, since the eigenfrequencies remain unchanged. Therefore, further processing will be carried out with an emphasis on the removal of seasonality.

In general, two main methods for creating models for describing and predicting time series can be distinguished: mathematical methods based on statistical data processing and machine learning methods, such as, for example, recurrent neural networks. Each of them was analyzed separately.

3.1 Integrated model of autoregression moving average (ARIMA)

The ARIMA model belongs to the class of statistical models for analysis and prediction of the time series. The model name is an acronym, the capital letters of which literally means the following:

AR: Autoregression is the use of a link between current and some lagging observations;

I: Integrated - a process that uses the difference between the current and previous observation so that the time series is unchanged;

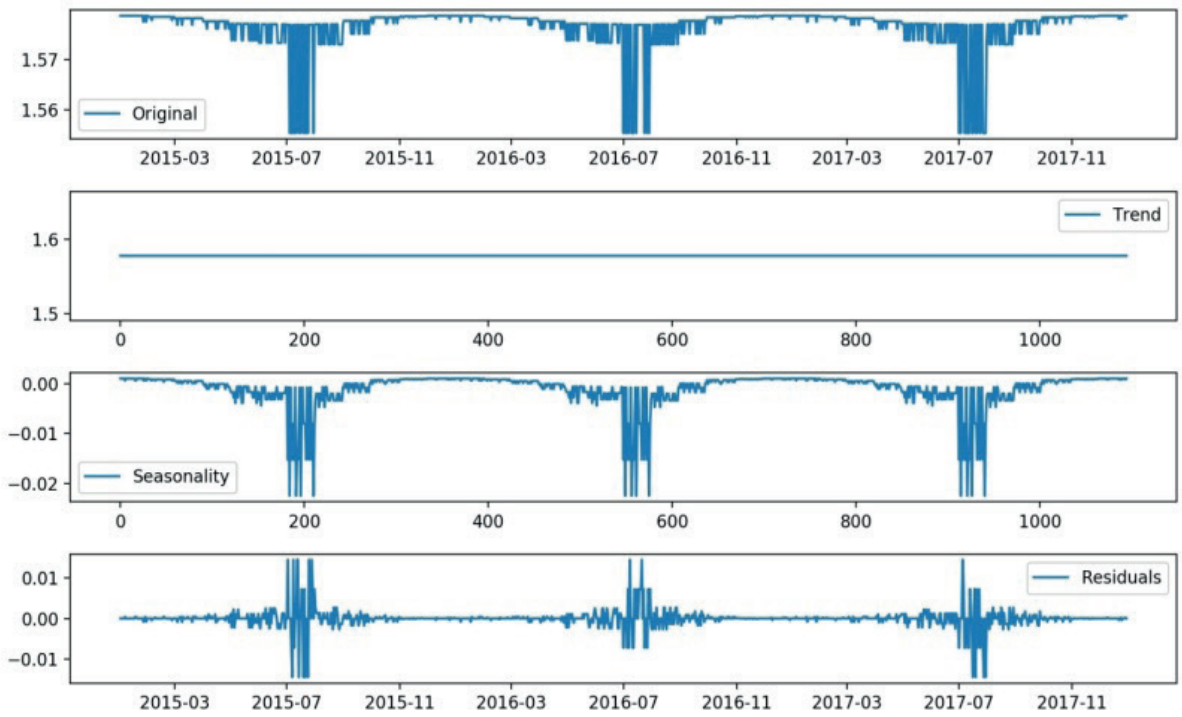

Figure 4 *Decomposition of the initial time series to the trend, seasonality and residuals*

MA: The moving average is a model where the relationship between observation and residual errors from the moving average model is used in relation to delayed observations.

Each of these components is explicitly specified as a model parameter. The standard notation used in the ARIMA (p, d, q), where each of the parameters is replaced by numbers in order to quickly specify the model being used. Model parameters mean:

p - the number of delayed observations contained in the model, also known as the order of lags;

d - number of order of difference of time series;

q - the size of the sliding-middle window (the order of the moving average).

In the case of the ARIMA type models, two main methods are distinguished in order to remove seasonality and trend in the time series: differentiation and decomposition [7]. In the generated data, trend is absent, so it is preferable to use the decomposition method, so trend would be represented as a horizontal line. In that case it is convenient to use the abstraction when the time series decomposes into several components: the remainder (the average value in a series), trend, seasonality and noise (random variation in a series). The first three components refer to systematic components of the time series that are consistent or repeatable and can be described and modeled. Noise, in turn, refers to the non-systematic component - it cannot be modeled directly.

According to Figure 3.b, it can be seen that seasonality has the same frequency and amplitude (width and height of cycles), that is, the linearity of the seasonal component. Then it seems possible to use an additive model describing the components of the time series, where the changes over time are consistently produced by the same amount:

$$y(t) = Residuals + Trend + Seasonality + Noise \quad (1)$$

After the decomposition is performed (Figure 4), the next step is to construct a mathematical model describing a stationary remainder of the time series. Building a model based on the ARIMA requires calculation of the parameters p, d, q, which can be performed in several ways. This article uses the method of iterative search for the best model by iterating through all of the basic combinations of parameters; the models are evaluated using the Akaike Information Criterion (AIC). This criterion measures how well the model fits the data, taking into account the overall complexity of the descriptive function.

A model that accurately describes data using multiple functions will have a larger AIC indicator than a model that uses fewer functions to achieve the same accuracy. Therefore, it is necessary to choose a model that gives the lowest value of the criterion. After iterative search, coefficients (0, 2, 0) gave the minimal result AIC:-7965,1. Figure 5 shows a graph of the time series and residuals description using the generated model ARIMA (0, 2, 0).

3.2 Model based on recurrent neural networks

From all the types of neural networks, the long-term memory (LSTM) is allocated to work with time series; it is well suited to learning on tasks of classification, processing and forecasting of time series in cases where important events are separated by time lags with indefinite duration and boundaries [8]. This recurrent network is trained using the back propagation in time - an algorithm that is used to update weights with all the network parameters taken into account. Use of a neural network can be rephrased as a question of constructing the regression dependence.

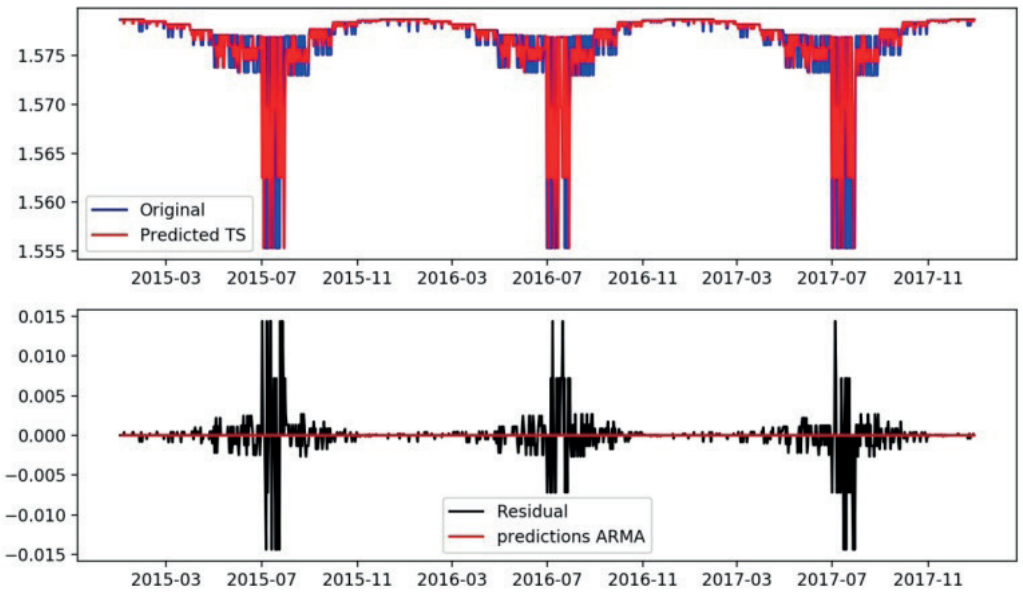

Figure 5 *Description of the original time series and residuals by the ARIMA model*

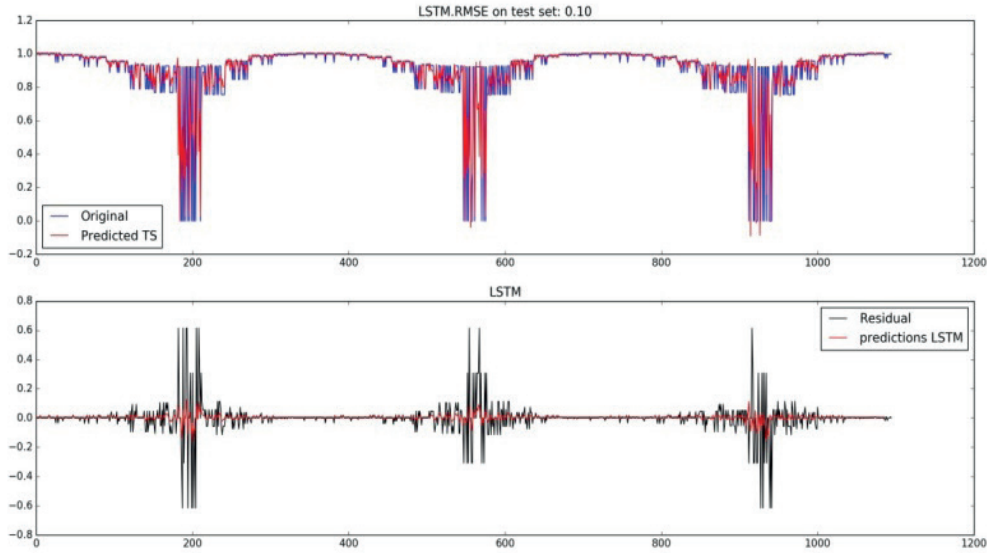

Figure 6 *Description of the original time series and residues by the LSTM model*

When using the time series, it is important to follow the order of using the values. The simplest method to use is to split an ordered set of data into a training and test data sets. The data was divided into a training data set with 67% of observations that can be used to train the model, leaving the remaining 33% for testing the model.

After the original data is modeled and the accuracy of the describing model is estimated by the training sample, one needs to get an idea of the predictive ability of the model with the new test data. For regression, this was done by using the cross-validation.

Form a network in which there is a visible layer with 1 input signal, a hidden layer with 4 LSTM blocks or neurons and an output level that makes one prediction value. For LSTM blocks, the default sigmoid activation function is used. Figure 6 presents a graph of the time series and remainder description using the generated model.

4. Conclusion

The article examines two main models of detrending and forecasting the time series. For the model building process a general data set was used, containing information about the dynamic response of the structure during the temperature

fluctuations. Development of the two models, allowing to predict the influence of environment on the dynamic behavior of a structure, is an urgent task in the field of monitoring of artificial structures. Its solution would lead to reduction in the number of parameters that require direct measurement and, consequently, to simplifying the monitoring systems and reducing their costs.

Both models give a good descriptive ability, the root-mean-square error is within acceptable limits. Constraints on the predictive ability of models are introduced in connection with the correlation of the data of the numerical experiment; in the future, with long-term monitoring of real objects, this can be avoided.

Further investigation in this direction would be to combine the two models and construct one predictor based on the method of voting (ensemble learning). This combination would improve the predictive ability, eliminate errors arising due to appearance of emissions and align the flaws of each model.

References

[1] KO, J. M., et al. Formulation of an uncertainty model relating modal parameters and environmental factors by using long-term monitoring data. SPIE 5057, Smart Structures and Materials 2003: Smart Systems and Nondestructive Evaluation for Civil Infrastructures : proceedings [online]. Vol. 5057. 2003, p. 298-307. Available from: https://doi.org/10.1117/12.482380

[2] RAMOS, L. F. Damage identification on masonry structures based on vibration signatures. PhD Thesis. Braga: University of Minho, 2007.

[3] MAECK, J., PEETERS, B., DE ROECK, G. Damage identification on the Z24-bridge using vibration monitoring. *Smart Materials and Structures* [online]. 2001, **10**(3), p. 512-517. ISSN 0964-1726/eISSN 1361-665X. Available from: https://doi.org/10.1088/0964-1726/10/3/313

[4] WONG, K. Y., MAN, K. L., CHAN, W. Y., Monitoring Hong Kong's bridges *real-time kinematic spans the gap*. *GPS World*. 2001, **12**(7), p. 10-18.

[5] International Federation for Structural Concrete. Task group 2.8. Safety and performance concepts: Reliability assessment of concrete structures: Guide to good practice. In: Bulletin / Feedeeration internationale du beeton. NO. 86. Lausanne, 2018. ISBN 978-2-88394-126-7.

[6] Recommendations for calculating the temperature and shrinkage effects on span structures of bridges. CNIIS, 2009.

[7] BOX, G. E. P., et al. *Time series analysis: Forecasting and control.* 5. ed. Hoboken, New Jersey: John Wiley & Sons, 2015. ISBN: 978-1-118-67502-1.

[8] CRONE, S. F., HIBON, M., NIKOLOPOULOS, K. Advances in forecasting with neural networks? Empirical evidence from the NN3 competition on time series prediction. *International Journal of Forecasting* [online]. 2011, **27**(3), p. 635-660. ISSN 0169-2070. Available from: https://doi.org/10.1016/j.ijforecast.2011.04.001

Mykola Sysyn - Vitalii Kovalchuk - Ulf Gerber - Olga Nabochenko - Bogdan Parneta*

LABORATORY EVALUATION OF RAILWAY BALLAST CONSOLIDATION BY THE NON-DESTRUCTIVE TESTING

The property of railway track to resist the irreversible deformation for a long-term operational loading considerably depends on the ballast layer. The ballast layer is the element of a railway track whose mechanical properties and state are formed in-situ with the help of the ballast cleaning, tamping and distributing machines. The varied properties of the ballast material to obtain the form during the maintenance and retain it during the operation are equally important for the ballast layer. The control over the processes of the ballast consolidation and deconsolidation by means of measurement methods could potentially provide great possibilities for improvement of its properties both during the maintenance and operation. The paper deals with an experimental study of the railway ballast consolidation and deconsolidation processes under the vibration loading of the sleeper. A non-destructive measurement method is proposed to investigate the distribution of the ballast consolidation along the sleeper. The method is based on the measurement of time of mechanical wave propagation. Modern low-cost sensors and powerful microcontroller techniques enable creating smart measurement systems for automatic multi-point data acquisition, online processing and statistical estimation of the ballast consolidation distribution.

Keywords: *railway ballast, tamping, consolidation, wave propagation, seismic method, non-destructive measurement*

1. Introduction

The operation of the railway track and its maintenance or construction depend considerably on the ballast layer. The ballast layer is an element of the track superstructure, where the residual deformations accumulate most quickly. The reason is that the ballast is a grained material that poorly absorbs the dynamic loads from the rolling stock. The occurrence of geometrical irregularities of the track, as a result of uneven settlements of the ballast layer, causes dynamic load on the track, which affects the work of all of its elements. Besides that, the ballast layer is an element of the track superstructure with the least industrialized degree of construction and maintenance. Unlike other elements, such as rails, sleepers, fastenings, the ballast layer formation occurs directly on the track during its construction. Thus, the property of the ballast material to easily change its shape during the construction and at the same time sustainably maintains a given shape throughout the lifecycle of the track are two contradictory requirements that are demanded of the ballast layer. The effect on these properties of the ballast is achieved during its consolidation. The control over this parameter and knowledge of its influence on the ballast deformation processes can allow to significantly optimize the track superstructure, as well as the work of the ballast tamping machines.

The quality control and the ballast layer influence on duration of the track lifetime are the subject of numerous studies and publications in recent years [1-6]. The investigations [7-8] have discovered a significant effect of the ballast layer consolidation and ballast filling on the construction of railroad engineering buildings. A simulation of railway track and turnout geometry deterioration due to inhomogeneous settlements of ballast layer is presented in [9-10].

Behavior of the ballast layer under the influence of a number of factors, including the initial stage of filling, the elasticity of the subgrade and the vibrational impact of the rolling stock have been studied in detail by the authors of [11-13]. Authors in [14] present theoretical analysis of the ballast vibration characteristics and their influence on a loose contact between the sleeper and ballast layer that causes a higher settlement of the ballast track.

The experimental determination of the quality of the ballast layer consolidation of the railway track is the basis of the authors' research [15-17]. A comprehensive review of the non-destructive methods of evaluation of the ballast layer consolidation is presented in [18].

The majority of methods of non-destructive evaluation of the ballast layer consolidation are based on measurements of the passage of elastic wave by geophones or accelerometers. The measurement of wave passage, analysis and determination of soil properties are the main tasks of a seismic survey. Application of the seismic survey methods for construction and transport purposes is based in SASW (Spectral Analysis Surface Waves) and MASW (Multichannel Analysis of Surface Waves) [19-20]. Those methods are based on the kinematic and dynamic interpretation of impact response of surface waves. The advantage of those methods is the simple arrangement of measuring sensors on the surface of the soil; the disadvantage is the relatively low resolution ability in inhomogeneous soil properties determination.

The methods of the wave propagation analysis are inextricably linked with mathematical methods of information processing, signal analysis and statistics. The application of

* [1]Mykola Sysyn, [2]Vitalii Kovalchuk, [1]Ulf Gerber, [2]Olga Nabochenko, [3]Bogdan Parneta
[1]Institute of Railway Systems and Public Transport, Technical University of Dresden, Germany
[2]Department of the rolling stock and track, Lviv branch of Dnipropetrovsk National University of Railway Transport, Lviv, Ukraine
[3]Department of Construction industry, Lviv Polytechnic National University, Lviv, Ukraine
E-mail: mykola.sysyn@tu-dresden.de

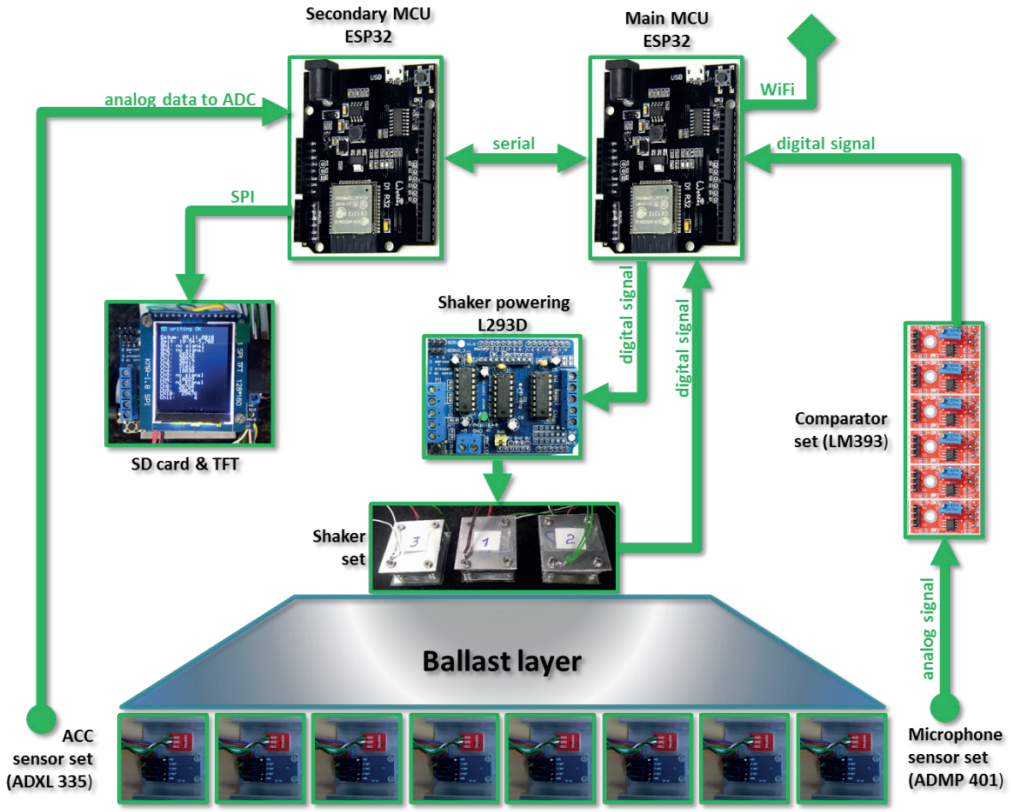

Figure 1 *Structural scheme of the device for measurements of ballast layer consolidation*

methods of machine and deep learning allow not only to automate the processing and interpretation of data, but also significantly increase the degree of information use and accuracy of measurements [21-22]. In the study [23] methods of cluster and discriminant analysis were used to identify the characteristic features of the ballast layer consolidation.

The purpose of this article is to develop the techniques for the laboratory determination of the ballast layer consolidation based on the non-destructive methods of geophysics. The method of measuring of the ballast layer consolidation should meet the following requirements:

- The measured value should vary depending on the ballast layer consolidation within considerable limits with regard to random fluctuations, providing sufficiently low relative error.
- The spatial separating ability of the ballast layer density measurement should not be less than a half of the thickness of the ballast layer; i.e. measurements must be performed simultaneously by a dense network of sensors.
- Dynamic and kinematic interpretation of the impulse response is based on the measurements of velocity of the wave propagation and acceleration.
- The measurement system should provide automatic measurements, data acquisition and their storing for the analysis.

Along with development of the method, it is necessary to determine the effect of the ballast layer consolidation on the measured velocity of the waves propagation and acceleration.

2. Development of the method for laboratory determination of ballast layer consolidation

The basis of the method for determining the ballast layer consolidation is measurement of velocity of the longitudinal waves passage through the ballast layer and recording of dynamic oscillations. The induction of dynamic oscillations and their registration are carried out by the developed device, the structural scheme of which is shown in Figure 1. The device consists of two programmable microcontrollers of type ESP-32, which control and create impulses, obtain digital signals and digitize analogue signals from sensors, pre-process, evaluate and store information with the output of current information about work fulfilment on the screen. Microcontrollers synchronously perform distributed tasks under direction of the main unit, which is synchronized with the Internet time. The elements of the periphery are three electromagnetic shakers that create a series of impacts in three points of the ballast layer. Shakers power management is performed by the program of the main microcontroller with digital control via Motor Shild L293D. MEMS sound microphones such as ADMP 401 (M1-M10) and ADXL 335 tri-axle accelerometers are used as sensors. The analogue information from the microphones about the time of wave propagation is digitized by the comparator system and transmitted digitally to the main controller. This method allows carrying out mass simultaneous measurements by the network up to 48 sensors per 1 microcontroller unit. The analogue information of acceleration signals of longitudinal and transverse waves from six accelerometers is digitized with the frequency of 15 kHz and is stored on an SD card.

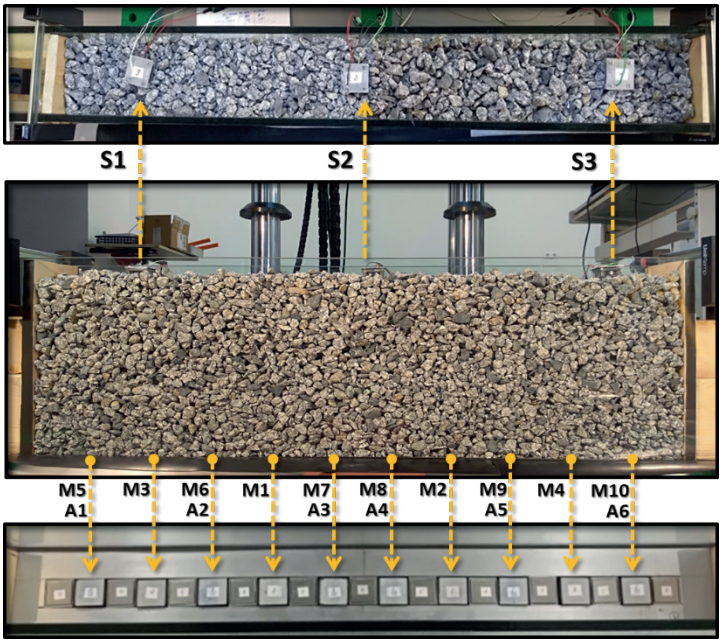

Figure 2 *Sensors and shaker location in the ballast box (bottom: accelerometers (A1-A6) and microphones (M1-M10) under the ballast, top: location of shakers on the ballast surface, middle: view from the ballast side in the box with glass walls)*

Before starting the measurement of the ballast layer consolidation, the microcontroller is synchronized with the real time through the server of the global Internet. After the synchronizing the microcontroller by means of the developed SeismoDens software, the programmed ESP-32 microcontroller launches Motor Shild, which controls the operation of shakers. The source of elastic waves from a shaker is an impact of an electromagnet on a metal plate with transverse dimensions of 5 cm by 3 cm, which is placed on the ballast after each stage of the ballast consolidation. The shakers consist of housing and a built-in electromagnet, which is attracted to the bottom of the metal housing; it creates an impulse while being powered. Shakers impulses occur in turn with the start time of the impulse recorder by means of separate digital channels on the main microcontroller board. At first, the impact is given by the shaker number 1 (left-hand side of the ballast layer), followed by the shaker number 2 (ballast layer center) and shaker number 3 (right-hand side of the ballast layer) in Figure 2. Getting statistically reliable data on time of the waves propagation in a granular ballast environment is provided by the program of a microcontroller, which creates a series of impacts from each of the shakers in the amount of 12 times. After fixing the initial wave propagation moment, by means of MEMS microphones ADMP401, the momentum passage through the ballast layer is recorded.

In addition to microphones to perform dynamic interpretation of the ballast consolidation signals, the recording of vibration accelerations, since the moment of impact, has been done using acceleration sensors ADXL 335 (accelerometers in Figure 1 have numbers from A1 to A6). The width of the impact of the shakers is chosen so that the wavelength is greater than the distance between the transmitter of impact (shaker) and receiving sensors (microphones and accelerometers). This is a compulsory condition for correct determination of speed of the sound signal propagation. After each measurement, the sound and acceleration measurements are recorded into a file with the name according to the recording date and the operating time of the device.

The laboratory bench for studying the degree of ballast consolidation is the ballast box filled with crushed stone of the size 1.0x0.17x0.33 m (Figure 2). The side walls of the box are thick-walled glass slabs to monitor the movement of ballast particles and perform photogrammetric measurements. This box is filled with crushed stone of granite fractions 8/16 to a depth of 0.27 m without consolidation. The end walls are capable to fulfil the longitudinal displacement when the ballast pressure reaches the friction resistance.

The bottom of the box consists of c-channel profiles where the signal cables and power supply to the sensors are placed. Sound sensors and accelerometers are placed in separate parts of the metal profile with the width and length of 40 mm and the height of 20 mm. These elements are separated from adjacent sensors and the base by the noise-isolation material in order to partially exclude the side-effects from the hydro-pulse. The total number of separate profiles with sensors is 10 pcs. Six of them are with common location of ADXL335 acceleration sensors and ADMP 401 microphones and four profiles are only with microphones. Microphones in Figure 2 have symbols from M1 to M10, accelerometers have symbols from A1 to A6 and shakers have symbols from S1 to S3.

3. Experimental studies of the ballast layer consolidation

The laboratory studies consisted of a sequence of cycles of the ballast layer consolidation and impact response measurements. The load was carried out by a servo-hydraulic test machine ZWICK HB 160. The load was applied to an I-beam placed in the ballast box that occupied the entire perimeter of the ballast prism.

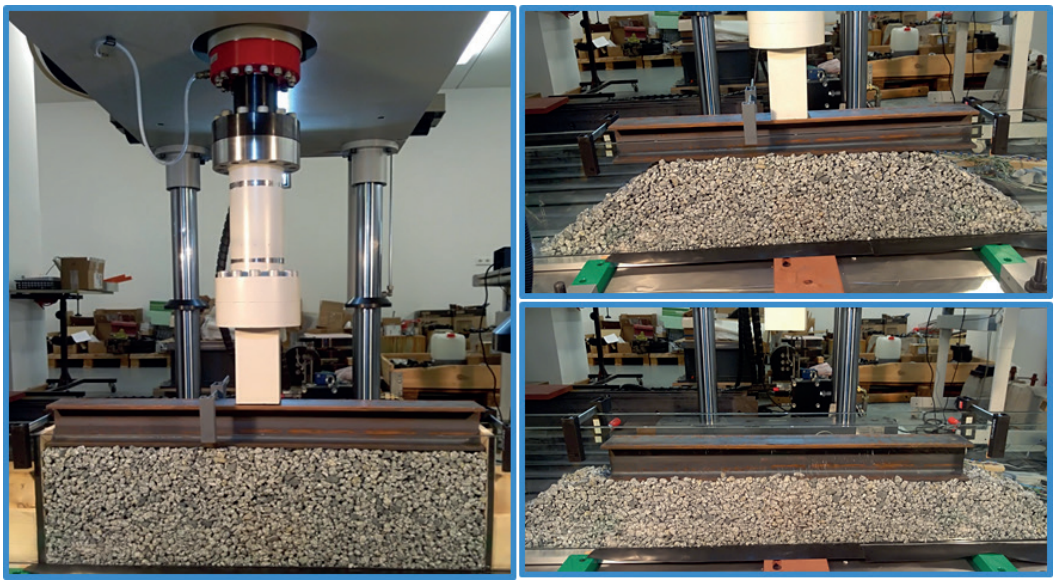

Figure 3 The ballast consolidation process in the laboratory experiment (left: initial state in cycle No1, right above: the ballast box without side enclosure after cycle No2, right below: the ballast settlement after cycle No2)

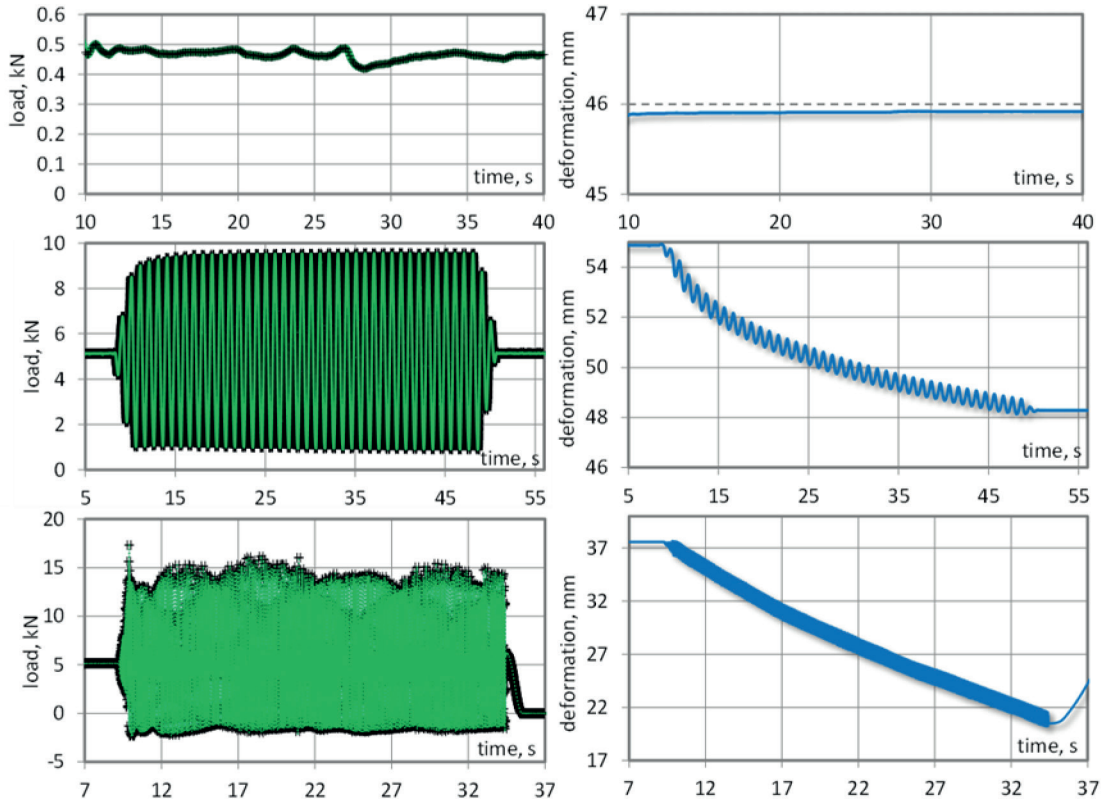

Figure 4 Load on the sleeper (on the left) and its settlement (on the right) in cycles No2 1 (above), No2 (in the middle) and No3 (bottom)

Figure 3 shows the ballast layer in 3 cycles of the experiment: before consolidation, intermediate state and after consolidation.

In each cycle of the experiment, static and dynamic loading were applied to the stamp, while the dynamic settlement of a sleeper was being measured. Dynamic loads and the results of a sleeper settlement in three cycles are shown in Figure 4. In the cycle No1, the constant loading through the stamp was 0.5 kN, while the residual settlement was almost not observed. During the cycle No2, a smooth change in loading from 0 kN to 5 kN was initially applied, and then the dynamic harmonic loading at a frequency of 1 Hz, ranging from 0 kN to 10.0 kN, was used. The overall stamp settlement is 6.7 mm in 25 load cycles. In the third cycle, the static load remained 5 kN and the total dynamic load on the sleeper was 15 kN with a frequency of 40 Hz. At the same time the ballast was completely unloaded. The settlement was 19 mm per 1000 load cycles.

After each consolidation cycle, measurements of the elastic oscillation propagation in the ballast layer were made using the

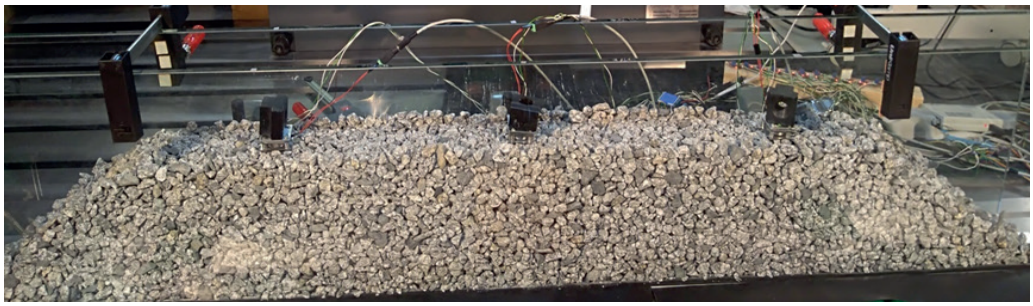

Figure 5 *Measuring the ballast layer consolidation*

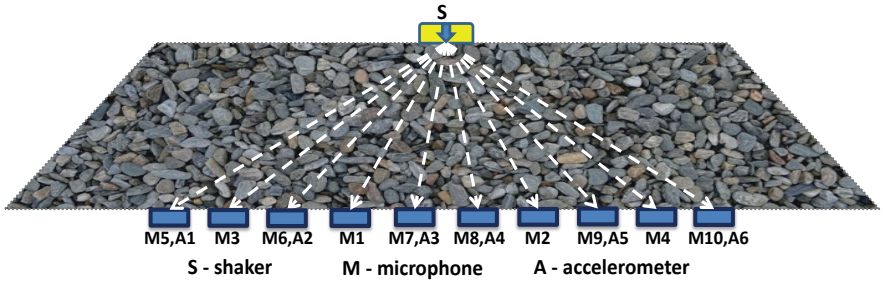

Figure 6 *Measuring the ballast layer consolidation*

developed method for determining the ballast layer consolidation. A group of shakers alternately created a series of 12 impacts, which were recorded and analysed by a series of ballast sensors of acceleration and sound distribution under the ballast. Figure 5 shows the process of measuring the ballast layer consolidation after the cycle No2 of the consolidation program with removed sleeper.

4. Analysis of influence of the ballast layer consolidation on the propagation of elastic waves in the ballast layer

The analysis of time and speed of waves propagation is carried out at three ballast consolidation states, namely: unconsolidated ballast, an intermediate state of the ballast consolidation and a ballast layer with maximum density of consolidation. The passage of elastic waves through a granular environment, which is the ballast layer of the railway, is determined according to the material and granulometric composition of the grains and, to a large extent, the number of contacts between grains, that is, the density of the ballast layer. Thus, measuring the velocity of elastic waves propagation after the shaker impact initiation, one can conclude about the degree of the ballast layer consolidation. The speed is determined by the known formula:

$$V = \frac{L}{t}, \tag{1}$$

where L - path of a wave propagation from a shaker to a microphone; t - time of wave passage from the impact (of a shaker) transmitter to the impact receiver (microphone).

The distance L is determined depending on the thickness of the ballast layer after each consolidation cycle and the relative position of the shaker and sensors. Figure 6 shows the scheme of L paths determination.

Then, the analysis of the impact of the ballast consolidation on the time and velocity of wave propagation in the case of shaker placing in the center of the ballast prism is carried out. The passage time of waves propagation from shaker No2 to sensors M3, M1, M2 and M4 at different consolidation cycles are shown in Figure 7. The passage time of a wave ranges from 1000 to 1500 μs for an unconsolidated state of the ballast and from 90 to 850 μs for maximum densities of the ballast. There is a significant increase in the passage time of a wave to side sensors, especially in the consolidated state. For sensors M1 and M2, which are the closest to the source of impacts, in the unconsolidated ballast, the average passage time of the wave through the granular medium is 1131 μs. For intermediate ballast compaction the average time is 737 μs, and for the maximum density of the ballast (according to experimental consolidation) the average propagation time of a wave is 298 μs. Consequently, the increase in the passage time of a wave through the ballast to a sensor in the ratio of propagation time of a wave in unconsolidated ballast to maximum density of the ballast is 3.7 times. Therefore, with increasing ballast consolidation, the passage time of a wave decreases. So, according to the time of the wave impact propagation from the source of impact to the receiving sensor, the degree of railway ballast consolidation can be assessed. The increase of time of the wave passage to side sensors is caused by the greater distance of the wave path.

To verify the method of determining the wave propagation time according to microphones records, the comparison of them to results of longitudinal waves records of accelerometers is performed. Figure 8 shows the records of longitudinal waves acceleration made by accelerometer A4 from shaker No2 after three cycles of consolidation, as well as the moment of impact start. The average propagation time of the pressure wave, determined by the accelerometer, is numbered after cycles No1, 2, 3, respectively, 1850 μs, 830 μs and 250 μs. Those results, taking into account the location of the accelerometer and the statistical

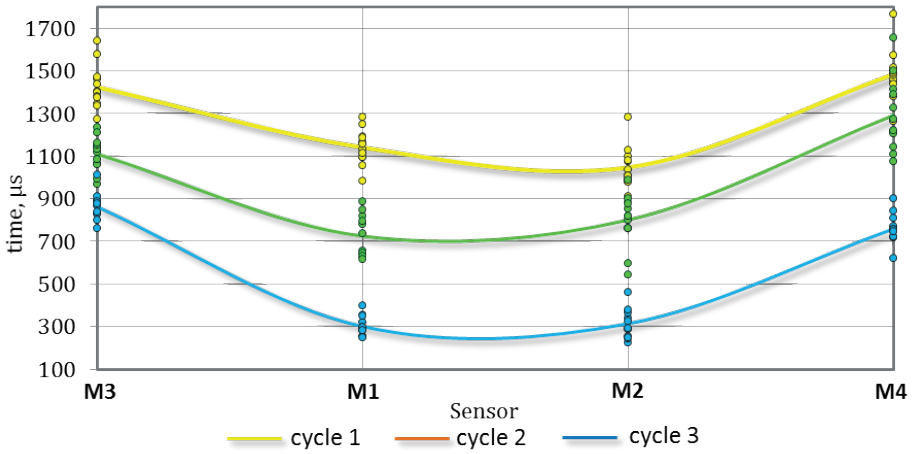

Figure 7 *Time of pressure waves propagation with the given impact from a shaker No2*

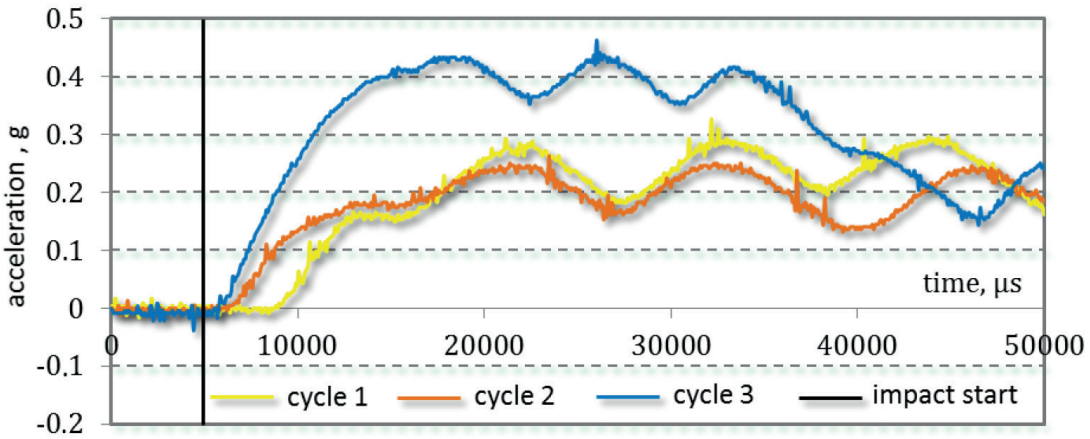

Figure 8 *Records of longitudinal waves acceleration by accelerometer A4 from shaker No2*

Table 1 *Wave propagation velocities for different compaction states*

Ballast compaction	Velocity, m/s			
	M3	M1	M2	M4
low	274	260	284	263
intermediate	333	377	344	289
high	386	732	717	440

spread, are fully consistent with measurements due to the sound propagation. However, the advantage of the microphone system is much greater accuracy of time measurement at high level of consolidation. In this case, according to the records of the wave passage time made by the accelerometer with the frequency of 13300 Hz at the highest density, the wave passage numbers 12 levels of a digitized signal. Accuracy increase can be achieved by the frequency increase, which inevitably leads to a proportional reduction of accelerometers in number and that is a disadvantage of this method of measurement. Thus, the proposed method of multisensory simultaneous measurement by microphones is a promising alternative to traditional methods.

The velocity of sound propagation according to times in Figure 7 is shown in Figure 9. In the case of impact setting from the central shaker No2 with unconsolidated ballast, an average wave propagation velocity to M1 microphone is 260 m/s, with an intermediate ballast compaction is 377 m/s and with the maximum compaction of the ballast is 732 m/s. An average wave propagation velocity to microphone M2 is 284 m/s, with an intermediate ballast compaction is 344 m/s and with the maximum compaction of the ballast is 717 m/s.

The velocity of wave propagation to remote microphones M3 and M4 is 274 m/s and 263 m/s, respectively, with unconsolidated ballast; with an intermediate ballast compaction is 333 m/s and 289 m/s, respectively and with the maximum compaction of the ballast is 386 m/s and 440 m/s, respectively. Results of measurement correspond to the values range from reference books [24] for sediment rocks. Results of determining the wave propagation velocities for three different compaction states are shown in Table 1.

The peculiarity of velocity distribution in Figure 9, in contrast to time distribution in Figure 8, is its almost the same indices at the initial stage. It is explained by the isotropy of ballast properties and homogeneity at all points of the ballast box. At the same

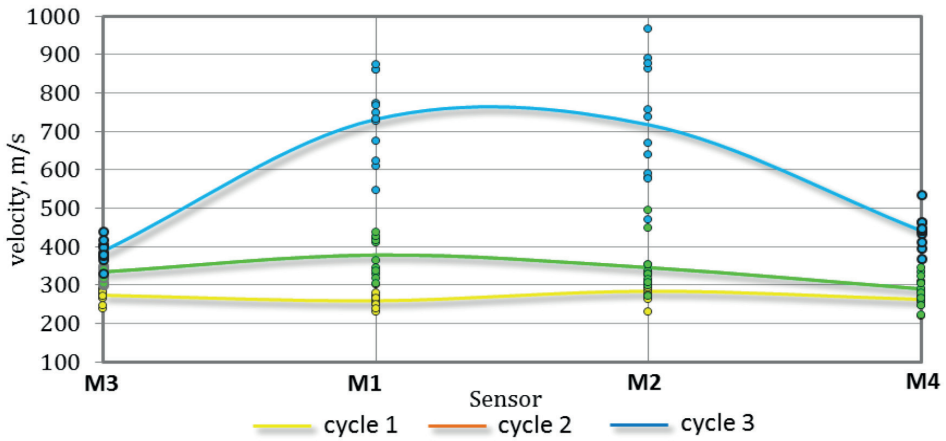

Figure 9 *Speed of impact waves passage at different stages of the ballast layer consolidation and impulse assignment from shaker No2*

time, it is necessary to underline the high level of measured speeds variations, which grows along with an average speed. Obtaining reliable values of velocity and consolidation of the ballast layer requires the use of modern statistical methods of data processing. Application of the newest powerful programmable microcontroller systems allows to automate statistical processing to online evaluation of the quality of measurements and the need for additional measurements.

5. Summary and subsequent studies

The ballast layer consolidation method has been developed and applied. It revealed a significant change in properties of the ballast during its deformation under the sleeper. The study proved the possibility of using the multi-sensory measurement by sound sensors in the field of wave front propagation instead of a complex method based on accelerometers. Results of measurements showed a significant local increase in the velocity of the longitudinal waves passage in the ballast layer. These results are confirmed by many studies that show the presence of consolidation zones under the sleeper.

The proposed approach will significantly improve the accuracy of determination of the ballast layer spatial consolidation during the tamping machines work, as well as in the process of modelling the operational deformations of the track. A promising area for further research is the application of computer statistics and machine learning algorithms for establishing interrelations between the ballast consolidation and characteristics of the impact response. Application of the modern sensor and microcontroller technologies allows simple and effective implementation of theoretical methods in creation of autonomous systems for monitoring the technical state of the track and engineering structures with the ballast layer.

References

[1] IZVOLT, L., HARUSINEC, J., SMALO, M. Optimisation of transition areas between ballastless track and ballasted track in the area of the tunnel Turecky vrch. *Communications - Scientific Letters of the University of Zilina* [online]. 2018, **20**(3), p. 67-76. ISSN 1335-4205/eISSN 2585-7878. Available from: http://komunikacie.uniza.sk/index.php/communications/article/view/256

[2] WANG, H., MARKINE, V. Modelling of the long-term behaviour of transition zones: prediction of track settlement. *Engineering Structures* [online]. 2018, **156**, p. 294-304. ISSN 0141-0296/eISSN 0141-0296. Available from: https://doi.org/10.1016/j.engstruct.2017.11.038

[3] FISCHER, S. Breakage test of railway ballast materials with new laboratory method. *Periodica Polytechnica Civil Engineering* [online]. 2017, **61**(4), p. 794-802. ISSN 0553-6626/eISSN 1587-3773. Available from: https://doi.org/10.3311/PPci.8549

[4] FISCHER, S., JUHASZ, E. Railroad ballast particle breakage with unique laboratory test method. *Acta Technica Jaurinensis* [online]. 2019, **12**(1), 26-54. eISSN 2064-5228. Available from: https://doi.org/10.14513/actatechjaur.v12.n1.489

[5] PLASEK, O., et al. Influence of under sleeper pads on track quality. *Akustika*. 2015, **23**(1), p. 28-33. ISSN 1801-9064.

[6] NAGY, R. Description of rail track geometry deterioration process in Hungarian rail lines no. 1 and no. 140. *Pollack Periodica* [online]. 2017, **12**(3), p. 141-156. ISSN 1788-1994/eISSN 1788-3911. Available from: https://doi.org/10.1556/606.2017.12.3.13

[7] KOVALCHUK, V., et al. Estimation of carrying capacity of metallic corrugated structures of the type multiplate mp 150 during interaction with backfill soil. *Eastern-European Journal of Enterprise Technologies* [online]. 2018, **1/1**(91), p. 18-26. ISSN 1729-3774/eISSN 1729-4061. Available from: https://doi.org/10.15587/1729-4061.2018.123002

[8] IZVOLT, L., SESTAKOVA, J., SMALO, M. Analysis of results of monitoring and prediction of quality development of ballasted and ballastless track superstructure and its transition areas. *Communications - Scientific Letters of the University of Zilina*. 2016, **18**(4), p. 19-29. ISSN 1335-4205/eISSN 2585-7878. Available from: http://komunikacie.uniza.sk/index.php/communications/article/view/284

[9] NABOCHENKO, O., et al. Studying the railroad track geometry deterioration as a result of an uneven subsidence of the ballast layer. *Eastern-European Journal of Enterprise Technologies* [online]. 2019, **1/7**(97), p. 50-59. ISSN 1729-3774/eISSN 1729-4061. Available from: https://doi.org/10.15587/1729-4061.2019.154864

[10] SYSYN, M., et al. Modelling and vehicle based measurements of ballast settlements under the common crossing. *European Transport* [online]. 2019, **71**, p. 1-19. ISSN 1825-3997. Available from: http://www.istiee.org/te/

[11] GERBER, U., FENGLER, W. Setzungsverhalten des Schotters / Settlement behaviour of ballast (in German). *Eisenbahntechnische Rundschau*. 2010, **59**(4), p. 170-175. ISSN 0013-2845.

[12] SYSYN, M., et al. The complex phenomenological model for prediction of inhomogeneous deformations of railway ballast layer after tamping works. *Archives of Transport* [online]. 2018, **47**(3), p. 91-107. ISSN 0866-9546/eISSN 2300-8830. Available from: https://doi.org/10.5604/01.3001.0012.6512

[13] HOLTZENDORFF, K. Untersuchung des Setzungsverhaltens von Bahnschotter und der Hohllagenentwicklung auf Schotterfahrbahnen. /Investigation of the settlement behavior of railway ballast and voids development on ballasted tracks (in German). Ph.D. thesis, TU Berlin. 2013.

[14] WANG, B., MARTIN, U., RAPP, S. Vibration characteristic analysis of ballast with different aspect ratios by means of the discrete element method. In: WALUBITA, L. F., HOLLERAN, I., MWANZA, A. D. (eds.): *Geo-China 2016: Resilient Railroad Materials and Structures to Mitigate Climate Change*. Geotechnical Special Publication (268 GSP)*,* 2016, p. 16-23. eISBN 9780784480113.

[15] SMUTNY, J., NOHAL, V. Vibration analysis in the gravel ballast by measuring stone method. *Akustika*. 2016, **25**(1), p. 22-28. ISSN 1801-9064.

[16] SADEGHI, J. Field investigation on dynamics of railway track pre-stressed concrete sleepers. *Advances in Structural Engineering* [online]. 2010, **13**(1), p. 139-151. ISSN 1369-4332/eISSN 2048-4011. Available from: https://doi.org/10.1260/1369-4332.13.1.139

[17] LAM, H., WONG, M. Railway ballast diagnose through impact hammer test. Procedia Engineering - The Twelfth East Asia-Pacific Conference on Structural Engineering and Construction : proceedings [online]. Vol 14. Elsevier, 2011. ISSN 1877-7058, p. 185-194. Available from: https://doi.org/10.1016/j.proeng.2011.07.022

[18] BOLD, R. D. Non-destructive evaluation of railway trackbed ballast. PhD Thesis, Institute for Infrastructure and Environment, School of Engineering, University of Edinburgh, 2011.

[19] PARK, C. B., MILLER, R. D., RYDEN, N. Roadside seismic survey utilizing traffic noise. NDE Conference on Civil Engineering : proceedings. St. Louis, MO, USA, 2006, p. 323-334.

[20] SUSSMANN, T. R., et al. Use of seismic surface wave testing to assess track substructure condition*. Construction and Building Materials* [online]. 2017, **155**, p. 1250-1255. ISSN 0950-0618/eISSN 1879-0526. Available from: https://doi.org/10.1016/j.conbuildmat.2017.02.077

[21] SYSYN, M., et al. Turnout monitoring with vehicle based inertial measurements of operational trains: a machine learning approach. *Communications - Scientific Letters of the University of Zilina* [online]. 2019, **21**(1), p. 42-48. ISSN 1335-4205/eISSN 2585-7878. Available from: http://komunikacie.uniza.sk/index.php/communications/article/view/1166

[22] SYSYN, M., KOVALCHUK, V., JIANG, D. Performance study of the inertial monitoring method for railway turnouts. *International Journal of Rail Transportation* [online]. 2019, **7**(2), p. 103-116. ISSN 2324-8378/eISSN 2324-8386. Available from: https://doi.org/10.1080/23248378.2018.1514282

[23] SYSYN, M., et al. Evaluation of railway ballast layer consolidation after maintenance works*. Acta Polytechnica* [online]. 2019, **58**(6), p. 1-16, 2019. ISSN 1210-2709/eISSN 1805-2363. Available from: https://doi.org/10.14311/AP.2019.59.0077

[24] DAHM, T. Grundlagen der Geophysik / Basics of Geophysics (in German). Lecture Notes [online]. Potsdam: Deutsches GeoForschungs Zentrum GFZ, 2005. Available from: https://doi.org/10.2312/GFZ.2.1.2015.001

Denis Kapski - Valery Kasyanik - Oleksii Lobashov - Aleksandra Volynets - Oleg Kaptsevich - Andrii Galkin*

ESTIMATING THE PARAMETERS OF TRAFFIC FLOWS ON THE BASIS OF PROCESSING OF LOCALIZATION DATA ON THE MOVEMENT OF VEHICLES

The article describes the method of estimating the parameters of transport flows using the two-fluid mathematical model of Herman-Prigogine and developed and based on the proposed method of estimating the parameters of the system on the basis of passive processing of navigation data on the movement of vehicles. The efficiency of the proposed algorithms, mathematical models for estimating the parameters of road traffic flow and system as a whole was confirmed during its testing using a set of tracks on the main highways of Commonwealth of Independent States.

Keywords: *vehicle, traffic flow, navigation system, the parameters of traffic flow, a mathematical model for evaluating traffic flow*

1. Introduction

At present, traffic congestion in road networks is a topical transport-related issue in most developed countries of the world. First of all, this problem is typical for the street and road networks of cities, where most of the fleet of personal vehicles is concentrated, as well as for key highways and transport corridors, which carry significant volumes of freight and passenger traffic.

Currently, significant experience in implementing measures aimed at solving this problem has been accumulated world-wide. These measures fall into three broad groups:

- measures aimed at increasing the maximum road network capacity (construction and reconstruction of road facilities);
- measures aimed at increasing the efficiency of using the existing road network capacity (improving traffic management);
- measures aimed at regulating the volume and structure of transport demand (introduction of various restrictions on the movement and parking of vehicles; reducing the need of the economy and the population for transport through measures in the field of territorial planning, etc.).

The basis for the development of such measures and the adoption of scientifically grounded solutions for their implementation is the application of mathematical modeling methods for the functioning of the existing and planned transport systems.

Predicting the effect of various measures aimed at managing the road network capacity requires solving various problems of transport modeling:

- predicting the effect of the construction or reconstruction of road facilities requires modeling the distribution of traffic flows over the road network;
- evaluating the effectiveness of measures on improving traffic management as a rule requires modeling the movement of individual vehicles in the traffic flow;
- evaluating the effectiveness of measures on regulating transport demand requires modeling the volume and structure of the need of the population and the economy for driving.

The necessity to use transport models will continue to grow as transport systems evolve (expansion and increase of connectivity of the road network, increased role of multimodal transport, introduction of intelligent transport systems, etc.), and as the already existing problem of congestion in road networks of major transport corridors and cities is worsening.

In order to use certain mathematical models to provide decision-making on the management of transport flows, it is necessary to correctly choose the criteria and methods for assessing traffic flows.

2. Choosing the optimal criteria for assessing traffic flows and the method for mathematical modeling of transport systems

When estimating street and road networks, a variety of tasks and situations may arise. This results in the need to use a number of partial and integral criteria for assessing traffic flows [1].

Partial criteria according to the nature of use can be divided into those used only as descriptors and those used as parameters of the management process. The latter include the average and total delays, the queue length, the leg length minus the queue length.

* [1]Denis Kapski, [2]Valery Kasyanik, [3]Oleksii Lobashov, [4]Aleksandra Volynets, [5]Oleg Kaptsevich, [6]Andrii Galkin
[1]Department of Transport Systems and Technologies, Automotive and Tractor Faculty, Belarusian National Technical University, Minsk, Belarus
[2]Brest Technical University, Belarus
[3]Department of Transport and Logistics, O. M. Beketov Kharkiv National University of Urban Economy, Ukraine
[4]State Enterprise Belarusian Road Scientific Research Institute, Belarus
[5]Department OJSC „AGAT - Control Systems“, company Geographic Information Management System, Belarus
[6]Department of Transport and Logistics, O. M. Beketov Kharkiv National University of Urban Economy, Ukraine
E-mail: galkin.tsl@gmail.com

The most significant criterion for the economic evaluation of the state of the traffic management is often considered to be the transport operation of the street and road network.

Another criterion is the stability of the street and road network functioning. This indicator is defined [2] as a property allowing to not reduce its capacity as a result of full or partial failure of its individual elements. Failure is considered as a change in road traffic conditions, which results in this element of the street and road network being partially or completely excluded from the transport process.

Criteria based on the magnitude of the delay and the queue length are also singled out. The duration of the average delay of the vehicle has been widely used as a criterion for optimizing traffic control at a separate intersection. It has been determined that the average delay closely correlates with such indicators as the total delay, queue length, traffic intensity, parameters of the traffic control mode.

The queue length means the number of vehicles in the queue or its length in linear units. This parameter is closely correlated with the average and maximum delays, traffic intensity, parameters of the traffic control mode, and affects such indicators as traffic speed, number of starting and braking per unit of length.

The queue length can be used as an indicator of the degree of saturation, comparing with the queue length passed per cycle. When the state of saturated flows is reached, the queue length and the associated indicators are considered to be the most acceptable for network management. In this case, the task of management is to minimize the probability of congestion.

The cost effectiveness of road traffic is estimated according to several criteria, the most important are the specific delay and the specific stop calculated per vehicle [2-4].

The density of street and road networks is defined as the ratio of the total length of streets and roads to the area size. The density of street and road networks and their traffic load indicators were considered in the works of A.V. Sigayev, S.A. Vaksman and a number of other authors. Typically, the subject of the research is statistical data that include the following indicators: the density of street and road networks, the length of streets and roads per capita, the number of registered vehicles per 1 km of streets and roads, the annual mileage of vehicles per 1 km of streets and roads, etc.

A number of researches are devoted to establish a connection between the density and capacity indicators [5]. The most important drawback of the density indicator and its modifications is the absence of any specific information about any street and road sections. In general, the above-mentioned density indicators are descriptors and give only a general assessment of the state of the network.

When using partial criteria, the question inevitably arises as to which indicators can be given preference and in what cases. It is impossible to find an unambiguous answer to this question.

However, it can be said with sufficient certainty that a significant number of specialists prefer the average delay value of vehicles as the most objective indicator of the quality of traffic control and management.

In case of heavy traffic flows, it is most expedient to estimate traffic conditions by the magnitude of the vehicle queue at the intersection or according to the indicators based on it:

- the queue length to the leg length ratio;
- the leg length minus the queue length.

A constant search for universal integral criteria is made that would allow evaluating both the quality of road traffic in general and the quality of its individual properties, since it is impossible to do this with the help of partial criteria.

D. Drew [6] proposed a valuating integral quality criterion for road traffic - Level of Service (LOS). The LOS is associated with such factors as traffic safety, operating speed, driving comfort and convenience, freedom of maneuvering, flow interruption, travel costs, etc. The usage of this criterion covers all stages of working with street and road networks - planning, design, and operation. Currently, the LOS criterion is used to estimate traffic conditions in both street and road network modeling programs and in highly specialized intersection and junction design programs. One of the drawbacks of the considered criterion is its difficulty and qualitative assessment as a whole, and sometimes the impossibility of quantitative assessment of the effectiveness of individual solutions.

Yu. A. Vrubel [7] proposed a new valuating integral criterion - “losses in road traffic”. The losses are understood as the socio-economic value of the unenforced costs of the movement process.

This criterion is applicable for assessing the quality of both road traffic in general and its individual properties. Quality assessment is carried out in monetary terms, which makes it possible to compare not only the quality of individual properties of road traffic, but also the costs of its accomplishment. This fact makes the comparison very clear and allows easily and quickly optimizing solutions for traffic management according to the criterion of loss minimization.

The variation of the traffic flow operating speed can be viewed as an integral criterion [8]. A significant variation of speeds is a distinctive feature of modern traffic on street and road networks of cities. The speed can range from 60 km/h allowed within the city limits to 5-10 km/h or less established in cases of congestion. The variation of the traffic flow operating speed evaluates the influence of a whole set of factors in a wide range of their changes, starting from free-flow conditions and ending with congestion situations. Thus, it is the integral criteria that are the most applicable to solving problems arising from the evaluation of the street and road network. When using integral criteria for assessing the quality of traffic management, it is inevitable that methods of mathematical modeling should be applied based on macroscopic models of traffic flow. In this regard, the integral criterion for assessing the quality of traffic management is developed on the basis of macroscopic models of traffic flow.

Historically, the first macroscopic model of the single-lane traffic flow was a model later named the Lighthill-Whitham-Richards model [9-10], in which the vehicle flow is regarded as a flow of a one-dimensional compressible fluid.

The Lighthill-Whitham-Richards model assumes that:

- there is a one-to-one relationship between the speed and the linear density of the flow;
- the law of conservation of mass - number of vehicles is fulfilled.

Another version of the Lighthill-Whitham-Richards model was proposed by Tanaka in 1963 [11].

The Tanaka model assumes that the vehicle speed cannot exceed a certain maximum value, and in view of this the density of the single-lane traffic flow is calculated. This model plays an important role in the study of traffic flows in terms of traffic safety.

The model developed by Whitham in 1974 takes into account the fact that drivers reduce speed when the density of traffic flow moving in front of them increases, and increase speed when the density decreases.

The Payne model [12] does not raise any assumptions about the dependence of speed on density, and is written as a conservation law.

Several drawbacks of the Payne model and many of the models subsequently proposed were indicated by C. Daganzo [13-14]. It was shown that with strong spatial in homogeneities of the initial conditions, negative speed values can appear (the congestion "dissipates back" as a result of viscosity influence). For certain parameter values, densities exceeding the maximum permissible values can occur ("bumper to bumper"). Moreover, according to these models, the vehicle movement is significantly influenced by vehicles located behind, which in the case of a single lane is hardly possible in the real-life traffic flow.

One of the macroscopic model varieties is the two-fluid mathematical model of Herman-Prigogine. This traffic flow model considers the nonlinear dependencies between the specific travel time and the specific time of delays expended per unit of distance. The scope of use of this model is the street and road network or its sections.

Due to the fact that the kinetic theory studies multilane traffic, Herman and Prigogine put forward the theory of two flows of city traffic. Vehicles in the traffic flow are divided into two groups - moving vehicles and stopped vehicles. The latter include vehicles stopped in the flow itself, i.e. vehicles stopped at intersections, stopped due to a regular congestion, stopped due to interference to traffic, etc., but exclude out-of-traffic vehicles, for example, parked vehicles.

An important property of the macroscopic model of Herman and Prigogine is that two different traffic operating modes can be displayed [15]. These are individual and collective flows, which are functionally dependent on the concentration of vehicles - flow density. With a low flow density, traffic moves in the individual flow mode. When the flow density increases, traffic starts moving in the collective flow mode. In this case, the flow becomes largely independent of the desires of individual drivers in the choice of the driving mode.

The two-flow model is based on two initial assumptions:

- the average operating speed along the street and road network is proportional to the fraction of vehicles in motion;
- the duration of delays of a vehicle moving along the street and road network is proportional to the number of vehicles stopped at a given time.

The studies confirmed the provisions of the two-fluid mathematical model of Herman-Prigogine [16]. Simultaneously, it was established that urban street networks can be characterized by two parameters of the model - *n* and *Tm*. These parameters were calculated on the basis of experimental data obtained from surveys of cities around the world.

The Herman-Prigogine model is very attractive for practical use, as it is easily applicable when conducting regular surveys of traffic conditions in comparison with other macroscopic models. The uniqueness of the model is that when assessing the impact of the street and road network load on traffic conditions, it is not necessary to determine the load level, i.e. to determine the traffic flow intensity and the capacity of the elements of the street and road network. To assess the n and Tm parameters, only the data on specific indicators of the travel time T and the standing time Ts are needed.

The Herman-Prigogine model can be applied:

- to compare street and road networks of different cities or to compare sections within one street and road network;
- to compare the peculiarities of behavior of drivers and the movement of certain types of vehicles;
- to give a detailed assessment of the influence of geometric and other parameters of the street and road network on traffic conditions;
- in the modeling of traffic flows in order to assess the projected traffic conditions.

3. Description of the traffic flow model

The parameters used in the Herman-Prigogine model [15] consisting of two flows (moving and standing vehicles) represent the average data determined on the scale of the whole street and road network for a given period of time.

In accordance with the above provisions, the traffic flow in the street and road network at any time consists of two parts: *fr* - moving vehicles; *fs* - standing vehicles. In this case, the condition $fr + fs = 1$ is observed, and the fraction of standing vehicles *fs* is determined by the ratio:

$$f_s = \frac{1}{T_S}, \tag{1}$$

where T_s - specific time expenditure caused by delays, min/km.

The average specific time expenditure T (min/km) is the sum of the average specific travel time T_r (min/km) and the specific delay time T_s (min/km):

$$T = T_r + T_s. \tag{2}$$

The average speed of moving vehicles *Vr* is defined as the product:

$$V_r = V_m \cdot f_r^n, \tag{3}$$

where V_m - the average maximum operating speed in the street and road network or in its considered section;

n - an indicator characterizing the quality of functioning of the street and road network or its considered section, which indicates how the speed decreases in the street and road network as the load increases.

Taking into account the delays, the average operating speed in the street and road network or its considered section *V* is calculated as

$$V = V_m \cdot f_r^{n+1}. \tag{4}$$

Taking into account the balance equation $f_r + f_s = 1$, Equation (4) can be represented in another form:

$$V = V_m \cdot f_r^{n+1} = V_m \cdot (1 - f_s)^{n+1}, \quad (5)$$

Taking the travel time per unit of length to be T, the travel time per unit of length to be T_r, and the average delay time for the passage of a section of the unit length T_s, we obtain the relations:

$$T = \frac{1}{V}; \quad (6)$$

$$T_m = \frac{1}{V_m}, \quad (7)$$

where V - the average operating speed in the street and road network including the delays;
T_m - the average minimal time for the passage of a section of the unit length.

The T_m parameter characterizes the minimum specific time expenditure for moving in the free conditions, i.e. at a very low level of network load, in which there is no interaction between vehicles in the flow.

In turn, the n parameter, called the Herman-Prigogine criterion, reflects the influence of the load level on the decrease in the operating speed of traffic flows. It can be considered as an indicator of the quality of service of traffic flows in the street and road network.

The second initial provision of the two-fluid model asserts that the duration of delays of a vehicle moving along the street and road network is proportional to the number of vehicles stopped at a given time. In accordance with this, the second assumption of the model is mathematically represented as

$$f_s = \frac{T_s}{t}. \quad (8)$$

Equation (5) can be reformulated in order to estimate the travel conditions according to the specific time expenditure as follows:

$$T = T_m (1 - f_s)^{-(n+1)}; \quad (9)$$

$$T = T_m \left(1 - \frac{T_s}{T}\right)^{-(n+1)}; \quad (10)$$

$$T_r = T_m^{\frac{1}{(n+1)}} \cdot T^{\frac{1}{(n+1)}}. \quad (11)$$

The general formula of the Herman-Prigogine model becomes as follows:

$$T_s = T - T_m^{\frac{1}{(n+1)}} \cdot T^{\frac{1}{(n+1)}}, \quad (12)$$

The model and the Herman-Prigogine criterion n represented above make it possible to obtain a systematic assessment of the transport situation in the street and road network as a whole, i.e. to quantify the sensitivity of traffic conditions to a change in the load of the street and road network.

The logarithmic transformation of Equation (12) is as follows:

$$\ln Ts = \frac{1}{(n+1)} \cdot \ln T_m + \frac{n}{(n+1)} \cdot \ln T, \quad (13)$$

In order to use linear regression, Equation (13) is transformed as follows:

$$\ln Ts = \ln T_m + n(\ln T - \ln T_m). \quad (14)$$

The linear dependence equation simplifies the procedure of regression analysis and allows using standard statistical methods for estimating the traffic flow parameters.

The classification of road networks based on the parameters included in the Herman-Prigogine model allows predicting the traffic speed and the time expenditure for travel at any given section of the road network. The classification can be constructed, for example, using the clustering analysis of the experimentally established values of the travel time parameters T and the standing time T_s.

4. Implementation of the traffic flow parameter assessment system

An integrated assessment of the quality of traffic management can be made on the basis of the Herman-Prigogine model using the data obtained from navigation equipment.

Satellite monitoring of transport is used for dispatch control and management of passenger transport, for solving problems of transport logistics in transportation management systems and automated fleet management systems [17]. Satellite monitoring of transport is a system for monitoring mobile objects, which is built on the basis of satellite navigation systems, cellular and/or radio communication equipment and technologies, computer technology, and digital maps [18].

The principle of monitoring is to track and analyze the spatial and temporal coordinates of a vehicle. Two monitoring options are available: “on-line” - with remote transfer of coordinate information, and “off-line” - information is read upon arrival at the dispatch center. A mobile module is installed on the vehicle, which consists of the following parts: a satellite receiver, storage and transmission modules for coordinate data.

Data on specific indicators of the travel time and standing time can be collected in an active way, using a specially equipped vehicle for driving through the examined sections of the street and road network.

A passive system can also be applied, in which specific indicators are calculated on the basis of navigational data collected from various vehicles participating in road traffic. Such data can be obtained from various sources, for example, from transportation company servers. Using a passive approach to data collection allows increasing the accuracy of the system, since more data can be examined that are collected from different vehicles controlled by different drivers.

The passive experiment methodology, along with the use of the Herman-Prigogine model, allows assessing the traffic flow parameters and constructing a decision-making support system for controlling transportation, selecting traffic routes, and assessing possible changes in the transport system.

Using the two-fluid model of Herman-Prigogine, a software system has been implemented that allows making quantitative assessment of traffic parameters using navigation data, as well as

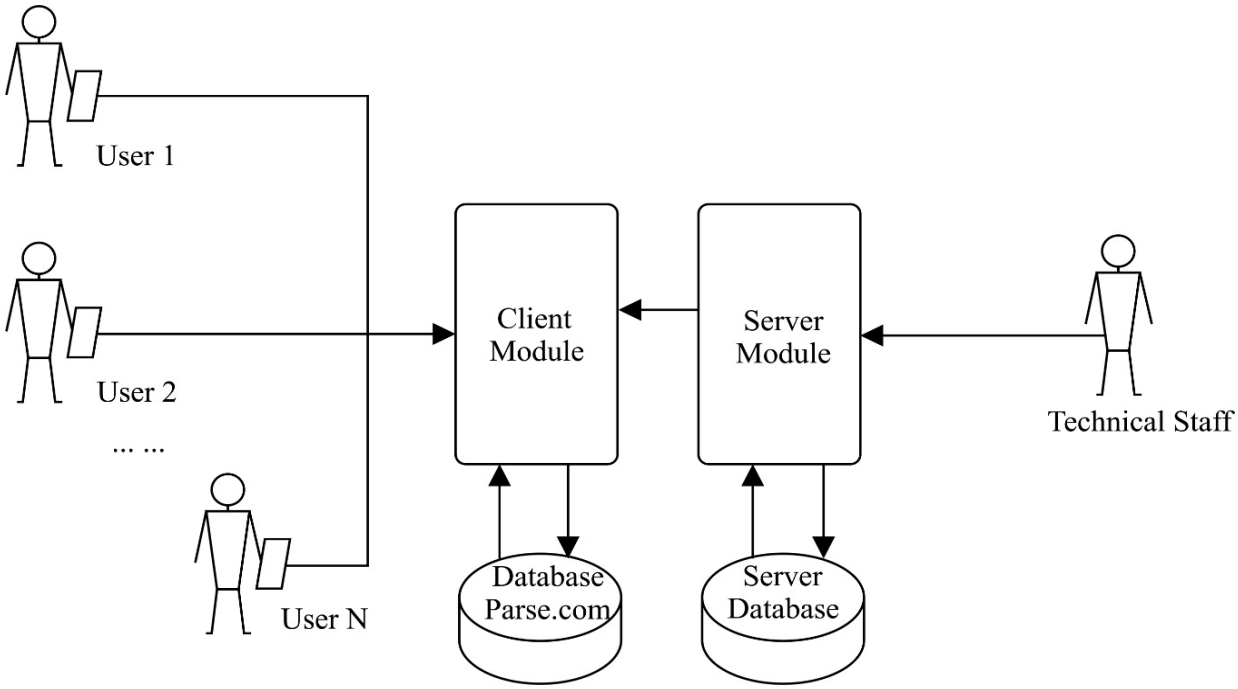

Figure 1 *System architecture*

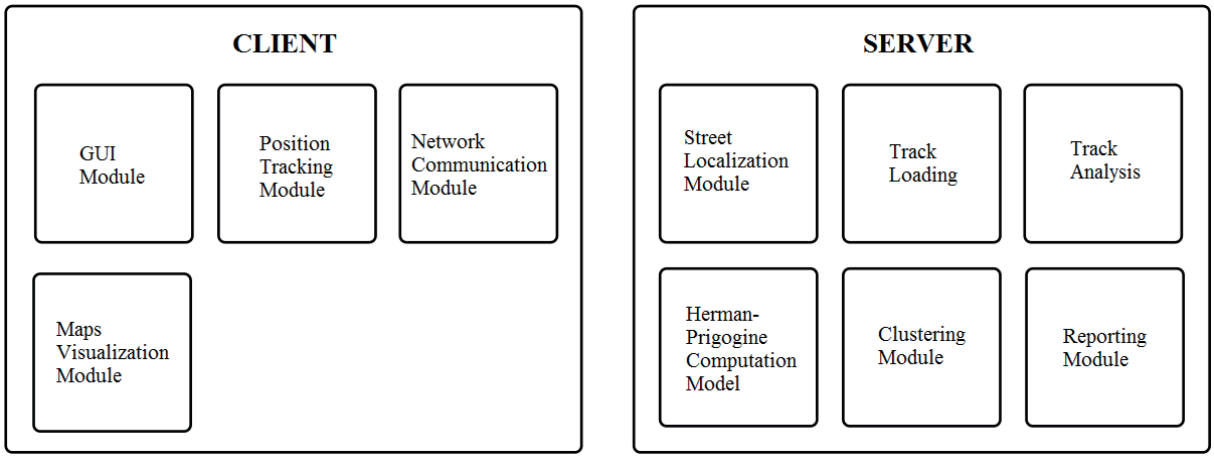

Figure 2 *Composition of the client and server subsystems*

their visualization using the Google Maps geographic information system.

The software system is designed to collect and analyze navigational data with further application in the assessment of traffic flow parameters on the basis of the two-fluid model of Herman-Prigogine [16, 19, 20]. The data are collected using a large number of navigation modules installed on vehicles or smartphones of users. Data analysis is performed centrally on a high-performance computer, as it requires a considerable amount of calculations.

The software package proposed for the solution of these tasks is implemented on the client-server architecture basis (Figures 1 and 2). Thus, data received from clients are transferred to the server end for further storage, as well as for processing and analysis of these data.

The client end is represented by two types of devices - a built-in navigation module integrated in the vehicle or a mobile application based on the Android OS. The built-in equipment automatically sends data on the vehicle location to the transportation company, which performs preliminary data collection with subsequent provision to the system under consideration. The second case is a client application installed on the user's mobile device.

In order to send tracks, users must have the GPS receiver activated on the smartphone or the vehicle, and data transfer must also be enabled. When driving over a certain period of time, users receive their current location. Also, an attempt is made to obtain the name of the street for the current coordinate. The client end of the application analyzes this information, calculating the following parameters on its basis: time, speed, coordinates.

User data are sent to the cloud server Parse.com for further storage and exported in the required format. The Parse.com library was used to work with data for Parse.com.

The implementation of the client end is represented by a mobile software system for data collection. This system was developed for the Android platform using the Java programming language. The user interface of the system was developed in accordance with the requirements of Google [4] for the interface of Android applications.

The server end of the system is a web application. The web application is used for:

- loading tracks from a file;
- processing tracks according to the Herman-Prigogine model;
- visualizing the obtained results with overlay on the Google Maps cartographic service [21];
- clustering sections of the street and road network according to the parameters of the Herman-Prigogine model.

After preliminary processing and storage in the cloud service, the data are uploaded as a file for further analysis. The file in the CSV format is sent to the server end of the system. The server end of the system at this stage receives all tracks from the file, processes and verifies them. The file in the CSV format containing tracks is sent to the input for analysis. After receiving all tracks for a particular street, the number of tracks, the standing time, and the average speed for this section of the road are determined. Every parameter is assigned a threshold value in advance, on the basis of which it is determined whether a track belongs to the group of unreliable tracks.

After passing the verification, the data are sent to the Herman-Prigogine module for calculating parameters. The following algorithm is used to implement the Herman-Prigogine model. All tracks for a particular street are selected from the track database, and information on time and speed at each point in time associated with obtaining of the location is extracted from them. Information on time allows calculating the total travel time, and the speed allows determining how much of this time is spent standing. Thus, two components are obtained, which are necessary for the Herman-Prigogine model. After receiving the data, a linear regression is constructed using the total time and the time in motion in order to solve an equation of the $y = kx + b$ type. After solving the linear regression, the k and b parameters are calculated, which are used for calculating the parameters of the Herman-Prigogine model.

After calculating the parameters of the Herman-Prigogine model, the data are transferred to the clustering module input. The FOREL algorithm [22] is used for clustering the obtained results. This algorithm is based on the idea of combining objects into one cluster in the areas with the most concentration. This algorithm was chosen because it does not need specifying the number of clusters in advance. After clustering of the entire sample, the application displays the charts and routes on the map, and then compiles a report in the TXT format.

The implementation of the server end is represented by a special system developed for the web platform [23-25]. Python was used for the development as the main programming language. The Flask framework [26] was used for displaying in the web environment. The cartographic service Google Maps v3 [27] was used in this system. The JavaScript programming language [23] was used for manipulating the map: constructing points and routes. ORM SqlAlchemy [28] and the SQLite database management system [25] were used for working with the database. The use of this DBMS is rational within this work in view of the mobility of deployment and maintenance. In the future, when developing this system, it will be necessary to use more powerful DBMS, as the increased amount of data will lead to limitations of the existing solution.

Thus, the hardware of the software package for assessing traffic flow parameters includes:

- mobile device for collecting traffic information - a navigation module integrated in the vehicle or a mobile device with a GPS receiver (Android OS 4.0 and higher) with the data transfer function enabled;
- software products of transportation companies that provide navigation data in the CSV format;
- automated workstation (AWS) of the operator that includes a personal computer running the Linux family operating system. The virtual environment was used to develop the AWS, as well as the Flask framework [29], and the web application was developed using the Python programming language [30].
- SDK Parse.com [31] for Android OS - a library that simplifies the work with the Parse.com platform on mobile devices;
- Parse.com cloud service [31] for storing data transmitted from customers.

5. Testing the software package for the assessment of traffic flow parameters using experimental data

The working efficiency of the proposed algorithms, mathematical models for the assessment of traffic flow parameters, and the system as a whole was confirmed during its testing, using a set of tracks on the main highways of Belarus. Similar calculations were made for the city of Minsk, where streets that function at the limit of their capabilities were identified.

To verify the functioning of the Herman-Prigogine model as part of the software package for the assessment of traffic flow parameters, the routes received from one of the transportation companies of the Republic of Belarus with the volume of 5,000,000 entries were used. A list of tracks for each street or route was used, which was obtained beforehand. Next, it was necessary to calculate the parameters of the Herman-Prigogine model for each street.

The parameters were calculated as follows:

1) two types of time were distinguished for each track: total travel time and standing time. In order to determine what state the vehicle was in - moving or standing, a speed limit of 5 km/h was adopted. If the speed was below this limit, the vehicle was considered standing, and if the speed was higher, the vehicle was considered moving;
2) after receiving the time of all tracks, the data was sent to the Herman-Prigogine model, after which the result was obtained. The result is a report file that contains the following information for each route:
   - route number - position number of the route in the list of streets or routes;
   - address - street, city, country for the current route;
   - starting point and end point - route boundary;

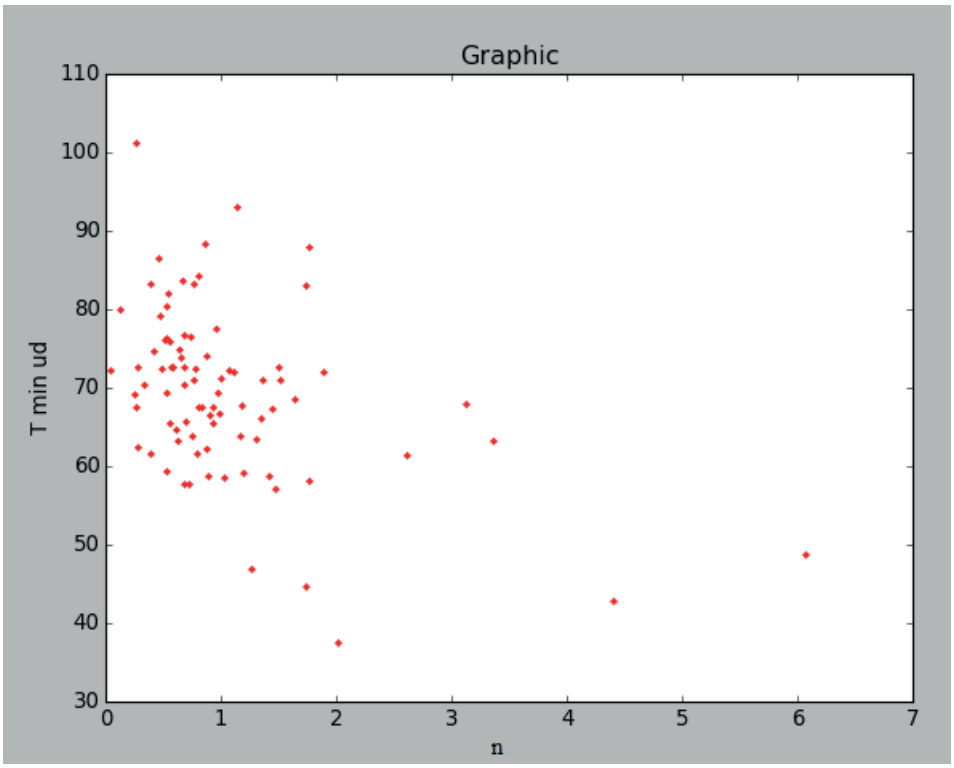

Figure 3 *Visualization graph of calculation results according to the Herman-Prigogine model*

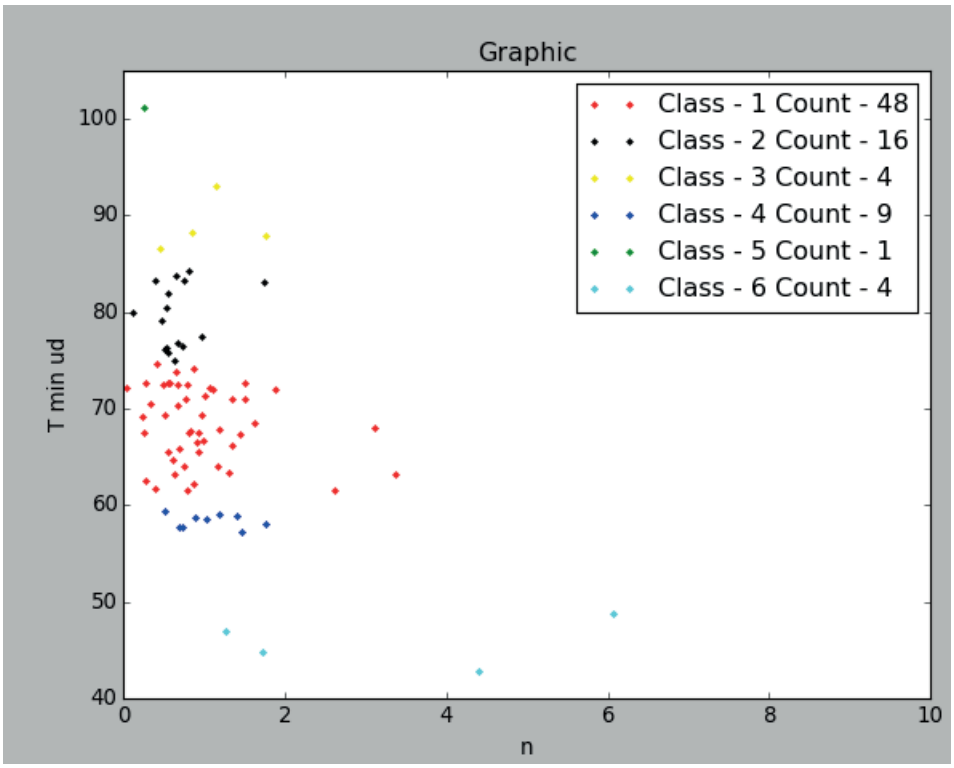

Figure 4 *Clustering of routes with a radius of 7 units*

- straight-line distance - distance between points in a straight line;
- road distance - distance between points along the road in compliance with traffic rules on this route;
- speed - minimum average speed obtained as a result of the analysis;
- table with intermediate data - table containing all the tracks for this route in the form of the total travel time,

Table 1 *Characteristics of the obtained clusters*

Cluster number	Number of streets	Range n	Range T	Brief description
1	48	[0.04; 3,36]	[61.51; 74.70]	Moderate response to increased street load
2	16	[0.12; 1.74]	[74.91; 84.30]	Weak response to increased load
3	4	[0.45; 1.76]	[86.60; 93.09]	Weak response to increased load
4	9	[0.52; 1.76]	[57.21; 59.39]	Weak response to increased load
5	4	[1.26; 6.07]	[42.86; 48.76]	Maximum response to increased load
6	1	[0.26; 0.26]	[101.17; 101.17]	No response to increased load

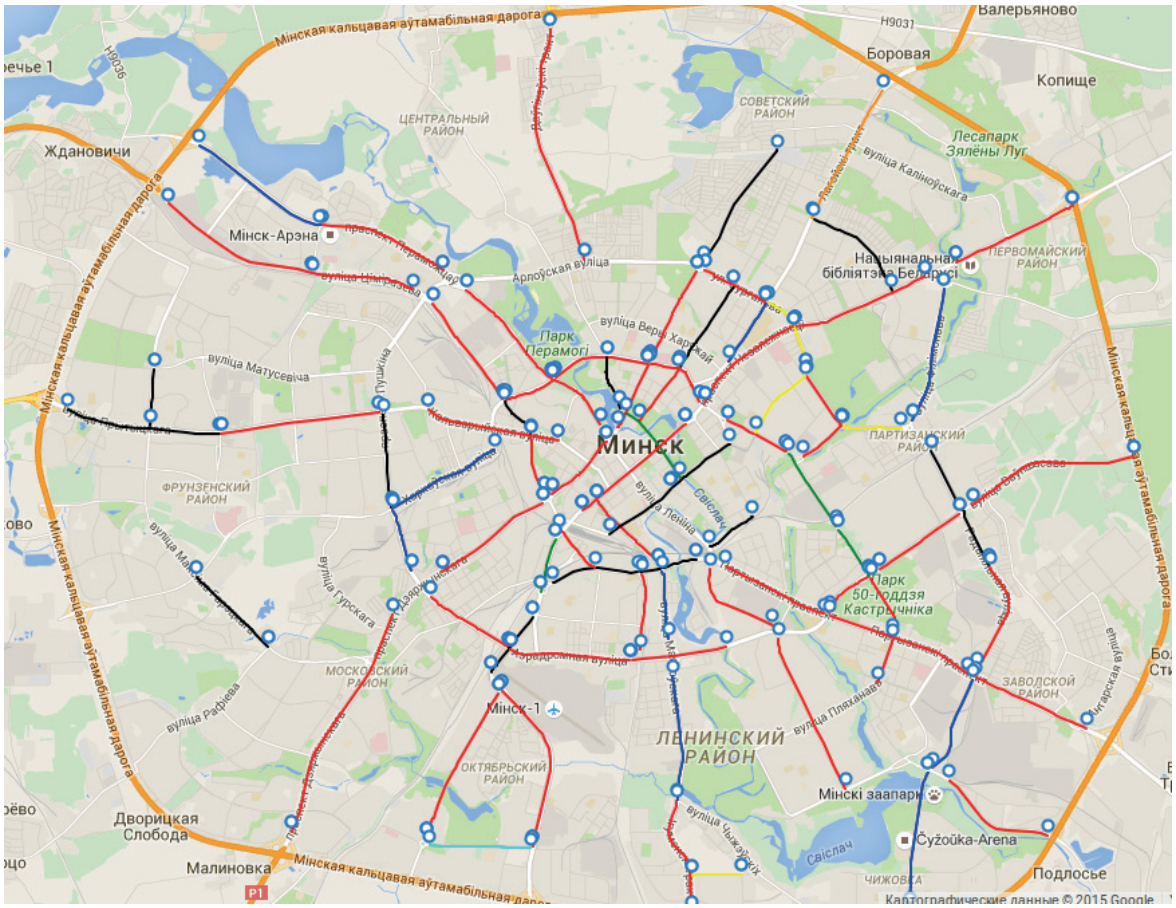

Figure 5 *Color differentiation of routes by classes*

as well as the standing time. The table also contains intermediate computational values;

- adjustable parameters for $y = kx + b$ - adjustable parameters k and b obtained during solving of the linear regression;
- parameters of the Herman-Prigogine model: the Herman-Prigogine indicator, the average minimum travel time, and the average minimum specific travel time.

As a result of testing of the subsystem for model calculations, data of the n and Tm parameters were obtained, which characterize the quality of traffic management in this section.

Having obtained the results of calculating the parameters of the Herman-Prigogine model for specific streets of the city of Minsk, the points of the minimum average specific travel time T_m and the indicator n of Herman-Prigogine for these streets were plotted in the graph (Figure 3). As seen here, the points are located irregularly, forming street clusters according to the quality of traffic management.

The FOREL algorithm was chosen for the clustering of this data set, since the number of clusters that should be obtained at the output was not known in advance. This algorithm requires specifying only the initial size of the expected clusters. By specifying the radius experimentally, the obtained output was a list of points with automatically generated cluster classes. The obtained clusters with a radius of 7 units are shown in Figure 4.

The illustration shows that the routes were divided into 6 clusters, each with a different number of streets. The parameters of each cluster are given in Table 1.

A brief description of road conditions is given for each cluster, which was determined on the basis of comparison with the indicators of other cities. Comparing the indicators of different cities, a conclusion can be made on the characteristics

Table 2 *Distribution of the streets of Minsk by clusters*

Cluster number	Street name
1	Igumensky trakt, Rokossovskogo ave., Radialnaya str. part 1, Akademicheskaya str., Kozlova lane, Svislochskaya str., Plekhanova str., Denisovskaya str., Partizansky ave. part 1, Partizansky ave. part 2, Partizansky ave. part 3, Tolstogo str., Sverdlova str., Nezavisimosti ave. part 1, Nezavisimosti ave. part 2, Nezavisimosti ave. part 3, Nezavisimosti ave. part 4, Kizhevatova str., Kazintsa str., Aerodromnaya str., Zhukova ave., Maksima Bogdanovicha str. part 1, Maksima Bogdanovicha str. part 2, Nemiga str., Dzerzhinskogo ave. part 1, Dzerzhinskogo ave. part 2, Prityckogo str., Kalvariyskaya str.,
	Pobediteley ave. part 1, Pobediteley ave. part 2, Pobediteley ave. part 3, Masherova ave. part 1, Masherova ave. part 2, Masherova ave. part 3, Timiryazeva str. part 1, Timiryazeva str. part 2, Timiryazeva str. part 3, Klary Tsetkin str., Kozlova str., Dolgobrodskaya str. part 1, Kuybysheva str., Surganova str, Vaneyeva str., Vaupshasova str. part 1, Vaupshasova str. part 2, Trostenetskaya str., Dolginovsky trakt, Volodko str.
2	Radialnaya str. part 2, Aranskaya str. Mogilyovskaya str., Brilevskaya str.,
	Pushkina ave., Maksima Goretskogo str., Prityckogo str., Storozhyovskaya str.,
	Timiryazeva str. part 4, Ulyanovskaya str., Pervomayskaya str., Kuybysheva str.,
	Smolenskaya str., Maksima Bogdanovicha str. part 3, Kuntsevshchina str., Volgogradskaya str.
3	Yanki Luchiny str., Stoletova str., Surganova str., Platonova str.
4	Mayakovskogo str. part 1, Tashkentskaya str., Kabushkina str., Mayakovskogo str. part 2, Zhukova ave., Kharkovskaya str., Pobediteley ave., Filimonova str.,
	Yakuba Kolasa str.
5	Moskovskaya str., Yanki Kupaly str., Dolgobrodskaya str. part 2, Dolgobrodskaya str. part 3
6	Korzhenevskogo str.

of traffic management in Minsk. Also, the degree of influence of the traffic flow load on the quality of service was determined in the "Brief description" column of Table 1.

The resulting route clustering was applied when plotting the routes on the map in different colors depending on the route class. This allows visually identifying road sections with different road conditions. The visualization results are shown in Figure 5.

The distribution of the streets of Minsk by clusters is given in Table 2.

Thus, the classification of the streets of Minsk according to the quality of traffic management was obtained, problematic streets were identified, and the results were visualized.

6. Conclusions

Mathematical modeling plays an increasingly important role in methodological support of the development and implementation of any measures to manage the road network capacity. The application of mathematical models in the planning of management activities in the field of transport offers an opportunity:

- to assess the quality of traffic management;
- to predict the operational efficiency of management activities and their combinations based on the obtained estimates;
- to predict possible negative consequences of the implementation of management activities.

These predictions and estimates allow significantly improving the quality of management decisions in the transport sector.

The widespread introduction of navigation systems in transport opens up wide possibilities for collecting information on traffic flows. There are mathematical tools that continue to improve, which provide a solution for current problems of transport modeling and the assessment of traffic flow parameters.

Thus, for successful application of mathematical modeling methods for the transport system, recommendations for transport modeling, as well as programs for optimizing the road network capacity should be developed.

As part of this work, a software system has been developed that includes modules for collection of navigational data, storage and verification of track data, management of street and road data, calculation of the Herman-Prigogine model indicators, and classification of streets according to these parameters on the basis of passive processing of navigational data on vehicle traffic on transport highways and street and roads networks of cities.

The main advantages and novelty of the developed system are as follows:

- cloud computing (using to store large amounts of cloud storage data);
- availability of a mobile client application for the Android OS for collecting data in addition to the ability to work with already collected navigation data from the navigation and information center and other sources;
- support for formats of modern GPS trackers;
- use for calculating and processing the data of modern web technologies;
- scalability and customizability of the system.

As a result of testing of the developed software, results confirming the working efficiency of the proposed algorithms were obtained. Also, as a result of using the navigational data collected in the Republic of Belarus, in particular in the city of Minsk, the ability of the software system to distinguish street classes with different conditions of traffic management and the influence of the traffic flow load on the capacity was demonstrated.

The obtained results of the assessment of traffic flow parameters can be used to improve the efficiency and quality of the activities of state bodies, services, and companies in the transport sector in order to support the decision-making on accounting and

redistribution of traffic flows within transport highways and street and road networks, on analyzing the transport load, on providing optimal traffic management, and when upgrading the existing road networks and designing new road networks. Moreover, this tool can be used to analyze transport corridors, main highways, and city streets in order to find sections that primarily require upgrading and improving.

References

[1] EBOLI, L., MAZZULLA, G., PUNGILLO, G. Measuring the driver's perception error in the traffic accident risk evaluation. IET Intelligent Transport Systems [online]. 2017, 11(10), 659-666. ISSN 1751-956X/eISSN 1751-9578. Available from: https://doi.org/10.1049/iet-its.2017.0084

[2] PERSIA, L. et al. Strategies and measures for sustainable urban transport systems. Transportation Research Procedia [online]. 2016, 14, p. 955-964. ISSN 2352-1465. Available from: https://doi.org/10.1016/j.trpro.2016.05.075

[3] GALKIN, A., et al. Perspective of decreasing of road traffic pollution in the cities. In: International Multidisciplinary Scientific GeoConference Surveying Geology and Mining Ecology Management SGEM 2018 : proceedings [online]. Vol. 18(4.2). Albena, Bulgaria, 2018. ISBN 978-619-7408-45-4, ISSN 1314-2704, p. 547-554. Available from: https://doi.org/10.5593/sgem2018/4.2/S19.071

[4] Material design - Google design guidelines [online]. Avaliable from: https://www.google.com/design/spec/material-design/introduction.html

[5] PONKRATOV, D., et al. Traffic streams and anti-congestions activities in city networks. International Journal of Automation, Control and Intelligent Systems [online]. 2015, 1(2), 21-26. ISSN 2381-7526/eISSN 2381-7534. Available from: http://files.aiscience.org/journal/article/html/70100016.html

[6] DREW, D. R. Traffic flow theory and control. New York: McGraw-Hill, 1968. ISBN 978-0070178311.

[7] VRUBEL, Y. A. Kapskiy, D. V., Kot, Y. N. The definition of losses in road traffic: a monograph (in Russian). Minsk: BNTU, 2006.

[8] EBOLI, L., et al. Experimental relationships between operating speeds of successive road design elements in two-lane rural highways. Transport [online]. 2015, 32(2), p. 138-145. ISSN 1648-4142/eISSN 1648-3480. Available from: https://doi.org/10.3846/16484142.2015.1110831

[9] LIGHTHILL, M. J., WHITHAM, G. B. On kinematic waves II. A theory of traffic flow on long crowded roads. Proceedings of the Royal Society A: Mathematical, Physical and Engineering Sciences [online]. 1955, 229(1178), p. 281-345. ISSN 0080-4630/eISSN 2053-9169. Available from: https://doi.org/10.1098/rspa.1955.0089

[10] RICHARDS, P. I. Shock waves on the highway. Operations Research [online]. 1956, 4(1), p. 42-51. ISSN 0030-364X/eISSN 1526-5463. Available from: https://doi.org/10.1287/opre.4.1.42

[11] GARTNER, N. H. MESSER, C. J. RATHI, A. K., eds. Traffic flow theory: A state-of-the-art report. Washington DC: Transportation Research Board, 2001.

[12] PAYNE, H. J. Models of freeway traffic and control. In: Bekey, G. A., ed., Mathematical Models of Public Systems. La Jolla, CA: Simulation Council, Inc. 1971, 1, p. 51-61.

[13] DAGANZO, C. F. Fundamentals of transportation and traffic operations. 1. ed. New York: Elsevier Science inc., 1997. ISBN 978-0080427850.

[14] SHVETSOV, V. I. Mathematical modeling of traffic flows (in Russian). Avtomatika i telemekhanika. 2003, 11, p. 3-46. ISSN 0005-2310.

[15] HERMAN, R., PRIGOGINC, I. A two-fluid approach to town traffic. Science [online]. 1979, 204(4389), p. 148-151. ISSN 0036-8075/eISSN 1095-9203. Available from: https://doi.org/10.1126/science.204.4389.148

[16] NELSON, P., SOPASAKIS, A. The prigogine-herman kinetic model predicts widely scattered traffic flow data at high concentrations. Transportation Research Part B: Methodological [online]. 1998, 32(8), p. 589-604. ISSN 0191-2615. Available from: https://doi.org/10.1016/S0191-2615(98)00020-4

[17] GECCHELE, G., et al. Data mining methods for traffic monitoring data analysis: A case study. Procedia-Social and Behavioral Sciences [online]. 2011, 20, p. 455-464. ISSN 1877-0428. Available from: https://doi.org/10.1016/j.sbspro.2011.08.052

[18] DERRMANN, T., et al. Estimating urban road traffic states using mobile network signaling data. In: IEEE 20th International Conference on Intelligent Transportation Systems ITSC 2017 : proceedings. 2017. eISSN 2153-0017, p. 1-7. Available from: https://doi.org/ 10.1109/ITSC.2017.8317718

[19] PRIGOGINE, I., HERMAN R. Kinetic theory of vehicular traffic. New York: American Elsevier Publishing Company, 1971.

[20] Blinkin, M. Ya., Tkachenko, B. A. Systemassessment of traffic conditions on the basis of the Herman–Prigogine [Sistemnaya otsenka uslovii dvizheniya na baze modeli Hermana-Prigozhina]. Sotsial'no-ekonomicheskie problem razvitiya transportnyh system gorodov i zon ih vliyaniya, 2009 [Electronic resource]: http://www.waksman.ru/Russian/Org&B/2008/blinkin1.htm. Last accessed: 1.03.2019

[21] Google Maps Javascript API - Google Developers [online]. Avaliable from: https://developers.google.com/maps/documentation/javascript/examples/event-simple

[22] Algorithms family FOREL (in Russian) - Wikipedia [online]. Avaliable from: https://ru.wikipedia.org/wiki/Algoritmy_semeystva_FOREL
[23] jQuery API Documentation - jQuery [online]. Avaliable from: http://api.jquery.com/
[24] Matplotlib 1.5.0 documentation [online]. Avaliable from: http://matplotlib.org/contents.html
[25] SQLite Documentation [online]. Avaliable from: https://www.sqlite.org/docs.html
[26] Flask (A Python Microframework) [online]. Avaliable from: http://flask.pocoo.org/
[27] Location and Sensors APIs - Android developers [online]. Avaliable from: http://developer.android.com/guide/topics/sensors/index.html.
[28] SQLAlchemy - The Database Toolkit for Python [online]. Avaliable from: http://www.sqlalchemy.org/
[29] Web "Flask (A Python Microframework)" [online]. Avaliable from: http://flask.pocoo.org/
[30] LUTZ, M. Learning Python (in Russian). 4. ed. Sebastopol, CA: O'Reilly Media, Inc. 2010. ISBN 978-0-596-15806-4.
[31] Parse Android Developers Guide - Web "Parse" [online]. Avaliable from: https://parse.com/docs/android/guide

Kiros Gebrearegawi Kebedow - Johan Oppen*

INCLUDING CONTAINERS WITH DANGEROUS GOODS IN THE CARGO MIX PROBLEM FOR CONTAINER VESSEL STOWAGE

The Cargo Mix Problem (CMP) chooses and distributes types of containers to load into bay subsections of a container vessel. In this paper, we extend existing Mixed Integer Programming models for the CMP by considering containers with dangerous goods. We show that our model can be optimally solved in reasonable time using standard software.

Keywords: *integer programming, container stowage, Cargo Mix Problem, dangerous goods*

1. Introduction

Maritime transportation has been, and still remains, the backbone of global trade. The introduction of containers in the maritime transportation have played an important role in modernization of the industry. The majority of containers is transported by container ships, which are specifically designed to carry containers. These ships are owned by different shipping companies. Except during the 2009 world economic crisis, the demand for sea transport has been increasing. However, the demand for efficient and cheap transportation and a fierce competition have driven shipping rates down. So, shipping companies are forced to utilize their vessels as efficiently as possible. Theoretically, the shipping companies know the nominal intake capacity of their container ships. The nominal intake capacity cannot be reached, unless the stability of the container vessel is perfect. This is a daily problem for a stowage coordinator. Stowage coordinators are the planners of the cargo, and have to find a load configuration (stowage plan) which not only suits the current cargo to be loaded, but also guarantees that the vessel can be utilized to its maximum in future ports. However, the ship size and available cargo mixes in different ports makes this work difficult.

The focus of this paper is the *Cargo Mix Problem* (CMP), which determines the cargo mix needed for a vessel to maximize its utilization on a given service. Differing from stowage planning, where a list of pre-selected containers must be stowed on the vessel, the Cargo Mix Problem aims at selecting the number of containers of each type that should be loaded on a vessel to maximize its intake. Moreover, standard stowage planning approaches only consider the current port, whereas the Cargo Mix Problem considers a cyclic service with multiple ports. The problem was introduced in the PhD thesis by Delgado [1] (in this work, the problem is referred to as the Container Composition Problem) and the paper by Christensen et al. [2]. The models presented in these works, however, did not take IMO containers into consideration.

The main contribution of our paper is that we include containers with dangerous goods, so-called *IMO containers* (IMO - the International Maritime Organization) in our model. We have not been able to find other research on the Cargo Mix Problem dealing with IMO containers.

The remainder of the paper is organized as follows: in Section 2 we provide a description of the Cargo Mix Problem. Section 3 gives a brief literature review. Our mathematical model is presented in Section 4, while we present computational results in Section 5. Finally, Section 6 concludes the paper.

2. Problem description

The Cargo Mix Problem requires understanding of the container ship architecture, and the shipping industry as a whole. Liner shipping companies transport containers between ports on a fixed cyclic schedule. A container is a metal box in which goods can be stored. The most commonly used container heights are 8'6'' and 9'6'', and lengths are 20', 40', and 45'. A 9'6'' container is called a high-cube container. High-cube 20' containers are rare and we assume that they do not exist when modeling the Cargo Mix Problem. Reefer containers are containers which should be kept cool and must be supplied with electricity. Containers carrying dangerous goods are referred to as IMO containers and should follow the respective segregation principles.

The longitudinal view of a container ship (container vessel) is shown in Figure 1. A container ship is partitioned into bays. Each bay is also partitioned into on deck and below deck parts using hatch covers which are metallic, flat, water proof structures which allow containers to be placed on top of them, and which can be removed during loading/unloading containers into/from the below deck part of the vessel. Furthermore, the below deck part of the ship is physically divided into several cargo holds by upright walls within the hull of the ship called *bulkheads*, which are indicated by the bold vertical lines in Figure 1.

Container ship capacity is measured in TEU. Both the on-deck and below deck parts of the vessel are partitioned into

* [1]Kiros Gebrearegawi Kebedow, [2]Johan Oppen
[1]School of Mathematical and Statistical Sciences, Hawassa University, Ethiopia
[2]Molde University College, Specialized University in Logistics, Norway
E-mail: Johan.Oppen@hiMolde.no

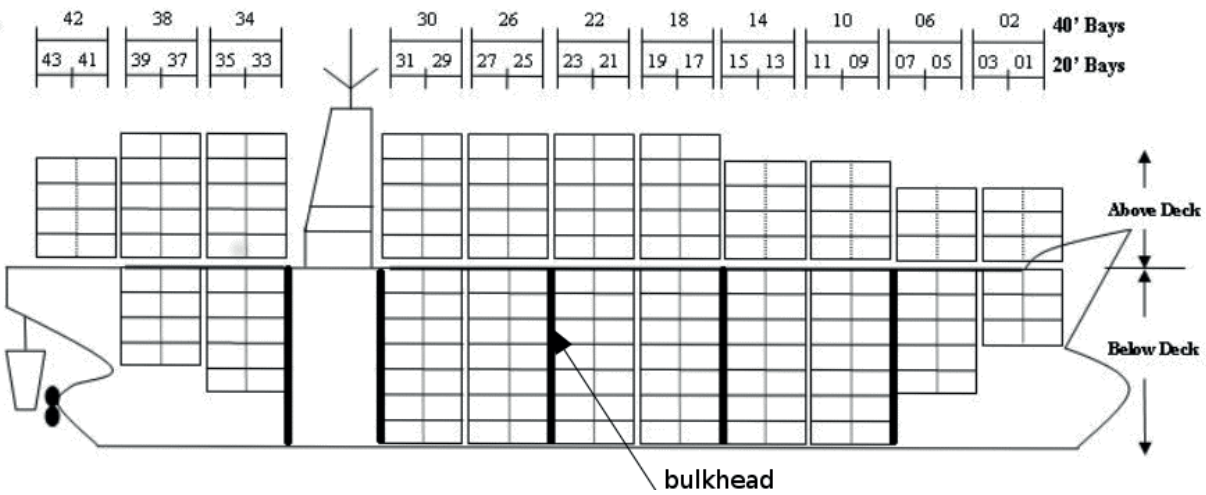

Figure 1 *The longitudinal view of a container ship*
The numbering of TEU and FEU bays are shown at the top [3]

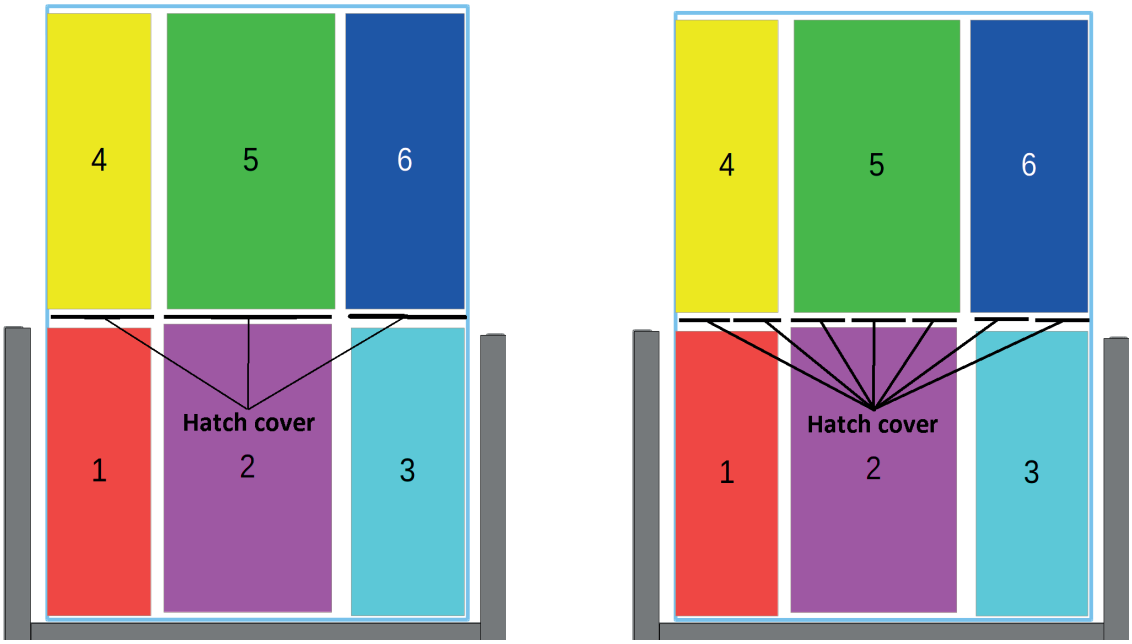

Figure 2 *Locations in a bay with three (left) and seven (right) hatch covers*

cells which contain two *Twenty foot Equivalent Unit* (TEU) or a single *Forty foot Equivalent Unit* (FEU) containers each. The cells are divided into two *slots*, a *fore* and an *aft* slot. A slot is described by three parameters called *bay*, *row*, and *tier*.

Most cells can hold one 40' or 45' container, or two 20' containers. 45' containers can only be loaded in cells meant for such containers or on the upper tier (on-deck) of an FEU bay, and some cells may be restricted to either 20' or 40' containers. Due to the physical layout of the vessel, there exist odd cells that hold only one 20' container.

Containers stowed in a row form a *stack*, which is one container wide, and is composed of two TEU bays and a single FEU bay. A location is a bay section, which consists of a set of stacks that are either on or below deck. The stacks are adjacent, and they coincide with the same hatch cover for bays with three hatch covers, or they coincide with two or three adjacent hatch covers for bays with seven hatch covers, as depicted in Figure 2. This definition of locations is different from the definitions in [2, 4], and we handle the problem according to the definition given here. Any location has a maximum TEU capacity, a maximum reefer container capacity, maximum capacities for different types of IMO containers, and weight limits.

Containers on a container ship are stowed one on top of the other in vertical stacks. As a result, a common situation is that, in the current port, a container with a downstream port as port of destination (POD) must be unloaded and reloaded in the current port in order to access the container below it, which has the current port as POD. This stowage configuration is called *over-stowage*, and costs both time and money for shipping lines. Two types of over-stowage are normally considered: when a container is unloaded, the containers above it in the same stack must be unloaded first. This situation is referred to as *over-stowage within location*. If the container is stowed below a hatch, all containers

IMO Class		1.1 1.2 1.5	1.3 1.6	1.4	2.1	2.2	2.3	3.0	4.1	4.2	4.3	5.1	5.2	6.1	6.2	7.0	8.0	9.0
Explosives	1.1 1.2 1.5	X	X	X	4	2	2	4	4	4	4	4	4	2	4	2	4	X
Explosives	1.3 1.6	X	X	X	4	2	2	4	3	3	4	4	4	2	4	2	2	X
Explosives	1.4	X	X	X	2	1	1	2	2	2	2	2	2	X	4	2	2	X
Flammable gases	2.1	4	4	2	X	X	X	2	1	2	X	2	2	X	4	2	1	X
Non-toxic, non-flammable gases	2.2	2	2	1	X	X	X	1	X	1	X	X	1	X	2	1	X	X
Toxic gases	2.3	2	2	1	X	X	X	2	X	2	X	X	2	X	2	1	X	X
Flammable liquid	3	4	4	2	2	1	2	X	X	2	1	2	2	X	3	2	X	X
Flammable solids	4.1	4	3	2	1	X	X	X	X	1	X	1	2	X	3	2	1	X
Substances liable to spontaneous combustion	4.2	4	3	2	2	1	2	2	1	X	1	2	2	1	3	2	1	X
Substances which, in contact with water emit flammable gases	4.3	4	4	2	X	X	X	1	X	1	X	2	2	X	2	2	1	X
Oxidizing substances (agents)	5.1	4	4	2	2	X	X	2	1	2	2	X	2	1	3	1	2	X
Organic peroxide	5.2	4	4	2	2	1	2	2	2	2	2	2	X	1	3	2	2	X
Toxic substance	6.1	2	2	X	X	X	X	X	X	1	X	1	1	X	1	X	X	X
Infectious substance	6.2	4	4	4	4	2	2	3	3	3	2	3	3	1	X	3	3	X
Radioactive material	7.0	2	2	2	2	1	1	2	2	2	2	1	2	X	3	X	2	X
Corrosive substance	8.0	4	2	2	1	X	X	X	1	1	1	2	2	X	3	2	X	X
Miscellaneous dangerous substances and article	9.0	X	X	X	X	X	X	X	X	X	X	X	X	X	X	X	X	X

Figure 3 *Segregation table, adopted from [7]*

above this hatch must also be unloaded in order to open the hatch; this is called *hatch over-stowage*.

When a container ship is ready to leave a port it must be declared seaworthy, which means that all loaded items, i.e., cargo, ballast water, fuel, etc., must be distributed along the vessel such that its stability is acceptable, all stress forces are within limits and the *draft, trim* and *metacentric height* of the ship are also within limits. We direct interested readers to [4], [5, 6] for a more detailed description of how vessel stability is computed and modelled. The constraints related to stability in this paper are similar to those in [6].

2.1 IMO classes and stowage rules

According to the International Maritime Dangerous Goods Code (IMDG Code), there are nine classes of dangerous goods, some of these are divided into subclasses, currently making up a total of 17 classes. Detailed information can be found in [7]. Due to their properties, many of these substances are incompatible to each other, and thus a minimum distance has to be kept between them. For this purpose, the IMDG Code provides a number of segregation rules as indicated in Figure 3.

As shown in Figure 3, there exist four specific segregation principles that must be followed for the stowage of dangerous goods, each of them giving detailed rules for how to separate pairs of containers holding incompatible goods: 1) Away from, 2) Separated from, 3) Separated by a complete compartment from, and 4) Separated longitudinally by an intervening complete compartment or hold from.

Principle 1) Away from

Principle 1) only affects the stowing of open top containers, which are not included in this paper, thus only principles 2-4 are considered here. The cells marked 'X' in Figure 3 refer to combinations of goods where the concrete substances will lead to a certain principle (1, 2, 3 or 4) to be applied.

Principle 2) Separated from

This principle means that the containers cannot be placed in the same stack (row), unless separated by a deck, while they can be stowed horizontally (in both longitudinal and transversal directions) separated by one container space. If there is a bulkhead between them, one container space is not necessary. For instance, given two incompatible IMO containers stowed according to principle 2, if one container is stowed in bay 15, row 09, tier 10, the other can be stowed in bay 17, row 09, tier 10, as illustrated in Figure 4.

Principle 3) Separated by a complete compartment from

This principle means that two containers on deck cannot be placed in the same stack, while they can be stowed longitudinally separated by one container space and transversally separated by two container spaces. For example, given two incompatible IMO containers stowed according to principle 3, if one container is stowed in bay 19, row 03, tier 88, the other cannot be stowed in on-deck locations of rows 02, 01, 03, 05, or 07 of bays 17, 19 or 21 as illustrated in Figure 4. Below deck, two containers stowed according to principle 3 cannot be placed in the same stack, horizontally they must be separated by a bulkhead. For instance, given two incompatible IMO containers stowed according to principle 3, if one container is put below deck in any row of bay 19, then the other cannot be put in any below deck locations belonging to bays 17, 19, 21 or 23 as illustrated in Figure 4. Note that there is a bulkhead between bay 14 and bay 18.

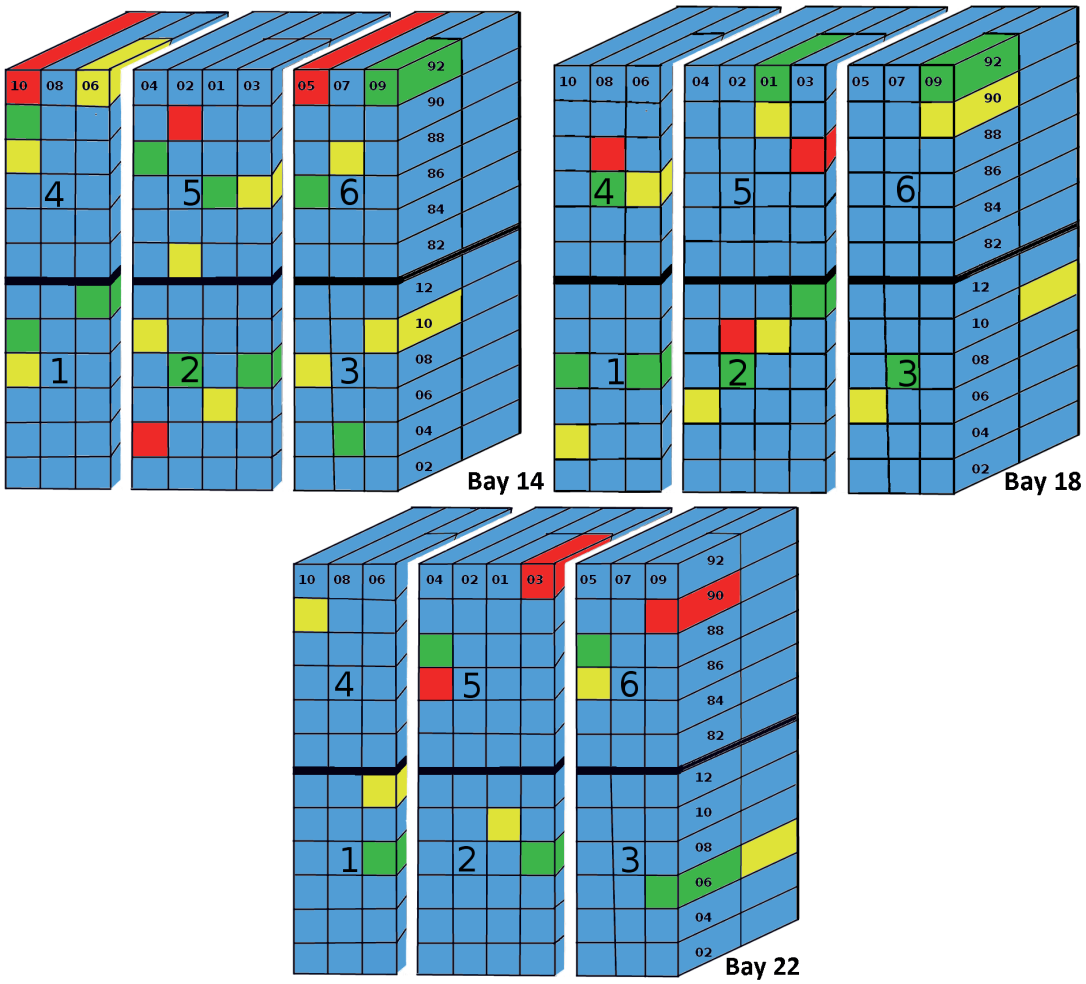

Figure 4 A container stowage configuration of two different incompatible groups of IMO containers following principle 2 (one group in yellow and the other group in green) and one incompatible group of IMO containers following principle 3 (in red) in three adjacent even bays. The setup is based on Figure 1, thus there is a bulkhead between bay 14 and bay 18

Principle 4) Separated longitudinally by an intervening complete compartment or hold from

This principle means that in on-deck locations, two containers cannot be placed in the same stack, longitudinally they require a minimum of 24 m (four 20' containers spaces[1]) separation, including a complete bay. Incompatible IMO containers stowed according to principle 4 in below deck locations in addition require a bulkhead separation. For example, given two incompatible IMO containers stowed according to principle 4, if one container is stowed in any location in bay 19, the other cannot be stowed in any location (both on-deck and below deck) of bay 13, 15, 17, 21, 23, or 25. The separation principles described above are summarized in Table 1, which is taken from [8].

2.2 Our version of the Cargo Mix Problem

In this paper, we focus on the Cargo Mix Problem. Our model is based on the mixed integer programming models presented by Christensen et al. [2] and Ambrosino et al. [6]. Christensen et al. [2] consider 20' dry and reefer containers, 40' dry and reefer containers both normal height and high-cube. A block stowage requirement is strictly enforced in their Cargo Mix Problem, thus the containers in each location must have the same discharge port. The model presented in Ambrosino et al. [6] is for the Multi Port Master Bay Planning Problem (MP-MBPP). Even though these two problems are different, the constraints regarding with stability are the same for both problems. Ambrosino et al. [6] considers 20' and 40' dry and reefer containers with three weight classes.

Our version of the Cargo Mix Problem extends these models by including 20' and 40', reefer and IMO containers as discussed above with three weight classes, and by splitting the locations as outlined in Figure 2. This definition of locations helps us to handle hatch over-stowage in a more realistic way, as there is no need to remove containers from more than one hatch cover to get access to a given below deck container for container ships with three hatch covers in each bay and there is no need to remove containers from more than three hatch covers to get access to a given below deck container for container ships with seven hatch covers in each bay. A feasible solution for the Cargo Mix Problem must then satisfy the following rules.

1 The open space between two consecutive even bays is 3 m.

Table 1 *Separation principles*

Principle	Vertical		Horizontal	
			On deck	Below deck
1	One on top of another allowed	Fore and aft	No restrictions	No restrictions
		Athwardship	No restrictions	No restrictions
2	Not in the same vertical line unless separated by deck	Fore and aft	One container space	One container space
		Athwardship	One container space	One container space
3	Not in the same vertical line unless separated by deck	Fore and aft	One container space	One bulkhead
		Athwardship	Two container spaces	One bulkhead
4	Not allowed	Fore and aft	Minimum horizontal distance of 24 m	One bulkhead and minimum horizontal distance of 24 m, at least 6 m from bulkhead
		Athwardship	Not allowed	Not allowed

R1: For each location and each port, the number of containers of length 20' and 40' must be within the TEU and FEU capacity limits of the location, respectively.

R2: For each location and each port, the number of reefer containers must be within the reefer capacity limit of the location.

R3: For each port, the numbers and positions of incompatible IMO2, IMO3 and IMO4 containers must be according to the separation rules given in Table 1.

R4: For each location and each port, the total weight of containers must be within the limits of the location.

R5: For each port, the transversal, and longitudinal stability must be secured when loading is completed.

The objective function of the Cargo Mix Problem is to maximize the weighted sum of stowed containers based on the group value of their type and length, and to minimize the weighted sum of the costs of hatch over-stowage, the makespan of the cranes along the trip, and stowage of non-reefer containers in reefer slots.

The mathematical formulation and its description in Section 4.2 gives a more precise and formal description of our version of the Cargo Mix Problem.

3. Literature review

The number of publications on the Cargo Mix Problem is limited. The earliest formal description was presented in the PhD thesis by Delgado [1], where a mixed integer programming model was presented. The author considered standard and reefer containers of length 20' and 40'. A decomposition approach, similar to stowage planning work in [4], was applied to achieve scalability. Christensen et al. [2] consider 20' dry and reefer containers, 40' dry and reefer containers of both normal and high-cube height. The block stowage requirement is strictly enforced in their Cargo Mix Problem, thus the containers in each location must have the same discharge port. The authors developed a matheuristic to solve the problem. The method combines a 3-phase decomposition with variable fixing and heuristic assignments. The method finds high-quality solutions in seconds, and they also claim that it can scale to industrial size instances. However, their model and solution method do not consider IMO containers.

Since the literature on the Cargo Mix Problems is scarce, we also consider literature related to stowage planning, as the Cargo Mix Problem can be viewed as a generalization of other stowage planning problems. Literature on stowage planning can be divided into two main categories: single phase and multi-phase approaches. Single phase approaches represent the stowage planning problem in a single optimization model, whereas multi-phase approaches decompose the problem into two or more phases.

Within the category of single phase approaches, integer programming models have been developed by Ambrosino et al. [6, 9-11] and Li et al. [12]. The binary integer programming model in [9] considers 20' and 40' standard containers with three weight classes. Over-stowage is modeled as constraints rather than as part of the objective, and containers with special requirements, such as reefer and IMO containers, are not included. The model considers only the current port, and the objective is to minimize berthing time. Li et al. [12] proposes a binary integer programming model for the multi-port stowage planning problem, aimed to determine the exact location of each container. Similar to [9], only standard containers of length 20' and 40' are considered. This work, however, does consider over-stowage as part of the objective, but does not consider weight limitations for individual containers. The objective minimizes re-handles and maximizes the stowage space utilization. The authors solve the model for different instances of a small vessel of 800 TEUs capacity. Ambrosino et al. [10] presents a mixed integer programming model for finding stowage plans for each port visited by the ship by taking into account the hatch covers and the irregular keel of a container ship, while minimizing the total berthing time, the number of unloaded containers, and over-stowage. Similar to [9, 12], only standard containers of length 20' and 40' are modeled, and the model is tested only with small instances. Ding and Chou [13] developed a heuristic algorithm which can generate stowage plans with a reasonable number of shifts (over-stowage) for the stowage planning problem. They handle the transversal and longitudinal stabilities similar to [6, 9-12]. Their algorithm can make a stowage plan based on the loading information of current port only, and also considers only 20' standard containers.

Multi-phase or decomposition approaches are commonly applied to solve stowage planning problems. The earliest decomposition approach that presented promising results was the work of Wilson and Roach [14] and Wilson et al. [15], where

the block based decomposition was introduced. In these works, a methodology for generating a stowage plan for a container ship on a multi-port journey is presented by decomposing the decision process into two planning phases: a strategic (Master Bay Planning) phase and a tactical (Slot Planning) phase. The strategic objective function includes minimizing over-stowage, imbalanced crane work, the cargo space occupied by each destination, and the cargo block (the set of stacks in a bay section i.e., location) occupied by containers.

Ambrosino et al. [11] introduce two mixed integer programming models for the MP-MBPP, dealing with practical and operational aspects of the problem: minimizing unmet demand, crane imbalance, and number of re-handles. Similar to [9-10, 12], only standard containers of length 20' and 40' are modeled. To solve the problem, the authors propose two different heuristic approaches based on the solution of relaxations, where all integer variables are relaxed to real values, whereas the binary variables remain constrained to {0,1}. These heuristics are tested using real life instances, and the authors claim that the models are applicable in real operations, even though the models do not consider containers with special requirements such as reefer and IMO. Ambrosino et al. [6] presents a new mixed integer programming model for the MP-MBPP that takes into account standard, reefer and open top containers of lengths 20' and 40', and hatch cover positions in the ships. The objective is to minimize the number of re-handles and imbalanced crane work. Unlike [9-10, 12], Ambrosino et al. [6, 11] assigns containers to the bays of the container ship i.e. only dealing with the Master Bay Planning problem. In the models presented in [6, 9-12], the constraints dealing with transversal and longitudinal stability are constructed by forcing the weight on the right side of the ship to be equal to the weight on the left side of the ship within given tolerances, and the weight on the stern of the ship to be equal to the weight on the bow of the ship within given tolerances. In addition, the constraints dealing with vertical stability and metacentric height are constructed by forcing containers to be stowed in ascending order of weight from the bottom to the top in the same stack.

Kang and Kim [16] present a two phase decomposition approach of the stowage planning problem: in the first phase they assign groups of standard containers of length 40' to the locations of the ship, in the second phase they determine the loading sequence of containers in each location aimed at minimizing the total berthing time at each port along the route. The constraints in the first phase are dealing with the stability of the ship, all containers in the load list must be loaded, and the containers loaded in a location must be within the capacity of the location. The authors propose heuristic methods to solve the problem. A decomposition of the multi-port stowage planning problem into two phases is also presented by Wei-Ying et al. [17], aimed at minimizing over-stowage and the number of bays occupied by containers at each port. In the first phase, containers are aggregated into homogeneous groups based on their type, length, height, weight and port of destination, the groups are then assigned to bays. This phase is solved using a bin packing algorithm where bays are regarded as bins, the number of slots in each bay are taken as capacities of bins, and containers with different characteristics (homogeneous container groups) are treated as items to pack. Pacino et al. [4] solve the stowage planning problem by decomposing it hierarchically into two phases: the Multi-Port Master Bay Planning Problem and the Slot Planning Problem. In the MP-MBPP, an integer programming model that assigns groups of different container types (standard light, standard heavy, reefer light and reefer heavy) to locations of the container ship is presented. This model is then solved after relaxing some of the variables. The Slot Planning Problem is solved by a constraint programming and local search procedure. Pacino et al. [4] develop a linear integer programming model with ballast tanks which leads to variable displacement for the MP-MBPP. They present a linearization approach for the center of gravity and hydrostatic data tables of the vessel, to formulate stability and stress constraints that can handle variable displacement. The objective is to minimize the changes in ballast water.

In Azevedo et al. [18], the problem is modelled as a 3D-stochastic stowage planning problem, and the authors propose a three-level solution to minimize unnecessary container movements and ship instability, but their assumptions are probably not fully applicable in a real world situation.

Parreno et al. [19] develop a binary programming model and a GRASP algorithm to solve the Slot Planning Problem where handling of IMO containers is included. To our knowledge, this is the only paper in the literature dealing with IMO containers.

4. A mathematical model for the Cargo Mix Problem

The Cargo Mix Problem (CMP) chooses and distributes types of containers to load into locations of a container vessel. We now introduce our mixed integer programming model formulated to solve the CMP.

4.1 Notation

In this subsection, we present the notation used in the model. Sets are listed in Table 2, constants are given in Table 3, and variables are listed in Table 4.

Containers are divided into groups by length (20' or 40'), weight classes (heavy (H), Medium(M) or Light (L)), type of container (S, R, IMOC1, IMOC2, IMOC3, ..., IMOC|D|), this grouping is used for different purposes in the model. IMO containers are split into different IMO classes (1, 2, 3, ..., |D|). As shown in Figure 3, there are currently 17 classes of dangerous goods. We consider the containers containing one class of dangerous goods as one IMO container type. The IMO containers of each class are incompatible with other IMO containers by respecting one of the segregation principles, so the incompatible containers must be stored according to the stowing rules for the given principle.

We include only FEU bays in the set B, as there is no need to keep track of the fore and aft parts of each bay in the Cargo Mix Problem.

Locations are also grouped based on different properties, the rules for separating IMO containers make it necessary to

Table 2 *Sets*

Notation	Explanation
W	weight classes of containers (light(l),medium (m),heavy (h))
C_L	lengths of containers (20‘, 40‘)
D	classes of dangerous goods
S	segregation principles {2, 3, 4}
T	container types (standard, reefer, imoc_1, imoc_2, ..., $\text{imoc}_{\lvert d\rvert}$)
T_R	reefer container types (reefer)
T_d	container types for dangerous goods of class d($IMOC_d$)
T_d^j	container types following segregation principle j with respect to containers of type T_d
H	bulkheads
H^{ADJ}	pairs of adjacent bulkheads {(1,2),(2,3),...,(|H|-1,|H|)}
B	even bays {2, 6, 10, ... }
B^{EX}	pairs of exclusive adjacent bays, each bay is included in two consecutive pairs of bays {(2,6), (10,14), ...}
B^{IN}	pairs of inclusive adjacent bays, each bay is included in only one pair of bays {(2,6), (6,10), ...}
V	set of positions for locations {*WS,C,PS*}
L	locations
L^O	on-deck locations
L^U	below deck locations
$L^U_{hh'}$	below deck location below on-deck location l
L_b^{EX}	water side locations (all locations to water side of a ship)
L_b^{IN}	port side locations (all locations to the port side of a ship)
L^A	aft locations (all locations to aft part of the ship from its center)
L^F	fore locations from its center (all locations to fore part of the ship)
$L^U_{hh'}$	below deck locations between two adjacent bulkheads h and h'
L_b^{EX}	locations in pair of exclusive adjacent bays
L_b^{IN}	locations in pair of inclusive adjacent bays
P	ports to be visited by the vessel
R	transports, represented by a load-discharge port pair (p_i,p_j)
R_p	transports with containers on the vessel at departure from port p
R_b^A	transports loaded or unloaded in port p
R_p^{OV}	transports which over-stow containers to load or unload in port p

keep track of below deck and on-deck locations and locations in adjacent bays.

A transport is a pair of load-discharge ports (p_i, p_j) where containers are transported from port p_i to port p_j, and port p_i is visited before port p_j.

The x^a variables are the decision variables of the problem, assigning the number of 20’ and 40’ containers of each type to be stowed in each location of the container ship during each transport. The binary variables δ indicate hatch over-stowage. The variables y^O calculate the amount of hatch over-stowage. The variables y^T and y^R calculate crane makespan and reduced reefer container capacity, respectively.

4.2 Formulation

The mixed integer programming model is formulated as follows:

$$\max \sum_{r\in R_p}\sum_{t\in T}\sum_{w\in W}\sum_{\alpha\in C_1} V_r^{\alpha wt}\sum_{l\in L} x_{rl}^{\alpha wt} - \\ -\sum_{p\in P}\sum_{l\in L}\left(C^O y_{pl}^O + C^R y_{pl}^R\right) - \sum_{p\in P} C^T y_p^T \tag{1}$$

subject to

$$\sum_{r\in R_p}\sum_{t\in T}\sum_{e\in W}\sum_{\alpha\in C_1} \Lambda_\alpha x_{rl}^{\alpha wt} \le C_{pl}^T,\ p\in P, l\in L \tag{2}$$

$$\sum_{r\in R_p}\sum_{t\in T}\sum_{w\in W}\sum_{\alpha\in C_1} \Lambda_\alpha x_{rl}^{\alpha wt} \le C_{pl}^R,\ p\in P, l\in L \tag{3}$$

$$\sum_{r\in R_p}\sum_{t\in T}\sum_{w\in W}\sum_{\alpha\in C_1} x_{rl}^{\alpha wt} \le \phi_{pl}^d M,\ p\in P, l\in L, d\in D \tag{4}$$

Table 3 *Constants*

Notation	Explanation
C_{pl}^{T}	TEU capacity of location *l* in port *p*
C_{pl}^{R}	reefer container capacity of location *l* in port *p*
C_{pl}^{α}	capacity of length α containers in location *l* in port *p*
C_{pl}^{jd}	capacity of containers incompatible with containers in T_d following segregation principle *j* in location *l* in port *p*
$L_{r}^{\alpha t}$	number of available containers of length α and type *t* in transport *r*
W_{pl}^{T}	maximum weight of all containers in location *l* in port *p*
$W^{\alpha w}$	average weight of length α and weight class *w*
Q_{T}	maximum cross (transversal) equilibrium
Q_{L}	maximum horizontal (longitudinal) equilibrium
$V_{r}^{\alpha wt}$	the value of container type *t* length α, and weight class *w* of transport *r*
$\Lambda_{\alpha} \in \{1,2\}$	TEU coefficient of a container with length α
C^{O}	cost of one hatch over-stowing container
C^{R}	cost of one unit reduction of reefer container capacity
C^{T}	cost of one time unit of crane makespan
C^{Time}	average crane time needed to load or unload a TEU unit
M	big number
M_{3}	sum of the TEU capacity of the locations in $L_{hh'}^{U}$
M_{4}	sum of the TEU capacity of the locations in L_{b}^{IN}
$M_{hh'}$	number of locations in $L_{hh'}^{U}$
M_{b}	number of locations in L_{b}^{IN}
R_{pl}^{D}	number of TEU units to be discharged from location *l* in port *p*
R_{pl}^{OV}	number of over-stowing TEU units in location *l* in port *p*
R_{pl}^{A}	number of TEU units to be loaded or discharged in location *l* in port *p*

Table 4 *Variables*

Notation	Explanation
$x_{rl}^{\alpha wt}$	number of containers with length α, weight *w* of type *t* stowed in location *l* during transport *r*
δ_{pl}	1 if there are containers to load or discharge in port *p* below on-deck location *l*, 0 otherwise
ϕ_{pl}^{d}	1 if there are containers containing dangerous goods of class *d* in location *l* when the vessel leaves port *p*, 0 otherwise
$\lambda_{(hh')p}^{d}$	1 if there are containers incompatible with class *d* following segregation principle 3 in under deck locations between two adjacent bulkheads *h* and *h'* when the vessel leaves port *p*, 0 otherwise
φ_{bp}^{d}	1 if there are containers incompatible with class *p* following segregation principle 4 in locations in pair *b* of inclusive adjacent bays when the vessel leaves port *p*, 0 otherwise
y_{pl}^{O}	number of hatch over-stowed TEU units to load or discharge in location *l* in port *p*
y_{p}^{T}	crane makespan in port *p*
y_{pl}^{R}	reduction of reefer TEU capacity in location *l* in port *p*

$$\sum_{r\in R_p}\sum_{t\in T_d^j}\sum_{w\in W}\sum_{\alpha\in C_1} x_{rl}^{\alpha wt} - (1-\phi_{pl}^{d})M \le C_{pl}^{jd}, \quad p\in P, l\in L, d\in D, j\in S \tag{5}$$

$$\sum_{r\in R_p}\sum_{l\in L_{hh'}^{U}}\sum_{t\in T_d^3}\sum_{w\in W}\sum_{\alpha\in C_L} x_{rl}^{\alpha wt} \le \lambda_{(hh')_p}^{d} M_3, \quad p\in P, d\in D, (hh')\in H^{ADJ} \tag{6}$$

$$\lambda_{(hh')p}^{d} + \frac{\sum_{l\in L_{hh'}^{U}}\phi_{pl}^{d}}{M_{(hh')}} \le 1, \quad p\in P, d\in D, (hh')\in H^{ADJ} \tag{7}$$

$$\sum_{r\in R_p}\sum_{l\in L_b^{IN}}\sum_{t\in T_d^4}\sum_{w\in W}\sum_{\alpha\in C_L} x_{rl}^{\alpha wt} \le \varphi_{bp}^{d} M_4, \quad p\in P, d\in D, b\in B^{IN} \tag{8}$$

Table 5 *Proportion of container types to be loaded in the Cargo Mix Problem. The column 'Principles' indicates the principles following the IMO containers in the given scenario*

Scenario	ST	R	$IMOC_1$	$IMOC_2$	$IMOC_3$	$IMOC_4$	Principles
S_1	70	10	7.5	7.5	3.5	1.5	2,3,4
S_2	71.5	10	7.5	7.5	3.5	0	2,3,4
S_3	75	10	7.5	7.5	0	0	2
S_4	82.5	10	7.5	0	0	0	-
S_5	90	10	0	0	0	0	-
S_6	100	0	0	0	0	0	-

Table 6 *Overview of instances: the columns under Vessel present ship dependent data: Loc is the total number of locations, Tot Cap is the total capacity of the ship in TEU and R Cap is the reefer capacity of the ship. Port indicates the number of ports along the route. The columns under Available containers to load presents the number of available containers of lengths 20', and 40', which will be loaded at current port and downstream ports. Transports is the total number of active transports, and the two rightmost columns show the maximum and minimum number of integer (binary) variables in the model*

ID	Vessel				Available containers to load				Tran	No of variables	
	Loc	Tot Cap	R Cap	Port	Current port		Downstream ports		sports	Integer (binary)	
					20'	40'	20'	40'		Max	Min
1	66	2376	250	6	800	800	1962	1962	15	28480 (7200)	6230 (132)
2	120	3600	370	6	1018	1018	1496	1962	15	56546 (9740)	11160 (360)
3	234	7800	800	6	2898	1920	7960	3984	15	91156 (10408)	21086 (468)
4	300	10000	1000	6	2898	1920	7910	3984	15	117035 (13725)	27026 (600)
5	276	18032	1680	6	4022	5990	7960	13868	15	116221 (12627)	25142 (552)

$$\varphi_p^d + \frac{\sum_{l \in L_{Bh}^{IN}} \phi_{pl}^d}{M_b} \leq 1,\ p \in P, d \in D, b \in B^{IN} \tag{9}$$

$$\sum_{r \in R_p} \sum_{t \in T} \sum_{w \in W} x_{rl}^{\alpha wt} \leq C_{pl}^{\alpha},\ p \in P, l \in L, \alpha \in C_L \tag{10}$$

$$\sum_{l \in L} \sum_{w \in W} x_{rl}^{\alpha wt} \leq L_r^{\alpha t},\ \alpha \in C_L, t \in T, r \in R \tag{11}$$

$$\sum_{r \in R_p} \sum_{t \in T} \sum_{w \in W} \sum_{\alpha \in C_L} W^{\alpha w} x_{rl}^{\alpha wt} \leq W_{pl}^T,\ p \in P, l \in L \tag{12}$$

$$\left| \sum_{r \in R_p} \sum_{t \in T} \sum_{w \in W} \sum_{\alpha \in C_L} \left(\sum_{l \in L^{WS}} W^{\alpha w} x_{rl}^{\alpha wt} \right) \right| \leq Q_T \tag{13}$$

$$\left| \sum_{r \in R_p} \sum_{t \in T} \sum_{w \in W} \sum_{\alpha \in C_L} \left(\sum_{l \in L^A} W^{\alpha w} x_{rl}^{\alpha wt} - \sum_{l \in L^F} W^{\alpha w} x_{rl}^{\alpha wt} \right) \right| \leq Q_L \tag{14}$$

$$\sum_{l' \in L_l^U} \left(R_{pl'}^D + \sum_{r \in R_p^A} \sum_{t \in T} \sum_{w \in W} \sum_{\alpha \in C_L} x_{rl'}^{\alpha wt} \right) \leq M \delta_{pl}, p \in P, l \in L^O \tag{15}$$

$$R_{pl}^{OV} + \sum_{r \in R_p^{OV}} \sum_{t \in T} \sum_{w \in W} \sum_{\alpha \in C_L} \Lambda_\alpha x_{rl}^{\alpha wt} - M(1 - \delta_{pl}) \leq y_{pl}^O,\ p \in P, l \in L^O \tag{16}$$

$$C^{Time} \sum_{r \in R_p^A} \sum_{l \in L_b^{EX}} \left(R_{pl}^A + \sum_{t \in T} \sum_{w \in W} \sum_{\alpha \in C_L} \Lambda_\alpha x_{rl}^{\alpha wt} \right) \leq y_p^T,\ p \in P, b \in B^{EX} \tag{17}$$

$$\sum_{r \in R_p} \sum_{t \in T} \sum_{w \in W} \sum_{\alpha \in C_L} F_{pl}^t \Lambda_\alpha x_{rl}^{\alpha wt} - C_{pl}^R \leq y_{pl}^R,\ p \in P, l \in L \tag{18}$$

$$x_{rl}^{\alpha wt} \in N \cup \{0\}, \alpha \in C_L, w \in W, t \in T, r \in R, l \in L \tag{19}$$

$$\delta_{pl} \in \{0,1\},\ p \in P, l \in L \tag{20}$$

$$\varphi_{bp}^d \in \{0,1\},\ p \in P, b \in B^{IN}, d \in D \tag{21}$$

$$\phi_{pl}^d \in \{0,1\},\ p \in P, l \in L, d \in D \tag{22}$$

$$\lambda_{(hh')p}^d \in \{0,1\},\ p \in P, (hh') \in H^{ADJ}, d \in D \tag{23}$$

$$y_{pl}^O \in N \cup \{0\},\ p \in P, l \in L \tag{24}$$

$$y_p^T,\ y_{pl}^R \geq 0,\ p \in P, l \in L \tag{25}$$

The objective function (1) maximizes the weighted sum of stowed containers based on the group value of their type and length, minus the weighted sum of costs of hatch over-stowage, the makespan of the cranes along the trip, and stowage of non-reefer containers in reefer slots.

The constraints in (2), (3) and (5) ensure that location capacities are not violated. Constraints (2) and (3) ensure that TEU and reefer container capacities of each location in each port are respected.

Constraints (4) set the binary variables ϕ_{pl}^d to 1 if there are containers with dangerous goods of class *d* to load, or already loaded, in port *p* in location *l*. Constraint (5) ensures that the number of incompatible containers following principles 2 and 3 in each location (for principle 3, only on-deck locations) never exceed the given limits.

Constraints (6) set the binary variables $\lambda_{(hh')p}^d$ to 1 if there are containers incompatible with containers containing dangerous goods of class *d* following principle 3 to load, or already loaded, in port *p* in the under deck locations between two adjacent bulkheads *h* and *h'*.

Constraint set (7) ensures that incompatible containers following principle 3 in below deck locations are separated by a bulkhead.

Constraint set (8) sets the binary variables φ_{bp}^d to 1 if there are containers incompatible with containers containing dangerous goods of class *d* following principle 4 to load, or already loaded, in port *p* in locations in pair *b* of inclusive adjacent bays.

***Table** 7 CMP results with one hour run time. The first and second columns are the instance Scenario and ID, respectively, the third column is the best found objective value. The fourth column shows the number of hatch over-stowing containers along the route. The fifth column is the run time used by the solver to find the best solution, and the last column is the optimality gap. We have used a maximum cross (transversal) equilibrium (Q_T) and maximum horizontal (longitudinal) equilibrium (Q_L) of 60 tons, which is equal to two 40' heavy containers*

Scen	ID	Obj (10^3)	HOS (TEU)	Runtime (s)	Gap (%)
	1	849.26	0	2990	0.13
	2	1145.48	0	2400	0.08
S_1	3	2965.26	1	360	0.02
	4	3067.08	0	3400	0.00
	5	6788.77	10	2700	0.23
	1	848.65	0	3500	0.22
	2	1145.91	0	1500	0.04
S_2	3	2965.16	0	2070	0.00
	4	3066.68	0	280	0.00
	5	6790.52	1	3470	0.23
	1	848.30	0	2680	0.24
	2	1145.52	0	3180	0.07
S_3	3	2965.22	0	1430	0.00
	4	3066.78	0	440	0.00
	5	6801.53	0	2740	0.04
	1	849.40	0	2680	0.10
	2	1144.67	0	480	0.03
S_4	3	2964.87	3	1890	0.02
	4	3066.70	0	370	0.00
	5	6800.79	0	2700	0.06
	1	850.17	0	1600	0.02
	2	1144.24	0	1870	0.00
S_5	3	2965.30	0	180	0.00
	4	3066.65	0	180	0.00
	5	6796.20	0	2600	0.04
	1	872.10	0	2780	0.00
	2	1187.44	0	410	0.00
S_6	3	2919.98	0	2780	0.00
	4	3028.38	0	65	0.00
	5	6721.24	0	1350	0.03

Constraint set (9) ensures that incompatible IMO containers following principle 4 are separated by at least two even bays longitudinally, including a complete compartment. When incompatible IMO containers following principle 4 are stowed in below deck locations, additional bulkhead separation is needed, but there are always enough bulkheads with two even bays separation.

Constraint set (10) ensures that the number of containers of each length in each location is within the location's capacity. This constraint set is quite similar to (2), but if a location has two odd cells, the constraints in (10) are needed to ensure that it is possible to load two 20' containers, but not one 40' container, in these two cells. The constraints in (11) ensure that the number of loaded containers in all transports do not exceed the number of available containers. Constraint set (12) ensures that the weight of all containers in each location is within the weight limit of the location.

The constraints (13) and (14) control the stability of the container ship in each port visited. The stability conditions are described in terms of the longitudinal and transversal equilibrium. This means that the difference of the weights of the water side and port side should be within the transversal equilibrium, and

Table 8 *CMP results with different values of Q_L and Q_R in one hour run time. For each pair of values for Q_L and Q_R the table shows the best found objective value, the optimality gap and the run time*

Scen	ID	$Q_L = Q_T = 30$ tons			$Q_L = Q_T = 90$ tons			$Q_L = Q_T = 120$ tons		
		Obj (10^3)	Time (s)	Gap (%)	Obj (10^3)	Time (s)	Gap (%)	Obj (10^3)	Time (s)	Gap (%)
	1	849.71	1850	0.10	849.00	3200	0.16	849.64	2290	0.09
	2	1146.07	940	0.03	1146.26	2920	0.00	1145.69	2060	0.06
S_1	3	2964.14	2490	0.06	2964.21	1840	0.05	2964.63	3464	0.04
	4	3067.00	1216	0.00	3067.04	1449	0.00	3066.96	164	0.00
	5	6796.09	2960	0.12	6801.00	3540	0.05	6801.75	2750	0.04
	1	849.73	2212	0.06	850.08	3510	0.02	849.08	1380	0.18
	2	1146.28	2370	0.00	1146.42	650	0.02	1146.14	2650	0.02
S_2	3	2964.79	3000	0.02	2958.83	2410	0.23	2956.66	3480	0.30
	4	3066.72	1505	0.00	3066.70	2252	0.00	3066.72	720	0.00
	5	6759.54	3190	0.66	6784.55	3400	0.29	6783.57	2380	0.30
	1	849.59	2960	0.11	849.70	2190	0.07	849.32	3430	0.12
	2	1146.28	2800	0.00	1146.36	1950	0.00	1146.28	1690	0.00
S_3	3	2964.79	2050	0.02	2965.23	1134	0.00	2965.34	1910	0.00
	4	3066.72	190	0.00	3066.67	526	0.00	3066.63	300	0.00
	5	6800.03	2920	0.06	6800.06	2810	0.06	6774.04	3080	0.44
	1	849.59	2510	0.08	849.57	3520	0.08	849.62	3060	0.08
	2	1144.30	390	0.06	1144.78	3580	0.02	1144.92	1810	0.00
S_4	3	2964.82	3390	0.02	2964.85	583	0.02	2965.12	670	0.01
	4	3066.76	580	0.00	3066.80	310	0.00	3066.78	58	0.00
	5	6799.83	2690	0.07	6799.15	1890	0.08	6801.37	2410	0.05
	1	849.93	1410	0.05	850.11	1900	0.02	850.08	3105	0.03
	2	1144.16	1320	0.00	1144.20	1580	0.00	1144.24	354	0.00
S_5	3	2964.83	2880	0.02	2964.80	170	0.02	2965.08	190	0.01
	4	3066.64	36	0.00	3066.56	44	0.00	3066.64	25	0.00
	5	6785.81	1710	0.20	6797.22	1960	0.03	6795.73	3560	0.06
	1	872.06	410	0.00	872.13	2420	0.01	872.05	1891	0.01
	2	1187.44	52	0.00	1187.34	158	0.00	1187.38	1051	0.00
S_6	3	2919.97	2800	0.00	2920.90	60	0.00	2920.11	1550	0.00
	4	3028.38	80	0.00	3028.24	23	0.00	3028.28	17	0.00
	5	6721.14	560	0.03	6721.77	2150	0.02	6721.42	480	0.02

the difference of the weights in the aft and fore parts should be within the longitudinal equilibrium. Since the expressions in the absolute values in (13) and (14) are linear, and since the RHS of both constraint sets are constant, each of the constraint sets are equivalent with two sets of linear constraints.

Constraints (15) - (18) compute values for some of the variables in the objective function. Constraint set (15) sets the binary variables δ_{pl} to 1 if there are containers to be handled in port p in the location below a given on-deck location l. Constraint (16) then calculates the number of hatch over-stow containers in on-deck location l in port p.

Crane makespan is the amount of time needed for the cranes to perform all loading and unloading operations, this is calculated by constraint set (17). In the Cargo Mix Problem, stacking rules are not taken explicitly into account. For this reason, some Slot Planning instances may be infeasible. A possible source of infeasibility is reefer containers, since they can only be stowed in slots with power plugs, which might be occupied by other container types. This is handled by reducing the capacity of reefer containers in a location by a proportional factor F^t_{pl}, where $F^t_{pl} = \frac{C^R_{pl}}{C^T_{pl}}$ for all non-reefer containers and a factor 1 for all

Table 9 *CMP results with different optimality gaps. For each gap, the table shows the optimality gap and the run time. A 0.00 in the Gap column means that the default Gurobi optimality gap of 0.01% or less was reached. The values for Q_T and Q_L are the same as their values in Table 7*

Scen	ID	1% Gap		0.5% Gap		0.1% Gap	
		Gap (%)	Time (s)	Gap (%)	Time (s)	Gap (%)	Time (s)
	1	0.79	100	0.43	135	-	-
	2	0.84	66	0.25	320	0.10	710
S_1	3	0.83	60	0.02	350	0.02	350
	4	0.76	160	0.01	570	0.01	570
	5	0.51	1830	0.29	2380	-	-
	1	0.96	111	0.42	335	-	-
	2	0.23	305	0.23	305	0.06	535
S_2	3	0.21	350	0.21	350	0.04	1950
	4	0.89	72	0.01	285	0.01	285
	5	0.73	2522	0.46	2524	-	-
	1	0.95	62	0.45	193	-	-
	2	0.43	238	0.43	238	0.10	2582
S_3	3	0.51	107	0.08	450	0.08	450
	4	0.50	41	0.50	41	0.08	441
	5	0.38	364	0.38	364	0.10	859
	1	0.79	41	0.36	66	0.10	2690
	2	0.47	103	0.47	103	0.05	151
S_4	3	0.91	50	0.11	170	0.06	340
	4	0.14	77	0.14	77	0.00	376
	5	0.53	583	0.23	747	0.06	2707
	1	0.67	14	0.46	19	0.10	1570
	2	0.08	44	0.08	44	0.08	44
S_5	3	0.71	65	0.19	143	0.03	189
	4	0.01	35	0.01	35	0.01	35
	5	0.96	239	0.17	369	0.10	725
	1	0.56	7	0.43	9	0.09	309
	2	0.09	9	0.09	9	0.09	9
S_6	3	0.04	41	0.04	41	0.04	41
	4	0.01	27	0.01	27	0.01	27
	5	0.92	57	0.05	153	0.05	153

reefer containers. Constraints (18) set the values for the variables y^R_{pl}, i.e., the reduction of the capacity of reefer containers within locations, which makes stowing non-reefer containers in reefer slots more costly.

Finally, constraints (19) - (25) give domains for the variables.

The mathematical formulation and the short explanation given here may be a bit hard to read and understand. A less formal and more understandable description of the objective and the constraints can be found in Section 2.2.

5. Computational results

In this section, we present the results from our computational experiments. Neither industrial contacts nor other researchers have been able or willing to share instances with us, so we have generated random instances, which we believe correspond closely to real world scenarios for the CMP related to container ships with capacities from 2376 to 18032 TEUs.

An overview of the considered container ships are reported in Table 6, in the columns under vessels.

The container demand has been randomly generated such that for each transport (origin-destination), there should be

a positive demand for standard, reefer, and IMO containers. In particular, six scenarios with different percentages of standard (S), reefer (R) and four classes of IMO ($IMOC_1$, $IMOC_2$, $IMOC_3$, $IMOC_4$) containers have been generated as listed in Table 5.

The weight classes we use for both 20' and 40' containers are the same as the weight classes used in [6]. In [6], containers of length 40' belong to light, medium and heavy classes corresponding to weights of 10, 20 and 30 tons, respectively, whereas the same classes are associated with 7, 14 and 21 tons for 20' containers.

We assume that the considered route has six ports, and, for each origin port, the possible destinations will be all downstream ports.

The proposed model was implemented in Pyomo [20] and solved with the MIP solver Gurobi 7.50 [21]. All the tests were executed on a Linux machine with Intel Core i7-5600U, CPU 2.60GHz x 4 and 16 GB of memory, no parallelism was used. In the tests reported in Table 7, all instances have been solved by considering the transversal equilibrium (Q_L) and longitudinal equilibrium (Q_T) of 60 tons (equivalent to two 40' heavy containers). A time limit of one hour has been assigned to the solver. As shown in Table 7, 13 instances are solved to optimality with the default Gurobi optimality gap of 0.01%. The remaining instances are solved with an optimality gap of less than 0.5%. In particular, 12 of the instances are solved with an optimality gap less than or equal to 0.\%, and the remaining five instances, which belong to Scenario S_1 (containing six container types and following all principles) and S_2 (containing five container types and following all principles) are solved with an optimality gap greater than 0.1%, but less than or equal to 0.5%. As expected, Scenario S_1 and S_2 seems to be more difficult to solve, whereas S_6 (containing only standard containers) is easy to solve.

In order to evaluate the robustness of the model, we tested with different values for transversal (Q_L) and longitudinal (Q_L) equilibriums, ranging from 30 to 120 tons. As can be seen from Table 8, most of the instances are solved with an optimality gap less than 0.1%, the remaining instances are solved with an optimality gap less than 1% within the time limit.

Finally, we have run the instances with larger optimality gaps to see how long time is needed to find a solution within the given gap, and how good this solution is compared to the "true" optimal solution. The results of these runs are given in Table 9. As expected, the run times decrease with increasing optimality gaps. With an optimality gap of 1% or 0.5%, almost all instances are solved within ten minutes (only two instances needed more than ten minutes with the given gaps). With 0.1% optimality gap, 17 instances are solved in less than ten minutes, but five instances are not solved with the given gap within one hour.

The results show that by increasing optimality gaps, the solution times can be brought down to quite acceptable levels without giving away much in terms of solution quality. Which gap to use and which amount of time to be regarded as "reasonable time" will depend on the situation, this has to be decided by the problem owner who is going to use the solution for planning.

6. Conclusions

This paper considers the Cargo Mix Problem (CMP), which is an important optimization problem in liner shipping, particularly for the efficiency of loading and unloading of container ships. We have extended existing models for the CMP by including IMO containers holding dangerous goods.

The proposed model was implemented in Pyomo and solved with Gurobi 7.5 for 30 instances with four different transversal and longitudinal equilibriums. The computational experiments show that our model can be solved to optimality or near optimality in reasonable time using a standard MIP solver.

References

[1] DELGADO, A. Models and algorithms for container vessel stowage optimization. PhD thesis, University of Copenhagen, 2013.

[2] CHRISTENSEN, J., PACINO, D. A matheuristic for the Cargo Mix Problem with Block Stowage. *Transportation Research Part E: Logistics and Transportation Review* [online]. 2017, **97**, p. 151-171. ISSN 1366-5545/e ISSN 1878-5794. Available from: https://doi.org/10.1016/j.tre.2016.10.005

[3] FAN, L., et al. Stowage planning of large containership with tradeoff between crane workload balance and ship stability. International MultiConference of Engineers and Computers Scientists : proceedings [online]. Vol. III. 2010. ISBN 978-988-18210-5-8/ISSN 2078-0958/eISSN 2078-0966, p. 1-7. Available from: http://www.iaeng.org/publication/IMECS2010/IMECS2010_pp1537-1543.pdf

[4] PACINO, D., et al. Fast generation of near-optimal plans for eco-efficient stowage of large container vessels. 2nd International Joint Conference on Artificial Intelligence : proceedings. 2011. ISSN 1045-0823, p. 286-301.

[5] PACINO, D., et al. An accurate model for seaworthy container vessel stowage planning with ballast tanks. 3rd International Conference on Computational Logistics : proceedings [online]. Springer, Berlin, Heidelberg, 2012. ISBN 978-3-642-33586-0/eISBN 978-3-642-33587-7, p. 17-32. Available from: https://doi.org/10.1007/978-3-642-33587-7_2

[6] AMBROSINO, D., PAOLUCCI, M., SCIOMACHEN, A. Computational evaluation of a MIP model for multi-port stowage planning problems. *Soft Computing* [online]. 2017, **21**(7), p. 1753-1763. ISSN 1432-7643/eISSN 1433-7479. Available from: https://doi.org/10.1007/s00500-015-1879-y

[7] AMBROSINO, D., SCIOMACHEN, A. Using a bin packing approach for stowing hazardous containers into containerships. In: FASANO, G., PINTER, J. D. (eds.) *Optimized packings with applications* [online]. Springer Optimization and Its Applications 105. Springer, Cham. 2015, **5**, p. 1-18. eISBN 978-3-319-18899-7/ISSN 1931-6828. Available from: https://doi.org/10.1007/978-3-319-18899-7_12

[8] International Maritime Organization. International Maritime Dangerous Goods code [online]. Vol. 1. London: Polestar Wheatons Ltd, 2006. ISBN 978-92-801-4214-3. Available from: https://law.resource.org/pub/us/cfr/ibr/004/imo.imdg.1.2006.pdf

[9] AMBROSINO, D., SCIOMACHEN, A., TANFANI, E. Stowing a containership: the master bay plan problem. *Transportation Research Part A: Policy and Practice* [online]. 2004, **38**(2), p. 81-99. ISSN 0965-8564/eISSN 1879-2375. Available from: https://doi.org/10.1016/j.tra.2003.09.002

[10] AMBROSINO, D., et al. Modelling the multi-port master bay problem. In: Dauer, R. R. M., Sagarra, R. M., de Oses, F. X. M (eds.): *Maritime Transport IV*. UPC (Universititat Politecnica de Catalunya), Barcelona, 2009. p. 63-73.

[11] AMBROSINO, D., PAOLUCCI, M., SCIOMACHEN, A. Experimental evaluation of mixed integer programming models for the multi-port master bay plan problem. *Flexible Services and Manufacturing Journal* [online]. 2015, **27**(2-3), p. 263-284. ISSN 1936-6582/eISSN 1936-6590. Available from: https://doi.org/10.1007/s10696-013-9185-4

[12] LI, F., et al. An Integer linear programming for container stowage problem. In: International Conference on Computational Science : proceedings. Lecture Notes in Computer Science, vol 5101 [online]. Springer, Berlin, Heidelberg, 2008. ISBN 978-3-540-69383-3/ eISBN 978-3-540-69384-0, p. 853-862. Available from: https://doi.org/10.1007/978-3-540-69384-0_90

[13] DING, D., CHOU, M. C. Stowage planning for container ships: A heuristic algorithm to reduce the number of shifts. *European Journal of Operational Research* [online]. 2015, **246**(1), p. 242-249. ISSN 0377-2217. Available from: https://doi.org/10.1016/j.ejor.2015.03.044

[14] WILSON, I. D., ROACH, P. A. Container stowage planning: a methodology for generating computerised solutions. *Journal of the Operational Research Society* [online]. 2000, **51**(11), p. 1248-1255. ISSN 0160-5682/e ISSN 1476-9360. Available from: https://doi.org/10.1057/palgrave.jors.2601022

[15] WILSON, I. D., ROACH, P. A., WARE, J. A. Container stowage pre-planning: using search to generate solutions, a case study. *Knowledge-Based Systems* [online]. 2001, **14**(3-4), p. 137-145. ISSN 0950-7051/eISSN 1872-7409. Available from: https://doi.org/10.1016/S0950-7051(01)00090-9

[16] KANG, J-G., KIM, Y-D. Stowage planning in maritime container transportation. *Journal of the Operational Research Society* [online]. 2002, **53**(4), p. 415-426. ISSN 0160-5682. Available from: https://doi.org/10.1057/palgrave.jors.2601322

[17] WEI-YING, Z., YAN, L., ZHUO-SHANG, J. Model and algorithm for container ship stowage planning based on bin-packing problem. *Journal of Marine Science and application* [online]. 2005, **4**(3), p. 30-36. ISSN 1671-9433/eISSN 1993-5048. Available from: https://doi.org/10.1007/s11804-005-0018-z

[18] AZEVEDO, A. T., et al. Solution of the 3D stochastic stowage planning for container ships through representation by rules. Fourth International Workshop on Knowledge Discovery, Knowledge Management and Decision Support : proceedings [online]. Atlantis Press. 2013. ISBN 978-90-78677-86-4/ISSN 1951-6851. Available from: https://doi.org/10.2991/.2013.15

[19] PARRENO, F., PACINO, D., ALVAREZ-VALDES, R. A GRASP algorithm for the container stowage slot planning problem. *Transportation Research Part E: Logistics and Transportation Review* [online]. 2016, **94**, p. 141-157. ISSN 1366-5545/eISSN 1 8 7 8 - 5794. Available from: https://doi.org/10.1016/j.tre.2016.07.011

[20] Pyomo [online]. Available from: www.pyomo.org

[21] MIP solver Gurobi [online]. Available from: www.gurobi.com

Vaclav Linkov - Martina Trepacova - Veronika Kureckova - Chih-Wei Pai*

NOVICE CZECH DRIVERS' ABILITY AND WILLINGNESS TO OFFER THE FIRST AID AFTER TRAFFIC ACCIDENTS: THE POSITIVE EFFECT OF THE FIRST-AID TRAINING

The first aid is an important tool to save people's lives after traffic accidents. Drivers are the most-likely bystanders, who might help injured people at the traffic accident site. The current research aims to explore Czech learner drivers' knowledge and attitudes towards the first aid and to evaluate whether the first aid education increases the likelihood that a driver will provide the first aid for injuries resulting from traffic accidents. A questionnaire survey was conducted in 2015 among a sample of 370 Czech learner drivers at driving schools. The two groups of student drivers were compared - those who had attended the first aid classes (FAC) and those who had not. The learner drivers who had attended an FAC are more likely to know how to treat burns and serious injuries, contain external bleeding, and unblock the respiratory track. Those who had not attended an FAC would more often hesitate to provide the first aid because they resisted taking a leadership role to organize the scene, or they did not have suitable equipment. This supports the idea that increasing the quality of the first aid training for Czech student drivers would improve the traffic safety in the Czech Republic.

Keywords: *traffic accident injuries; the first aid education; learner drivers; driving schools*

1. Introduction

Importance of the first aid training for improving safety has been acknowledged for a long time [1]. There is a great effort to provide the adequate first aid to people in need [2]. Since the first aid classes are included in the regular education [3], people are better trained to be able to provide the first aid, which increases its quality. Therefore, training people in the first aid is a way to improve the pre-hospital care for injured [4].

Not all the people know how to administer the first aid. For example, in Jordan, 72% of university students know how to treat a spinal fracture, but only 45% know how to check respiration and 37% to treat a burn [5]. Even people who might need it in their profession do not know how to provide the first aid: less than 20% of Slovenian kindergarten teachers know how to provide cardiopulmonary resuscitation or know what to do in the case of intoxication [6]. In Norway, where the first aid tends to be taught from the primary-school level [7], 90% of the population surveyed by Bakke et al. [8] had received the first aid training and 72% of the population felt that they would be able to provide the first aid in case of an emergency. Of those who had had an opportunity to use the knowledge learned in an FAC, 78% felt that the training had prepared them well. People who had attended an FAC were more knowledgeable about the necessity of providing the first aid after a traffic accident.

Witnesses of accidents where the first aid is necessary might feel helpless and unable to provide the first aid [9]. They might feel too physically weak or that they lack enough knowledge to provide the first aid. They might also hesitate to provide the first aid because of the unpleasant circumstances, like patient vomiting, obesity or blood. The fear of an infectious disease might also lead to hesitation [10]. According to Bakke et al. [8], some people have reservations regarding providing the first aid - 12% are "unwilling to perform certain first aid measures" (p. 4) and one third of those (4% of the total sample) have these reservations because of a fear of infection. Reservations regarding the first aid are not related to presence or absence of the first aid training [8].

Driver training and the ability to provide the first aid vary around the world. In Nigeria, 76% of professional drivers know how to make sure that a patient is breathing properly, 90% know how to stop bleeding and 76% know how to treat fractures [11]. Only 32% of Ethiopian taxi drivers can identify the correct first step for providing the first aid, 28% know how to unblock an obstructed airway, 12% know how to apply direct pressure to serious bleeding, and 20% know how to transport an unconscious patient [12]. Larsson et al. [13] report that 7% of Swedish drivers trained in the first aid actually used their knowledge after a traffic accident. Over 80% of Polish drivers would offer the first aid in the case of an accident, 60% of Polish drivers would hesitate to offer the first aid because of their lack of competence, 20% would hesitate because they are afraid of their own health and 10% would hesitate because of possible legal consequences. About 40% Polish drivers know how to unblock the respiratory track, 24% know how to make the chest compressions and 60% know how to treat a person with a spinal injury [14]. The ability to provide the first aid might also be influenced by the fact that traffic accidents mostly happen when drivers are tired [15], so the witnesses may also be tired.

Research generally shows that when drivers attend an FAC, it increases their ability to provide the first aid. Adelborg et al. [16] compared the first aid knowledge of Danish learner drivers before and after they took an FAC. Knowledge to prioritize the

* [1]Vaclav Linkov, [1]Martina Trepacova, [1]Veronika Kureckova, [2]Chih-Wei Pai
[1]CDV - Transport Research Centre, Brno, Czech Republic
[2]Graduate Institute of Injury Prevention and Control, College of Public Health, Taipei Medical University, Taipei, TAIWAN
Email: vaclav.linkov@hotmail.com

treatment among several casualties increased to 95% from 62%; how to control arterial bleeding to 75% from 30%; how to relieve a foreign body from airway construction to 97% from 68%; how to offer the first aid for a neck injury to 89% from 77%; and for shock to 71% from 50%; while the knowledge of how to offer the first aid for a concussion did not increase (84% before, 80% after). In a Polish sample, 8% of drivers would not offer help because they were afraid that they might harm the patient [17]. When the knowledge of drivers who had attended an FAC was compared with those who had not, the knowledge about checking for consciousness was 60% for the former and 47% for the latter; for checking the breathing it was 42% and 27%, respectively and for how to synchronize chest compression with rescue breaths 62% and 47%, respectively [17]. Vakili et al. [18] collected a sample of 500 professional Iranian drivers who had encountered a traffic accident and gave them the first aid training. Before the training they asked whether they had provided the first aid in the accident(s) they had encountered. Six months after the training they asked those drivers who had encountered a new accident the same questions and compared whether the percentage of those who provided the first aid had improved. The percentage of those who administered the first aid increased to 96% from 65% for airway management; to 98% from 79% for control of bleeding; to 97% from 71% for fracture management; and to 92% from 55% for putting the injured person in a recovery position.

In this study the focus was on the first aid skills of Czech learner drivers. Children in Czech primary schools have about 4 hours of the first aid classes every year from the 5th to the 9th grade. Czech learner drivers additionally have four hours of the first aid classes during their driving course. Nevertheless, those classes consist only of watching videos and students do not practice the skills. Only about 60% of Czech drivers would give the first aid after a traffic accident [19]. This situation might be improved if additional first aid training is incorporated into Czech driving courses [20]. This research aims to assess Czech drivers' ability to provide specific types of the first aid and the obstacles they might feel when deciding to administer it. While Kureckova et al. [20] compared different types of the first aid training for learner drivers, the aim here is to show that any type of training is efficient in comparison to absence of training: The differences between drivers who have attended the first aid classes (FAC) and those who have not were compared through a questionnaire. In this way the intention was to bring additional evidence that the first aid training increases the traffic safety in the Czech Republic.

2. Study

Sample

Hundred and twenty driving schools in the South Moravian, Vysocina, Olomouc, and Prague regions of the Czech Republic were contacted. They were asked whether they would distribute a questionnaire to their students. Six of the schools agreed to do so, two in Brno, two in Trebic, one in Olomouc, and one in Prague. We distributed the questionnaire among their students in the end of 2013 and the first half of 2014. The sample consisted of 400 participants, however, 30 questionnaires were excluded for too many missing answers resulting in having data from 370 subjects - 312 men, 53 women and 5 did not provide their gender. The mean age of the participants was 21.2 (SD = 7.2). More than a half of the participants (n = 189, 52%) took the first aid course, the rest (n = 181) had no experience with the first aid course.

Measure

The questionnaire was created by Adelborg et al. [16], which was translated to the Czech language by professional interpreter. The questionnaire contains questions about gender and age; whether the participant had experience with providing the first aid, had ever attended some first aid course and had witnessed a traffic accident. It contained the 5-point Likert scale (rating scale with five rankings: certainly yes, rather yes, I don't know, rather no, certainly no) items about whether the subject was able and willing to provide the first aid after a traffic accident, what kind of the first aid the participant thought they would be able to offer and how satisfied they were with the first aid education in their driving school. There were several 4-point Likert scales (certainly yes, rather yes, rather no, certainly no) about why the participant might hesitate to offer the first aid (the reasons for refusing the first aid are in Table 3).

3. Results

This study aims to determine whether groups of those who attended the first aid course and those who did not differ in their declared knowledge of the first aid and the willingness to provide it. The t-tests for independent samples were used for analysis of obtained data. All reported probability values are two-tailed. For all analyses, an alpha of .05 or .01 was used. The assumptions of normality and the homogeneity of variance were examined and met. The percentages in the text below mean how many people answered "certainly yes" or "rather yes" on the Likert scales.

The majority of participants (n = 287, 78%) did not have experience with providing the first aid. The length of the traffic aid course was an average of 4.8 hours (SD = 8.4). A quarter of the participants (n = 102, 28%) had witnessed a traffic accident.

The majority of participants (n = 226, 62%) felt that they would be able to provide the first aid after a traffic accident. Those who had attended the first aid course felt more confident about their ability than those who had not ($t = 2.8$, $p < .01$).

The majority (n = 282, 78%) knew how to stop large-scale external bleeding; those who had attended an FAC knew how to contain it more often than those who had not ($t = 2.2$, $p < .05$). Participants (n = 211, 58%) also knew how to treat burns; those who had attended an FAC knew more often than those who had not ($t = 2.0$, $p < .05$). Only one third of the participants (n = 123, 34%) knew how to treat a spinal or neck injury; those who had attended an FAC knew it more often ($t = 2.7$, $p < .01$). Over three quarters (n = 286, 78%) knew how to provide chest compressions. Three quarters (n = 273, 75%) knew how to unblock the respiratory track; those who had attended an FAC knew it more often ($t = 2.0$, $p < .05$). More than a half of participants (n = 190, 52%) knew how to treat a serious injury; those who had attended an FAC knew it more often ($t = 3.0$, $p < .01$). Nearly all of the participants (n = 349, 96%) knew how to call for help. See Tables 1 and 2 for details.

Table 1 *Descriptions of participants who had and had not attended the first aid course (FAC)*

	Certainly yes or rather yes		Certainly/ rather yes and attended the FAC		Certainly/ rather yes and did not attend the FAC	
Item	n	%	n	%	n	%
Feels able to provide the first aid after a traffic accident	226	61.8	128	68.4	93	55.4
Knows how to...						
Stop large external bleeding	282	76.2	153	81.8	121	72.0
Treat a burn	211	57	119	63.6	86	51.2
Treat a spinal or neck injury	123	33.2	70	37.6	47	28.0
Provide chest compressions	286	77.3	146	78.1	135	80.4
Clear the lungs/unblock respiratory track	273	73.8	144	77.0	124	73.8
Prioritize serious injuries	190	51.4	107	57.2	75	44.6
Call for help	349	94.3	178	95.2	161	95.8
	N = 370		N = 187		N = 168	

Table 2 *Differences in the first aid knowledge between participants who had and had not attended the first aid course (FAC)*

Item	M1	M2	t	p	d
Feels able to provide the first aid after a traffic accident	2.18	2.39	2.8	0.006	.29
Knows how to...					
Stop large external bleeding	2.02	2.21	2.2	0.032	.23
Treat a burn	2.30	2.49	2.0	0.044	.22
Treat a spinal or neck injury	2.85	3.16	2.7	0.007	.30
Provide chest compressions	1.90	1.96	0.5	0.590	
Clear the lungs/unblock respiratory track	1.89	2.08	2.0	0.042	.22
Prioritize serious injuries	2.40	2.70	3.0	0.003	.32
Call for help	1.20	1.17	-0.5	0.630	

Note: M1 - mean for those who had attended FAC, M2 - mean for those who had not attended FAC, t - Student's t - test value, p - statistical significance, d - Cohen's d

Table 3 *Descriptions of participants who had and had not attended the first aid course (FAC) for a question: which of the following situations would stop them from providing the first aid*

	Certainly yes or rather yes		Certainly/ rather yes and attended the FAC		Certainly/ rather yes and did not attend the FAC	
Item	n	%	n	%	n	%
The following situation would stop me from providing the first aid:						
Someone else will help or helps	96	26	36	19.3	56	33.1
Someone else would see me, it is embarrassing	29	7.8	14	7.5	14	8.3
I would not dare to organize others to provide help	123	33.2	57	30.5	63	37.3
When no one else is helping there is no need to provide help	57	15.4	19	10.2	36	21.3
I do not have suitable equipment	79	21.4	34	18.2	43	25.4
I have suitable equipment but I do not know how to use it	71	19.1	29	15.5	39	23.1
I have the first aid kit but I do not know how to use it	35	3.7	11	5.9	23	13.6
I cannot ensure my own safety	197	53.2	109	58.3	82	48.5
Injury looks repulsive	131	35.4	61	32.6	67	40.1
	N = 370		N = 187		N = 169	

Regarding the reasons someone would not offer the first aid after a traffic accident, 8% (29/357) said they would feel ashamed with someone observing them. One third (123/364, 34%) would not because they would not dare organizing others to help; however, this would be a lesser obstacle for those who had attended an FAC than for those who had not ($t = -2.5$, $p < .05$). One quarter of the participants (79/362, 22%) would not offer the first aid because they feared that they might not have suitable equipment; this would be less of an obstacle for those who had attended an FAC ($t = -2.5$, $p < .05$). For 20% of the participants (71/361), the lack of knowledge about how to use the first aid equipment would be a reason not to offer help; again,

Table 4 *Differences between participants who had and had not attended the first aid course (FAC) for question which of the following situations would stop them from providing the first aid*

Item	M1	M2	t	p	d
The following situation would stop me from providing the first aid:					
Someone else will help or helps	3.18	2.83	-3.2	.002	-.36
Someone else would see me, it is embarrassing	3.56	3.51	-.64	.520	
I would not dare to organize others to provide help	2.91	2.68	-2.5	.014	-.26
When no one else is helping there is no need to provide help	3.54	3.2	-3.7	.000	-.39
I do not have suitable equipment	3.23	3.02	-2.5	.013	-.26
I have suitable equipment but I do not know how to use it	3.24	3.01	-2.6	.009	-.27
I have the first aid kit but I do not know how to use it	3.10	3.20	-1.1	.230	
I cannot ensure my own safety	2.29	2.48	1.8	.07	0.2
Injury looks repulsive	2.83	2.74	-.88	0.38	

Note: M1 - mean for those who had attended FAC, M2 - mean for those who had not attended FAC, t - Student's t-test value, p - statistical significance, d - Cohen's d

this would be more common for those who had not attended an FAC ($t = -2.6$, $p < .01$) and other participants (35/179, 20%) did not know the contents of the first aid kit in their car. Half of the participants (197/360, 55%) would not offer help when they could not guarantee their own safety. One third (131, 37%) would not offer help when an injury was grotesque or disgusting. See Tables 3 and 4 for details.

4. Discussion and Conclusion

Over one quarter of surveyed Czech student drivers had experience with a traffic accident and one fifth had provided some kind of the first aid. This is quite a large proportion of drivers and, given that they were not well informed about treating several types of injuries, this shows that improving the first aid training of Czech drivers is an important step to increasing the traffic safety.

The presented results support the argument that an FAC is associated with the ability to provide the first aid. Participants who had attended FACs felt more able to provide the first aid and more often knew how to treat specific health issues. The only exception was for the chest compressions: FAC students did not know more than those without an FAC. Additionally, the FAC also reduces some reservations that block people from helping. People with FAC experience would hesitate less to offer help because of a fear about not having the suitable equipment and being unable to organize others.

The sample and method that were used has several limitations. First, our sample was not randomly selected. This enhances probability of a sample bias. Second, the large number of statistical comparisons were performed, so the probability of type 1 error increased. Third, the sample represents only central and south eastern part of the Czech Republic and it is questionable whether the results could be generalized to the whole country.

Obtained results support the hypothesis that the first aid training is important for boosting self-confidence for providing the first aid. Health educators should provide the best possible first aid training to learner drivers. With increased training, the number of people who actually would help will probably increase and many human lives could be saved. The recommendation is to increase the number of the first aid lectures for the learner drivers with the aim of improving the traffic safety. The first aid is more important after the traffic accidents for the elderly patients, because they die before reaching the hospital more often than the younger people [21]. It would be beneficial if the first aid training was organized for older drivers who might more often have the opportunity to save other elderly patients' lives. The first aid training makes people behave safer in their normal life [22]. Training learner drivers in the first aid might help to increase the general safety of society.

Acknowledgements

This research was produced with the financial support of the Ministry of Education, Youth and Sports within National Sustainability Programme I, a project of the Transport R&D Centre (LO1610), on a research infrastructure acquired from the Operation Programme Research and Development for Innovations (CZ.1.05/2.1.00/03.0064).

References

[1] GLENDON, A. I., MCKENNA, S. P. Using accident injury data to assess the impact of community first aid training. *Public Health* [online]. 1985, **99**(2), p. 98-109. ISSN 0033-3506/eISSN 1476-5616. Available from: https://doi.org/10.1016/S0033-3506(85)80006-8

[2] VAN DE VELDE, S., et al. European first aid guidelines. *Resuscitation* [online]. 2007, **72**(2), p. 240-251. ISSN 0300-9572/eISSN 1873-1570. Available from: https://doi.org/10.1016/j.resuscitation.2006.10.023

[3] WILKS, J., PENDERGAST, D. Skills for life: First aid and cardiopulmonary resuscitation in schools. *Health Education Journal* [online]. 2017, **76**(8), p. 1009-1023. ISSN 0017-8969/eISSN 1748-8176. Available from: https://doi.org/10.1177/0017896917728096

[4] IBRAHIM, N., A., et al. Road traffic injury in Lagos, Nigeria: Assessing prehospital care. *Prehospital and Disaster Medicine* [online]. 2017, **32**(4), p. 1-7. ISSN 1049-023X/eISSN 1945-1938. Available from: https://doi.org/10.1017/S1049023X17006410

[5] KHATATBEH, M. First aid knowledge among university students in Jordan. *International Journal of Preventive Medicine* [online]. 2016, **7**(1), p. 24. ISSN 2008-7802/eISSN 2008-8213. Available from: https://doi.org/10.4103/2008-7802.174772

[6] SLABE, D., FINK, R. Kindergarten teachers' and their assistants' knowledge of first aid in Slovenian kindergartens. *Health Education Journal* [online]. 2012, **72**(4), p. 398-407. ISSN 0017-8969/eISSN 1748-8176. Available from: https://doi.org/10.1177/0017896912446555

[7] BAKKE, H., K., BAKKE, H., K., SCHWEBS, R. First-aid training in school: Amount, content and hindrances. *Acta Anaesthesiologica Scandinavica* [online]. 2017, **61**, p. 1361-1370. ISSN 0001-5172/eISSN 1399-6576. Available from: https://doi.org/10.1111/aas.12958

[8] BAKKE, H., K., et al. A nationwide survey of first aid training and encounters in Norway. *BMC Emergency Medicine* [online]. 2017, **17**(6), p. 1-7. eISSN 1471-227X. Available from: https://doi.org/10.1186/s12873-017-0116-7

[9] AXELSSON, Å., HERLITZ, J., FRIDLUND, B. How bystanders perceive their cardiopulmonary resuscitation intervention; a qualitative study. *Resuscitation* [online]. 2000, **47**(1), p. 71-81. ISSN 0300-9572/eISSN 1873-1570. Available from: https://doi.org/10.1016/S0300-9572(00)00209-4

[10] SKORA, J., RIEGEL, B. Thoughts, feelings, and motivations of bystanders who attempt to resuscitate a stranger: A pilot study. *American Journal of Critical Care*. 2001, **10**(6), p. 408-416. ISSN 1062-3264/eISSN 1937-710X.

[11] OLUGBENGA-BELLO, A., I., et al. First aid knowledge and application among commercial inter-city drivers in Nigeria. *African Journal of Emergency Medicine* [online]. 2012, **2**(3), p. 108-113. ISSN 2211-419X/eISSN 2211-4203. Available from: https://doi.org/10.1016/j.afjem.2012.06.003

[12] TESHALE, A., A., ALEMU, Z., A. Knowledge, attitude and practice of first aid and factors associated with practice among taxi drivers in Addis Ababa, Ethiopia. *Ethiopian Journal of Health Development* [online]. 2017, **31**(3), p. 200-207. ISSN 1021-6790/eISSN 2309-7388. Available from: https://www.ejhd.org/index.php/ejhd/article/view/1357/1015

[13] LARSSON, E., M., MARTENSSON, N., L., ALEXANDERSON, K., A., E. First-aid training and bystander actions at traffic crashes - A population study. *Prehospital and Disaster Medicine* [online]. 2002, **17**(3), p. 134-141. ISSN 1049-023X/eISSN 1945-1938. Available from: https://doi.org/10.1017/S1049023X00000352

[14] FRYDRYSIAK, K., GRZESKOWIAK, M. Czy kierowcy potrafia udzielic pierwszej pomocy poszkodowanemu w wypadku drogowym? / Can drivers give first aid to causalities in road accident? (in Polish). *Anestezjologia i Ratownictwo* [online]. 2013, **7**, p. 305-311. ISSN 1898-0732. Available from: http://www.akademiamedycyny.pl/wp-content/uploads/2016/05/201303_AiR_005.pdf

[15] Tvarozkova, L., et al. Unava za volantem, rizikove casy behem dne a dopravni nehodovost / Drowsy driving, vulnerable times of the day and traffic accidents (in Czech). *Psychologie a jeji kontexty* [online]. 2017, **8**(2), p. 85-100. ISSN 1803-9278/ ISSN 1805-9023. Available from: http://psychkont.osu.cz/fulltext/2017/2017_2_7_Tvarozkova.pdf

[16] ADELBORG, K., et al. Benefits and shortcomings of mandatory first aid and basic life support courses for learner drivers. *Resuscitation* [online]. 2011, **82**(5), p. 614-617. ISSN 0300-9572/eISSN 1873-1570. https://doi.org/10.1016/j.resuscitation.2010.12.018

[17] KARYS, J., et al. Knowledge of first aid in road traffic accidents among drivers from the Staszow County. *Archives of Physiotherapy and Global Researches* [online]. 2015, **19**(1), p. 29-33. ISSN 2353-4389/eISSN 2353-7183. Available from: https://doi.org/10.15442/apgr.19.2.4

[18] VAKILI, M., A., et al. The efficacy of a first aid training course for drivers: An experience from northern Iran. *Chinese Journal of Traumatology* [online]. 2014, **17**, p. 289-292. ISSN 1008-1275. Available from: https://doi.org/10.3760/cma.j.issn.1008-1275.2014.05.008

[19] ZAMECNIK, P., et al. Vyuka prvni pomoci v autoskolach - zbytecnost nebo relevantni opatreni s velkym potencialem? / First aid training in driving schools - uselessness or relevant measure with considerable potential? (in Czech). *Psychologie a jeji kontexty* [online]. 2014, **5**(Suppl.), p. 107-115. ISSN 1803-9278/ ISSN 1805-9023. Available from: http://psychkont.osu.cz/fulltext/2014/Zamecnik_etal_2014_S.pdf

[20] KURECKOVA, V., et al. First aid as an important traffic safety factor - Evaluation of the experience-based training. *European Transport Research Review* [online]. 2017, **9**(5), p. 1-8. ISSN 1867-0717/eISSN 1866-8887. Available from: https://doi.org/10.1007/s12544-016-0218-4

[21] KATAYAMA, Y., et al. Factors associated with prehospital death among traffic accident patients in Osaka City, Japan: A population-based study. *Traffic Injury Prevention* [online]. 2017, **19**(1), p. 49-53. ISSN 1538-9588/eISSN 1538-957X. Available from: https://doi.org/10.1080/15389588.2017.1347645

[22] LINGARD, H. The effect of first aid training on Australian construction workers' occupational health and safety motivation and risk control behavior. *Journal of Safety Research* [online]. 2002, **33**(2), p. 209-230. ISSN 0022-4375/eISSN 1879-1247. Available from: https://doi.org/10.1016/S0022-4375(02)00013-0

Errata: Communications - Scientific Letters of the University of Zilina, **21**(1), 2019, Passsenger Ride Comfort and International Roughness Index Specifications in the Slovak Republic, p. 15-22.

Authors have identified incorrect results in their paper [1]. Trend removal of measured acceleration signal in Matlab code was *inadvertently* not turned on. This caused incorrect and overstated acceleration RMS values after acceleration data processing (predominantly on the seat surface). Further, the correct multiplying factors in Equation (1) should be $k_{Sx} = k_{Sy} = 1.4$. Presented incorrect results of total vibration a_v in [1] were substantially higher than the correct values. The authors would like to apologise for any inconvenience caused.

Corrected text, figure and tables should read as follows:

6. Whole-body vibration and IRI road classes

...

Median a_v value (P50) exceeds the lower bound of expected "fairly uncomfortable" human reaction (a_v = 0.5 m/s^2, Table 1) for two IRI road classes (#2 and #3) and motorways and three IRI road classes (#3–#5) for the 1st and 2nd class roads (Table 4). For IRI road class #3 and motorways and IRI road class #3–#5 and the 1st and 2nd class roads a lower bound of "uncomfortable" level (a_v = 0.8 m/s^2) was exceeded by the 90th percentile (P90) of a_v (Table 4).

The median values of a_v are shown in Figure 3. Comparison shows higher vibration total value a_v by 16 %, 20 % and 9 % for motorways in the same IRI road class.

On motorways, 27.1 % of processed segments induced passenger's vibrations higher than the lower bound of expected "fairly uncomfortable" human reaction (0.5 m/s^2) and 2.9 % segments exceeded the lower bound of "uncomfortable" level. On the 1st and 2nd class roads it was 55.8 % ("fairly uncomfortable") and 22.8 % ("uncomfortable").

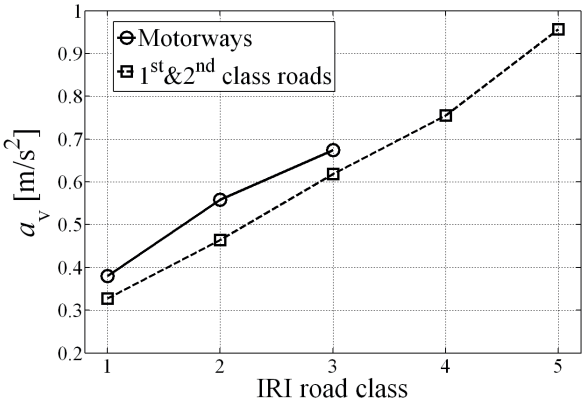

Figure 3 *Median of the passenger vibration total value a_v as a function of IRI road class and road category*

Results in Table 5 may be commented as follows:

Negligible portion of sections falls in the worst comfort likely reaction levels "very uncomfortable" and "extremely uncomfortable".

Table 3 *Fitting parameters of function IRI = f(a_v,v) [Equation (2)] as a function of road category*

Road category	*N*	Length (km)	b_1	b_2	b_3	RMSE	*R*	R^2
Motorways	3808	380.8	2.099	-0.0056	1.226	0.50	0.538	0.290
1st class roads	4684	468.4	4.237	-0.0377	3.886	1.01	0.719	0.517
2nd class roads	5462	546.2	3.664	-0.0368	5.210	1.42	0.545	0.297
1st and 2nd class roads	10146	1014.6	4.605	-0.0445	4.675	1.34	0.682	0.465

Table 4 *Vibration total value statistics as a function of IRI road classes and road category*

N	Length (km)	IRI road class	*v* (km/h)		IRI (mm/m)				Vibration total value a_v (m/s^2)						
			mean	std	min	max	mean	std	mean	std	P10	P25	P50	P75	P90
Motorways															
2940	294	1	118.3	14.4	0.65	1.89	1.2	0.32	0.405	0.124	0.281	0.321	0.380	0.461	0.560
837	83.7	2	118.5	14.5	1.9	3.28	2.3	0.34	0.561	0.167	0.345	0.442	0.558	0.672	0.771
31	3.1	3	111.5	14.0	3.31	4.31	3.7	0.38	0.643	0.321	0.274	0.313	0.674	0.883	1.096
3808	380.8	All	118.3	14.4	0.65	4.31	1.5	0.60	0.441	0.153	0.287	0.332	0.403	0.518	0.654
1st and 2nd class roads															
601	60.1	1	81.1	14.7	0.71	1.88	1.5	0.28	0.339	0.098	0.229	0.270	0.327	0.392	0.465
2604	260.4	2	76.7	16.9	1.9	3.29	2.6	0.40	0.484	0.142	0.323	0.381	0.464	0.562	0.678
3468	346.8	3	71.8	18.1	3.3	4.99	4.2	0.49	0.644	0.209	0.400	0.497	0.619	0.766	0.909
3375	337.5	4	68.2	19.1	5	9.94	6.2	1.02	0.770	0.274	0.423	0.575	0.755	0.942	1.122
98	9.8	5	48.7	10.1	10.03	16.47	11	0.95	0.877	0.320	0.399	0.658	0.957	1.102	1.224
10150	1015	All	72.2	18.5	0.71	16.47	4.4	1.84	0.629	0.254	0.343	0.438	0.586	0.779	0.970

Table 5 *Percentage of travelled sections in comfort level according to the ISO 2631-1 as a function of IRI road classes for motorways*

IRI road class	IRI (mm/m)		a_v (m/s^2)					
			< 0.315	0.315-0.63	0.5-1	0.8-1.6	1.25-2.5	> 2
	min	max	not uncomfortable	a little uncomfortable	fairly uncomfortable	uncomfortable	very uncomfortable	extremely uncomfortable
Motorways								
1	0	1.9	22.4	72.3	17.1	1.2	0.1	0
2	1.9	3.3	6	60.6	61.3	7.8	0	0
3	3.3	5	29	16.1	48.4	32.3	6.5	0
All	0.65	4.31	18.9	69.2	27.1	2.9	0.1	0
1st and 2nd class roads								
1	0	1.9	46.6	52.2	6.3	0.2	0	0
2	1.9	3.3	8.4	77.2	38.9	3.1	0	0
3	3.3	5	2.1	49.8	68.9	20.4	0.7	0
4	5	10	2.5	29.6	64.8	43.4	4.6	0.1
5	10	–	2	22.4	35.7	64.3	8.2	0
All	0.71	16.47	6.5	50	55.8	22.8	1.9	0

Comfort levels “a little uncomfortable” and “fairly uncomfortable” prevailed for all road categories.

Higher percentage of road segments in the same IRI road class corresponds to “fairly uncomfortable” (by 28.7 %) and “uncomfortable” (by 19.9 %) levels for the 1st and 2nd class roads than for motorways. The comparison is influenced with an unequal number of segments N in groups and higher mean speed by 30 to 40 km/h on motorways on the section of the same road class.

Road class #1 for motorways and road class #2 for the 1st and 2nd class roads indicate similar percentage of acceleration response in “uncomfortable” category (1.2 % vs. 3.1 %).

Road class #3 for motorways and road class #4 for the 1st and 2nd class roads indicate similar percentage of acceleration response in “uncomfortable” category (32.3 % vs. 43.4 %).

...

Using Equation (2) to compare IRI thresholds, the correction factor in relation IRI(130) = f(IRI(90)) would be lower at about 0.30-0.35.

7. Conclusions

...

3. Indication of comfort levels “very uncomfortable” and “extremely uncomfortable” was very rare. Comfort levels “a little uncomfortable” and “fairly uncomfortable” prevailed. About fifty percent of all the processed sections exceeded a lower bound of expected “fairly uncomfortable” reaction (a_v = 0.5 m/s^2). About 1.9 % of all the processed sections of the 1st and 2nd road class exceeded a “very uncomfortable” level.
4. Different passenger’s WBV was identified for the same IRI road classes between motorways and the 1st and 2nd class roads. For the same IRI road class, the median total passenger vibration was about 10-20 % higher on motorways.

References

[1] MUCKA, P., STEIN, G. J., TOBOLKA, P. Passenger ride comfort and International Roughness Index specifications in the Slovak Republic. *Communications - Scientific Letters of the University of Zilina* [online]. ISSN 1335-4205, 2019, **21**(1), p. 15-22. ISSN 1335-4205/eISSN 2585-7878. Available from: http://komunikacie.uniza.sk/index.php/communications/issue/view/36